# Inaugural-Dissertation

zur
Erlangung der Doktorwürde
der
Naturwissenschaftlich-Mathematischen Gesamtfakultät
der
Ruprecht-Karls-Universität
Heidelberg

vorgelegt von
Diplom-Mathematiker Jochen Siehr
aus Hardheim

Tag der mündlichen Prüfung: 26. April 2013

**Numerical optimization methods within a continuation strategy for the reduction of chemical combustion models**

Gutachter: Prof. Dr. Dres. h. c. Hans Georg Bock
Prof. Dr. Dirk Lebiedz

To my family and friends

*juvat integros accedere fontis*
*atque haurire juvatque novos decerpere flores*

Titus Lucretius Carus

# Abstract

Model reduction methods in chemical kinetics are used for simplification of models which involve a number of different time scales. Slow invariant manifolds in chemical composition space are supposed to be identified. A selection of state variables serve for parametrization of these manifolds. Species reconstruction methods are used to compute the values of the remaining variables in dependence of the parameters. We discuss theoretical results and numerical methods for an application of a model reduction method that is developed by D. Lebiedz based on optimization of trajectories. The main focus of this work is an application of the model reduction method to models of chemical combustion. The existence of a solution of the semi-infinite optimization problem, which has to be solved to obtain a local approximation of the slow manifold, is proven. A finite optimization problem for the same purpose is presented which can be solved with a generalized Gauss–Newton method. This method is used with an active set strategy. A filter framework and iterations with second order correction are employed for globalization of convergence. Families of neighboring optimization problems can be solved efficiently in a predictor corrector continuation scheme. The tangent space of the slow manifold can be computed by evaluation of sensitivity equations for the parametric optimization problem. A step size strategy is applied in the continuation scheme for efficient progress along the homotopy path. Results of an application of the presented method are shown and discussed. The test models range from simple test examples to realistic models of syngas combustion in air.

# Zusammenfassung

Methoden der Modellreduktion in der chemischen Reaktionskinetik werden zur Vereinfachung von Modellen eingesetzt, welche eine große Zahl verschiedener Zeitskalen beinhalten. Langsame invariante Mannigfaltigkeiten im chemischen Zustandsraum sollen hierfür identifiziert werden. Eine Auswahl von Zustandsvariablen dienen als Parameter zur Parametrisierung dieser Mannigfaltigkeiten. Speziesrekonstruktionsmethoden werden benutzt, um die Werte der verbleibenden Variablen in Abhängigkeit von den Parametern zu berechnen. Wir diskutieren theoretische Resultate und numerische Methoden zur Anwendung einer von D. Lebiedz entwickelten Modellreduktionsmethode basierend auf der Optimierung von Trajektorien mit dem Ziel dieser Arbeit, die Modellreduktionsmethode auf Modelle der chemischen Verbrennung anzuwenden. Die Existenz einer Lösung des zur Berechnung einer lokalen Approximation der langsamen Mannigfaltigkeit zu lösenden Optimierungsproblems wird gezeigt. Ein endliches Optimierungsproblem mit demselben Zweck wird präsentiert, welches mit einem verallgemeinerten Gauß–Newton-Verfahren gelöst werden kann. Diese Methode wird mit einer Aktive-Mengen-Strategie, einer Filter-Methode und Iterationen mit Korrektur zweiter Ordnung zur Globalisierung der Konvergenz genutzt. Familien benachbarter Probleme können effizient mit einem Prädiktor-Korrektor-Fortsetzungsschema gelöst werden. Der Tangentialraum der langsamen Mannigfaltigkeit kann durch Auswertung der Sensitivitätsgleichungen für das parametrische Optimierungsproblem berechnet werden. Eine Schrittweitenstrategie wird in der Fortsetzungsmethode für effizienten Fortschritt entlang des Homotopie-Pfades verwendet. Ergebnisse einer Anwendung der präsentierten Methode werden gezeigt und diskutiert. Die Testmodelle reichen dabei von einfachen Testbeispielen zu realistischen Modellen von Synthesegas-Verbrennung in Luft.

# Acknowledgment

I would like to thank my advisor Hans Georg Bock for the possibility to do research in combination of numerical optimization and chemical combustion.
I wish to thank my advisor Dirk Lebiedz. I thank him for committing the topic "model reduction in chemical kinetics" to me. His professional mentoring, his many ideas, and support during the last five years made this thesis possible.
I wish to thank the late Jürgen Warnatz. His work sparked my interest in combustion research.

I am grateful to Ingrid Hellwig and Margret Rothfuß for administration.
I wish to thank Marc Fein, Marcel Rehberg, Dominik Skanda, and Jonas Unger for their help in many respects.
I would like to thank the research group "Reactive Flows", especially Markus Nullmeier and Volkmar Reinhardt for their advice and Jürgen Moldenhauer and Joachim Simon for computer administration.
In addition, I wish to thank Christian Kirches, Mario Mommer, and Andreas Potschka for a lot of hints.

I like to thank everybody who contributed to software that is used for this work and everybody who improved my English language skills and the style of this thesis.

Funding by the German Research Council (DFG) via project B2 within the Collaborative Research Center (SFB) 568 is gratefully acknowledged.

# Contents


**1 Introduction** **1**
- 1.1 Mathematical models and model reduction . . . . . 1
- 1.2 Results and new contributions . . . . . 4
- 1.3 Outline of the thesis . . . . . 5

**I Theory and modeling** **7**

**2 Theory of dyn. systems and model reduction methods** **9**
- 2.1 Theory of dynamical systems and ODE . . . . . 9
  - 2.1.1 Basic definitions and theorems . . . . . 9
  - 2.1.2 Exponentially attracting manifolds . . . . . 12
- 2.2 Singularly perturbed systems . . . . . 14
  - 2.2.1 Theory of singularly perturbed systems . . . . . 14
  - 2.2.2 Examples of singularly perturbed systems . . . . . 16
- 2.3 Slow invariant manifolds . . . . . 17
  - 2.3.1 Slow manifolds . . . . . 17
  - 2.3.2 Tangent space . . . . . 19
- 2.4 Methods for model reduction . . . . . 19
  - 2.4.1 Early model reduction methods . . . . . 19
  - 2.4.2 Automatic model reduction methods . . . . . 20

**3 Theory of optimization and continuation** **25**
- 3.1 Solution theory of optimization problems . . . . . 25
  - 3.1.1 Semi-infinite optimization problems . . . . . 25
  - 3.1.2 Nonlinear programming problems . . . . . 26
- 3.2 Parametric optimization . . . . . 28
- 3.3 Continuation method . . . . . 30

**4 Models for combustion chemistry** **33**
- 4.1 Basic variables and equations . . . . . 33
  - 4.1.1 State variables . . . . . 33
  - 4.1.2 Thermodynamic variables . . . . . 35
  - 4.1.3 Equilibrium constant and Gibbs free energy . . . . . 37
- 4.2 Conservation laws . . . . . 38

4.2.1 Mass conservation . . . 38
4.2.2 Energy balance . . . 38
4.2.3 NASA polynomials . . . 39
4.3 Chemical kinetics . . . 44
4.3.1 Mass action kinetics . . . 44
4.3.2 Arrhenius kinetics . . . 46
4.3.3 Troe kinetics . . . 47
4.4 Models for homogeneous combustion . . . 48
4.4.1 Change of the mass of the species . . . 48
4.4.2 Conservation of energy . . . 49
4.4.3 Conservation of enthalpy . . . 50

**5 Model reduction method based on optimization 53**
5.1 Basic ideas of the method . . . 53
5.2 Choice of the objective functional . . . 55
5.2.1 Entropy based objective functions . . . 55
5.2.2 Curvature based objective functions . . . 55
5.3 Optimization problems for model reduction . . . 57
5.3.1 Semi-infinite optimization problem . . . 57
5.3.2 Local optimization problem . . . 58
5.4 Existence of solutions . . . 58
5.5 Tools for analysis of the manifold . . . 61
5.5.1 Selection of the reaction progress variables . . . 61
5.5.2 A posteriori analysis . . . 63
5.5.3 Visual tests . . . 65

**II Numerical methods, implementation, and results 67**

**6 Solution methods for the semi-infinite opt. problem 69**
6.1 Numerical quadrature . . . 69
6.1.1 Newton–Cotes quadrature . . . 69
6.1.2 Gaussian and Radau quadrature . . . 70
6.2 Numerical solution of ODE systems . . . 71
6.2.1 Collocation methods . . . 71
6.2.2 Backward differentiation formulae methods . . . 74
6.3 Numerical solution methods for semi-infinite opt. problems . . . 74

**7 Numerical methods for nonlinear programming problems 77**
7.1 Generalized Gauss–Newton method . . . 77
7.1.1 Basic solution method . . . 78
7.1.2 Local convergence . . . 80
7.1.3 Global convergence . . . 81
7.2 Interior point method . . . 88

7.3 Computation of derivatives for the optimization algorithm . . 90

**8 Path following** **93**
8.1 Predictor corrector scheme . . . . . 94
8.1.1 Parameter sensitivities . . . . . 94
8.1.2 Predictor with full step . . . . . 99
8.2 Step size strategy in the predictor corrector method . . . . . 100
8.2.1 Computation of the step size ratio . . . . . 102
8.2.2 Newton-bisection method . . . . . 103
8.3 Computation of the tangent space in the sequential approach 103
8.4 Equilibration of the KKT matrix . . . . . 104
8.5 Warm start of interior point methods . . . . . 105

**9 Results of application** **107**
9.1 Basic tests . . . . . 108
9.1.1 Davis–Skodje model . . . . . 108
9.1.2 Verhulst model . . . . . 110
9.1.3 Singularly perturbed system of catalysis . . . . . 113
9.2 Advanced tests . . . . . 114
9.2.1 Simple three species model . . . . . 114
9.2.2 Lindemann mechanism . . . . . 115
9.2.3 Bioreactor . . . . . 116
9.3 Models based on kinetic mechanisms . . . . . 117
9.3.1 Six species test mechanism . . . . . 117
9.3.2 Simplified six species hydrogen combustion . . . . . 121
9.3.3 Ozone decomposition . . . . . 131
9.4 Models for combustion . . . . . 135
9.4.1 Hydrogen combustion . . . . . 135
9.4.2 Syngas combustion . . . . . 138

**10 Summary, conclusion, and outlook** **145**
10.1 Summary and conclusion . . . . . 145
10.2 Outlook . . . . . 149

**A Mechanisms** **151**
A.1 Simplified six species hydrogen combustion . . . . . 151
A.2 Ozone decomposition . . . . . 152
A.3 GRI-Mech 3.0 . . . . . 153

**B Notation** **157**
B.1 General notation . . . . . 157
B.2 Symbols in combustion models . . . . . 158
B.3 Acronyms . . . . . 160

**C External software and hardware** **161**

**D Work flow of the model reduction code** **163**
D.1 First call . . . . . 163
D.2 Warm start . . . . . 166
D.3 Input variables and options . . . . . 168

*Most of mathematical models that really work are simplifications of the basic theoretical models and use in the backgrounds an assumption that some terms are small enough to neglect or almost neglect them.*

Alexander N. Gorban et al. [75]

# 1 Introduction

The aim of model reduction methods is the simplification of mathematical models. Mathematical models are used, e.g. in natural sciences, to describe processes in the language of mathematics. In this way, these processes can be analyzed with the methods of mathematics. Simplified models allow for a faster simulation of the model and eventually allow for more insight into the process under consideration.

## 1.1 Mathematical models and model reduction

Not only natural scientists are modeling or deal with mathematical models, but hardly any definition of a *mathematical model* can be found. A simple but not rigorous definition can be found in the textbook of P. Tannenbaum [156].

**Definition 1.1.1** (Mathematical model [156])
*When a mathematical structure such as a graph is used to describe and study a real world problem we call such a structure a* mathematical model *for the original problem.*

A similar definition is given by E. A. Bender in [20].

**Definition 1.1.2** (Mathematical model [20])
*A* mathematical model *is an abstract, simplified, mathematical construct related to a part of reality and created for a particular purpose.*

Both definitions are very general and leave it to a "user" to decide if a mathematical structure can be considered as a model. On the other hand, these

imprecise definitions make clear, that the term *model reduction* calls for more explanation in the remainder.
The benefit of mathematical modeling itself is discussed in philosophy, see e.g. [85]. In particular, the increasing computational power has amplified the importance of simulations strongly [78].

### Mathematical models in this thesis

The action of deriving a mathematical model is called *mathematical modeling*. The phenomena which are under consideration can be divided into three categories: things whose effects can be neglected, things that effect the model but whose behavior the model is not intended to study, and things the model is supposed to study the behavior of [20].
A lot of data and parameters are given with kinetic mechanisms. A model based on such large mechanisms often includes species, reaction pathways, etc. whose effects can be neglected. Kinetic model reduction methods aim at removing such features to downsize the model. In this work, the models are usually described by ordinary differential equations. The state of the system formulated by the dependent variables of the differential equation undergoes changes which are modeled by means of kinetic mechanisms as the right hand side of these ordinary differential equations.
During the progress of science and mathematical modeling, amplified by the largely increasing computational power in high performance computing, the size of models has increased highly. Especially in combustion research, the size of available models – the number of species and reactions involved – increased in an extraordinary manner. Whereas only small models have been considered in early times, current models include hundreds of species and thousands of reactions. For example, methane combustion mechanisms typically consist of about 30 species and 200 reactions, hexane combustion mechanisms include 450 species and 1500 reactions, and cetane combustion mechanisms include about 1200 species and 7000 reactions [169].
Driven by the need to use regenerative fuels, new compounds have to be considered in the mechanisms. Biofuel is a term used for chemically different substances: alcohols, ethers, esters, and others in dependence of the biomass they are based on [96]. New mechanisms are created for this new type of fuel [80].

### Gain of (reduced) models

As stated before, we mainly deal with models arising in combustion science. These models very often involve many time scales and can be extremely large. When a technical combustion process, e.g. in an engine or in a gas turbine, is modeled, this is usually done in a reactive flow framework. This means, there is not only reaction but also convection and diffusion taking

place in a spatial domain. Therefore, the model is usually formulated as a set of partial differential equations [93, 173].
Such a system of partial differential equations is solved numerically on a fine grid in the spatial domain. Yet limited by modern computer power, there is a discrepancy between the number of species that are needed for a meaningful simulation and the size of the spatial grid.
This is the point where kinetic model reduction methods come into play. Roughly spoken, if it is possible to delete unimportant species and reactions without affecting the dynamics of the simulated species considerably, the system of partial differential equations is reduced by the number of the less important species and reactions. This means, a system of equations for a smaller number of species is supposed to be solved in the spatial domain, and less reaction rates have to be computed. Consequently, much less computational effort is needed.
A common aim of many kinetic model reduction methods is the identification of so-called *slow invariant manifolds* (SIM) [74]. In order to achieve this, a model reduction method is applied only to the (chemical) source term, the term in the system of equations that represents the source of the reaction. This means, we consider a (thermodynamic) system which consists of a homogeneous mixture in the model reduction method. In the phase space, spanned by the state variables, the desired SIM are supposed to exist. Trajectories in the phase space relax onto these SIM of successively lower dimension, before they converge toward equilibrium that can be interpreted as a zero-dimensional manifold. This behavior is related to multiple time scales present in the system, which appear as spectral gaps in the set of eigenvalues of the Jacobian of the kinetic source term. The SIM represent the slow chemistry in the sense of the slow directions tangential to the manifold. The invariance property of the SIM is given by the fact that a trajectory started at a point of a SIM can never leave it; trajectories started in a neighborhood of a SIM are attracted to that SIM.
It is desirable to compute such a SIM locally for a given parametrization and not to compute a representation of a SIM as a whole. The values for a predefined number of species are given for parametrization of the SIM. These represented species are often called *reaction progress variables* as their value is a measure for the state of the system after the "beginning of the reaction" (the start of a simulation) before asymptotically reaching a state of equilibrium. The result of the model reduction method is a mapping from the represented species (the reaction progress variables) to the unrepresented ones. This can be found as *species reconstruction* in literature. Not only the "reconstructed" values of the species in the sense of a local approximation of a point on the SIM are of interest, but also their derivative with respect to the reaction progress variables is needed. These are the tangent vectors of the SIM.
The approximation of points on the SIM can be used in several applica-

tions. As stated before, reaction-diffusion-convection systems are very often simplified. To achieve this, equations for unrepresented species are canceled. Whenever their value is needed e.g. in simulation, the model reduction method is applied for species reconstruction. More sophisticated methods have to be used for the treatment of reaction-diffusion interaction. An approach for using the SIM approximation in reactive flow simulations can be found in [48].
If (spatially) homogeneous systems are modeled, the SIM approximation can directly be used for a numerical integration of the ordinary differential equations that describe the dynamics of the system. Fast time scales are eliminated such that explicit integration methods are utilizable. In this context, the SIM approximation can also be used for solving optimal control problems, see [134].

## 1.2 Results and new contributions

New developments and results in context of a model reduction method published by D. Lebiedz in [101] are presented in this thesis. The method is based on the identification of special trajectories. These trajectories are special as a mathematically formulated criterion for slowness is minimal. The method is refined and applied to example problems in a number of publications [102, 103, 104, 135, 136, 137, 161, 175]. The aim of this thesis is a presentation of numerical methods and considerations for the application of this model reduction method to models of combustion processes.
A computer code is implemented in `C++` for solving the semi-infinite optimization problem, which identifies the SIM approximation. The solution method is based on shooting or collocation approaches. A local (in time) optimization problem for model reduction is presented which can be solved with a generalized Gauss–Newton method. Globalization of convergence of the generalized Gauss–Newton method is achieved with a filter method. Following the recommendation of D. Lebiedz, parameter sensitivities of the optimization problem are analyzed, such that the tangent space of the manifold can be computed. This is done in context of an interior point method and the generalized Gauss–Newton method as solution methods for optimization problems. The sensitivities are used in a predictor corrector scheme for a continuation method to solve families of neighboring optimization problems. In this context, an efficient step size strategy is used based on the contraction of the corrector. The corrector iteration here corresponds to an iteration in the computation of a numerical solution of the optimization problem. Additionally, a proposal for an *a priori* computation of a suitable selection of the reaction progress variables is made. A proof for the existence of a solution of the optimization problem which is valid for the reduction of models describing isothermal combustion is extended to models for adiabatic systems. The

implementation is tested in application to several models that range from simple examples to realistic models of syngas combustion in air.
Parts of the results presented in this thesis are also contents of [105, 106, 107, 108, 147, 148].

## 1.3 Outline of the thesis

The structure of this thesis is as follows. **Part I** deals with theoretical considerations of model equations, their solution, and reduction. Furthermore, theoretical properties of the methods to solve and reduce these model equations are discussed. Afterward, **Part II** contains numerical aspects of an implementation of the model reduction method. Results of an application to different models are presented.
In **Chapter 2**, a short overview of theory for dynamical systems and existing methods for model reduction is given. A focus lies on singularly perturbed systems of ordinary differential equations as sample systems with known time scale separation. The conceptual basis of slow invariant manifolds is presented.
**Chapter 3** deals with the theory of optimization. Optimality conditions are considered as well as a presentation of theory of parametric optimization problems. This is extended by theory of continuation methods to follow the solution of parametric optimization problems.
An application of the model reduction method to models for combustion processes is the aim of this thesis. Therefore, the basic equations for combustion models based on chemical and physical laws are discussed in detail in **Chapter 4**. Obstacles for an application of the optimization based model reduction method to these models are identified. Solutions for the problems are discussed.
The first part merges in **Chapter 5** with a presentation of the model reduction method based on optimization. The presentation includes the most important steps in the development of the method as well as the current state. Different optimization problems are presented that can be solved to compute an approximation of a point on the slow manifold, and the choice of the objective functional is discussed. The existence of a solution of the optimization problems is proven on the condition that the feasible set is nonempty. Ideas for an improvement of the results are shown.
Solution methods for the semi-infinite optimization problem are shown in **Chapter 6**. These are shooting methods with integration schemes based on backward differentiation formulae and collocation methods based on Gauss–Radau quadrature.
Numerical methods to compute a solution of finite nonlinear optimization problems are discussed in **Chapter 7**. For a special form of constrained least squares problems, a generalized Gauss–Newton framework with filter

approach for globalization and iterations for second order correction is presented. In the further course of the chapter, we restrict ourselves to interior point methods.
Path following methods which are suitable to solve neighboring optimization problems efficiently are presented in **Chapter 8**. Special attention is paid to the step size strategy. Numerical strategies are shown that are needed in context of the different optimization methods that serve as corrector method in the predictor corrector scheme.
An implementation in agreement with the methods presented in this thesis is applied to a large number of different models. The results are shown and discussed in **Chapter 9**. The models are simple test models with analytically representable SIM, large test models, and realistic models for the combustion of hydrogen and syngas, respectively, in air.
The thesis is summarized in **Chapter 10**, and an outlook on future research is given.
The **appendix** contains reaction mechanisms for the computations where the results are discussed in Chapter 9, an overview of the notations, flowcharts explaining the `C++` code developed with this work, and a list of external software that is used therein.

### Related publications

The method discussed in this thesis is raised, discussed, extended, and applied in a large number of articles, where the important are [101, 102, 103, 104, 105, 106, 107, 108, 135, 136, 137, 147, 148, 161, 175]. An obsolete version of the implementation developed with this work is used for the numerical results in [161]. In this thesis, content of all articles where the author of this thesis is coauthor (these are [105, 106, 107, 108, 147, 148] as well as our extended abstracts for the second and third International Workshop on Model Reduction in Reacting Flows) may be used without clear citation.

# I Theory and modeling

*And the answer quite generally has the form of a new system (well posed problem) for the solution to satisfy, although it is sometimes obscured because the new system is so easily solved that one is led directly to the solution without noticing the intermediate step.*

Martin David Kruskal

# 2

# Theory of dynamical systems and model reduction methods

In this chapter, an overview of the theory of model reduction methods is given. At first, basic theory of dynamical systems and ordinary differential equations is shortly considered. Subsequently, the purpose of model reduction is clarified. Different methods of model reduction and their theoretical background are shortly explained.

## 2.1 Theory of dynamical systems and ordinary differential equations

We consider dynamical systems that are given in form of a system of ordinary differential equations. The most important definitions and theorems for these are collected in this section.

### 2.1.1 Basic definitions and theorems

A general definition of a dynamical system is the following one taken from [98].

**Definition 2.1.1** (Dynamical system [98])
*A* dynamical system *is a triple* $(T, X, \phi^t)$*, which consists of a* set of time *$T$, a* state space *$X$, and a* family of evolution transformations $\phi^t : X \to X$ *parametrized by $t \in T$ and satisfying*

(i) $\phi^0 = \mathrm{id}$,

(ii) $\phi^{t+s} = \phi^t \circ \phi^s, \quad t, s, t+s \in T.$

The state space is also called *phase space*. In all combustion models considered in this thesis, the state of the system converges to a stable equilibrium.

**Definition 2.1.2** (Fixed point/equilibrium [98])
*A point $z^0 \in X$ is called a* fixed point *or* equilibrium *of the dynamical system $(T, X, \phi^t)$ if*

$$\phi^t z^0 = z^0 \quad \forall t \in T.$$

We only consider dynamical systems that are given as a system of ordinary differential equations (ODE)*.

**Definition 2.1.3** (Ordinary differential equation [155])
*A (system of) differential equation(s) of the form*

$$\mathrm{D}z(t) = S(t, z(t)), \quad z(t) \in \Gamma, \tag{2.1}$$

*where $S : D \to \mathbb{R}^d$, $D = I_T \times \Gamma \subset \mathbb{R} \times \mathbb{R}^d$, $d \in \mathbb{N}$, is at least $\mathcal{C}^1$, is called* (system of) ordinary differential equation(s).

It is convenient to consider autonomous (systems of) ODE only.

**Definition 2.1.4** (Autonomous ordinary differential equation [155])
*A (system) of ordinary differential equations $\mathrm{D}z(t) = S(t, z(t))$ is called* autonomous*, if its right hand side does not explicitly depend on time $t$, i.e. if it is given in the form*

$$\mathrm{D}z(t) = S(z(t)), \quad z(t) \in \Gamma.$$

By adding a dependent variable $z_{d+1} := t$ and the differential equation $\mathrm{D}z_{d+1} = 1$, any system of ODE can be transformed into an autonomous one. The equilibria of an autonomous ODE are exactly the points $z(t)$, where $S(z(t)) = 0$. The state at some time $t$ is given by the continuously differentiable solution of an ODE system through an initial point $(t_0, z_0) \in D$.

**Definition 2.1.5** (Initial value problem (IVP) [155])
*An* initial value problem *is given as an ODE (2.1) together with an initial condition $z(t_0) = z_0 \in \Gamma$ at time $t_0 \in I_T \subset \mathbb{R}$.*

**Definition 2.1.6** (Trajectory [155])
*The continuously differentiable solution $z(t; z_0)$ of the IVP given in Definition 2.1.5 with initial value $z_0$ is called* trajectory *through the point $z_0$ at $t = t_0$.*

The next theorems guarantee a unique solution for IVP.

*For the notation of derivatives, see Section B.1. Note that the operator D for differentiation with respect to time $t$ differs from the later used symbol $D$.

**Theorem 2.1.7** (Peano [133])
*Let $S(t, z)$ be continuous in $\bar{D}$ in both arguments,*

$$\bar{D} = \left\{(t, \bar{z}) \in \mathbb{R} \times \mathbb{R}^d : |t - t_0| \leqslant \alpha, \|\bar{z} - z_0\|_2 \leqslant \beta\right\}.$$

*Then there exists a solution $z(t)$ of the IVP given in Definition 2.1.5 with $\bar{t} := \min(\alpha, \beta/M)$ and $M := \max_{(\bar{z},t)\in\bar{D}} \|S(t, \bar{z})\|_2$ in the (time) interval $I_{\bar{t}} = [t_0 - \bar{t}, t_0 + \bar{t}]$.*

*Proof.* See [133, 155]. □

**Definition 2.1.8** (Lipschitz continuity [133])
*A function $S : D \subset \mathbb{R}^d \to \mathbb{R}^k$, $d, k \in \mathbb{N}$, is called* Lipschitz continuous *if*

$$\|S(y_1) - S(y_2)\|_2 \leqslant L\|y_1 - y_2\|_2, \quad y_1, y_2 \in D,$$

*holds with a so-called* Lipschitz constant $L > 0$. *The function $S$ is called* contraction *if $L < 1$.*

**Theorem 2.1.9** (Picard–Lindelöf [133])
*Let additionally $S(t, \bar{z})$ in Theorem 2.1.7 be Lipschitz continuous with respect to $\bar{z}$, then the solution given by Theorem 2.1.7 is unique.*

*Proof.* See [81, 133, 170]. □

There are various definitions for stability of invariant sets. We use the definition of an invariant set of [174].

**Definition 2.1.10** (Invariant set [174])
*A set $M_0 \subset \mathbb{R}^n$ is called* invariant *under the vector field $\mathrm{D}z(t) = S(t, z(t))$ if for any $z_0 \in M_0$ we have $z(t; z_0) \in M_0$ for all $t \in \mathbb{R}$.*

The set $M_0$ is called *positively invariant set* if this condition is fulfilled for $t > 0$, and it is called *negatively invariant set* if the condition is fulfilled for $t < 0$. Sometimes the notion *invariant set* is used instead of *positively invariant set*.

**Definition 2.1.11** (Lyapunov stability [174])
*A set $M_0 \subset \mathbb{R}^n$ is called* Lyapunov stable *if for all $\epsilon > 0$ there exists a $\delta = \delta(\epsilon) > 0$ such that for all $z(t; z_0)$ with $\|M_0 - z(t_0; z_0)\| < \delta$ it holds that $\|M_0 - z(t; z_0)\| < \epsilon$ for every $t \geqslant 0$.*

In other words, a set $M_0$ is Lyapunov stable if nearby trajectories do not leave the neighborhood of $M_0$[†].

**Definition 2.1.12** ((Asymptotic) Stability [174])
*An invariant set $M_0 \subset \mathbb{R}^n$ is called* stable *if two conditions hold:*

[†]The norm $\|\cdot\|$ may be any norm in $\mathbb{R}^n$ due to norm equivalence.

(i) *For any sufficiently small neighborhood* $U$, $M_0 \subset U$, *there is a neighborhood* $V$, $M_0 \subset V$, *such that* $\phi^t x \in U$ *for all* $x \in V$, $t > 0$, *and*

(ii) *there is a neighborhood* $U_0 \supset M_0$ *such that for all* $x \in U_0$

$$\phi^t x \to M_0 \text{ as } t \to \infty.$$

This means, trajectories starting near the equilibrium set $M_0$ converge to $M_0$. Lyapunov stability is a weaker type of stability than asymptotic stability. In Section 2.1.2, exponentially attracting manifolds are defined, a property that is closely related to stability.

### 2.1.2 Exponentially attracting manifolds

Lyapunov functions for exponentially attracting manifolds are described by L. B. Ryashko and E. E. Shnol. We follow the results of [143] in this section. We consider a smooth[‡] autonomous ODE system. It is formulated as

$$\mathrm{D}z(t) = S(z(t)) \tag{2.2}$$

with $z(t) \in \mathbb{R}^n$ and $S \in \mathcal{C}^\infty(\mathbb{R}^n)$.
Let $M \subset \mathbb{R}^n$ be a compact submanifold in the following, invariant with respect to this system, and $z$ be a solution of the ODE. We define the distance of a point to this manifold $M$ as the standard definition of the distance of a point to a set.

**Definition 2.1.13** (Distance of a point to a manifold [143])
*Let* $M$ *be a smooth, compact submanifold in the Euclidean space* $\mathbb{R}^n$ *and* $\hat{z} \in \mathbb{R}^n$. *The real number*

$$\rho(\hat{z}, M) = \min_{y \in M} \|\hat{z} - y\|$$

*is called* distance of $\hat{z}$ to $M$.

**Notation 2.1.14** (Tangent space and normal space [143])
*Let* $y$ *be a point of* $M$. *We denote the tangent space of* $M$ *at* $y$ *with* $\tilde{T}_y$ *and the corresponding normal space with* $\tilde{N}_y$.

**Definition 2.1.15** (Neighborhood [143])
*A* neighborhood of a manifold $M$ *is the set* $U_\epsilon = \{\hat{z} \in \mathbb{R}^n \mid \rho(\hat{z}, M) < \epsilon\}$ *for a small* $\epsilon > 0$.

[‡]In this work, the notion *smooth* for a function means continuously differentiable. The notion *sufficiently smooth* means that the function is continuously differentiable as often as necessary in the current context.

**Definition 2.1.16** (Exponentially attracting manifold [143])
*A compact manifold $M$ is called* exponentially attracting *if there is a neighborhood $U$ of $M$ and constants $K, \gamma > 0$ such that for all initial values $a \in U$, $z(0) = a$ and $t \geqslant 0$ it holds that*

$$\rho(z(t), M) \leqslant K \exp(-\gamma t)\rho(a, M).$$

**Proposition 2.1.17** ([143])
*Let $U_\epsilon$ be a neighborhood of a smooth, compact submanifold $M \subset \mathbb{R}^n$. If $\epsilon$ is sufficiently small, the following statements are true:*

(i) *For all $\hat{z} \in U_\epsilon$ there exists a unique $y_*(\hat{z}) \in M$, which is nearest, i.e. where $\rho(\hat{z}, M)$ is minimal.*

(ii) *All $\hat{z}$ for which $y_*(\hat{z}) = a$ with $a \in \mathbb{R}^n$ are in $\tilde{N}_a$. The normal spaces $\tilde{N}_a \cap U_\epsilon$ for all $a \in M \cap U_\epsilon$ are disjoint and $\bigcup_{a \in M \cap U_\epsilon} (\tilde{N}_a \cap U_\epsilon) = U_\epsilon$.*

(iii) *The function $\rho^2$ is smooth in $U_\epsilon$.*

*Proof.* See [47]. □

**Definition 2.1.18** ($\rho^2$-function [143])
*A function $g : \mathbb{R}^n \to \mathbb{R}$ is called* $\rho^2$-function*, if there exist positive real constants $c_1$ and $c_2$ with*

$$c_1 \rho^2(z) \leqslant g(z) \leqslant c_2 \rho^2(z).$$

**Proposition 2.1.19** (Lemma 1 in [143])
*Let $M$ be a compact, exponentially attracting manifold of (2.2). There exists a nonnegative function $\Lambda : U_\epsilon \subset \mathbb{R}^n \to \mathbb{R}$ in a neighborhood $U_\epsilon$ of $M$ with the following properties*

(i) $\Lambda(\hat{z}) = 0 \Leftrightarrow \hat{z} \in M$

(ii) $\langle \nabla \Lambda(\hat{z}), S(\hat{z}) \rangle \leqslant 0$

(iii) $\langle \nabla \Lambda(\hat{z}), S(\hat{z}) \rangle < 0 \ \forall \hat{z} \notin M$

(iv) *$\Lambda$ and $-\langle \nabla \Lambda(\hat{z}), S(\hat{z}) \rangle$ are $\rho^2$-functions.*

*Conversely: If a function $\Lambda$ exists with property* (iv)*, then $M$ is exponentially attracting.*

*Proof.* See [143]. □

**Proposition 2.1.20**
*The function*

$$\Lambda(z) := \int_{t_0}^{t_\mathrm{f}} \rho^2(z(t)) \, \mathrm{d}t$$

*fulfills the four conditions in Proposition 2.1.19 with $t_0 = 0$ and $t_\mathrm{f} > 0$ such that $K \exp(-\gamma t_\mathrm{f}) < \frac{1}{2}$.*

*Proof.* See [143]. □

It is clear with Propositions 2.1.19 and 2.1.20 that there exists a function which characterizes points on exponentially attracting manifolds.

## 2.2 Singularly perturbed systems

In context of kinetic model reduction methods, singularly perturbed systems of ODE are often considered. In his series of articles [49, 50, 51, 52], N. Fenichel analyzes the existence of slow manifolds for flows and their stability properties in case of singularly perturbed systems. In the following, the discussion is mainly based on these articles, [74], and [86].

### 2.2.1 Theory of singularly perturbed systems

A singularly perturbed system of ODE is a system of ODE of the form

$$\begin{aligned} \mathrm{d}_t z_\mathrm{f} &= S_1(z_\mathrm{f}, z_\mathrm{s}; \varepsilon) \\ \mathrm{d}_t z_\mathrm{s} &= \varepsilon S_2(z_\mathrm{f}, z_\mathrm{s}; \varepsilon) \end{aligned} \tag{2.3}$$

where $\mathrm{d}_t$ denotes the derivative with respect to $t$. The right hand side consists of the two functions $S_1 : \mathbb{R}^{n_\mathrm{f} \times n_\mathrm{s}} \to \mathbb{R}^{n_\mathrm{f}}$ and $S_2 : \mathbb{R}^{n_\mathrm{f} \times n_\mathrm{s}} \to \mathbb{R}^{n_\mathrm{s}}$ which depend on the variables $z_\mathrm{f}(t) \in \mathbb{R}^{n_\mathrm{f}}$ and $z_\mathrm{s}(t) \in \mathbb{R}^{n_\mathrm{s}}$ and the real parameter $\varepsilon$. It is assumed to be small in the sense that $0 < \varepsilon \ll 1$ and measures the separation of time scales. The functions $S_1$ and $S_2$ are assumed to be smooth and $\mathcal{O}(1)$. The so-called fast variables $z_\mathrm{f}$ change at a rate of $\mathcal{O}(1)$ and the slow variables $z_\mathrm{s}$ at a rate of $\mathcal{O}(\varepsilon)$.
The ODE system can be reformulated as

$$\begin{aligned} \varepsilon \mathrm{d}_\tau z_\mathrm{f} &= S_1(z_\mathrm{f}, z_\mathrm{s}; \varepsilon) \\ \mathrm{d}_\tau z_\mathrm{s} &= S_2(z_\mathrm{f}, z_\mathrm{s}; \varepsilon) \end{aligned} \tag{2.4}$$

by exchanging the independent variable $t$ with the new variable $\tau = \varepsilon t$. The two systems (2.3) and (2.4) are equivalent for $\varepsilon \neq 0$. The independent variable $t$, interpreted as time, is called fast time, and $\tau$ is called slow time. Analogously, system (2.3) is called fast and (2.4) is called slow system.
In the limit $\varepsilon \to 0$, the two systems behave different. System (2.3) converges to

$$\begin{aligned} \mathrm{d}_t z_\mathrm{f} &= S_1(z_\mathrm{f}, z_\mathrm{s}; 0) \\ \mathrm{d}_t z_\mathrm{s} &= 0. \end{aligned} \tag{2.5}$$

This means, only $z_\mathrm{f}$ varies whereas $z_\mathrm{s}$ remains constant. An assumption of that type is made when the quasi steady state assumption is applied, see the

discussion in Section 2.4.1. System (2.4) instead converges for $\varepsilon \to 0$ to the differential algebraic system

$$\begin{aligned} 0 &= S_1(z_\mathrm{f}, z_\mathrm{s}; 0) \\ \mathrm{d}_\tau z_\mathrm{s} &= S_2(z_\mathrm{f}, z_\mathrm{s}; 0) \end{aligned} \tag{2.6}$$

which leads to a varying value of $z_\mathrm{s}(\tau)$ on a manifold defined by all points $(\bar{z}_\mathrm{f}^\mathrm{T}, \bar{z}_\mathrm{s}^\mathrm{T})^\mathrm{T}$ which fulfill $S_1(\bar{z}_\mathrm{f}, \bar{z}_\mathrm{s}; 0) = 0$. A similar assumption is used in the partial equilibrium assumption as explained in Section 2.4.1.
If all eigenvalues of the Jacobian $\mathrm{D}_{z_\mathrm{f}} S_1$ have negative real part, the implicit function theorem guarantees existence of a continuously differentiable function $h^0 : \tilde{K} \to \mathbb{R}^{n_\mathrm{f}}$ on a on open subset $\tilde{K} \subset \mathbb{R}^{n_\mathrm{s}}$, that we further restrict to a compact subset $K \subset \tilde{K}$. The graph of $h^0$ represents the manifold along which all solutions of (2.6) for given initial values $z_\mathrm{s}(t_0)$ evolve via the mapping $h^0(z_\mathrm{s}) = z_\mathrm{f}$. The slow manifold of the slow system (2.6) is defined as the set

$$\mathcal{W}_0 = \{(\bar{z}_\mathrm{f}^\mathrm{T}, \bar{z}_\mathrm{s}^\mathrm{T})^\mathrm{T} : \ S_1(\bar{z}_\mathrm{f}, \bar{z}_\mathrm{s}; 0) = 0\} \subset \mathbb{R}^{n_\mathrm{f}+n_\mathrm{s}}.$$

The dynamics can be described with $\mathcal{W}_0$ by the smaller system

$$\mathrm{d}_\tau z_\mathrm{s} = S_2\left(h^0(z_\mathrm{s}), z_\mathrm{s}; 0\right).$$

In a number of theorems, N. Fenichel studies existence and properties of manifolds $\mathcal{W}_\varepsilon$ for system (2.3) or (2.4), respectively, in case $\varepsilon > 0$.

**Theorem 2.2.1** (Fenichel's invariant manifold theorem 1 [86])
*For $\varepsilon > 0$ sufficiently small, there exists a manifold $\mathcal{W}_\varepsilon$ that lies within $\mathcal{O}(\varepsilon)$ of $\mathcal{W}_0$ and is diffeomorphic to $\mathcal{W}_0$.*

*Proof.* See [49]. □

**Definition 2.2.2** (Locally invariant set [86])
*A set $\mathcal{W}$ is called* locally invariant *under the flow from system (2.3) if it has a neighborhood $\mathcal{V}$ such that no trajectory can leave $\mathcal{W}$ without also leaving $\mathcal{V}$.*

**Theorem 2.2.3** (Existence of a mapping onto $\mathcal{W}_\varepsilon$ [86])
*For $\varepsilon > 0$ sufficiently small, there exists a function $h^\varepsilon(\bar{z}_\mathrm{s}) = \bar{z}_\mathrm{f}$ defined on a compact set $K \subset \mathbb{R}^{n_\mathrm{s}}$ such that the graph*

$$\mathcal{W}_\varepsilon = \{(\bar{z}_\mathrm{f}^\mathrm{T}, \bar{z}_\mathrm{s}^\mathrm{T})^\mathrm{T} : \ h^\varepsilon(\bar{z}_\mathrm{s}) = \bar{z}_\mathrm{f}\}$$

*is locally invariant under the flow from system (2.3).*

*Proof.* See [49]. □

There exists a locally invariant manifold $\mathcal{W}_\varepsilon$ along which the slow dynamics evolve for a finite, but sufficiently small time scale separation.

**Singularly perturbed systems and model reduction** Singularly perturbed systems are special as they are in an explicit fast-slow form. Model reduction approaches can be tested with these systems. The accuracy of the manifold approximation given by the model reduction method in comparison to the analytically representable slow manifold $\mathcal{W}_\varepsilon$ can be determined in powers of $\varepsilon$.

### 2.2.2 Examples of singularly perturbed systems

In many applications of model reduction methods, it is not clear how a small parameter $\varepsilon$ in the model under consideration can be determined and how to transform the system into a singularly perturbed form [74].
An example of a singularly perturbed system in chemical kinetics is given in [74, p. 230]. It is similar to a Michaelis–Menten kinetic system [117]. The small parameter $\varepsilon$ arises in a catalytic reaction. Due to the large difference in the concentrations of educt and catalyst, it is possible to transform the system into a singularly perturbed form.
The model is a catalytic reaction with two steps

$$\mathrm{A} + \mathrm{Z} \overset{k_1^\pm}{\rightleftharpoons} \mathrm{AZ} \overset{k_2^\pm}{\rightleftharpoons} \mathrm{P} + \mathrm{Z},$$

where Z has the function of a catalyst and A is some substrate that reacts to some product P. After using the rules of mass action and formulating an ODE system in concentrations, the following nondimensionalization can be applied: $y_\mathrm{A} = \frac{c_\mathrm{A}}{B_\mathrm{A}}$ and $y_\mathrm{Z} = \frac{c_\mathrm{Z}}{B_\mathrm{Z}}$. Here $B_\mathrm{A}$ is the sum of all $c_\mathrm{A}$, $c_\mathrm{AZ}$, and $c_\mathrm{P}$ in the system. Analogously, $B_\mathrm{Z}$ is the sum of $c_\mathrm{AZ}$ and $c_\mathrm{Z}$.
With the nondimensional mass conservation laws

$$\begin{aligned} y_\mathrm{AZ} &= 1 - y_\mathrm{Z} \\ y_\mathrm{P} &= 1 - y_\mathrm{A} - \frac{B_\mathrm{Z}}{B_\mathrm{A}} y_\mathrm{AZ}, \end{aligned}$$

we arrive at a singularly perturbed system

$$\mathrm{D}y_\mathrm{A} = B_\mathrm{Z}\left(-k_1^+ y_\mathrm{A} y_\mathrm{Z} + \frac{k_1^-}{B_\mathrm{A}} y_\mathrm{AZ}\right) \tag{2.7a}$$

$$\mathrm{D}y_\mathrm{Z} = B_\mathrm{A}\left(-k_1^+ y_\mathrm{A} y_\mathrm{Z} + \frac{k_1^-}{B_\mathrm{A}} y_\mathrm{AZ} + \frac{k_2^+}{B_\mathrm{A}} y_\mathrm{AZ} - k_2^- y_\mathrm{Z} y_\mathrm{P}\right). \tag{2.7b}$$

It holds that $y_i \geqslant 0$, $i = \mathrm{A}, \mathrm{P}, \mathrm{Z}, \mathrm{AZ}$. This is a singularly perturbed system of ODE as the overall amount of catalyst is usually much lower than the amount of educt and product: $B_\mathrm{A} \gg B_\mathrm{Z}$.
In the article [74], no concise parameters are given. We use the following values for the rates

$$k_1^+ = 1.0, \quad k_1^- = 0.01, \quad k_2^+ = 0.01, \quad k_2^- = 10^{-5};$$

for the amounts of substance, we use

$$B_{\mathrm{A}} = 1.0, \quad B_{\mathrm{Z}} = 10^{-6}$$

in the computations, results of which are discussed in Section 9.1.3. There we also compare the results of our model reduction method to an approximation of the graph of the function $h^{\varepsilon}$.

## 2.3 Slow invariant manifolds

Inspired by the theory of singularly perturbed systems and observations of the behavior of trajectories in the phase space of ODE models, many model reduction methods are designed for the identification of slow invariant manifolds.

### 2.3.1 Slow manifolds

It can be observed in the phase space of ODE models of e.g. combustion or biochemical systems that trajectories bundle on hierarchically ordered manifolds of low dimension.
It is assumed that there exists a diffeomorphism between the actual dynamics under consideration and an unknown singularly perturbed system. Additionally, it is assumed that there exists a parameter $\varepsilon$ in the unknown singularly perturbed system that is sufficiently small such that a manifold $\mathcal{W}_{\varepsilon}$ exists. The diffeomorphic manifestation of $\mathcal{W}_{\varepsilon}$ in the observed space are the manifolds of slow motion.
A sketch of the idealistic situation can be seen in Figure 2.1. The phase space of the ODE system as defined in Definition 2.1.1 is also called *(chemical) composition space* and is spanned by the dependent state variables. The state, here also called the chemical composition, is restricted to a physically meaningful domain which is given by the positivity of the values of the state variables[§] and several (elemental mass and/or other) conservation relations. This *effective* or *realizable* phase space or (chemical) composition space is depicted as a polytope whose edges are shown as blue dotted lines in Figure 2.1. Trajectories in the phase space are shown as green dashed curves. It can be observed that these trajectories bundle hierarchically on submanifolds, here shown as first bundling onto a two-dimensional manifold (red bounded) followed by a bundling onto a one-dimensional manifold before they converge to equilibrium.
Along its course through the phase space, the speed of a trajectory slows down (the norm of the right hand side of the ODE system decreases) in correspondence to the slow evolution of the solutions of singularly perturbed

[§]We formulate this as nonnegativity in the mathematical problem.

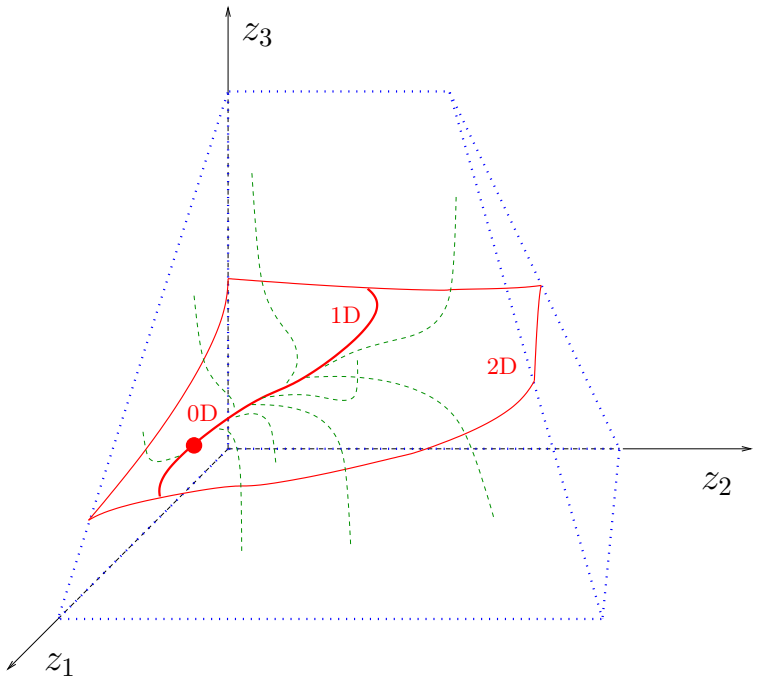


**Figure 2.1:** Sketch of the phase space. The domain which is physically feasible is the interior of the blue-bounded polytope, here three-dimensional. Within this polytope, there is a two-dimensional manifold (bounded red), where trajectories (shown in green) relax onto. The trajectories relax afterward onto the one-dimensional manifold within the two-dimensional one. Finally, the trajectories converge toward the zero-dimensional manifold: the equilibrium.

systems on the slow manifold. These manifolds are invariant sets under the dynamics and attract nearby trajectories. Hence, these manifolds represent the slow reaction part of the model under consideration, and it is desirable to find a constructive representation of such manifolds, which are called slow invariant manifolds (SIM) in literature [149, 162].

Many model reduction approaches allow for the computation of an approximation of a SIM via a species reconstruction. A number of species are selected as slow species $z_\mathrm{s}$. These are called *reaction progress variables* or *represented species*. The species reconstruction method allows for a computation of the fast, *unrepresented* species. This is analogous to the map $h^\varepsilon : K \subset \mathbb{R}^{n_\mathrm{s}} \to \mathbb{R}^{n_\mathrm{f}}$, $\bar{z}_\mathrm{s} \mapsto \bar{z}_\mathrm{f} = h^\varepsilon(\bar{z}_\mathrm{s})$. A sketch of this species reconstruction is shown in Figure 2.2.

For illustration, two variables $z_2$ and $z_1$ are chosen as represented species, and their value is given. Such a choice usually is based on experience and defines the dimension as well as the coordinate system of the desired manifold approximation. The value of the unrepresented species $z_3$ is given by a model

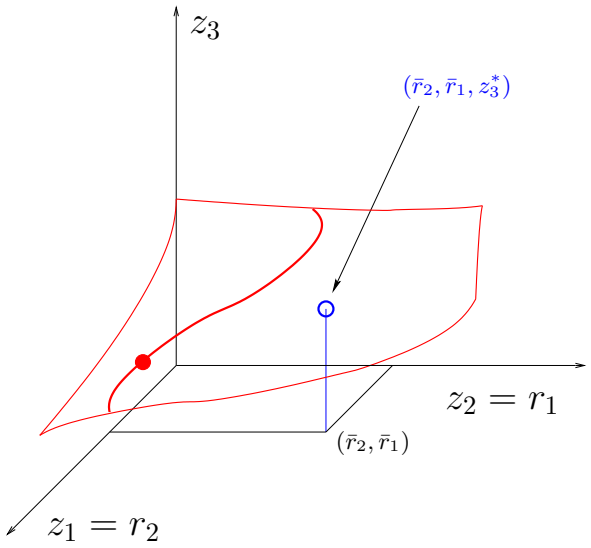


**Figure 2.2:** Sketch of the species reconstruction method. Fixed values $\bar{r}_1$ and $\bar{r}_2$ are given for the represented species $z_2$ and $z_1$, respectively, to approximate a point on the two-dimensional manifold. The value $z_3^*$ of the remaining variable is computed with a model reduction method for species reconstruction.

reduction method with species reconstruction.

### 2.3.2 Tangent space

Together with a SIM approximation, a representation and computation of the tangent space of the SIM is desirable, see Figure 2.3. The tangent vectors are needed for the usage of a reduced reaction model in a reactive flow simulation, e.g. in the close parallel assumption (CPA) of Ren et al. [139, 141].

## 2.4 Methods for model reduction

In this section, an overview of important model reduction methods and methods related to the optimization based method discussed in this thesis is given.

### 2.4.1 Early model reduction methods

Very early model reduction approaches are the quasi steady state assumption (QSSA) and the partial equilibrium assumption (PEA). These methods are performed manually by a user.
In the QSSA method [30, 31, 35], certain species are assumed to be in steady state: The rate of formation and consumption are assumed to equalize.

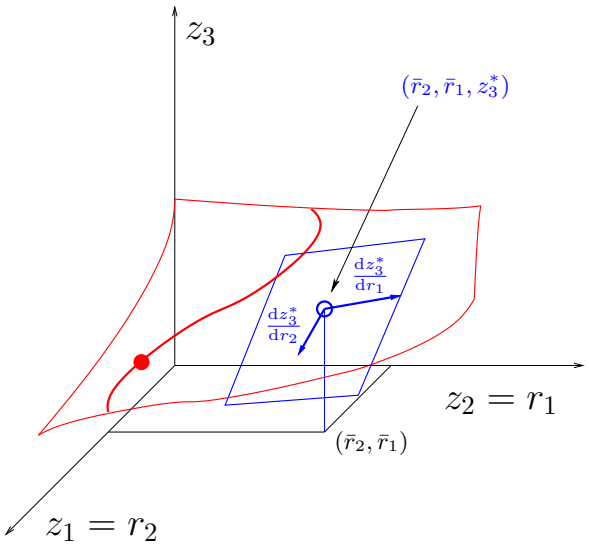


**Figure 2.3:** Sketch of the manifold. In addition to the point on the two-dimensional SIM, the tangent space spanned by the tangent vectors in that point is supposed to be computed.

Therefore, the state variables which represent such species can be considered as constant. The resulting system can be considered as the system in Equation (2.5) from singular perturbation theory. A widely known example of an effective application of this assumption is Michaelis–Menten kinetics [117]. The error of this method is analyzed e.g. in [145, 159].
In contrast, it is assumed in the PEA that a reaction step is in partial equilibrium. The forward and reverse rates of the reaction are assumed to be exactly the same [173]. Consequently, this reaction can be replaced by an algebraic equilibrium equation.
It is shown by D. A. Goussis in his talk [76] that the PEA and the QSSA are limit cases of leading order asymptotic. Furthermore, the QSSA is a limit case of the PEA [76].
It is obvious that detailed expert knowledge of chemical kinetics and the underlying dynamics is needed for the identification of steady state species and balanced reactions. There are also implementations for an automatic application of these methods, see e.g. [123].

### 2.4.2 Automatic model reduction methods

Modern numerical model reduction methods automatically compute a reduced model via a slow manifold, its tangent space, etc. without the need for a detailed expert knowledge by the user.
Many of these modern techniques are explicitly or implicitly based on a time scale analysis of the system under consideration with the purpose to

identify a slow, invariant, and attracting manifold in the phase space. For a comprehensive overview, see e.g. [72, 157] and references therein.

### Model reduction methods based on time scale separation

A very popular method for model reduction is the intrinsic low dimensional manifold (ILDM) method. Another powerful method is the computational singular perturbation (CSP) method, especially because it provides tools for an analysis of the dynamics and the reduced model, e.g. CSP pointers.
Let

$$\mathrm{D}z(t) = S(z(t))$$

again be the ODE system under consideration with $z(t) \in \mathbb{R}^n$ and the smooth function $S : \mathbb{R}^n \to \mathbb{R}^n$.

**ILDM method** U. Maas and S. B. Pope introduce the ILDM method in their article [111] in 1992. It is very popular and widely used in the reactive flows community, e.g. in [5, 120, 150].
A local time scale analysis is performed on the Jacobian $J_S$ of the right hand side $S$ of the ODE system. With a Schur decomposition, an upper block triangular matrix is computed of the form

$$Q^{\mathrm{T}}\, J_S\, Q = T = \begin{bmatrix} T_{11} & T_{12} & \dots & T_{1n} \\ 0 & T_{22} & \dots & T_{2n} \\ \vdots & \vdots & \ddots & \vdots \\ 0 & 0 & \dots & T_{nn} \end{bmatrix} = \begin{bmatrix} T_{\mathrm{fast}} & T_{\mathrm{coup}} \\ 0 & T_{\mathrm{slow}} \end{bmatrix}.$$

Via the Sylvester equation [70], fast and slow submatrices can be fully decoupled [135]

$$T_{\mathrm{r}}^{-1}\, J_S\, T_{\mathrm{r}} = \tilde{T} = \begin{bmatrix} \tilde{T}_{\mathrm{fast}} & 0 \\ 0 & \tilde{T}_{\mathrm{slow}} \end{bmatrix}.$$

Fast time scales are assumed to be fully relaxed. This means

$$\mathrm{D}z = T_{\mathrm{r,fast}}^{-1} S(z) = 0.$$

Together with the parameter equation for the reaction progress variables and additional conservation relations [135], the ILDM equations can be stated as

$$\begin{bmatrix} T_{\mathrm{r,fast}}^{-1} S(z) \\ P(z, c) \end{bmatrix} = 0.$$

A drawback of this method is that a solution of the ILDM equation does not necessarily exist. It is shown that the ILDM method in application to singularly perturbed systems of ODE identifies the SIM to order $\mathcal{O}(\varepsilon)$ [89, 142]. For recent developments and extensions of the ILDM method, see e.g. [34] and references therein.

**CSP method** The CSP method is proposed by S. Lam in 1985 [99, 100]. It is also widely used for model reduction as well as for model analysis as e.g. in the recent publications [121] and [131]. In the two manuscripts [178, 179], the authors reveal that the application of the CSP method improves its approximation of the SIM of singularly perturbed systems of ODE by order one per CSP iteration.
The basic concept of this method is a representation of the dynamical system in a set of basis vectors locally such that fast and slow modes decouple. With a set of basis vectors $\{a_i\}$, $i = 1, \ldots, n$, and (row) covectors $\{b^i\}$ ($b^i\, b_j = \delta_{ij}$ with Kronecker delta $\delta_{ij}$), the right hand side is split into fast and slow components

$$S(z) = S_\mathrm{s}(z) + S_\mathrm{f}(z) = \sum_{i=1}^{m} a_i h^i + \sum_{i=m+1}^{n} a_i h^i,$$

where the vectors $h^k = b_k S$. As a result the system

$$\mathrm{D}z(t) = S_\mathrm{s}(z(t))$$

describes the slow dynamics of the system constrained to the SIM described by

$$S_\mathrm{f}(z) = 0.$$

The crucial point is the appropriate choice of the basis vectors. Consider the matrices $A = (a_i)_{i=1}^n$ and $B = (b^i)_{i=1}^n$. The dynamics $S$ split into the amplitudes $\Omega$ of $S$: $\Omega = BS$ with

$$\Omega = \begin{bmatrix} \Omega_\mathrm{f} \\ \Omega_\mathrm{s} \end{bmatrix},$$

the fast amplitudes $\Omega_\mathrm{f}$, and the slow ones $\Omega_\mathrm{s}$. The amplitudes solve the ODE

$$\mathrm{D}\Omega = B(\mathrm{D}S) + (\mathrm{D}B)S = BJ_S S + (\mathrm{D}B)S = \Pi\Omega$$

with

$$\Pi := BJ_S A + (\mathrm{D}B)A = BJ_S A - B\mathrm{D}A.$$

An ideal basis $A$ leads to a block diagonal $\Pi$ such that $\Omega_\mathrm{f}$ and $\Omega_\mathrm{s}$ decouple. Starting with an initial basis $A^0$, one iterates

$$\Pi^k = B^k J_S A^k - B^k \mathrm{D}A^k = \begin{bmatrix} \Pi_{11}^k & \Pi_{12}^k \\ \Pi_{21}^k & \Pi_{22}^k \end{bmatrix}$$

and updates

$$A^{k+1} = A^k \left( I - \begin{bmatrix} 0 & (\Pi_{11}^k)^{-1}\Pi_{12}^k \\ 0 & 0 \end{bmatrix} \right) \left( I + \begin{bmatrix} 0 & 0 \\ \Pi_{21}^k (\Pi_{11}^k)^{-1} & 0 \end{bmatrix} \right).$$

**Iterative methods** Other iterative methods are based on an evaluation of functional equations that describe the central characteristics of a slow manifold: invariance and stability. Examples are Fraser's algorithm [43, 60, 122] and methods for generation of invariant grids [36, 37, 39, 72, 73].
Another method is proposed in [62] and analyzed in [177]. For identification of the SIM, the equation

$$\mathrm{d}_t^{m+1} z_\mathrm{f} = 0$$

has to be solved – in practice iteratively –, where the vector $z_\mathrm{f}(t)$ consists of the fast species and $\mathrm{d}_t^{m+1}$ is the $(m+1)$st derivative with respect to time $t$. It is shown in [177] that the result approximates the SIM of singularly perturbed systems of ODE up to order $\mathcal{O}(\varepsilon^m)$.

**Other methods** Stretching rates are studied and applied in [2, 3, 4].
The motivation to use stretching rates for model reduction purposes is basically the same as the motivation to use finite time Lyapunov exponents and vectors which are analyzed for evaluation of time scale information in [114, 115].
In [6, 7], the authors connect fixed points via heteroclinic orbits for identification of one-dimensional slow manifolds.
Together with a tabulation method, the invariant constrained equilibrium edge preimage curve (ICE-PIC) method [138, 140] is used in simulations of reactive flows. It is shown that the manifold computed with the ICE-PIC method has the important properties of invariance, smoothness, consistency with physical laws, existence, uniqueness, and local computability.
The ICE-PIC method [138, 140] extends the rate-controlled constrained equilibrium (RCCE) method [92].
Lumping techniques and sensitivity based methods are in use, too. Consider e.g. the overview in [157].
In many applications, as e.g. in [95, 97], flamelet-generated manifolds (FGM) are used [44, 125] which are based on tabulated data of a simulated one-dimensional laminar flame.
The authors of [118] formulate an integer linear programming problem explicitly minimizing the number of species in the reduced model subject to a given error constraint.

*The subject of optimization is a fascinating blend of heuristics and rigor, of theory and experiment.*

Roger Fletcher

# 3 Theory of optimization and continuation

In this work, a model reduction method is discussed which is based on the solution of optimization problems. Therefore, theory of optimization problems is presented in this chapter.

## 3.1 Solution theory of optimization problems

Nonlinear optimization problems with both equality and inequality constraints occur in the problems considered in this thesis. These can be subdivided into semi-infinite and finite ones.

### 3.1.1 Semi-infinite optimization problems

In our case, the dynamics are given as a system of ODE and enter the optimization problem as constraints. Therefore, we only consider a special type of semi-infinite optimization problems. In the following, the notation is partially taken from [144] and adapted to our situation. The general semi-infinite optimization problem (sufficient for our purposes) is given in the form

$$\min_z \Psi(z) \tag{3.1a}$$

subject to

$$\mathrm{D}z(t) = S(z(t)) \tag{3.1b}$$
$$C(z(t)) \geqslant 0 \tag{3.1c}$$
$$r(z(t_*)) = 0 \tag{3.1d}$$

with time $t \in [t_0, t_\mathrm{f}] \subset \mathbb{R}$ and a point fixed in time $t_* \in [t_0, t_\mathrm{f}]$. The state variables $z : [t_0, t_\mathrm{f}] \to \mathbb{R}^{n_z}$ are solutions (see Definition 2.1.6) of the dynamics in (3.1b). The right hand side $S : D \to \mathbb{R}^{n_z}$, $D \subset \mathbb{R}^{n_z}$ open, is assumed to be at least piecewise Lipschitz. The objective function is given in Bolza form

$$\Psi(z) := \int_{t_0}^{t_\mathrm{f}} L(z(t))\,\mathrm{d}t + M(z(t_\mathrm{f})).$$

The Bolza objective functional is the sum of the Lagrange term $\int_{t_0}^{t_\mathrm{f}} L(z(t))\mathrm{d}t$ and the Mayer term $M(z(t_\mathrm{f}))$. The functions $L$, $M$, $C$, and $r$ are assumed to be at least $\mathcal{C}^2$. Additional parameters are introduced in Section 3.2.
Under these assumptions the solution trajectory $z$ of the dynamics (3.1b) through a given point $z(t_*)$ depends continuously on the data $z(t_*)$. An application of a suitable discretization method to the semi-infinite optimization problem (3.1) or an integration method to solve (3.1b) yields a finite optimization problem, see also Chapter 6.

### 3.1.2 Nonlinear programming problems

In this section, the theory of finite optimization problems is considered as presented in standard literature, as e.g. [124]. The standard (finite) nonlinear programming (NLP) problem for our considerations is given in the form

$$\min_{x \in \mathbb{R}^n} f(x) \tag{3.2a}$$

subject to

$$g(x) = 0 \tag{3.2b}$$

$$h(x) \geqslant 0 \tag{3.2c}$$

with the objective function $f : D \subset \mathbb{R}^n \to \mathbb{R}$, the equality constraints $g : D \subset \mathbb{R}^n \to \mathbb{R}^{n_2}$, and the inequality constraints $h : D \subset \mathbb{R}^n \to \mathbb{R}^{n_3}$. The three functions $f$, $g$, and $h$ are assumed to be sufficiently smooth, which in this section means at least $\mathcal{C}^2(D)$. We need the notions of the following definition in the remainder of this chapter.

**Definition 3.1.1** (Basic notions)

(i) *The set* $\Omega := \{x \in \mathbb{R}^n \mid g(x) = 0,\ h(x) \geqslant 0\}$ *is called* feasible set *and any element* $\bar{x} \in \Omega$ *is called* feasible point.

(ii) *A feasible point* $\bar{x}$ *is called* local solution *or* local minimizer *of the NLP problem (3.2) if there is a neighborhood* $U(\bar{x})$ *of* $\bar{x}$ *such that* $f(\bar{x}) \leqslant f(x)$ *for all* $x \in U(\bar{x}) \cap \Omega$.

(iii) *A feasible point* $\bar{x}$ *is called* strict local solution *or* strict local minimizer *of the NLP problem (3.2) if there is a neighborhood* $U(\bar{x})$ *of* $\bar{x}$ *such that* $f(\bar{x}) < f(x)$ *for all* $x \in U(\bar{x}) \cap \Omega$, $x \neq \bar{x}$.

It has to be known for the characterization of a feasible point $x$ as a potential local solution if $x$ is at the boundary of the feasible set, and if so, which inequality constraints are fulfilled exactly, i.e. $h_i(x) = 0$.

**Definition 3.1.2** (Active set)
*The* active set *(AS) at any feasible point $x$ of (3.2) is the set of the indices of the inequality constraints, for which $h_i(x) = 0$ holds:*

$$\mathcal{A}(x) = \{i \mid h_i(x) = 0,\ i = 1, \ldots, n_3\}.$$

*The inequality constraint $i$ is called* active (in $x$) *if $i \in \mathcal{A}(x)$; otherwise it is called* inactive (in $x$).

**Definition 3.1.3** (Linear independence constraint qualification)
*A feasible point $x$ of (3.2) with active set $\mathcal{A}(x)$ is said to fulfill the linear independence constraint qualification (LICQ) if the set of equality constraint gradients and active inequality constraint gradients*

$$\{\nabla g_i(x),\ i = 1, \ldots, n_2\} \cup \{\nabla h_i(x),\ i \in \mathcal{A}(x)\} \tag{3.3}$$

*is linearly independent.*

**Definition 3.1.4** (Lagrangian function)
*The* Lagrangian function $\mathcal{L}$ *for the general NLP problem (3.2) is defined as*

$$\begin{aligned} \mathcal{L} : \mathbb{R}^n \times \mathbb{R}^{n_2} \times \mathbb{R}^{n_3} &\to \mathbb{R} \\ (x, \lambda, \mu) &\mapsto \mathcal{L}(x, \lambda, \mu) := f(x) - \lambda^{\mathrm{T}} g(x) - \mu^{\mathrm{T}} h(x), \end{aligned}$$

*where $\lambda \in \mathbb{R}^{n_2}$ and $\mu \in \mathbb{R}^{n_3}$ are the* Lagrange multipliers.

First order necessary conditions for optimality can be stated with these preparations.

**Theorem 3.1.5** (Karush–Kuhn–Tucker conditions)
*Let $x^*$ be a local minimizer of (3.2), $f$, $g$, and $h$ continuously differentiable, and $x^*$ fulfill LICQ. Then there exist Lagrange multipliers $\lambda^* \in \mathbb{R}^{n_2}$ and $\mu^* \in \mathbb{R}^{n_3}$ such that the triple $(x^*, \lambda^*, \mu^*)$ satisfies the following Karush–Kuhn–Tucker (KKT) conditions*

$$\nabla_x \mathcal{L}(x^*, \lambda^*, \mu^*) = 0 \tag{3.4a}$$
$$g(x^*) = 0 \tag{3.4b}$$
$$h(x^*) \geqslant 0 \tag{3.4c}$$
$$\mu^* \geqslant 0 \tag{3.4d}$$
$$\mu_j^*\, h_j(x^*) = 0 \quad \forall j = 1, \ldots, n_3. \tag{3.4e}$$

*Proof.* See e.g. [56, 124]. □

**Definition 3.1.6** (KKT point)
*A point* $(x^*, \lambda^*, \mu^*)$ *which satisfies all conditions (3.4) is called* KKT point.

Second order necessary and sufficient conditions can be formulated with the critical cone.

**Definition 3.1.7** (Linearized feasible directions)
*For a feasible point* $x$ *of (3.2) and its corresponding active set* $\mathcal{A}(x)$*, the set of* linearized feasible directions *is defined as*

$$\mathcal{F}(x) := \{d \in \mathbb{R}^n \mid d^{\mathrm{T}} \nabla g_i(x) = 0,\ i = 1, \ldots, n_2;\ d^{\mathrm{T}} \nabla h_j(x) \geqslant 0,\ j \in \mathcal{A}(x)\}.$$

The critical cone is a subset of all feasible directions, namely:

**Definition 3.1.8** (Critical cone)
*For a KKT point* $(x^*, \lambda^*, \mu^*)$ *with linearized feasible directions* $\mathcal{F}(x^*)$*, the* critical cone *is defined as*

$$\mathcal{C}(x^*, \lambda^*, \mu^*) := \{d \in \mathcal{F}(x^*) \mid d^{\mathrm{T}} \nabla h_i(x) \geqslant 0\ \forall i \in \mathcal{A}(x)\ \textit{with}\ \mu_i^* > 0\}.$$

**Theorem 3.1.9** (Second-order necessary conditions)
*Let* $x^*$ *be a local minimizer of (3.2),* $f$*,* $g$*, and* $h$ *twice continuously differentiable, and* $x^*$ *fulfill LICQ. Let* $\lambda^*$ *and* $\mu^*$ *be the Lagrange multipliers for which the KKT conditions are satisfied. Then it holds*

$$v^{\mathrm{T}}\ \nabla_{xx}^2 \mathcal{L}(x^*, \lambda^*, \mu^*)\ v \geqslant 0 \quad \forall v \in \mathcal{C}(x^*, \lambda^*, \mu^*).$$

*Proof.* See e.g. [56, 124]. □

**Theorem 3.1.10** (Second-order sufficient conditions (SSC))
*Let* $x^*$ *be a feasible point of (3.2) for which the KKT conditions are satisfied with Lagrange multipliers* $(\lambda^*, \mu^*)$*. Suppose further that*

$$v^{\mathrm{T}} \nabla_{xx}^2 \mathcal{L}(x^*, \lambda^*, \mu^*) v > 0 \quad \forall v \in \mathcal{C}(x^*, \lambda^*, \mu^*),\ v \neq 0.$$

*Then* $x^*$ *is a strict local minimizer for (3.2).*

*Proof.* See e.g. [56, 124]. □

## 3.2 Parametric optimization

In the optimization problem for model reduction purposes which is presented in Chapter 5, there is a parameter dependence in the equality constraints. Therefore, we consider parametric NLP problems in the following. The basic problem is given as

$$\min_{x \in \mathbb{R}^n} f(x, r) \tag{3.5a}$$

subject to

$$g(x, r) = 0 \tag{3.5b}$$
$$h(x, r) \geqslant 0, \tag{3.5c}$$

where the objective function $f : D \times \tilde{D} \to \mathbb{R}$, the equality constraint function $g : D \times \tilde{D} \to \mathbb{R}^{n_2}$, and the inequality constraint function $h : D \times \tilde{D} \to \mathbb{R}^{n_3}$ depend on the parameter vector $r \in \tilde{D}$ with $D \subset \mathbb{R}^n$, $\tilde{D} \subset \mathbb{R}^{n_r}$ open.
The Lagrangian function can be written as

$$\mathcal{L}(x, \lambda, \mu, r) := f(x, r) - \lambda^{\mathrm{T}} g(x, r) - \mu^{\mathrm{T}} h(x, r).$$

First order sensitivity results are given by the following theorem of Fiacco [55]. These results are used in context of real-time optimization, see e.g. [33], and nonlinear model predictive control, e.g. in [53, 180].

**Theorem 3.2.1** (Parameter sensitivity [55])
*Let the functions $f$, $g$, and $h$ in problem (3.5) be twice continuously differentiable in a neighborhood of $(x^*, 0)$. Let the second order sufficient conditions hold for a local minimum of (3.5) at $x^*$ with $r = 0$ and Lagrange multipliers $\lambda^*$, $\mu^*$. Furthermore, let LICQ be valid in $(x^*, 0)$ and strict complementary slackness, i.e. $\mu_i^* > 0$ if $h_i(x^*, 0) = 0$, $i = 1, \ldots, n_3$. Then the following holds:*

(i) *The point $x^*$ is a local isolated minimizer of (3.5) with $r = 0$, and the associated Lagrange multipliers $\lambda^*$, $\mu^*$ are unique.*

(ii) *For $r$ in a neighborhood of $0$, there exists a unique once continuously differentiable function $(x(r), \lambda(r), \mu(r))$ satisfying the second order sufficient conditions for a local minimum of (3.5) such that*

$$(x(0), \lambda(0), \mu(0)) = (x^*, \lambda^*, \mu^*),$$

*and $x(r)$ is a local minimizer of (3.5) with Lagrange multipliers $\lambda(r)$ and $\mu(r)$.*

(iii) *Strict complementarity with respect to $\mu(r)$ and LICQ hold at $x(r)$ for $r$ near $0$.*

*Proof.* See [55]. □

For different fixed values of the parameter $\bar{r}$, a family of parametric optimization problems (3.5) is supposed to be solved for the results presented in Chapter 9. The aim of numerical algorithms is the computation of a root of a function $K$ which (basically – see also Section 8.1.1) represents the KKT conditions

$$K(x, \lambda, \mu, \bar{r}) = 0$$

in order to solve (3.5) with parameter $\bar{r}$.
We are interested in the derivative of a solution $(x^*, \lambda^*, \mu^*)$ of the optimization problem (3.5) with respect to the parameter. The implicit function theorem yields for $(x^*(r), \lambda^*(r), \mu^*(r))$

$$\mathrm{D}_{(x,\lambda,\mu)}K \; \mathrm{D}_r(x^*, \lambda^*, \mu^*) = -\mathrm{D}_r K.$$

This can be rewritten in a matrix equation form as

$$\begin{bmatrix} \mathrm{D}_x K & \mathrm{D}_\lambda K & \mathrm{D}_\mu K \end{bmatrix} \begin{bmatrix} \mathrm{D}_r x^* \\ \mathrm{D}_r \lambda^* \\ \mathrm{D}_r \mu^* \end{bmatrix} = -\mathrm{D}_r K. \tag{3.6}$$

The matrix

$$\begin{bmatrix} \mathrm{D}_x K & \mathrm{D}_\lambda K & \mathrm{D}_\mu K \end{bmatrix}$$

is called KKT matrix. It is nonsingular if LICQ and second order sufficient optimality conditions as stated in Theorem 3.1.10 are fulfilled.
The usage of the sensitivities $\mathrm{D}_r(x^*, \lambda^*, \mu^*)$ within a continuation method is explained in Chapter 8.

## 3.3 Continuation method

In this section, we deal with the theory of continuation methods, also called homotopy methods or embedding methods. Homotopy methods are in use since the work of Poincaré. We mainly follow the presentation in [9] in context of optimization methods.
The aim of homotopy methods often is to trace the zero of a function while a parameter varies. In our context, KKT points are followed in dependence of parameters which are the reaction progress variables. Not only a single point as approximation of a point on the SIM needs to be computed in application of a model reduction method but a number of neighboring points. This can be done efficiently with a continuation method. For a family of optimization problems, a solution of a previously solved problem can be used as initial value for the next problem to be solved.
Consider a sufficiently smooth mapping $F : \mathbb{R}^{\tilde{n}} \to \mathbb{R}^{\tilde{n}}$. A zero of this function $F$ can be computed with a Newton-like method, e.g. The contraction of Newton's method depends on the initial guess, which might be very poor.
The goal of continuation methods usually is to define a deformation, the homotopy $H : \mathbb{R}^{\tilde{n}} \times \mathbb{R} \to \mathbb{R}^{\tilde{n}}$ with $H(x, 0) = F(x)$ and $H(x, 1) = G(x)$, where $G : \mathbb{R}^{\tilde{n}} \to \mathbb{R}^{\tilde{n}}$ is a sufficiently smooth function with known zeros at $x_1 \in \mathbb{R}^{\tilde{n}}$, e.g. of a previously solved problem. The strategy is to trace an implicitly defined curve $c$ from a starting point $(x_1, 1)$ to the desired solution $(\bar{x}, 0)$. Some preconditions have to be fulfilled to guarantee for the existence of such a curve.

**Assumption 3.3.1** (Assumptions 2.1.1 and 2.1.2 in [9])

(i) *Let* $H : \mathbb{R}^{\tilde{n}} \times \mathbb{R} \to \mathbb{R}^{\tilde{n}}$, $(x,t) \mapsto H(x,t)$ *be a sufficiently smooth map.*

(ii) *There exists a* $u_0 \in \mathbb{R}^{\tilde{n}+1}$ *such that*

- $H(u_0) = 0$
- *the Jacobian* $\mathrm{D}_x H(u_0)$ *has maximum rank* $\tilde{n}$.

In this case, the implicit function theorem allows for a local parametrization of the solution curve of $H^{-1}(0)$.

**Lemma 3.3.2** (Lemma 2.1.3 in [9])
*Under Assumption 3.3.1, there exists a smooth curve* $c : J \to \mathbb{R}^{\tilde{n}+1}$ *with* $\alpha \mapsto c(\alpha)$ *for an open interval* $J \subset \mathbb{R}$, $0 \in J$ *such that*[*]

(i) $c(0) = u_0$

(ii) $H(c(\alpha)) = 0$

(iii) $\operatorname{rank}(\mathrm{d}_y H(c(\alpha))) = \tilde{n}$

(iv) $\mathrm{d}_\alpha c(\alpha) \neq 0$.

*Proof.* See [9]. □

It follows that $\mathrm{d}_y H(c(\alpha))\mathrm{d}_\alpha c(\alpha) = 0$, i.e. the tangent $\mathrm{d}_\alpha c(\alpha)$ spans the kernel of $\mathrm{d}_y H(c(\alpha))$. For theoretical purposes, it is helpful to parametrize the curve with respect to arc length parameter $s$. That means,

$$\|\mathrm{d}_s c(s)\|_2 = 1, \quad s \in \bar{J}$$

with a new interval $\bar{J}$. This is achieved by setting

$$\mathrm{d}s = \|\mathrm{d}_\alpha c(\alpha)\|_2 \, \mathrm{d}\alpha.$$

To define a direction in the kernel of the matrix $\mathrm{d}_y H(c(s))$, the augmented Jacobian is defined as

$$\begin{pmatrix} \mathrm{d}_y H(c(s)) \\ \mathrm{d}_s c(s)^{\mathrm{T}} \end{pmatrix},$$

which has full rank $\tilde{n}+1$ as a direct consequence of Assumption 3.3.1 and Lemma 3.3.2. So we can define the orientation of the curve as positive if the determinant of the augmented Jacobian is positive and negative otherwise. Application of the implicit function theorem to $H(x(t),t) = 0$ under Assumption 3.3.1 leads to

$$\mathrm{D}x = -\mathrm{D}_x H(x,t)^{-1} \mathrm{D}_t H(x,t),$$

the *Davidenko differential equation* [42, 61]. The main theoretical result in [9, Chapter 2] is the following theorem.

[*]The expression $\mathrm{d}_y H(y)$ is the derivative of $H$ with respect to the variable $y \in \mathbb{R}^{\tilde{n}+1}$.

**Theorem 3.3.3** (Theorem 2.1.14 in [9])
*Let zero be a regular value of $H$ (i.e. $\mathrm{d}_y H(0)$ has maximum rank). Then the curve $c$ is defined on all of $\mathbb{R}$ and satisfies one of the following conditions:*

- *The curve $c$ is diffeomorphic to a circle.*
- *The curve $c$ is diffeomorphic to the real line.*

*Proof.* See [9]. □

In case of the optimization based model reduction method, the KKT conditions play the role of the function $H$. The function $H$ is regular if and only if the KKT matrix is nonsingular which is the case if LICQ and second order sufficient optimality conditions as stated in Theorem 3.1.10 are fulfilled.

*In der Flamme eines Lichts sind alle Naturkräfte thätig (...)*

Novalis

# 4 Models for combustion chemistry

In this chapter, equations to describe the chemical reactions of combustion processes are discussed. It concludes with formulae for the description of a combustion process via an ODE model and conservation relations in the sense of algebraic equations. Results of a reduction of such models with the optimization based model reduction approach described in Chapter 5 are shown in Chapter 9.
We mainly follow the detailed discussion in [173] and [93] with a collection of aspects important for this thesis. Lists of symbols used in this chapter are given in Appendix B.

## 4.1 Basic variables and equations

In the following, important quantities and relations between them are subsumed.

### 4.1.1 State variables

We consider a (spatially) homogeneous system. The state of this system can be described in amount of substance of the $n_{\text{spec}}$ species with symbol $n_s$, $s = 1, \ldots, n_{\text{spec}}$ in mole (mol) together with the temperature of the system $T$ in Kelvin (K).

**Notation 4.1.1**
*The index $s$ iterates through the species in the following. We assume bijections between the natural numbers $1, \ldots, n_{\text{spec}}$ and the names of the species,*

*as well as between* $1, \ldots, n_{\text{elem}}$ *and the names of the chemical elements, and another bijection between* $1, \ldots, n_{\text{tb}}$ *and the names* $\mathrm{M}_i$, $i = 1, \ldots, n_{\text{tb}}$ *of the third body collision partners. Hence, numbers and names are used interchangeable, e.g. if* $\mathrm{H}_2$ *has number* 5*, we might use for the amount of substance of* $\mathrm{H}_2$ *both the symbol* $n_{\mathrm{H}_2}$ *or equivalently* $n_5$*. If indices as* $\mathrm{H}_2$ *occur in a formula, e.g. in a sum, they should be understood as the dedicated one.*

The state of the system can also be represented in other variables. In general, the choice depends on the assumed thermodynamic environment. We consider systems within one of the four classical standard thermodynamic environments [74], i.e.

- isothermal and isochoric
- isothermal and isobaric
- adiabatic and isochoric (hence isoenergetic)
- adiabatic and isobaric (hence isenthalpic)

systems.
The species in the system can be described in amount of substance $n_s$, such that the overall amount of substance is $n = \sum_{s=1}^{n_{\text{spec}}} n_s$. One might also use the mass of the species $m_s = M_s n_s$ with the molar mass $M_s$ of species $s$. The molar mass of species $s$ can be computed by the molar mass of the chemical elements $\bar{M}_i$, $i = 1, \ldots, n_{\text{elem}}$, and the atomic composition coefficient $\chi_{i,s}$ with the sum $M_s = \sum_{i=1}^{n_{\text{elem}}} \chi_{i,s} \bar{M}_i$. The coefficient $\chi_{i,s}$ is the number of element $i$ in species $s$. The total mass of the system is $m = \sum_{s=1}^{n_{\text{spec}}} m_s$. Another possibility for describing the state of our system are mole fractions $x_s = \frac{n_s}{n}$ and mass fractions $w_s = \frac{m_s}{m}$. Similarly, the mass densities of the species $\rho_s = \frac{m_s}{V}$ can be used, such that the identity $\rho V = m$ holds for the total mass density $\rho = \sum_{s=1}^{n_{\text{spec}}} \rho_s$. The inverse mass densities of the species $v_s = \rho_s^{-1}$ are the specific volumes of the species. The partial pressure $p_s = p x_s$ can also be used to describe the system. Concentrations $c_s = \frac{n_s}{V}$ are typical variables used to describe chemical processes because mass action kinetics are formulated in terms of concentration. With the total concentration $c = \sum_{s=1}^{n_{\text{spec}}} c_s$, the important formula $c = \frac{n}{V}$ is valid.
In the following, we prefer the representation of the state of the system in specific moles

$$z_s = \frac{n_s}{m} = \frac{w_s}{M_s}, \quad s = 1, \ldots, n_{\text{spec}}$$

in $\mathrm{mol\,kg^{-1}}$, because it simplifies the evaluation of the ODE model and allows for a fast computation of the other variables if the values of the conserved quantities are known, e.g. the concentrations can be computed via

$$c_s = \frac{n_s}{V} = z_s \, \rho, \quad s = 1, \ldots, n_{\text{spec}}.$$

Another important quantity is the mean molar mass

$$\bar{M} = \sum_{s=1}^{n_{\text{spec}}} x_s M_s = \frac{m}{n} = \frac{\rho}{c} = \left( \sum_{s=1}^{n_{\text{spec}}} z_s \right)^{-1}. \tag{4.1}$$

The conversions

$$w_j = \frac{M_j n_j}{\sum_{s=1}^{n_{\text{spec}}} M_s n_s} = \frac{M_j x_j}{\sum_{s=1}^{n_{\text{spec}}} M_s x_s}$$
$$x_j = \bar{M} \frac{w_j}{M_j} = \bar{M} z_j = \frac{w_j}{M_j \sum_{s=1}^{n_{\text{spec}}} \frac{w_s}{M_s}}$$

for $j = 1, \ldots, n_{\text{spec}}$ are often used.
The ideal gas law is assumed to be valid in our models. It connects the important macroscopic variables pressure $p$, volume $V$, amount of substance $n$, and temperature $T$ via

$$pV = nRT$$

with the gas constant $R = 8.314\,471\,\mathrm{J\,mol^{-1}\,K^{-1}}$. For its value, see the latest published version of CODATA recommended values 2006 [119]. New experiments have lead to the more recent CODATA 2010 recommendation $R = 8.314\,462\,1\,\mathrm{J\,mol^{-1}\,K^{-1}}$. As the combustion mechanisms used in the following are created with the old recommendation, we use CODATA 2006 values in this work.
The ideal gas law leads to a relation between mass density $\rho$ and pressure $p$

$$p\bar{M} = \rho RT, \tag{4.2}$$

which can be verified with the identity $\rho V = m$ and Equation (4.1).

### 4.1.2 Thermodynamic variables

In the following, we need the definition of thermodynamic quantities. These are introduced in this section with the three fundamental laws of thermodynamics. We consider *open* systems which exchange energy and matter with their surroundings, *closed* systems which only exchange energy with their surroundings, and *isolated* (adiabatic) systems which exchange neither energy nor matter with their surroundings.
The first law of thermodynamics states that the sum of all energies is constant in an isolated system [173].
This means, a change $\mathrm{d}E$ in the internal energy $E$ of a system can be written as the sum of the heat $\delta Q$ transferred and the work $\delta W$ done to the system

$$\mathrm{d}E = \delta Q + \delta W.$$

In the cases considered in this thesis, only compression work $-p\mathrm{d}V$ occurs such that the first law of thermodynamics for an isolated system can be written as

$$\mathrm{d}E + p\mathrm{d}V = 0. \tag{4.3}$$

The first law of thermodynamics can be written for closed isochoric systems as

$$\mathrm{d}E = \delta Q.$$

The enthalpy $H$ is used for isobaric systems to describe the state of the system. It is defined as

$$H = E + pV,$$

and this yields in differential form

$$\mathrm{d}H = \mathrm{d}E + \mathrm{d}(pV) = \mathrm{d}E + p\mathrm{d}V + V\mathrm{d}p.$$

We get

$$\mathrm{d}H - p\mathrm{d}V - V\mathrm{d}p + p\mathrm{d}V = \mathrm{d}H - V\mathrm{d}p = 0 \tag{4.4}$$

with law (4.3).
In the models considered later, the heat capacity $C$ is used. It describes the amount of heat $\delta Q$ that is needed to change the temperature of a system by a certain amount: $C\mathrm{d}T = \delta Q$. This depends on the thermodynamic environment of the system, because the added heat can eventually be used for compression (or expansion) work. With the first law of thermodynamics, it is clear that for constant volume and pressure, respectively,

$$\mathrm{d}U = \delta Q = C_V \mathrm{d}T$$
$$\mathrm{d}H = \delta Q = C_p \mathrm{d}T$$

are valid.
The entropy $S$ is defined (in thermodynamics) via the relation

$$\mathrm{d}S = \frac{\delta Q_\mathrm{r}}{T},$$

i.e. the change in entropy is the heat absorbed in a process, which is carried out reversibly, divided by the equilibrium temperature. Therefore, it holds in an isolated system for the reversible and irreversible change in entropy that

$$\mathrm{d}_\mathrm{r}S = 0$$
$$\mathrm{d}_\mathrm{i}S > 0.$$

This can be seen as the second law of thermodynamics. The third law of thermodynamics states that the entropy for a perfect crystal of a pure substance at a temperature $T = 0\,\mathrm{K}$ is zero

$$\lim_{T \to 0} S = 0.$$

**Notation 4.1.2**
*In the following, thermodynamic variables with a bar are molar values, e.g.*

$$\bar{H} = \frac{H}{n},$$

*and lowercase thermodynamic variables are specific values, e.g.*

$$h = \frac{H}{m}.$$

### 4.1.3 Equilibrium constant and Gibbs free energy

The Gibbs free energy is defined as

$$G := H - TS,$$

with enthalpy $H$, entropy $S$, and temperature $T$. In an isothermal process, the change of the Gibbs free energy

$$\Delta G = \Delta H - T\Delta S$$

can be calculated from the sum of the free energies of all product species minus the sum of the free energies of all educt species in the chemical reaction. The changes $\Delta H$ and $\Delta S$ can be computed analogously.
The Gibbs free energy change of formation of a species at temperature $T$ in its standard form from its elements in their standard form at $T$ is called $\Delta G_\mathrm{f}^\circ$. The standard state for a gaseous species is a pressure of $p^\circ := 10^5\,\mathrm{Pa}$. Important equations are the pressure dependence of $G$

$$\frac{\partial G}{\partial p}\Big|_T = V$$

and the temperature dependence of $G$ – the Gibbs–Helmholtz equation –

$$\frac{\partial \frac{G}{T}}{\partial T}\Big|_p = -\frac{H}{T^2}.$$

The equilibrium constant of a chemical reaction in terms of pressure values and the standard Gibbs free energy of the reaction are connected via the relation

$$\Delta G_\mathrm{r}^\circ = -RT \ln K_p. \tag{4.5}$$

The definition of the equilibrium constant in terms of partial pressures can be found in Section 4.3.1. The dependence of $K_p$ on the temperature is given via the famous van't Hoff equation

$$\frac{\mathrm{d} \ln K_p}{\mathrm{d}T} = \frac{\Delta H_\mathrm{r}^\circ}{RT^2}$$

with the standard enthalpy of the reaction $\Delta H_\mathrm{r}^\circ$.

## 4.2 Conservation laws

The basis of all models considered here are physical conservation laws. The models comprise $n_{\text{spec}}$ chemical species composed by $n_{\text{elem}}$ chemical elements. The chemical source term obeys the law of elemental mass conservation, which is considered in Section 4.2.1, and an energetic balance, which is presented in Section 4.2.2.

### 4.2.1 Mass conservation

The conservation of the total mass of each chemical element in the system is formulated in specific moles as

$$\check{z}_i = \sum_{s=1}^{n_{\text{spec}}} \chi_{i,s} z_s, \quad i = 1, \ldots, n_{\text{elem}}, \tag{4.6}$$

where $\chi_{i,s}$ is the atomic composition coefficient. There is also a restriction on the values of the constant elemental specific moles $\check{z}_i$ which requires that the mass fractions sum to one

$$\sum_{i=1}^{n_{\text{elem}}} \bar{M}_i \check{z}_i = 1, \tag{4.7}$$

where $\bar{M}_i$ is the molar mass of element $i$. This is equivalent to the conservation of the total mass of the system.

### 4.2.2 Energy balance

The energy balance has to be considered additionally. As stated in Section 4.1.1, we consider only systems in one of the four traditional thermodynamic environments. A fixed temperature is assumed in the isothermal cases. The adiabatic cases are discussed in the following.

#### Adiabatic and isochoric systems

As stated in Section 4.1.2, the first law of thermodynamics for an adiabatic system yields

$$\mathrm{d}E + p\mathrm{d}V = 0.$$

In the isochoric case, $\mathrm{d}V = 0$ implies the conservation of internal energy. In practice, we can only compute the standard molar enthalpy of the species, see Section 4.2.3. Hence, the equation for the conservation of a fixed internal

energy $\check{E}$, which is considered in the final model, is

$$\begin{aligned}\check{E} &= H - pV \\ &= m \sum_{s=1}^{n_{\text{spec}}} h_s^\circ \, w_s - \frac{V \rho R T}{\bar{M}} \\ &= m \left( \sum_{s=1}^{n_{\text{spec}}} \frac{\bar{H}_s^\circ}{M_s} \, w_s - \frac{RT}{\bar{M}} \right) \\ &= m \left( \sum_{s=1}^{n_{\text{spec}}} \bar{H}_s^\circ \, z_s - \frac{RT}{\bar{M}} \right),\end{aligned}$$

where we make use of the ideal gas law. Alternatively,

$$\check{e} = \sum_{s=1}^{n_{\text{spec}}} \bar{H}_s^\circ \, z_s - \frac{RT}{\bar{M}} \tag{4.8}$$

can be used for a fixed specific internal energy $\check{e}$.

#### Adiabatic and isobaric systems

The first law of thermodynamics for an adiabatic system also states

$$\mathrm{d}H - V \mathrm{d}p = 0,$$

see Section 4.1.2. In the isobaric case, $\mathrm{d}p = 0$ implies the conservation of enthalpy. Thus, the equation for a fixed enthalpy $\check{H}$ to be fulfilled in the final model is

$$\check{H} = m \sum_{s=1}^{n_{\text{spec}}} \bar{H}_s^\circ \, z_s.$$

One could also use a fixed specific enthalpy $\check{h}$ and

$$\check{h} = \sum_{s=1}^{n_{\text{spec}}} \bar{H}_s^\circ \, z_s. \tag{4.9}$$

### 4.2.3 NASA polynomials

Thermodynamic quantities are necessary for a combustion model. So-called NASA polynomials are evaluated to obtain the standard molar heat capacity (at constant pressure), enthalpy, and entropy of the species.

**Listing 4.1:** NASA polynomial coefficients for $H_2O$ for use with the mechanism given in Section A.1.

```
H2O               20387H   2O   1          G  0300.00   5000.00  1000.00      1
 0.02672145E+02 0.03056293E-01-0.08730260E-05 0.12009964E-09-0.06391618E-13    2
-0.02989921E+06 0.06862817E+02 0.03386842E+02 0.03474982E-01-0.06354696E-04    3
 0.06968581E-07-0.02506588E-10-0.03020811E+06 0.02590232E+02                   4
```

### Evaluation of the NASA polynomials

The parameter values representing the coefficients of the NASA polynomials are given in a specific form. In Listing 4.1, the values for $H_2O$ taken from a thermodynamical data set are shown. The first line in Listing 4.1 determines the name of the species and some additional information. The last three values are of importance. In this example $T_{\mathrm{lb}} = 300\,\mathrm{K}$, $T_{\mathrm{ub}} = 5000\,\mathrm{K}$, and $T_{\mathrm{sw}} = 1000\,\mathrm{K}$ are given.
Fourteen coefficients for the NASA polynomials are given in line two to four. We call the first seven $a_i^{\mathrm{high}}$, $i = 1, \ldots, 7$, and the rest $a_i^{\mathrm{low}}$, $i = 1, \ldots, 7$. The temperature at which the polynomials shall be evaluated defines which set (high or low) has to be taken. If $T$ is between $T_{\mathrm{lb}}$ and $T_{\mathrm{sw}}$, the numbers $a_i^{\mathrm{low}}$ have to be taken, and between $T_{\mathrm{sw}}$ and $T_{\mathrm{ub}}$, the values for high temperature $a_i^{\mathrm{high}}$ are used. Formulae in the following are valid for both $a_i^{\mathrm{low}}$ and $a_i^{\mathrm{high}}$ such that we just use the notation $a_i$, $i = 1, \ldots, 7$.
The standard molar heat capacity at constant pressure of a certain species at high or low temperature is computed via a five term polynomial of order four in $T$

$$\frac{\bar{C}_{p,s}^{\circ}(T)}{R} = a_1 + a_2 T + a_3 T^2 + a_4 T^3 + a_5 T^4. \tag{4.10}$$

Formulae for the computation of enthalpy and entropy can be deduced via the integrals

$$\bar{H}_s^{\circ}(T) = R a_6^* + \int_{T'=298}^{T} \bar{C}_p^{\circ}(T')\,\mathrm{d}T' \tag{4.11}$$

and

$$\bar{S}_s^{\circ}(T) = R a_7^* + \int_{T'=298}^{T} \frac{\bar{C}_p^{\circ}(T')}{T'}\,\mathrm{d}T', \tag{4.12}$$

where $a_i^*$, $i = 6, 7$, are chosen to be the integration constants in the formulae. This means, the standard molar enthalpy and entropy of a species can be computed via

$$\frac{\bar{H}_s^{\circ}(T)}{R} = a_6 + a_1 T + \frac{a_2}{2} T^2 + \frac{a_3}{3} T^3 + \frac{a_4}{4} T^4 + \frac{a_5}{5} T^5 \tag{4.13}$$

and

$$\frac{\bar{S}_s^{\circ}(T)}{R} = a_7 + a_1 \ln(T) + a_2 T + \frac{a_3}{2} T^2 + \frac{a_4}{3} T^3 + \frac{a_5}{4} T^4. \tag{4.14}$$

The constants $a_6$ and $a_7$ are chosen such that $\bar{H}_s^\circ(298\,\mathrm{K}) = \Delta H_\mathrm{f}^\circ(298\,\mathrm{K})$ is valid and the value of the entropy $\bar{S}^\circ(298\,\mathrm{K})$ matches.
Based on enthalpy and entropy, the Gibbs free energy can be computed via

$$G = H - TS.$$

This means, the equilibrium constant for a chemical reaction is given solely by the NASA coefficients, see also Section 4.1.3.

### Transition between the branches

The use of the NASA polynomials causes a problem within the optimization framework for model reduction. Consider e.g. the coefficients in Listing 4.2 valid for O in case of the ozone decomposition mechanism given in Table A.2. Obviously, the switching temperature is at $T_\mathrm{sw} = 1000\,\mathrm{K}$ again. The transi-

**Listing 4.2:** NASA polynomial coefficients for O for use with the ozone mechanism given in Table A.2.

```
O                 120186O   1               G  0300.00   5000.00  1000.00      1
 0.02542059E+02-0.02755061E-03-0.03102803E-07 0.04551067E-10-0.04368051E-14    2
 0.02923080E+06 0.04920308E+02 0.02946428E+02-0.16381665E-02 0.02421031E-04    3
-0.16028431E-08 0.03890696E-11 0.02914764E+06 0.02963995E+02                   4
```

tion between the two branches of the molar heat capacity at the switching temperature $T_\mathrm{sw}$ is discontinuous as depicted in Figure 4.1. We apply the idea of [32, 151] and use the hyperbolic tangent for generating a $\mathcal{C}^\infty$-transition.
The temperature is varied in the optimization algorithm for model reduction. It is not important to limit the temperature between the bounds $T_\mathrm{lb}$ and $T_\mathrm{ub}$, as the function formed by the connected polynomials is $\mathcal{C}^\infty(\mathbb{R}^+)$, except at the switching point. However, positivity should be guaranteed for the temperature. Otherwise some (kinetic) expressions might not be evaluable. The temperature should be between the bounds at the solution computed by the optimization algorithm to guarantee a valid model.
We denote the low temperature branch of the standard molar heat capacity of species $s$ at constant pressure with $\bar{C}_{p,s}^\mathrm{low}$ and the high temperature branch with $\bar{C}_{p,s}^\mathrm{high}$ (without $^\circ$). We redefine the molar heat capacity at standard state of species $s$ via the convex combination

$$\bar{C}_{p,s}^\circ(T) = (1 - \sigma(T))\bar{C}_{p,s}^\mathrm{low}(T) + \sigma(T)\bar{C}_{p,s}^\mathrm{high}(T),$$

where $\sigma$ is a sufficiently smooth transition function with parameter $\gamma$ defined by

$$\begin{aligned} \sigma &: \mathbb{R} \to (0,1) \\ T &\mapsto \sigma(T) := \frac{1}{2}\tanh[\gamma(T - T_\mathrm{sw})] + \frac{1}{2}. \end{aligned}$$

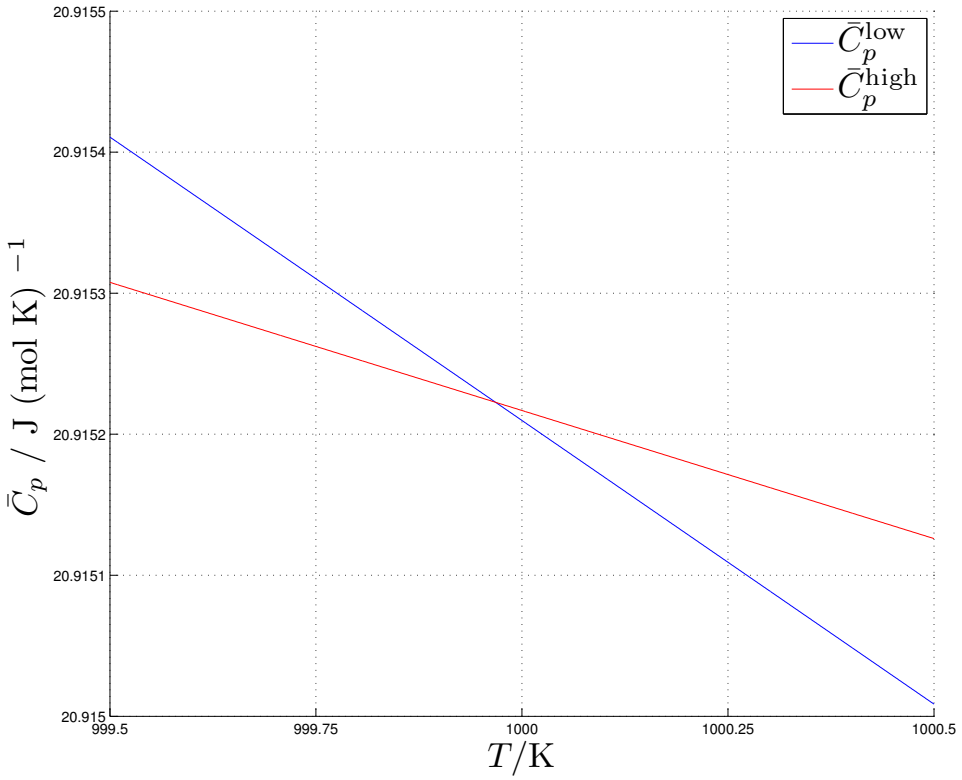


**Figure 4.1:** Visualization of the molar heat capacity $\bar{C}^{\circ}_{p,\mathrm{O}}$ versus $T$ near a temperature value of $T_{\mathrm{sw}} = 1000\,\mathrm{K}$. The transition from the low temperature branch (blue) to the high temperature branch (red) is discontinuous.

This means, we use a convex combination of the two branches. As tanh is an odd function, it holds that

$$1 - \sigma(T_{\mathrm{sw}} - T) = \sigma(T_{\mathrm{sw}} + T),$$

which results in a symmetric overlay. Analogously, the branches for enthalpy and entropy can be coupled

$$\bar{H}^{\circ}_s(T) = (1 - \sigma(T))\bar{H}^{\mathrm{low}}_s(T) + \sigma(T)\bar{H}^{\mathrm{high}}_s(T)$$
$$\bar{S}^{\circ}_s(T) = (1 - \sigma(T))\bar{S}^{\mathrm{low}}_s(T) + \sigma(T)\bar{S}^{\mathrm{high}}_s(T).$$

Derivatives of first and second order of the function

$$\sigma(T) = \frac{1}{2}\tanh[\gamma(T - T_{\mathrm{sw}})] + \frac{1}{2}$$

are necessary in our computations. These are

$$\mathrm{d}_T\sigma(T) = \frac{\gamma}{2}\left(1 - \tanh^2[\gamma(T - T_{\mathrm{sw}})]\right)$$
$$\mathrm{d}^2_T\sigma(T) = -\gamma^2\tanh[\gamma(T - T_{\mathrm{sw}})]\left(1 - \tanh^2[\gamma(T - T_{\mathrm{sw}})]\right).$$

Because $\mathrm{d}_T\sigma(T_{\mathrm{sw}}) = \frac{\gamma}{2}$, we can consider $\gamma$ as a parameter for the slope of the transition function at the switching temperature. Hence, large $\gamma$ mean a steep transition, small $\gamma$ a smooth one. The parameter $\gamma = 20$ for $\sigma$ is used as it leads to a reasonable compromise; see also Figure 4.2.

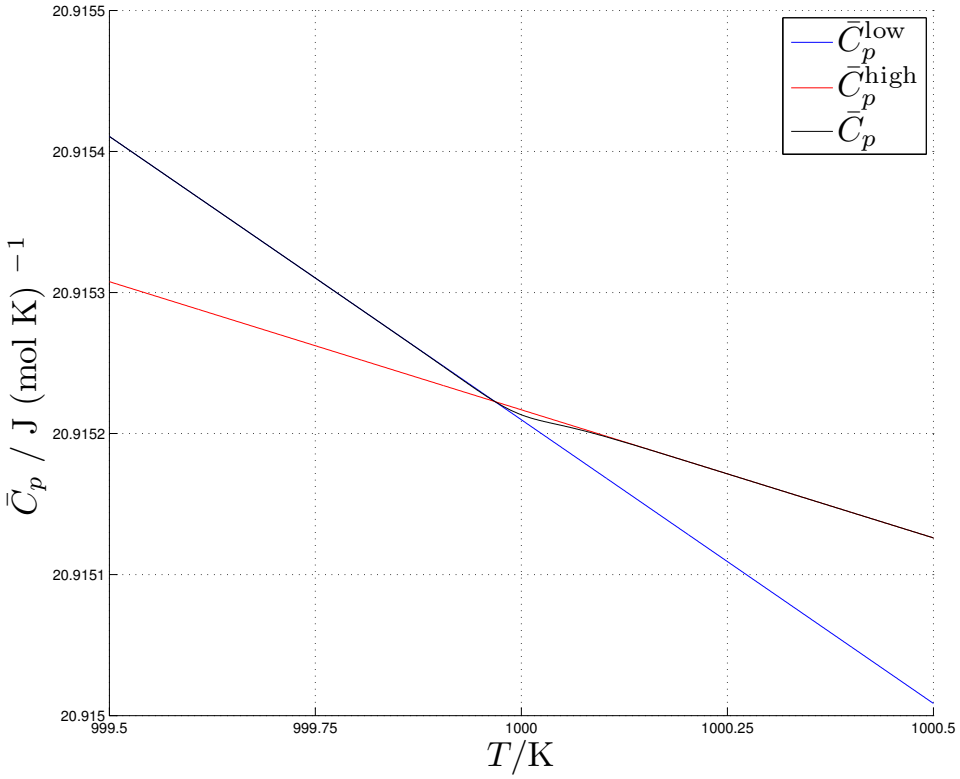


**Figure 4.2:** Plot of the heat capacity $\bar{C}^\circ_{p,\mathrm{O}}$ versus $T$ near a temperature value of $T_{\mathrm{sw}} = 1000\,\mathrm{K}$. The black curve depicts the combined $\bar{C}^\circ_p(T)$ that smoothly connects the low temperature branch (blue) with the high temperature branch (red).

**Implementation** The hyperbolic tangent is implemented via the hyperbolic sine and cosine in an old version of the automatic differentiation package `CppAD` [17, 18] that is used in the code developed with this thesis, see Section 7.3. This leads to an overflow for large values of $T - T_{\mathrm{sw}}$. As a remedy, we use another transition function $\zeta$ with the parameter $\tau$ and its derivatives

$$\begin{aligned}
\zeta(T) &= \frac{1}{\pi}\arctan[\tau(T - T_{\mathrm{sw}})] + \frac{1}{2} \\
\mathrm{d}_T\zeta(T) &= \frac{\tau}{\pi[1 + \tau^2(T - T_{\mathrm{sw}})^2]} \\
\mathrm{d}_T^2\zeta(T) &= -\frac{2\tau^3(T - T_{\mathrm{sw}})}{\pi[1 + \tau^2(T - T_{\mathrm{sw}})^2]^2}.
\end{aligned}$$

**Resulting error** The error in the physical relations between heat capacity, enthalpy, and entropy resulting from the introduced transition function is given as

$$\begin{aligned}|\mathrm{d}_T \bar{H}_s^\circ - \bar{C}_{p,s}^\circ| &= \Big|\Big(-\bar{H}_s^{\mathrm{low}}\mathrm{d}_T\sigma + (1-\sigma)\bar{C}_{p,s}^{\mathrm{low}} + \bar{H}_s^{\mathrm{high}}\mathrm{d}_T\sigma + \sigma\bar{C}_{p,s}^{\mathrm{high}}\Big) \\ &\quad - \Big((1-\sigma)\bar{C}_{p,s}^{\mathrm{low}} + \sigma\bar{C}_{p,s}^{\mathrm{high}}\Big)\Big| \\ &= \Big|\Big(-\bar{H}_s^{\mathrm{low}} + \bar{H}_s^{\mathrm{high}}\Big)\,\mathrm{d}_T\sigma\Big|\end{aligned}$$

and

$$\begin{aligned}|T\mathrm{d}_T \bar{S}_s^\circ - \bar{C}_{p,s}^\circ| &= \Big|\Big(-T\bar{S}_s^{\mathrm{low}}\mathrm{d}_T\sigma + (1-\sigma)\bar{C}_{p,s}^{\mathrm{low}} + T\bar{S}_s^{\mathrm{high}}\mathrm{d}_T\sigma + \sigma\bar{C}_{p,s}^{\mathrm{high}}\Big) \\ &\quad - \Big((1-\sigma)\bar{C}_{p,s}^{\mathrm{low}} + \sigma\bar{C}_{p,s}^{\mathrm{high}}\Big)\Big| \\ &= \Big|\Big(-\bar{S}_s^{\mathrm{low}} + \bar{S}_s^{\mathrm{high}}\Big)\,\mathrm{d}_T\sigma\Big|.\end{aligned}$$

The function $\mathrm{d}_T\sigma$ has a large influence. The maximum of $\mathrm{d}_T\sigma$ is at $T = T_{\mathrm{sw}}$. It can be stated that the parameter $\gamma$ is a trade off between a steep transition, meaning small error in the values of heat capacity, enthalpy, and entropy near $T_{\mathrm{sw}}$, and a smooth transition resulting in an error in the violation of Equations (4.11) and (4.12) near $T_{\mathrm{sw}}$. In our implementation, we use the value $\gamma = 20$ for $\sigma$ and $\tau = 1000$ for $\zeta$ as standard values.

## 4.3 Chemical kinetics

All combustion models considered here are based on mechanisms which themselves are based on the law of mass action. In this section, all formulae needed for the computation of the reaction rates in dependence of the kinetic parameters are discussed. The section concludes with the computation of the molar net chemical production rate, which is needed for the right hand side of an ODE model as it is assembled in the following Section 4.4.

### 4.3.1 Mass action kinetics

It is important to distinguish between *overall* or *net* reactions and *elementary* reactions. The rate of destruction of species A for the general chemical reaction

$$a\,\mathrm{A} + b\,\mathrm{B} \to c\,\mathrm{C} + d\,\mathrm{D}$$

is of the form

$$-\frac{\mathrm{d}c_{\mathrm{A}}}{\mathrm{d}t} = k c_{\mathrm{A}}^{\alpha} c_{\mathrm{B}}^{\beta},$$

where $k$, $\alpha$, and $\beta$ are empirically evaluated rate constants and reaction orders with respect to the species, respectively. In contrast, elementary reactions proceed at molecular level as they are noted. Consider

$$a\,\mathrm{A} + b\,\mathrm{B} \rightarrow c\,\mathrm{C} + d\,\mathrm{D}$$

an elementary reaction. The rate of destruction of species A is

$$-\frac{\mathrm{d}c_\mathrm{A}}{\mathrm{d}t} = kac_\mathrm{A}^a c_\mathrm{B}^b,$$

where the stoichiometric constants are the exponents or reaction orders. For this reason, a chemical mechanism usually is given as a set of elementary reactions.

### General situation

A general set of elementary reactions (numbered by $r$) might be written in the form

$$\sum_{s=1}^{n_\mathrm{spec}} \nu'_{sr}\mathrm{X}_s \rightleftharpoons \sum_{s=1}^{n_\mathrm{spec}} \nu''_{sr}\mathrm{X}_s, \quad r = 1, \ldots, n_\mathrm{reac}.$$

The rate of progress of reaction $r$ is described by

$$q_r = \underbrace{k_{\mathrm{f},r} \prod_{s=1}^{n_\mathrm{spec}} c_s^{\nu'_{sr}}}_{=:r_{\mathrm{f},r}} - \underbrace{k_{\mathrm{r},r} \prod_{s=1}^{n_\mathrm{spec}} c_s^{\nu''_{sr}}}_{=:r_{\mathrm{r},r}}.$$

A third body is necessary in some reactions. In that case, the rate of progress of reaction $r$ is

$$q_r = \left(\sum_{s=1}^{n_\mathrm{spec}} \alpha_{sr} c_s\right)\left(k_{\mathrm{f},r} \prod_{s=1}^{n_\mathrm{spec}} c_s^{\nu'_{sr}} - k_{\mathrm{r},r} \prod_{s=1}^{n_\mathrm{spec}} c_s^{\nu''_{sr}}\right),$$

where $\alpha_{sr}$ is the collision efficiency of species $s$ in reaction $r$. Third bodies often have the same collision efficiency in several reactions. Hence, symbols for third bodies $\mathrm{M}_i$ are defined, and $\alpha_{sr}$ is replaced by $\alpha_{si}$ if third body $i$ takes part in reaction $r$. We can define the concentration of third body $\mathrm{M}_i$, $i = 1, \ldots, n_\mathrm{tb}$, as

$$c_{\mathrm{M}_i} = \sum_{s=1}^{n_\mathrm{spec}} \alpha_{si} c_s. \tag{4.15}$$

Unspecified collision efficiencies are meant to have the value 1 [171]. This is used for all mechanisms considered in this work.
The molar chemical production rate $\omega_s$ of species $s$ is defined as

$$\omega_s = \sum_{r=1}^{n_\mathrm{reac}} \nu_{sr} q_r, \tag{4.16}$$

where $\nu_{sr}$ is the net stoichiometric coefficient

$$\nu_{sr} := \nu''_{sr} - \nu'_{sr}.$$

The chemical potential of forward and reverse reactions in equilibrium are the same. Therefore, the equilibrium constant for reaction $r$ can be defined as

$$K_{p,r} := \prod_{s=1}^{n_{\text{spec}}} \left( \frac{p_s}{p^\circ} \right)_{\text{e}}^{\nu_{sr}},$$

where the index e denotes that all values are considered in equilibrium and the index $p$ clarifies the constant being in terms of pressure values.
The equilibrium constants of reaction $r$ are connected via the relation

$$K_{c,r} = K_{p,r} \left( \frac{p^\circ}{RT} \right)^{\nu_r} \tag{4.17}$$

with the net change of the number of species present in the gas phase

$$\nu_r := \sum_{s=1}^{n_{\text{spec}}} \nu_{sr}.$$

### 4.3.2 Arrhenius kinetics

Rate constants strongly depend on temperature. This dependence is modeled with a three-parameter modified Arrhenius equation

$$k_{\text{f},r}(T) = A\, T^b\, \text{e}^{-\frac{E_\text{a}}{RT}}. \tag{4.18}$$

The constants $A$, $b$, and $E_\text{a}$ are given for each reaction. For an interpretation of the pre-exponential factor $A$, see e.g. [93, 173].
The reverse rate coefficient of reaction $r$ also depends on temperature. It can also be given in the Arrhenius form*. Alternatively, the connection of forward and reverse rate coefficient via the equilibrium constant is used with the relation

$$\frac{k_{\text{f},r}}{k_{\text{r},r}} = K_{c,r}.$$

The equilibrium constant in terms of concentrations is computed with NASA polynomials via the following equation for $K_{p,r}$,

$$K_{p,r} = \exp\left( \frac{\Delta S^\circ_{\text{r},r}(T)}{R} - \frac{\Delta H^\circ_{\text{r},r}(T)}{RT} \right),$$

* In some publications, the reverse rate coefficients of Arrhenius type reactions are computed with fitted Arrhenius parameters for the reverse reactions. We also use this strategy in previous publications as e.g. [105, 106]. However, this is impossible in case of pressure dependent reactions, and it may lead to inconsistent values of thermodynamic quantities in the mass action kinetics in relation to the heat of the reaction. Therefore, we prefer the thermodynamic approach in this thesis.

see Equations (4.5) and (4.17), where

$$\Delta H^\circ_{\mathrm{r},r}(T) = \sum_{s=1}^{n_{\mathrm{spec}}} \nu_{sr} \bar{H}^\circ_s(T)$$
$$\Delta S^\circ_{\mathrm{r},r}(T) = \sum_{s=1}^{n_{\mathrm{spec}}} \nu_{sr} \bar{S}^\circ_s(T)$$

are the molar reaction enthalpy and entropy, respectively. The computation of the standard molar enthalpy $\bar{H}^\circ_s(T)$ of species $s$ and entropy $\bar{S}^\circ_s(T)$ is described in Section 4.2.3.

### 4.3.3 Troe kinetics

The reaction rate constants can also depend on pressure. A detailed discussion of this issue can be found in [93, Section 9.4]. In summary, both the low pressure rate constant $k^{(2)}_{\mathrm{uni},0}$ and the high pressure constant $k_{\mathrm{uni},\infty}$ are given in the modified Arrhenius form (4.18). These are used together with a third body M to compute the reduced pressure (a dimensionless parameter)

$$p_{\mathrm{r}} = \frac{k^{(2)}_{\mathrm{uni},0} c_{\mathrm{M}}}{k_{\mathrm{uni},\infty}},$$

where $c_{\mathrm{M}}$ is defined as in Equation (4.15). With this parameter, the final rate constant $k_{\mathrm{f},r} = k_{\mathrm{uni}}$ of reaction $r$ is computed as

$$k_{\mathrm{uni}} = k_{\mathrm{uni},\infty} \frac{p_{\mathrm{r}}}{1 + p_{\mathrm{r}}} F$$

with a function $F$. To compute this $F$, Gilbert, Luther, and Troe [63, 158] introduced the formula

$$\lg F = \left\{ 1 + \left[ \frac{\lg p_{\mathrm{r}} + c}{n - d(\lg p_{\mathrm{r}} + c)} \right]^2 \right\}^{-1} \lg F_{\mathrm{c}},$$

with a set of simplifications

$$c = -0.4 - 0.67 \lg F_{\mathrm{c}}$$
$$n = 0.75 - 1.27 \lg F_{\mathrm{c}}$$
$$d = 0.14$$

and the F-center-value

$$F_{\mathrm{c}} = (1 - a) \exp\left( -\frac{T}{T^{***}} \right) + a \exp\left( -\frac{T}{T^{*}} \right) + \exp\left( -\frac{T^{**}}{T} \right),$$

which includes the four parameters $a$, $T^*$, $T^{**}$, and $T^{***}$. These are given for each so-called Troe reaction. In the mechanisms used here, only the Troe form is used for pressure dependent reactions, so we skip a discussion of other possibilities like the SRI form and its extension.

## 4.4 Models for homogeneous combustion

In this section, ODE models for homogeneous combustion are contemplated. We consider again the four classical thermodynamic environments. A thermodynamic Lyapunov function is known in all four cases [74]. These are

1. isothermal, isochoric systems: $\frac{F}{RT}$
2. isothermal, isobaric systems: $\frac{G}{T}$
3. adiabatic, isochoric systems : $-\frac{S}{R}$
4. adiabatic, isobaric systems: $-\frac{S}{R}$.

Here $F = E - TS$ is the Helmholtz energy. All other quantities are introduced in Sections 4.1.2 and 4.1.3.
We consider the state of a system given in specific moles and the conserved quantity from energy balance. The realizable phase space of the system is the polytope defined by the positivity of the specific moles and the linear mass conservation (4.6). This polytope is depicted in Figure 2.1.
In all four systems, there is a unique equilibrium point in the realizable phase space which attracts all trajectories. It is defined by the minimum of the corresponding Lyapunov function. The proof can be found in [130].

### 4.4.1 Change of the mass of the species

The mass of the species in the system change in accordance to

$$\mathrm{D}m_s = \omega_s \, M_s \, V, \quad s = 1, \ldots, n_{\mathrm{spec}}.$$

This can be expressed in terms of mass fractions

$$\mathrm{D}w_s = \frac{\omega_s \, M_s}{\rho}, \quad s = 1, \ldots, n_{\mathrm{spec}}$$

or specific moles

$$\mathrm{D}z_s = \frac{\omega_s}{\rho}, \quad s = 1, \ldots, n_{\mathrm{spec}}. \tag{4.19}$$

**Isothermal, isochoric systems**

In isothermal systems, the value of the temperature $T$ is used as a parameter. The pressure $p(t)$ can be computed with Equation (4.2) as $\rho$ is constant in this case and $V$ and $m$ are known.

We can reformulate the ODE for a system in this thermodynamic environment for $s = 1, \dots, n_{\text{spec}}$ as

$$\begin{aligned} \rho \, \mathrm{D}z_s &= \omega_s \\ \mathrm{D}(\rho \, z_s) &= \omega_s + z_s \mathrm{D}\rho \\ \mathrm{D}c_s &= \omega_s \end{aligned}$$

with $\mathrm{D}\rho(t) = 0$.

**Isothermal, isobaric systems**

In the isothermal, isobaric case, the right hand side of system (4.19) can directly be written as

$$\mathrm{D}z_s = \frac{\omega_s}{p} \frac{RT}{\bar{M}}, \quad s = 1, \dots, n_{\text{spec}}.$$

### 4.4.2 Conservation of energy

The internal energy is conserved in adiabatic, isochoric systems, because compression work can not occur. We want to derive a differential equation in the temperature for the energy conservation in this section.
The internal energy can be computed by specific partial internal energies of the species

$$E = m \sum_{s=1}^{n_{\text{spec}}} w_s \, e_s.$$

It is conserved, so the chain rule yields

$$\mathrm{d}_t E = m \sum_{s=1}^{n_{\text{spec}}} w_s \, \mathrm{d}_t e_s + m \sum_{s=1}^{n_{\text{spec}}} e_s \, \mathrm{d}_t w_s = 0.$$

With identities for the specific heat capacity at constant volume

$$\begin{aligned} \mathrm{d}_t e &= c_V \mathrm{d}_t T \\ \mathrm{d}_t e_s &= c_{V,s} \mathrm{d}_t T, \quad s = 1, \dots, n_{\text{spec}} \\ c_V &= \sum_{s=1}^{n_{\text{spec}}} w_s c_{V,s} \end{aligned}$$

and the ODE system for mass fractions, the differential equation for the temperature is

$$\mathrm{d}_t T \, c_V = - \sum_{s=1}^{n_{\text{spec}}} e_s \, \frac{\omega_s \, M_s}{\rho}.$$

This formula has to be reformulated using terms of molar enthalpy for computation. The conversion factor between specific enthalpy $h_s = \frac{H_s}{m_s}$ and molar enthalpy $\bar{H}_s = \frac{H_s}{n_s}$ is the molar mass:

$$h_s = \frac{\bar{H}_s}{M_s}, \quad s = 1, \ldots, n_{\text{spec}}.$$

The analogous formula holds for the internal energy

$$e_s = \frac{\bar{E}_s}{M_s}, \quad s = 1, \ldots, n_{\text{spec}}.$$

With the ideal gas law, the difference between molar enthalpy and molar energy of species $s$ is $RT$:

$$\bar{H}_s^\circ - RT = \bar{E}_s^\circ, \quad s = 1, \ldots, n_{\text{spec}}.$$

The specific heat capacity at constant volume can be computed by the standard molar heat capacity at constant pressure and the specific moles

$$\begin{aligned} c_V^\circ &= \frac{C_V^\circ}{m} \\ &= \frac{C_p^\circ - nR}{m} \\ &= \frac{\sum_{s=1}^{n_{\text{spec}}} n_s \bar{C}_{p,s}^\circ - nR}{m} \\ &= \sum_{s=1}^{n_{\text{spec}}} z_s \bar{C}_{p,s}^\circ - \frac{R}{\bar{M}}. \end{aligned}$$

The differential equation for the temperature is

$$\begin{aligned} \mathrm{D}T = \mathrm{d}_t T &= \frac{-\sum_{s=1}^{n_{\text{spec}}} \bar{E}_s^\circ \, \omega_s}{\rho c_V} \\ &= \frac{-V \sum_{s=1}^{n_{\text{spec}}} (\bar{H}_s^\circ - RT)\omega_s}{m \left( \sum_{s=1}^{n_{\text{spec}}} z_s \bar{C}_{p,s}^\circ - R \sum_{s=1}^{n_{\text{spec}}} z_s \right)}. \end{aligned}$$

### 4.4.3 Conservation of enthalpy

In an adiabatic, isobaric system, the enthalpy is conserved as can be seen in Equation (4.4). In analogy to the presentation in the previous section, a differential equation for the temperature is derived.
The enthalpy is conserved. This can be written as

$$\begin{aligned} \mathrm{d}_t(E + pV) &= 0 \\ \mathrm{d}_t h &= 0. \end{aligned}$$

As in the section before, a formulation in terms of partial quantities is needed. Analogously, the chain rule yields

$$\mathrm{d}_t \sum_{s=1}^{n_{\mathrm{spec}}} (h_s w_s) = 0$$

$$\sum_{s=1}^{n_{\mathrm{spec}}} (w_s \mathrm{d}_t h_s + h_s \mathrm{d}_t w_s) = 0.$$

The equation for the specific heat capacity is

$$\mathrm{d}_t h_s = c_{p,s} \mathrm{d}_t T, \quad s = 1, \ldots, n_{\mathrm{spec}}$$

$$c_p = \sum_{s=1}^{n_{\mathrm{spec}}} w_s \, c_{p,s} = \sum_{s=1}^{n_{\mathrm{spec}}} z_s \, \bar{C}_{p,s}.$$

With the differential equation for the mass fractions, we arrive at

$$\sum_{s=1}^{n_{\mathrm{spec}}} w_s \, c_{p,s} \, \mathrm{d}_t T = - \sum_{s=1}^{n_{\mathrm{spec}}} h_s \, \frac{\omega_s \, M_s}{\rho}.$$

We rearrange this equation to get

$$\mathrm{d}_t T = - \frac{\sum_{s=1}^{n_{\mathrm{spec}}} h_s \, \omega_s \, M_s}{\rho \, c_p},$$

where the unknown $\rho(t)$ is computed with Equation (4.2). The ODE for the temperature in case of enthalpy conserving systems is

$$\mathrm{D}T = - \frac{RT \sum_{s=1}^{n_{\mathrm{spec}}} (\bar{H}_s^\circ \, \omega_s) \sum_{s=1}^{n_{\mathrm{spec}}} z_s}{p \, \sum_{s=1}^{n_{\mathrm{spec}}} (z_s \, \bar{C}_{p,s}^\circ)}.$$

*Nature optimizes.*

Jorge Nocedal and
Stephen J. Wright

# 5 Theory of the model reduction method based on optimization

The idea to use an optimization approach for model reduction in the context presented in this work is raised in [101]. Similar ideas exist already before. In 1999, L. Petzold and W. Zhu introduce an optimization based method for model reduction switching on and off different reaction pathways [126]. Already in 1998, S. S. Girimaji introduces an optimization approach minimizing the evolution rate of the dynamics [69].

## 5.1 Basic ideas of the method

D. Lebiedz introduces a model reduction method based on minimal entropy production trajectories (MEPT) in 2004 [101]. The basic idea is that the SIM is supposed to be characterized by maximum relaxation of the system dynamics under given constraints of fixed reaction progress variables [148]. More general, this means that the objective function in the optimization problem captures essential properties of a SIM [106] and should represent the assumption that chemical forces are – under the given constraints – maximally relaxed along trajectories on the SIM [148]. From the inverse point of view, this means that the remaining relaxation of chemical forces along the trajectories is minimal while they converge toward chemical equilibrium [105]. Hence, an appropriate characterization of maximum "slowness", e.g. in terms of an integral over suitably defined *curvature* (velocity change) of trajectories measured in the Euclidean norm, is reasonable. The SIM is generally characterized by the property that all trajectories in its neighborhood

converge faster to the manifold than to the attractor, the chemical equilibrium point [106].
The optimization problem to compute an approximation of a point on a SIM can be written as

$$\min_{z} \ \Psi(z) \tag{5.1a}$$

subject to

$$\mathrm{D}z(t) = S(z(t)) \tag{5.1b}$$
$$0 = \bar{C}(z(t)) \tag{5.1c}$$
$$0 = z_j(t_*) - z_j^{t_*}, \quad j \in \mathcal{I}_{\mathrm{pv}} \tag{5.1d}$$
$$0 \leqslant z(t) \tag{5.1e}$$

and

$$t \in [t_0, t_\mathrm{f}] \tag{5.1f}$$
$$t_* \in [t_0, t_\mathrm{f}] \quad \text{(fixed)}, \tag{5.1g}$$

where temperature $T$ is omitted for simplification of the discussion. The vector $z(t) = (z_i(t))_{i=1}^n$ denotes the state vector (in specific moles in a combustion model). The system dynamics, e.g. chemical kinetics determined by the reaction mechanism, are described by (5.1b) and enter the optimization problem as equality constraints. Hence, an optimal solution $z^*$ of (5.1) always satisfies the system dynamics of the full ODE system; it represents a solution trajectory of (5.1b).
Dimension and parametrization of the manifold to be computed have to be set *a priori* by the user; see also the discussion in Section 5.5.1. The set $\mathcal{I}_{\mathrm{pv}} \subset \{1, ..., n\}$ is an index set that contains the indices of a selection of state variables, denoted as *reaction progress variables* in chemical kinetics, see Section 2.3.1. The values at time $t_*$ are fixed for these variables and are used to parametrize the reduced model, i.e. the SIM to be computed. These values are fixed via the equality constraint (5.1d) at $t_*$. It is clear that the solution of the optimization problem (5.1) allows for species reconstruction of the values $z_j^*(t_*)$, $j \notin \mathcal{I}_{\mathrm{pv}}$ as introduced in Section 2.3.1. Additional constraints are collected in a function $\bar{C}$ in (5.1c). These are explained later.
The objective functional in form of a Lagrange term

$$\Psi(z) := \int_{t_0}^{t_\mathrm{f}} \Phi\left(z(t)\right) \, \mathrm{d}t \tag{5.2}$$

with a function $\Phi : \mathbb{R}^n \to \mathbb{R}$ represents a mathematical formulation of characteristic properties of a SIM. This is discussed in Section 5.2. We call the function $\Phi$ *criterion* in the following as it should indicate a property which qualifies the trajectory piece $z(t)$, $t \in [t_0, t_\mathrm{f}]$ for being on the SIM.

## 5.2 Choice of the objective functional

During the development of the optimization based model reduction method, a lot of criteria $\Phi$ have been suggested. Numerical experiments with several different objective functions $\Psi$ are compared especially in [135] and [105], but no clear preference can be found. We present an overview of the most important suggestions.

### 5.2.1 Entropy based objective functions

The first objective function used for model reduction purposes in the presented context is raised with the method in [101], where D. Lebiedz creates the notion *minimal entropy production trajectory* (MEPT). The concept is based on choosing trajectories along which the entropy production is minimal. The entropy production of an elementary reaction $j$ (due to irreversible processes) is defined as

$$\frac{\mathrm{d_i}S_j}{\mathrm{d}t} := R(r_{\mathrm{f},j} - r_{\mathrm{r},j}) \ln\left(\frac{r_{\mathrm{f},j}}{r_{\mathrm{r},j}}\right). \tag{5.3}$$

See Chapter 4 for the meaning of the symbols. The total entropy production is the sum over the entropy production of all elementary reactions. Hence, the criterion $\Phi$ used in the objective function (5.2) of the optimization problem (5.1) would be

$$\Phi_{\mathrm{EP}}(z(t)) = \sum_{j=1}^{n_{\mathrm{reac}}} \frac{\mathrm{d_i}S_j}{\mathrm{d}t}.$$

Several similar objective functionals are discussed in [135] as the reparametrized entropy production $\sum_{j=1}^{n_{\mathrm{reac}}} \frac{\mathrm{d_i}S_j}{\mathrm{d}t} \|S(z)\|_2$ or a version with a semi-norm, which only respects those variables that do not serve as reaction progress variables $\sum_{j=1}^{n_{\mathrm{reac}}} \frac{\mathrm{d_i}S_j}{\mathrm{d}t} \|S(z)\|_{2,\text{non-pv}}$.
In [103], the idea to use the entropy production is extended and discussed with the definition of entropy in a mathematical sense.

### 5.2.2 Curvature based objective functions

Later on, e.g. in [136], the idea is discussed that the velocity and the curvature are related to the force relaxation of the system. In [136], this idea is compared to MEPT. Comparing formula (5.3) and formula (4.16), it is clear that there is a "similarity" between the minimization of the entropy production on the one hand and the minimization of the chemical production rate on the other hand.
A similar approach is raised in [65, 66, 67], where J.-M. Ginoux introduces the flow curvature method, which identifies flow curvature manifolds. It is

shown there that these manifolds correspond to the manifolds defined by the graph of the map $h^\varepsilon$ in singular perturbation theory, see Section 2.2.
The rate of change of the right hand side of the ODE (5.1b) is closely related to the curvature of the trajectories as geometrical objects in the phase space; it is the second derivative

$$\mathrm{D}^2 z(t) = J_S(z(t))\ S(z(t)).$$

This can be interpreted as a directional derivative of the chemical source with respect to its own normalized direction $v := \frac{\mathrm{D}z}{\|\mathrm{D}z\|_2} = \frac{S}{\|S\|_2}$

$$\frac{\mathrm{d}}{\mathrm{d}\alpha} S(z(t) + \alpha v)\Big|_{\alpha=0} = J_S(z(t)) \frac{S(z(t))}{\|S(z(t))\|_2}. \tag{5.4}$$

The evaluation of this expression within the integral formulation of the objective functional (5.2) should be a path integral along the trajectory

$$\int_{l(0)}^{l(t_\mathrm{f})} \Phi(z(l(t)))\ \mathrm{d}l(t),$$

where $l(t)$ is the Euclidean length of the curve $z$ at time $t$ given by

$$l(t) = \int_0^t \|\mathrm{d}_\tau z(\tau)\|_2\ \mathrm{d}\tau.$$

This results in the reparametrization

$$\mathrm{d}l(t) = \|\mathrm{D}z(t)\|_2\ \mathrm{d}t.$$

Hence, the reparametrization cancels out $\|S(z(t))\|_2$ in (5.4) such that a second choice for the criterion $\Phi$ in a notation that coincides with the general problem (5.1) with (5.2) would be

$$\Phi(z(t)) = \|J_S(z(t))\ S(z(t))\|_2^2. \tag{5.5}$$

This can be seen as minimizing the length of a trajectory in a suitable Riemannian metric. The length of a continuously differentiable curve $z$ on a Riemannian manifold is defined as the curve integral

$$L(z) = \int_z \sqrt{g_z(\mathrm{D}z(t), \mathrm{D}z(t))}\ \mathrm{d}t$$

with a scalar product $g_z$ on the tangent space of the curve in each point. The choice of $g_z(S, S) = S^\mathrm{T} J_S^\mathrm{T} J_S S$ with the symmetric positive definite (in case there are no conservations $\bar{C}$ in (5.1c)) matrix $J_S^\mathrm{T} J_S$ leads to $\sqrt{\Phi}$ as given in Equation (5.5). Therefore, the solution curve can be interpreted as a geodesic, i.e. a curve which minimizes the length of a path between two

points in a manifold. This duality of minimal velocity change and minimal length arises naturally as a minimal curvature coincides with a minimal distance that is covered and vice versa.

There are a lot more suggestions for objective functions in the optimization based model reduction approach. For example, a weighting with the Shashahani norm [146] improves the results for some example applications but also leads to numerical difficulties [105]. The local curvature defined as

$$\kappa(z) := \left\| \frac{\mathrm{D}^2 z}{\|\mathrm{D}z\|_2^2} - \left\langle \mathrm{D}z, \mathrm{D}^2 z \right\rangle_2 \frac{\mathrm{D}z}{\|\mathrm{D}z\|_2^4} \right\|_2 .$$

is tested as criterion $\Phi(z)$ in [105], too.

## 5.3 Optimization problems for model reduction

Optimization problems for model reduction of combustion models are formulated in this section.

### 5.3.1 Semi-infinite optimization problem

In [106], it is shown that the solution of (5.1) with criterion

$$\Phi(z(t)) = \|J_S(z(t))\, S(z(t))\|_2^2$$

in the objective function (5.2) identifies the SIM in case of a linear test model and in case of the nonlinear Davis–Skodje test model (see Equation (9.2)) exactly for an infinite spectral gap or for an infinite integration horizon with $t_* = t_\mathrm{f}$ and $t_0 \to -\infty$. This means, the following optimization problem should be used to reduce models of chemical combustion as discussed in Chapter 4:

$$\min_{z,T} \int_{t_0}^{t_\mathrm{f}} \Phi(z(t))\, \mathrm{d}t \tag{5.6a}$$

subject to

$$\mathrm{D}z(t) = S^\mathrm{m}(z(t), T(t)) \tag{5.6b}$$
$$\mathrm{D}T(t) = S^\mathrm{e}(z(t), T(t)) \tag{5.6c}$$
$$0 = C(z(t_*), T(t_*)) \tag{5.6d}$$
$$0 = z_j(t_*) - z_j^{t_*}, \quad j \in \mathcal{I}_\mathrm{pv} \tag{5.6e}$$
$$0 \leqslant z(t), T(t) \tag{5.6f}$$

and

$$t \in [t_0, t_\mathrm{f}] \tag{5.6g}$$
$$t_* \in [t_0, t_\mathrm{f}] \quad \text{(fixed)} \tag{5.6h}$$

with

$$\Phi(z(t)) = \| J_{S^{\mathrm{m}}}(z(t))\ S^{\mathrm{m}}(z(t)) \|_2^2,$$

where the source term of the species $S^{\mathrm{m}}$ in (5.6b) is as in Equation (4.19). The additional constraints in comparison to (5.1) are the evolution equation for the temperature in (5.6c) and function $C$ in (5.6d). The function $C$ comprises the conservation equations of elemental mass as in Equation (4.6) and a conservation of temperature, of energy as in Equation (4.8), or of enthalpy as in Equation (4.9), respectively.

### 5.3.2 Local optimization problem

It turned out in application that the computation of a solution of the dynamics (5.6b) and (5.6c) within the solution algorithm for (5.6) on the time horizon $[t_0, t_{\mathrm{f}}]$ and the computation of the derivatives needed in the optimization algorithm is very time consuming. If a solution of the optimization problem is needed *in situ* in an application, e.g. for the simulation of a reactive flow with reduced chemistry, a numerical solution of (5.6) is not computable in a reasonable time. Hence, an optimization problem replacing (5.1) is needed that is "local in time". It is (cf. [69])

$$\min_{z(t_*), T(t_*)} \quad \Phi(z(t_*)) \tag{5.7a}$$

subject to

$$0 = C(z(t_*), T(t_*)) \tag{5.7b}$$

$$0 = z_j(t_*) - z_j^{t_*}, \quad j \in \mathcal{I}_{\mathrm{pv}} \tag{5.7c}$$

$$0 \leqslant z(t_*), T(t_*) \tag{5.7d}$$

with again $\Phi(z(t_*)) = \| J_{S^{\mathrm{m}}}(z(t_*))\ S^{\mathrm{m}}(z(t_*)) \|_2^2$.

## 5.4 Existence of solutions

In [108], the authors study theoretical properties of the optimization based model reduction method as described in the sections before. It is shown that for linear (mass conservation) constraints there always exists a solution of the optimization problems (5.6) and (5.7), respectively, if there exists a feasible point.
In case of a realistic combustion model for a system in an adiabatic thermodynamic environment, the nonlinear internal energy conservation or enthalpy conservation comes into play. The proof of existence is extended to these cases, see also [148]. The following results are valid for both (5.6) and (5.7). The crucial point is the compactness of the feasible set, which is more complicated to ensure in the case of nonlinear constraints.

A simple way to guarantee compactness of the feasible set would be an upper bound for the temperature. Together with the compactness argument for the linear constraints [108], the compactness of the feasible set is obvious. But it is not evident where to choose the upper cut off for the temperature.
We avoid the cut off of the temperature and make use of the definition of the specific enthalpy via NASA polynomials. Thereby, we accept the temperature to leave the domain where the NASA polynomials approximate the standard molar enthalpy of the species appropriately.
As in Section 4.2.2, the specific enthalpy $h$ of a system is given by

$$h = \sum_{s=1}^{n_{\text{spec}}} \bar{H}_s^\circ(T)\, z_s, \tag{5.8}$$

where $n_{\text{spec}}$ is the number of chemical species in the system, see Chapter 4. That means, the phase space of the ODE system (5.6b) and (5.6c) has dimension $n_{\text{spec}} + 1$.
The equation for the specific internal energy $e$ is

$$e = h - RT \sum_{s=1}^{n_{\text{spec}}} z_s. \tag{5.9}$$

The standard molar enthalpy $\bar{H}_s^\circ(T)$ of species $s$ is a continuous function in the temperature $T$. In our case, it is computed by evaluation of the NASA polynomials. Their formula for $s = 1, \ldots, n_{\text{spec}}$ is

$$\frac{\bar{H}_s^\circ(T)}{R} = a_6 + a_1 T + \frac{a_2}{2}T^2 + \frac{a_3}{3}T^3 + \frac{a_4}{4}T^4 + \frac{a_5}{5}T^5 \tag{5.10}$$

with two sets of coefficients $a_i$, $i = 1, \ldots, 6$. One set is given for a temperature lower than a certain switch temperature $T < T_{\text{sw}}$ and one set of coefficients for high temperature $T \geqslant T_{\text{sw}}$. The two branches are connected at $T_{\text{sw}}$ at least continuously. There are upper and lower bounds for the temperature, where the polynomial approximation is valid. We ignore these bounds for the following consideration.

**Definition 5.4.1** (Proper map [109])
*Let $X$ and $Y$ be topological spaces. A map, continuous or not, $H : X \to Y$ is called* proper *if the preimage $H^{-1}(K)$ of each compact subset $K \subset Y$ is compact.*

To formulate a sufficient condition for properness, we need the notion of divergence to infinity.

**Definition 5.4.2** (Divergence to infinity [109])
*If $X$ is a topological space, a sequence $(x_\nu)$ in $X$ is said to* diverge to infinity *if for every compact set $K \subseteq X$ there are at most finitely many indices $\nu$ with element $x_\nu \in K$.*

A sufficient condition for properness is formulated in the following lemma.

**Lemma 5.4.3** (Properness condition [109])
*Suppose $X$ and $Y$ are topological spaces and $H : X \to Y$ is a continuous map. If $X$ is a second countable Hausdorff space and $H$ takes sequences diverging to infinity in $X$ to sequences diverging to infinity in $Y$, then $H$ is proper.*

*Proof.* See [109, p. 119]. □

**Lemma 5.4.4** (Properness of $h$ and $e$)
*The specific enthalpy $h$ and the specific internal energy $e$ defined via NASA polynomials seen as functions in $T$ and $z$ are proper maps.*

*Proof.* The vector space $\mathbb{R}^{n_{\text{spec}}+1}$ is a second countable Hausdorff space. Any nonconstant polynomial takes sequences diverging to infinity in $\mathbb{R}^n$, equipped with its Euclidean metric induced topology, to sequences diverging to infinity in $\mathbb{R}$. We can see $h$ and $e$ as polynomials of sixth degree in $z_s$ and $T$, see Equations (5.8), (5.9), and (5.10). Therefore, $h : \mathbb{R}^{n_{\text{spec}}+1} \to \mathbb{R}$ and $e : \mathbb{R}^{n_{\text{spec}}+1} \to \mathbb{R}$ are proper maps. □

Using this information, we can extend Lemma 2.1 for existence as stated in [108].

**Lemma 5.4.5** (Compactness of the feasible set)
*The feasible set at $t_*$*

$$\Omega = \{(\hat{z}, \hat{T}) : C(\hat{z}, \hat{T}) = 0;\ \hat{z}_j - z_j^{t_*} = 0,\ j \in \mathcal{I}_{\text{pv}};\ (\hat{z}, \hat{T}) \geqslant 0\}$$

*is compact.*

*Proof.* Case 1: isothermal combustion
Equations for mass conservation together with nonnegativity of the specific moles $\hat{z}_s$ and fixed temperature define a polytope in $\mathbb{R}^{n_{\text{spec}}+1}$ which is closed and bounded, hence (Heine–Borel theorem) compact.
Case 2: adiabatic combustion
As in the isothermal case, the variables $\hat{z}_s$ are restricted to a compact polytope due to elemental mass conservation and nonnegativity constraints. Following Lemma 5.4.4, the preimage of the singleton of the fixed energy or enthalpy, respectively, is a compact subset of $\mathbb{R}^{n_{\text{spec}}+1}$. This subset may only be further constrained by the polytope defined by the mass conservation and nonnegativity. The intersection of the two compact subsets is compact. □

**Lemma 5.4.6** (Existence of a solution)
*If the objective functional of the optimization problem* (5.6) *or* (5.7) *is a continuous function and the feasible set is not empty, there exists a solution of problem* (5.6) *or* (5.7)*, respectively.*

*Proof.* Following the argumentation in [108], the semi-infinite optimization problem (5.6) can be reduced to a finite optimization problem by construction of a continuous map $(z,T)(t_*) \mapsto \int_{t_0}^{t_f} \Phi\left(z(t)\right) \mathrm{d}t$. The feasible set $\Omega$ is compact as seen in Lemma 5.4.5. Therefore, existence follows from the Bolzano–Weierstrass theorem. □

## 5.5 Tools for analysis of the manifold

It is necessary to check if the results of the optimization problem are a sufficient approximation of a SIM. The quality of the results can depend on the selection of the reaction progress variables. A bad choice may cause that a parametrization of the SIM to be approximated is not possible. Expert knowledge of the full model in the phase space domain under consideration is needed for a good decision.

### 5.5.1 Selection of the reaction progress variables

The number and also the choice of the reaction progress variables is a difficult task. An analysis of the system dynamics can be helpful. It is based on the time scales and an analysis of the Jacobian of the right hand side of the ODE model.

#### Feasible points for analysis

A guess for a solution of the optimization problem has to be given by a user for initialization of the computations to solve the optimization problem (5.1), but this initial value might not fulfill the desired conservation laws $\bar{C} = 0$, see (5.1c). The feasibility restoration phase of the generalized Gauss–Newton method discussed in Section 7.1.3 can be used to compute a nearest point in the Euclidean distance to the initial guess which fulfills $\bar{C} = 0$ and (if necessary) has only nonnegative coordinates. This point $\bar{z}$ can be used for an *a priori* analysis.

#### Number of reaction progress variables

The number of reaction progress variables should be directly related to the time scales. The (local) time scales are

$$\tau_i = \frac{1}{\mathrm{abs}(\Re(\lambda_i))}, \quad i = 1, \ldots, n,$$

where $\lambda_i$ are the eigenvalues of the Jacobian matrix $J_S$ of the right hand side of the dynamics (5.1b) at point $\bar{z}$ in the phase space, i.e.

$$\lambda_i = \mathrm{eig}(J_S(\bar{z}))_i, \quad i = 1, \ldots, n.$$

Small time scales $\tau_i$ correspond to fast directions in the phase space whereas large time scales correspond to slow directions. There are infinite time scales corresponding to fixed states, e.g. the temperature in isothermal systems or the specific moles of inert nitrogen or argon. If the time scales are ordered by size from fast to slow $0 =: \tau_0 \leqslant \tau_1 \leqslant \cdots \leqslant \tau_n$, the differences

$$\Delta\tau_i := \tau_i - \tau_{i-1}, \quad i = 1, \ldots, n,$$

are a measure for the gap in the time scales. In face of the theoretical results shown in [108], a large spectral gap should be chosen. Hence, $n - \iota + 1$ many reaction progress variables should be selected, where $\iota$ is the index of the largest $\Delta\tau_i$. This number has to be reduced by the number of balances (e.g. mass and energy) that the system obeys. This strategy might fail in case of species with rates that change much.

### Selection of reaction progress variables

The choice which species should serve as reaction progress variables is crucial, as they should be chosen in a way that the *a priori* unknown SIM can be uniquely parametrized. Hence, the value of the reaction progress variables should de- or increase monotonously in time.
Another idea is proposed in [69]. S. S. Girimaji's analysis is motivated by the residence time of a trajectory in a volume element. A perturbation of a trajectory is interpreted as a neighboring trajectory, and the distance of the state vectors along the trajectories is analyzed in dependence of time. Let the state be denoted as $\bar{z} \in \mathbb{R}^n$ again and the ODE $\mathrm{D}z = S(z)$. It is proposed in [69] to use the value

$$\bar{\sigma}_i(\bar{z}) := \left[\sum_{s=1}^{n} \left(\frac{\partial S_i(\bar{z})}{\partial \bar{z}_s}\right)^2\right]^{\frac{1}{2}}, \quad i = 1, \ldots, n,$$

the Euclidean norm of the $i$-th row of the Jacobian of $S(\bar{z})$, as an indicator for the slowness of species $\bar{z}_i$, $i = 1, \ldots, n$. This means, the smaller $\bar{\sigma}_i(\bar{z})$ is, the better species $\bar{z}_i$ should serve as reaction progress variable. This is only valid for well-scaled systems. In this work and the related computer code, the values

$$\hat{\sigma}_i(\bar{z}) := \left[\sum_{s=1}^{n} \left(\frac{1}{\bar{z}_i}\frac{\partial S_i(\bar{z})}{\partial \bar{z}_s} - \frac{S_i(\bar{z})}{\bar{z}_i^2}\right)^2\right]^{\frac{1}{2}}, \quad i = 1, \ldots, n, \tag{5.11}$$

are used as a scaled alternative. This strategy does not guarantee for the desired monotonous behavior of the reaction progress variable, but gives a good advice, see the results in Chapter 9.

### 5.5.2 A posteriori analysis

There are several ideas for an analysis of a SIM that usually are based on the system dynamics. Many of these ideas can be used for an *a posteriori* analysis of the results computed with a model reduction method.

#### Eigenvalues and timescales

As in the analysis before, the eigenvalues of the Jacobian of the right hand side of the ODE and the real parts of their inverse values in modulus – the time scales – can be used to judge the reasonability of an approximation of a SIM. An approximation of a SIM should be acceptable for a large spectral gap for the chosen number of reaction progress variables.

#### Singular values

The singular values of the Jacobian of the source term can also serve as a check for a SIM approximation. The singular values

$$\eta_i := (\mathrm{svd}(J_S(z,T)))_i$$

are the square roots of the eigenvalues of the symmetric matrix $J_S^{\mathrm{T}} J_S$. They describe the propagation of disturbances in the different directions in the phase space. A similar gap as in the time scales should be observable.

#### Finite time Lyapunov exponents

Finite time Lyapunov exponents are used for model reduction purposes in [114, 115]. This method is similar to the method for complexity reduction described in [88]. We consider again the ODE system

$$\mathrm{D}z = S(z).$$

The linearized dynamics are

$$\mathrm{D}v = J_S(z)v, \quad v(t) \in \mathbb{R}^n.$$

This ODE describes the rate of change of a disturbance $v(t)$ in the phase space at a point $z(t)$. The combined evolution of $(z(t), v(t)) \in T_z\mathbb{R}^n$ with a point $(z_0, v_0) \in T_z\mathbb{R}^n$ as initial value at $t_0$ in the tangent space $T_z\mathbb{R}^n$ is described by

$$(z(t), v(t)) = (z(t), W(t, z_0)v_0).$$

The disturbance $v(t)$ is given by a linear transformation of the initial value $v_0$ multiplied with the sensitivity matrix

$$W(t, z_0) = \frac{\mathrm{d}z(t; z_0)}{\mathrm{d}z_0}.$$

The forward and backward finite time Lyapunov exponents at time $t_\mathrm{f}$ with initial time $t_0 = 0$ are defined as

$$\mu^+(t_\mathrm{f}, z, \bar{v}) := \frac{1}{t_\mathrm{f}} \log \frac{\|W(t_\mathrm{f}, z_0)\bar{v}\|_2}{\|\bar{v}\|_2}$$
$$\mu^-(t_\mathrm{f}, z, \bar{v}) := \frac{1}{t_\mathrm{f}} \log \frac{\|W(-t_\mathrm{f}, z_0)\bar{v}\|_2}{\|\bar{v}\|_2}.$$

Finite time Lyapunov exponents describe the averaged exponential rate of growth or decay of the disturbance $\bar{v}$. They can be computed via a singular value decomposition

$$\mu_i^+(t_\mathrm{f}, z, \bar{v}) = \frac{1}{t_\mathrm{f}} \log[\mathrm{svd}(W(t_\mathrm{f}, 0))_i].$$

K. D. Mease et al. analyze the finite time Lyapunov exponents for gaps to identify slow and fast directions. Lyapunov exponents and vectors are suitable for this task as they are independent of the current coordinate system and metric [114, 115]. We can use this information to check if there is a large gap in the finite time Lyapunov exponents for our computed solution.

### Stretching ratio

A model reduction approach which is based on stretching ratios is discussed in [2, 3, 4]. It is applied to models of explosive kinetics in [40, 68].
We consider the same ODE system as before with the differential equation for the linearized system

$$\mathrm{D}v = J_S(z)v, \quad v(t) \in \mathbb{R}^n.$$

The rate of change of the length of the disturbance $v$ is described by

$$\mathrm{D}\left(\|v\|_2^2\right) = \frac{2\langle J_S(z)v, v\rangle_2}{\|v\|_2^2}\|v\|_2^2.$$

Based on this observation, the local stretching ratio $r$ at $\bar{z} \in \mathbb{R}^n$ is defined as the ratio

$$r := \frac{\omega_\nu}{\omega_\tau}$$

of the normal stretching rate

$$\omega_\nu(\bar{z}) := \max_{\|\hat{n}\|_2=1} \langle J_S(\bar{z})\hat{n}, \hat{n}\rangle_2$$

to the tangential stretching rate

$$\omega_\tau(\bar{z}) := \langle J_S(\bar{z})\hat{S}(\bar{z}), \hat{S}(\bar{z})\rangle_2,$$

where $\hat{S} := \frac{S}{\|S\|_2}$ is the normalized right hand side. The maximum is taken over all vectors $\hat{n}$ in the normal space to the manifold in $\bar{z}$. It can be

computed with a variant of Gram–Schmidt orthogonalization. Furthermore, the corresponding time averaged values

$$\langle \omega_\tau \rangle(t_\mathrm{f}) = \tfrac{1}{t_\mathrm{f}} \int_0^{t_\mathrm{f}} \omega_\tau(z(t))\ \mathrm{d}t$$
$$\langle \omega_\nu \rangle(t_\mathrm{f}) = \tfrac{1}{t_\mathrm{f}} \int_0^{t_\mathrm{f}} \omega_\nu(z(t))\ \mathrm{d}t$$

can be used for analysis. The comparison of the stretching rates $r$ for the results of neighboring SIM point approximations can help to identify outliers.

In the Gram–Schmidt algorithm, an orthogonal decomposition of the Jacobian matrix is computed of the form $A = QR$, $A, Q, R \in \mathbb{R}^{n\times n}$, where $A$ is the Jacobian matrix to be decomposed, $Q$ is an orthogonal matrix, and $R$ is an upper triangular matrix. In the implementation, a stabilized version of the Gram–Schmidt algorithm is used as described in [70, p. 231f.]. We need the normalized first column of $A$ as first column of $Q$. Therefore, an accordingly adapted version of the algorithm is implemented.

### 5.5.3 Visual tests

"Eye inspection" can be helpful in case of test problems which consist of a low-dimensional ODE. The SIM approximation should attract nearby trajectories. This can be tested by an analysis of the course of trajectories started in the neighborhood of the results of the optimization problem.
Furthermore, a SIM approximation should be on an invariant manifold. This is of special importance if the approximation is used in an integration scheme as e.g. in [48, 134]. The invariance condition defined in [74, p. 218] is related to the consistency property defined in [105].

**Definition 5.5.1** (Consistency property [105])
*Suppose an optimal trajectory $\tilde{z}(t)$ is identified by a solution of the optimization problem (5.6) or (5.7), respectively. Take the values of the reaction progress variables $\tilde{z}_j(t_1)$, $j \in \mathcal{I}_\mathrm{pv}$, at some time $t_1 > t_*$ as new fixed parameter values $z_j(t_*^\mathrm{new})$, $j \in \mathcal{I}_\mathrm{pv}$ for the same problem (5.6) or (5.7), and solve the optimization problem again. If the condition $\hat{z}(t_*^\mathrm{new} + t) = \tilde{z}(t_* + t_1 + t)$ holds with the solution and its associated trajectory $\hat{z}(t)$ of the second optimization problem, the optimization problem with criterion $\Phi$ and its solutions $\tilde{z}(t_*)$ and $\hat{z}(t_*^\mathrm{new})$ are called consistent.*

The consistency property is illustrated in Figure 5.1. It poses a strong demand that is not *a priori* incorporated into the optimization problems (5.6) or (5.7). In general, it is not fulfilled for solutions of the optimization problems as can be seen in Chapter 9.

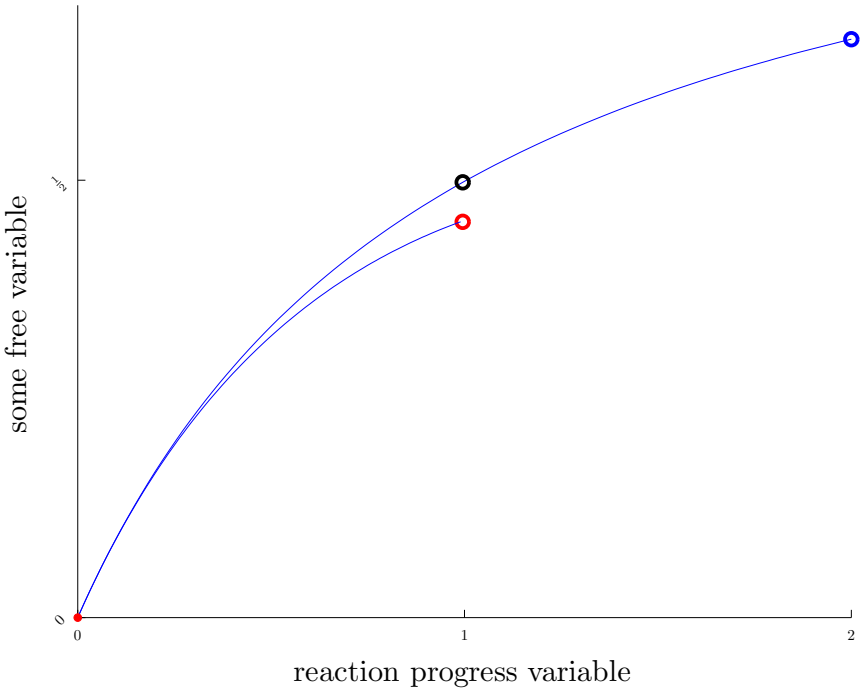


**Figure 5.1:** Illustration of the consistency property. An optimization problem of type (5.6) or (5.7) is solved for a fixed value (here: 2) for the reaction progress variable. Its solution defines the trajectory $\tilde{z}(t)$ starting from the blue circle and converging toward equilibrium (red dot in in the coordinate origin). At a later point in time $t_1 > t_*$, the progress variable is fixed to the value on the trajectory $\tilde{z}_j(t_1)$ (it is 1, here), $j \in \mathcal{I}_{\text{pv}}$, and the optimization problem is solved again. If the "new" solution trajectory (the trajectory starting at the black circle) $\hat{z}(t)$ coincides with the remaining part of the previous one, we call the objective function of optimization problem (5.6) or (5.7) and its solutions $\tilde{z}(t_*)$ and $\hat{z}(t_*^{\text{new}})$ shown as blue and black circle, respectively, consistent. Otherwise (e.g. if the second solution is as the trajectory which starts at the red circle), they are called inconsistent.

# II Numerical methods, implementation, and results

*The most likely reason for the adoption of a relatively small number of discrete intervals as the tonal material for music is that discretization or categorization is a typical, if not universal, strategy used by animals in order to reduce information overload and facilitate processing (...)*

Edward M. Burns

# 6 Solution methods for the semi-infinite optimization problem

The semi-infinite optimization problems (5.1) and (5.6) are solved numerically with a shooting or a collocation approach to obtain the results presented in Chapter 9. In this chapter, we have a look at numerical quadrature. This is the base for collocation methods. We also consider backward differentiation formulae methods that can be used in a shooting approach to compute a solution of (5.1) or (5.6), respectively.

## 6.1 Numerical quadrature

The aim of numerical quadrature is the numerical approximation of the value of a definite integral of a real-valued function $f : \mathbb{R} \to \mathbb{R}$

$$\int_a^b f(x)\,\mathrm{d}x. \tag{6.1}$$

with $a, b \in \mathbb{R}$. In the following, we follow the presentation in [155].

### 6.1.1 Newton–Cotes quadrature

The Newton–Cotes formulae can be obtained by replacing the integrand $f$ in (6.1) by a polynomial $P(x)$. Consider an equidistant partition of the interval $[a, b]$ with the nodes

$$x_i = a + jh, \quad j = 0, \ldots, n,$$

step length $h = \frac{b-a}{n}$, and the number of sub-intervals $0 < n \in \mathbb{N}$. Let $P_n$ be the interpolating polynomial of degree $n$ or less which adopts the values of $f$ at $x_j$ exactly

$$P_n(x_j) = f(x_j), \quad j = 0, \ldots, n.$$

The Lagrange interpolation formula gives

$$P_n(x) = \sum_{j=0}^{n} f(x_j) L_j(x), \quad L_j(x) = \prod_{k=0,\, k\neq j}^{n} \frac{x - x_k}{x_j - x_k}.$$

With an affine parameter shift to $t$ defined as $x = a + ht$, we have

$$L_j(x) = \phi_j(t) := \prod_{k=0,\, k\neq j}^{n} \frac{t-k}{j-k}.$$

This means

$$\begin{aligned}\int_a^b P_n(x)\,\mathrm{d}x &= \sum_{j=0}^{n} f(x_j) \int_a^b L_j(x)\,\mathrm{d}x \\ &= h \sum_{j=0}^{n} f(x_j) \int_0^n \phi_j(t)\,\mathrm{d}t \\ &= h \sum_{j=0}^{n} f(x_j) w_j\end{aligned}$$

with the weights

$$w_j := \int_0^n \phi_j(t)\,\mathrm{d}t.$$

These weights only depend on $n$, are tabulated, and are suitable for numerical quadrature up to $n = 6$ [155, p. 148].

### 6.1.2 Gaussian and Radau quadrature

Gaussian quadrature not only allows for freely chosen weights, but also the grid of nodes $x_j$ on which the function $f$ has to be evaluated is not necessarily equidistant.
The general problem in case of Gaussian quadrature methods is the evaluation of an integral of the real-valued function $f : \mathbb{R} \to \mathbb{R}$

$$I(f) = \int_a^b \omega(x) f(x)\,\mathrm{d}x$$

with a nonnegative weight function $\omega$ on the interval $[a, b]$, where the bounds can be infinite. The weight function must be measurable on $[a, b]$; all its moments $\int_a^b x^k \omega(x)\mathrm{d}x$ (for all $k = 0, 1, \ldots$) must exist and be finite. For any

polynomial $s(x)$ which is nonnegative on $[a, b]$, relation $\int_a^b \omega(x)s(x)\mathrm{d}x = 0$ has to imply $s \equiv 0$.
The integration formula is supposed to have the form

$$\tilde{I}(f) = \sum_{i=1}^{n} w_i f(x_i)$$

where the weights $w_i$ as well as the nodes/abscissas $x_i$ have to be determined. In general, these are constructed via orthogonal polynomials. This allows for an exact numerical integration of polynomials of maximum possible degree. The values of $x_i$ and $w_i$ are tabulated e.g. in [1].
Radau quadrature is a Gaussian quadrature, where $\omega \equiv 1$ is chosen for the weighting function and Legendre polynomials as orthogonal polynomials on the finite interval are used. One abscissa is fixed at one end of the interval, i.e. $x_0 = a$. This reduces the order of the method but is beneficial if the value $f(a)$ is needed as well.
The values of the weights and abscissas for Radau quadrature are given in the tables in the next section, taken from [46]. The values given there correspond to the integration interval $[a, b] = [0, 1]$.

## 6.2 Numerical solution of ODE systems

The ODE system which describes the dynamics of the model, e.g. in (5.6b) and (5.6c), has to be solved for computing a solution of the optimization problem (5.6). Therefore, methods for computing a numerical solution of ODE systems are presented here. The time scale separation which is supposed to be exploited in model reduction methods (see Section 2.2.1) leads to the phenomenon of *stiffness* in the context of numerical solution methods for ODE. There are fast components in the solution of the ODE that correspond to large eigenvalues of the Jacobian of the right hand side, and there are slow components that correspond to small eigenvalues. Hence, only implicit methods are suitable. We restrict ourselves to a presentation of collocation methods and differentiation methods based on backward differentiation formulae (BDF).

### 6.2.1 Collocation methods

Collocation methods are described e.g. in [15] and [46], where the following presentation is taken from. We consider the autonomous scalar ODE

$$\mathrm{D}z = S(z) \tag{6.2}$$

with $S : \mathbb{R} \to \mathbb{R}$ sufficiently smooth for simplicity. We want to compute a solution $z : \mathbb{R} \to \mathbb{R}$ of the ODE with initial value $z(t_0) = a$ in the sense

of an IVP on the time horizon $[t_0, t_\mathrm{f}]$. The interval is partitioned with an equidistant grid $t_0 < t_1 < \cdots < t_K = t_\mathrm{f}$ into $K$ subintervals $[t_j, t_{j+1}]$, $t_{j+1} - t_j = h$. In a collocation method, a function $p$ is constructed which fulfills the ODE in $k$ nodes $c_i$, $i = 1, \ldots, k$ on each subinterval $[t_j, t_{j+1}]$. In general, a polynomial of degree at most $k$ is used. On each subinterval $j = 1, \ldots, K$, $k + 1$ conditions

$$\begin{aligned} p(t_{j-1}) &= z(t_{j-1}) \\ \mathrm{D}p(t_{j-1} + hc_i) &= S(p(t_{j-1} + hc_i)), \quad i = 1, \ldots, k \end{aligned}$$

are required. Usually, $0 \leqslant c_1 \leqslant \cdots \leqslant c_k \leqslant 1$ are chosen. The polynomials are connected at the ends of the subintervals $t_j$ via a matching condition

$$p(t_j) = z(t_j), \quad j = 1, \ldots, K - 1.$$

The initial value $z(t_0) = a$ is required at the first subinterval.
This results in an $s$-stage implicit Runge–Kutta formula [46]. It can be written as

$$p(t_{j-1} + hc_i) = z(t_{j-1}) + h \sum_{l=1}^{k} a_{il} k_l, \quad i = 1, \ldots, s$$

with the coefficients

$$k_i = S\left( z(t_{j-1}) + h \sum_{l=1}^{s} a_{il} k_l \right), \quad i = 1, \ldots, s.$$

The value of the approximated solution at the ends of the subintervals are

$$p(t_{j-1} + h) = z(t_{j-1}) + h \sum_{l=1}^{s} b_l k_l,$$

where the values of $b_i$, $i = 1, \ldots, s$, are computed as integrals of Lagrangian polynomials.
The equivalence of collocation and Runge–Kutta methods (see [46]) allows to write the coefficients of collocation methods in form of a Butcher tableau as in Table 6.1, where the implicit Euler method is shown that corresponds to the Gauss(–Radau) collocation method of first order. The coefficients $a_{ij}$ are given in the top right. The abscissas are in the left column and the weights in the row at the bottom. The order of a collocation method is the order of the quadrature method, that the corresponding Runge–Kutta method is based on.
Gaussian collocation methods based on Gaussian quadrature are of highest order. These are also A-stable (see [46, p. 242] for the definition of A-stability). In this work, we consider highly stiff systems. Therefore, we

**Table 6.1:** Butcher tableau for the Radau collocation method of order 1. In the left column are the abscissas; at the bottom are the weights; at the top right are the zeros ($a_{il}$) of Lagrangian polynomials [46].

| | |
|---|---|
| 1 | 1 |
| | 1 |

**Table 6.2:** Butcher tableau for the Radau collocation method of order 3 arranged in the same manner as Table 6.1 [46].

| | | |
|---|---|---|
| $\frac{1}{3}$ | $\frac{5}{12}$ | $\frac{-1}{12}$ |
| 1 | $\frac{3}{4}$ | $\frac{1}{4}$ |
| | $\frac{3}{4}$ | $\frac{1}{4}$ |

prefer Gauss–Radau collocation methods as they "have stiff decay" and "are particularly suitable for the solution of stiff initial value ODEs" [15]. Coefficients for three L-stable (see again [46, p. 249] for the concise definition of L-stability) Gauss–Radau methods of order 1, 3, and 5 are given in Tables 6.1, 6.2, and 6.3, respectively, as used in our implementation.

We assume that the manifolds we approximate are exponentially attractive in the sense of Definition 2.1.16. Therefore, it can be helpful not to use an equidistant partitioning of the interval $[t_0, t_\mathrm{f}]$ but to enlarge the size of the subintervals exponentially. In order to achieve this, a factor is implemented by which the subinterval $[t_i, t_{i+1}]$ is larger than the preceding subinterval $[t_{i-1}, t_i]$, $i = 1, \ldots, K-1$. This means, it is possible to concentrate many collocation points in the beginning of the time interval, where the relaxation phase to the SIM occurs. Less points are sufficient in the latter part of the trajectory piece which is assumed to be relaxed onto the SIM. In this way, it is possible to reduce the number of collocation points. However, this factor

**Table 6.3:** Butcher tableau for the Radau collocation method of order 5 arranged in the same manner as Table 6.1 [46].

| | | | |
|---|---|---|---|
| $\frac{4-\sqrt{6}}{10}$ | $\frac{88-7\sqrt{6}}{360}$ | $\frac{296-169\sqrt{6}}{1800}$ | $\frac{-2+3\sqrt{6}}{225}$ |
| $\frac{4+\sqrt{6}}{10}$ | $\frac{296+169\sqrt{6}}{1800}$ | $\frac{88+7\sqrt{6}}{360}$ | $\frac{-2-3\sqrt{6}}{225}$ |
| 1 | $\frac{16-\sqrt{6}}{36}$ | $\frac{16+\sqrt{6}}{36}$ | $\frac{1}{9}$ |
| | $\frac{16-\sqrt{6}}{36}$ | $\frac{16+\sqrt{6}}{36}$ | $\frac{1}{9}$ |

should be handled with care as it has an exponential effect.

### 6.2.2 Backward differentiation formulae methods

Other popular methods for the numerical solution of stiff ODE systems are methods based on BDF. These integration methods are a special type of linear multistep methods for the solution of ODE, where the right hand side of the ODE system is only evaluated at the end point of the current step interval in each step [15, 41].
We consider again ODE (6.2). A number of $R$ values $z_i^h \in \mathbb{R}$ are computed, $i = 1, \ldots, R$, e.g. with a starting procedure, that approximate the solution $z(t_i)$ of (6.2) at $t_i$. In a BDF method, a polynomial is constructed which interpolates the last computed values $z_i^h$, $i = 1, \ldots, R$ for the fixed number $R$. Additionally, the polynomial has to fulfill the ODE at a new point $t_n \in \mathbb{R}$. This $R$ step method has (consistency) order $R$. It can be written for (6.2) as [15]

$$\sum_{j=0}^{R} \gamma_j \, z_{n-j}^h = h \, \beta_0 \, S(z_n^h)$$

with coefficients $\gamma_j$, $j = 0, \ldots, R$, $\beta_0$, and step size $h$. These methods are implicit as $\beta_0 \neq 0$ and solved with Newton's method or variants of it. BDF methods are 0-stable up to order 6 and A($\alpha$) stable, where the value of the angle $\alpha$ depends on the order $R$.
More information can be found e.g. in [15, 82]. The implementation of D. Skanda [151] is used for a part of the results presented in Chapter 9.

## 6.3 Numerical solution methods for semi-infinite optimization problems

In this section, methods for solving the semi-infinite optimization problem (5.6) numerically (and (5.1) analogously) are compared, which are used in this work: single shooting, also called sequential approach, and collocation, also called simultaneous approach. Multiple shooting is a hybrid approach between sequential and simultaneous. We use multiple shooting only in form of a double shooting.

#### Single shooting

The solution method to solve (5.6b) and (5.6c) and the solution method to solve the optimization problem (5.6) are decoupled in the sequential – in optimal control called *direct single shooting* – approach. The initial values $(z(t_0), T(t_0))$ are used as optimization variables. Starting at $t_0$, the ODE system is integrated with an integration scheme. In our case of stiff ODE

systems, a stiff ODE solver based on BDF methods is used. The integrand in the objective function formulated as a Lagrange term, see Section 3.1.1, is integrated itself. The value at the end point $t_\mathrm{f}$ is evaluated in form of a Mayer term objective functional.
The resulting nonlinear programming (NLP) problem is solved independently. Derivatives required in the algorithm for solving the NLP problem are computed by the ODE solver, e.g. via an internal numerical differentiation (IND) scheme [22, 23].
It can be stated that the single shooting method is very effective in the cases $t_* = t_0$ and $t_* = t_\mathrm{f}$ in problem (5.6) in case of stable ODE systems (5.6b) and (5.6c); see the results in Chapter 9.

### Collocation

Often, especially in case of instable or extremely stiff systems, it is beneficial to use an all-at-once approach to solve (5.6). In this simultaneous approach, the methods to solve the ODE system and to solve the optimization problem are coupled. The state profiles are fully discretized "in time using collocation of finite elements" [21].
As described in Section 6.2.1, polynomials are constructed for each state $z_s$, $T$ with $s = 1, \ldots, n_\mathrm{spec}$ on each sub-interval $[t_j, t_{j+1}]$, $j = 1, \ldots, K$ that fulfill (5.6b) and (5.6c) at the collocation points. All state variables at all collocation points are used as optimization variables in the NLP problem. The Lagrange term objective function is evaluated with the Gauss–Radau quadrature of corresponding order.
Kameswaran and Biegler analyze convergence rates for Gauss–Radau collocation in application to optimal control problems in [87]. Their results are applicable in the cases considered here by omitting the control variables.

### Multiple shooting

Multiple shooting is a hybrid approach combining the benefits of the sequential and the simultaneous approach. It is very useful for instable and stiff systems of ODE in the constraints. It is used to solve boundary value problems e.g. in [94] and to solve optimal control problems in [29, 128].
The interval $[t_0, t_\mathrm{f}]$ is split into subintervals $[t_j, t_{j+1}]$, $j = 0, \ldots, M-1$, that are usually larger than in case of the collocation approach described before. The initial value problem to solve the ODE constraints (5.6b) and (5.6c) with initial values $z(t_0)$, $T(t_0)$ is decomposed into $M$ independent initial value problems on the subintervals. We consider the scalar ODE (6.2) again. On each subinterval $[t_j, t_{j+1}]$, $j = 0, \ldots, M-1$, the problem

$$\begin{aligned} \mathrm{D}z_j(t) &= S(z_j(t)) \\ z_j(t_j) &= s_j \end{aligned}$$

is solved with $s_j \in \mathbb{R}$. Continuity of the solution is assured by matching conditions

$$s_{j+1} = z_j(t_{j+1}; s_i), \quad j = 0, \ldots, M-1$$

with $s_0 = a$. These conditions are additional constraints in the resulting NLP problem. This NLP problem has more degrees of freedom and in general is large in comparison to the resulting NLP problem in the single shooting approach, but sophisticated condensing strategies can be applied [24].
For the solution of the optimization problem (5.6) in case of $t_* \in (t_0, t_\mathrm{f})$, we divide the interval into the two sub-intervals $[t_0, t_*]$ and $[t_*, t_\mathrm{f}]$ and apply one matching condition. A solution method for the resulting NLP problem is discussed in the next chapter.

*People optimize.*

Jorge Nocedal and
Stephen J. Wright

# 7

# Numerical methods for nonlinear programming problems

In this chapter, numerical methods for the solution of nonlinear programming (NLP) problems are considered. We start with generalized Gauss–Newton methods for the computation of the solution of problem (5.7). We prefer interior point (IP) methods to solve (5.6) after suitable discretization with a collocation method or in a shooting approach.

For results of an application of the presented methods, see Chapter 9. We mainly adopt the notation of [124].

## 7.1 Generalized Gauss–Newton method

Generalized Gauss–Newton (GGN) methods can be used to solve the optimization problem (5.7). GGN methods are often used to compute a numerical solution of constrained least squares problems which typically have to be solved in parameter estimation problems.

The presentation in this section mainly consists of content of [24] and the lectures [25] and [27] by H. G. Bock as taught in winter term 2006 and summer term 2007 at the University of Heidelberg. This section further includes the filter method as described in [167, 168] and some ideas from [57].

### 7.1.1 Basic solution method

We consider constrained nonlinear least squares (CNLLS) problems of the form

$$\min_{x\in\mathbb{R}^n} \ \tfrac{1}{2}\|F_1(x)\|_2^2 \tag{7.1a}$$

subject to

$$F_2(x) = 0 \tag{7.1b}$$
$$F_3(x) \geqslant 0, \tag{7.1c}$$

where the functions $F_i : D \to \mathbb{R}^{n_i},\ i = 1, 2, 3$, are supposed to be at least twice continuously differentiable in a domain $D \subset \mathbb{R}^n$. The problem is solved iteratively with the iterates $x_{k+1} = x_k + t_k d_k$, where $d_k \in \mathbb{R}^n$ is the increment and $t_k \in (0, 1]$ the step length. Let us first assume a full step method (which means that $t_k = 1$ for all $k$).

#### Linearization

The increment $d_k \in \mathbb{R}^n$ is computed as the solution of the linearization of problem (7.1), which itself is a constrained linearized least squares (CLLS) problem

$$\min_{d\in\mathbb{R}^n} \ \tfrac{1}{2}\|F_1(x_k) + J_1(x_k)d\|_2^2 \tag{7.2a}$$

subject to

$$F_2(x_k) + J_2(x_k)d = 0 \tag{7.2b}$$
$$F_3(x_k) + J_3(x_k)d \geqslant 0, \tag{7.2c}$$

where $J_i$ is the Jacobian matrix of $F_i$ for $i = 1, 2, 3$.

**Lemma 7.1.1** (Lemma 3.1.18 in [24])
*The point $(x^*, \lambda_1^*, \lambda_2^*)$ is a KKT point of the CNLLS problem (7.1) if and only if the point $(0, \lambda_1^*, \lambda_2^*)$ is a KKT point of the CLLS problem (7.2) at $x_k = x^*$.*

*Proof.* See [24]. □

We assume that LICQ, second order sufficient optimality conditions, and strict complementarity are valid at the solution of the optimization problems. Hence, the active set in a neighborhood of the solution does not change. We omit inequality constraints which can be treated with an active set strategy in the further discussion of local convergence: Active inequality constraints are considered as equality constraints; inactive inequality constraints are neglected.
We make the assumption that LICQ is fulfilled and $J_1^{\mathrm{T}} J_1$ is positive definite on the kernel of $J_2$ in the iterate $x_k$. Thus, there exists a solution operator

$J^+(x_k) : \mathbb{R}^{n_1+n_2} \to \mathbb{R}^n$ for the equality constrained problem (7.2a) subject to (7.2b) such that $d = J^+F$ with $F^{\mathrm{T}} := (F_1^{\mathrm{T}}, F_2^{\mathrm{T}})$ [24]. This $J^+$ is a generalized inverse for

$$J := \begin{bmatrix} J_1 \\ J_2 \end{bmatrix},$$

i.e. $J^+JJ^+ = J^+$. Its explicit form is given by

$$J^+ = \begin{bmatrix} I_n & 0_{n_2} \end{bmatrix} \begin{bmatrix} J_1^{\mathrm{T}} J_1 & J_2^{\mathrm{T}} \\ J_2 & 0 \end{bmatrix}^{-1} \begin{bmatrix} J_1^{\mathrm{T}} & 0 \\ 0 & I_{n_2} \end{bmatrix},$$

where $I_n$ is the unit matrix of dimension $n$. In case of an unconstrained optimization problem, $J^+$ reduces to the Moore-Penrose pseudo inverse $J^\dagger$. The theory of CNLLS problems is studied extensively in [24].

### Solution method

In order to solve the CLLS problem (7.2), we use the following strategy as proposed by Stoer in 1971 [25, 154]. The argument $x_k$ is omitted in the following presentation for a clear notation. This method is chosen because it does not require positive definiteness of $J_1^{\mathrm{T}} J_1$ on the null space of $J_2$ in every iterate.

**Remark 7.1.2**
In the optimization problems considered in this thesis, LICQ is always fulfilled by mass and energy balances in the constraints. This can be seen via Equation (4.6) if we assume that there are no two chemical elements that can be found in every chemical species at the same amount, i.e.*

$$\forall (i,j),\ i \neq j,\ i,j \in \{1,\dots,n_{\mathrm{elem}}\}\ \exists s \in \{1,\dots,n_{\mathrm{spec}}\} : \chi_{i,s} \neq \chi_{j,s}.$$

All chemical species and the temperature make a contribution to the value of the internal energy and enthalpy as can be seen in Equations (4.8) and (4.9). These arguments ensure that LICQ holds.

First, the Jacobian matrix of the constraints is decomposed in the form $J_2 = LQ$ with a lower triangular matrix $L$ and an orthogonal matrix $Q$. In our code, we use the `LAPACK` routine `dgeqrf.f`, which is an implementation of efficient Householder transformations. With the matrix $Q$, the Jacobian matrix $J_1$ of $F_1$ is transformed to $J_1 = [A_1\ A_2]Q$. We denote the triangular matrix as $L = [\tilde{L}\ 0]$. The composed Jacobian matrix $J$ can be written as

$$J = \begin{bmatrix} J_1 \\ J_2 \end{bmatrix} = \begin{bmatrix} A_1 & A_2 \\ \tilde{L} & 0 \end{bmatrix} Q.$$

*See Chapter 4 and Section B.2 for the notation.

The transformed vector increment $\tilde{d}$ is defined as $\tilde{d} = Qd$. It can be split into $\tilde{d}^{\mathrm{T}} = (\tilde{d}_1^{\mathrm{T}}\ \tilde{d}_2^{\mathrm{T}})$ with $\tilde{d}_1 \in \mathbb{R}^{n_2}$ and $\tilde{d}_2 \in \mathbb{R}^{n_1-n_2}$. The equality constraint (7.2b) allows to compute $\tilde{d}_1$ via

$$F_2 + \tilde{L}\tilde{d}_1 = 0.$$

The remaining unknown $\tilde{d}_2$ is the solution of the unconstrained least squares problem

$$\min_{\tilde{d}_2}\ \tfrac{1}{2}\|F_1 + A_1\tilde{d}_1 + A_2\tilde{d}_2\|_2^2.$$

There are several strategies to solve this. In our implementation, we use the `LAPACK` routine `dgelsy.f` based on a QR decomposition. Finally, the increment $d$ is given as $d = Q^{\mathrm{T}}\tilde{d}$.
The Lagrange multipliers $\lambda = \lambda(x_k)$ are needed together with the current iterate, e.g. for an evaluation of a merit function or within an active set strategy. The formula for a root of the gradient of the Lagrangian function (of the CLLS problem) is

$$J_1^{\mathrm{T}}J_1 d + J_1^{\mathrm{T}}F_1 = J_2^{\mathrm{T}}\lambda.$$

The residuum is defined as $R_1 := F_1 + J_1 d$. The resulting equation

$$J_2^{\mathrm{T}}\lambda = Q^{\mathrm{T}}L^{\mathrm{T}}\lambda = J_1^{\mathrm{T}}R_1$$

can be solved directly with the decomposed $J_2$.

### 7.1.2 Local convergence

In [24], a local contraction theorem is shown. It guarantees a well-defined iteration, convergence to the solution, a linear rate of convergence, and gives an *a priori* estimate for the distance of the iterates to the solution.

**Theorem 7.1.3** (Bock's local contraction theorem [24])
*Let $D$ be a region, $F : D \to \mathbb{R}^{n_1+n_2}$, $F = (F_1^{\mathrm{T}}, F_2^{\mathrm{T}})^{\mathrm{T}} \in \mathcal{C}^1(D)$, $J$ the derivative of $F$, and $J^+$ the corresponding generalized inverse. Let furthermore for all $x, y \in D$, $t \in [0,1]$ with $y - x = -J^+(x)F(x)$ and initial value $x_0 \in D$ the conditions*

(1) $\|J(y)^+(J(x + t(y-x)) - J(x))(y-x)\|_2 \leqslant \omega t\|y-x\|_2^2$
*with $\omega < \infty$*

(2) $\|(J(y)^+ - J(x)^+)R(x)\|_2 \leqslant \kappa(x)\|y-x\|_2$
*with $R(x) = F(x) - J(x)J(x)^+F(x)$ and $\kappa(x) \leqslant \kappa < 1$*

(3) $\delta_0 = \kappa + \frac{\omega}{2}\|\Delta x_0\|_2 < 1$
*with $\delta_k := \kappa + \frac{\omega}{2}\|\Delta x_k\|_2 < 1$ and $\Delta x_k := -J(x_k)^+F(x_k)$*

(4) $D_0 := \left\{ z \;\middle|\; \|z - x_0\|_2 \leqslant \frac{\|\Delta x_0\|_2}{1-\delta_0} \right\} \subset D$

*be fulfilled. Then it holds:*

(i) *The iteration* $x_{k+1} = x_k + \Delta x_k$ *is well defined and remains in* $D_0$.

(ii) *There exists an* $x^* \in D_0$ *with* $x_k \to x^*$ *for* $k \to \infty$.

(iii) *There is an* a priori *estimate* $\|x_{k+j} - x^*\|_2 \leqslant \frac{\|\Delta x_k\|_2}{1-\delta_k} \delta_k^j$.

(iv) *The rate of convergence is linear with*

$$\|\Delta x_{k+1}\|_2 \leqslant \delta_k \|\Delta x_k\|_2 = \kappa \|\Delta x_k\|_2 + \tfrac{\omega}{2} \|\Delta x_k\|_2^2.$$

*Proof.* See [24]. □

The meaning of the two Lipschitz constants $\omega$ and $\kappa$ is discussed in [24], too.

#### Curvature

In our case, the function $F$ is $\mathcal{C}^\infty$ in the compact feasible domain (the realizable composition space with its boundary). Hence, the existence of an $\omega < \infty$ under optimality conditions can be proven. The value of $\omega$ can be understood as a measure for the nonlinearity of the model. Its inverse $\omega^{-1}$ characterizes the region, where the linear approximation of $F$ is sufficiently good [24].

#### Incompatibility

The constant $\kappa$ is called *incompatibility constant*. Existence of a finite $\kappa$ can be guaranteed by a similar argumentation as in case of $\omega$. However, it is important that $\kappa < 1$. This is the case for a small residuum $R(x^*)$ [25]. In case of so called *large residual solutions*, the GGN full step method does not necessarily converge, but global convergence can be achieved with e.g. a line search method based on a merit function, see Section 7.1.3.

### 7.1.3 Global convergence

In case the initial guess $x_0$ is not in the local contraction region of the GGN method, a globalization strategy has to be used. This can be based on a trust region, a merit function, a filter, or the restrictive monotonicity test [28, 124], which are all restrictions to the step size $t_k$ in the iteration $x_{k+1} = x_k + t_k d_k$.

### Merit function

Merit functions find a compromise between the desire to minimize the objective function and to fulfill the constraints. A line search is performed in direction of the increment $d$ to find a minimum of the merit function.
In our implementation, the $\ell_1$ penalty function is used as merit function. It is defined in the current context as

$$\ell_1(x) = \tfrac{1}{2}\|F_1(x)\|_2^2 + \sum_{i=1}^{n_2} \alpha_i |F_{2,i}(x)| + \sum_{j=1}^{n_3} \beta_j |\min\{0, F_{3,j}(x)\}|$$

with the penalty parameter vectors $\alpha \in \mathbb{R}^{n_2}$, $\beta \in \mathbb{R}^{n_3}$. In some publications, the authors propose to use a fixed $\alpha_i = \beta_j = \tau \in \mathbb{R}$ for all $i, j$. This is an exact merit function (i.e. a minimum $x^*$ of $\ell_1$ is also a minimum of the corresponding CNLLS problem) if $\alpha_i > |\lambda_i^*|$ with the Lagrange multipliers $\lambda_i^*$ at the solution for all $i = 1, \ldots, n_2$ and the same condition holds for $\beta_j$ with the corresponding multipliers $\mu_j$, $j = 1, \ldots, n_3$. The directional derivative of $\ell_1(x)$ in direction of the increment $d$ is given by

$$\begin{aligned}\partial_d \ell_1(x, d) = F_1(x)J_1(x)d + &\sum_{F_{2,i}(x)>0} \alpha_i J_{2,i}(x)d \\ - &\sum_{F_{2,i}(x)<0} \alpha_i J_{2,i}(x)d + \sum_{F_{2,i}(x)=0} \alpha_i |J_{2,i}(x)d| \\ - &\sum_{F_{3,i}(x)<0} \beta_i J_{3,i}(x)d + \sum_{F_{3,i}(x)=0} \beta_i \min\{0, J_{3,i}(x)d\}\end{aligned}$$

with $J_{j,i}(x)$ the derivative of the $i$-th component function of $F_j(x)$, $j = 2, 3$ [26].
As the Lagrange multipliers at the solution $\lambda_i^*$ are unknown during the iterations, they have to be estimated. Two different strategies are implemented. The maximum strategy uses the maximum absolute value of the current Lagrange multipliers $\lambda_j^k$ as proposed in [124] increased by a small parameter $\epsilon$ (and the same for $\beta_i^k$ with the corresponding multipliers $\mu_i$)

$$\alpha_i^k = \max_{j=1,\ldots,n_2} (|\lambda_j^k|) + \epsilon, \quad i = 1, \ldots, n_2.$$

The second, "inheritance" based version includes also the old values $\alpha_i^{k-1}$ of the last iteration [26]

$$\alpha_i^k = \max\{|\lambda_i^k|, \tfrac{1}{2}(|\lambda_i^k| + \alpha_i^{k-1})\} + \epsilon, \quad i = 1, \ldots, n_2,$$

and analogously for $\beta_i^k$.
The line search is implemented with an Armijo-type condition [14] with backtracking. In both cases for the choice of $\alpha_i^k$ and $\beta_i^k$, the line search condition very often only accepts small step sizes in praxis in our experience.

### Second order correction

Many algorithms employing a step size strategy for globalization of convergence suffer from the Maratos effect: As described before, the goal of the merit function is to find a trade off between the minimization of the objective function and the violation of the constraints. It can occur that the constraint violation is penalized too sharply. A temporary violation could improve the progress of the algorithm. Different strategies are possible to overcome this effect.
In a *watch dog strategy*, a small fixed number of full step iterations are performed. The progress of the algorithm is analyzed, and it is decided if the full steps are acceptable or a reduced step size is preferable.
Another strategy to prevent the Maratos effect is a second order correction (SOC). The SOC increment is defined as [124]

$$\hat{d} := -J_2(x)^{\mathrm{T}}(J_2(x)J_2(x)^{\mathrm{T}})^{-1}F_2(x+d),$$

where we omit the index $k$ of the iterates.
In the current context, the following interpretation from [124] is adequate. Assume the full step with increment $d$ causes a large violation of the constraint $F_2$. We want to reduce this in another correction step, which means

$$F_2(x+d+\hat{d}) = 0.$$

We linearize the expression around the full step $x+d$. This leads to

$$F_2(x+d+\hat{d}) \doteq F_2(x+d) + J_2(x+d)\hat{d}.$$

As this is an underdetermined system, we use a minimal norm formulation

$$\min_{\check{d}} \ \|\check{d}\|_2^2 \tag{7.3a}$$

subject to

$$F_2(x+d) + J_2(x+d)\check{d} = 0. \tag{7.3b}$$

This calls for a new evaluation of the constraints $F_2$ and the Jacobian matrix $J_2$. Since $J_2(x)$ is already decomposed, see Section 7.1.1, we assume that $J_2(x+d) \doteq J_2(x)$ in problem (7.3)[†].

[†]In our application, the nonconstant entries of $J_2$ are given as (see Chapter 4 for the notation)

$$\frac{\mathrm{d}}{\mathrm{d}T}\left(\sum_{s=1}^{n_{\mathrm{spec}}} \bar{H}_s^\circ\, z_s - \frac{RT}{\bar{M}}\right) = \sum_{s=1}^{n_{\mathrm{spec}}} \bar{C}_{p,s}^\circ\, z_s - R\sum_{s=1}^{n_{\mathrm{spec}}} z_s$$
$$\frac{\mathrm{d}}{\mathrm{d}z_i}\left(\sum_{s=1}^{n_{\mathrm{spec}}} \bar{H}_s^\circ\, z_s - \frac{RT}{\bar{M}}\right) = \bar{H}_i^\circ - RT, \quad i = 1,\ldots,n_{\mathrm{spec}}$$

for isoenergetic systems, see also Equation (4.8). In case of isenthalpic systems, the subtrahends in the two formulae fall away, cf. Equation (4.9).

The solution of the resulting problem

$$\min_{\check{d}} \ \|\check{d}\|_2^2$$

subject to

$$F_2(x+d) + J_2(x)\check{d} = 0$$

is [19]

$$\hat{d} = -J_2(x)^{\mathrm{T}}(J_2(x)J_2(x)^{\mathrm{T}})^{-1}F_2(x+d).$$

We can recycle the decomposition $J_2(x) = LQ$ and $L = [\tilde{L}\ 0]$ from Section 7.1.1 such that $\hat{d}$ is computed as

$$\begin{aligned}\hat{d} &= -J_2(x)^{\mathrm{T}}(LL^{\mathrm{T}})^{-1}F_2(x+d)\\ &= -J_2(x)^{\mathrm{T}}\tilde{L}^{-\mathrm{T}}\tilde{L}^{-1}F_2(x+d).\end{aligned}$$

### Filter method

In our experience, the merit function approach restricts the step size $t_k$ too much in our application. The SOC strategy described in the section before yields no reasonable improvement in our application, too. Hence, a modern filter approach is used as an alternative to the merit function.
Filter approaches are proposed in [57] as a globalization strategy for a sequential quadratic programming (SQP) [129] trust region algorithm. Global convergence results for this method are shown in [58]. Global convergence for a filter method combined with interior point methods is shown in [160]. In [167], a filter method is presented which is applicable for globalization of sequential quadratic programming or interior point frameworks, and global convergence is proven. The filter approach that we use for globalization of the GGN method is an implementation similar to the filter used in `Ipopt` [167, 168].
The basic idea of a filter method is that the optimization problem is treated as a bi-objective problem: minimize the constraint violation and minimize the objective function. So a step is accepted when it reduces the constraint violation or the objective function. It is clear that there should be an equilibration between the two "objectives" in such a way that a reduction in the constraint violation is favorable to a reduction in the objective function.
The infeasibility measure is defined via

$$\Theta(x) := \sum_{i=1}^{n_2} |F_{2,i}(x)| + \sum_{i=1}^{n_3} |\min\{0, F_{3,i}(x)\}|,$$

similar as in [57], and

$$f(x) := \tfrac{1}{2}\|F_1(x)\|_2^2$$

is a short notation for the least squares objective function. As in the original publication [167], we accept a step length $t_k$ for the step $x_k + t_k d_k$ if it provides sufficient reduction in comparison to the current iterate $x_k$, i.e. if

$$\Theta(x_k + t_k d_k) \leqslant (1 - \gamma_\Theta)\Theta(x_k) \tag{7.5a}$$

or

$$f(x_k + t_k d_k) \leqslant f(x_k) - \gamma_f \Theta(x_k) \tag{7.5b}$$

with the two small parameters $\gamma_\Theta$ and $\gamma_f$, for which in the implementation $10^{-5}$ is taken.
As stated in [167], this could lead to a feasible but nonoptimal point, as these conditions are based on the infeasibility measure in the current iterate. Therefore, a so-called *f-type switching condition* is introduced [168]

$$f_x(x_k)d_k < 0 \quad \text{and} \quad t_k(-f_x(x_k)d_k)^{s_f} > \delta(\Theta(x_k))^{s_\Theta} \tag{7.6}$$

with the partial derivative

$$f_x(x_k) = F_1(x_k)J_1(x_k)$$

and constants for which the same values are used as in `Ipopt` [168], namely $\delta = 1$, $s_f = 2.3$, and $s_\Theta = 1.1$. If condition (7.6) holds and $\Theta(x_k)$ is smaller than a certain threshold ($\Theta^{\min} = 10^{-4}$ in our implementation), an Armijo type condition [14] is used. If

$$f(x_k + t_k d_k) \leqslant f(x_k) + \eta_f t_k f_x(x_k) d_k \tag{7.7}$$

with constant $\eta_f = 10^{-8}$ holds, the trial point $x_k + t_k d_k$ is also acceptable.
If a trial point $x_k + t_k d_k$ is acceptable for the sufficient reduction criterion (7.5) or for (7.6) and (7.7), it still has to be acceptable to the filter for being accepted as new iterate. The filter $\mathcal{F}_k$ is a set – in the implementation a list of pairs –

$$\mathcal{F}_k \subseteq \{(\vartheta, \varphi) \in \mathbb{R}^2 \mid \vartheta > 0\}.$$

A trial point $x_k + t_k d_k$ is acceptable to the filter, if it is not contained in the filter $x_k + t_k d_k \notin \mathcal{F}_k$. The initial filter is given with a large $\vartheta_0 > 0$ as the half plane $\mathcal{F}_0 = \{(\vartheta, \varphi) \in \mathbb{R}^2 \mid \vartheta > \vartheta_0\}$.
Every time a point is accepted as new iterate via the sufficient reduction criterion (7.5) (and the filter) and at the beginning of the feasibility restoration phase (see the section below), the filter is updated

$$\mathcal{F}_{k+1} := \mathcal{F}_k \cup \left\{(\vartheta, \varphi) \in \mathbb{R}^2 \mid \vartheta \geqslant (1 - \gamma_\vartheta)\Theta(x_k) \text{ and } \varphi \geqslant f(x_k) - \gamma_\varphi \Theta(x_k)\right\}$$

with the constants $\gamma_\vartheta = 10^{-5}$ and $\gamma_\varphi = 10^{-5}$ which ensure sufficient progress of the algorithm.
In our implementation, the filter method replaces the merit function approach as it shows better convergence properties.

### Active set strategy

For the treatment of a detailed combustion model as described in Chapter 4, it is crucial for the iterates to be nonnegative as the model can not be evaluated in the negative domain. The linearization of the nonnegativity constraints $x \geqslant x_\mathrm{l} := 0 \in \mathbb{R}^n$ is given by

$$x + I \cdot d \geqslant x_\mathrm{l}. \tag{7.8}$$

We use an active set (AS) strategy to deal with this inequality. The AS $\mathcal{I}$ is defined as the indices of the active inequality constraints in the current iterate. Suppose a candidate $x + td$ for a step violates Equation (7.8). If this is the case, the smallest step length

$$t_\mathrm{min} = \min_{i \in \{1,\ldots,n\} \setminus \mathcal{I}} \left( \frac{x_{\mathrm{l},i} - x_i}{d_i} \right)$$

is identified such that the border of the feasible domain is precisely reached $x_i + t_\mathrm{min} d_i = x_{\mathrm{l},i}$ for one index $i$. If the shortened step $x + t_\mathrm{min} d$ is accepted by any of the ways described before, the exactly fulfilled equation is added to the equality constraints, $\mathcal{I} = \mathcal{I} \cup \{i\}$, and the shortened step is accepted as new iterate.
If a previously accepted step does not violate any inequality constraint, it is checked if the active set is too large. That means, if the Lagrange multipliers related to one or more active inequality constraints are lower than zero ($\lambda_i < 0$), one active inequality for which this is the case, e.g. the active inequality constraint of these with the largest Lagrange multiplier in modulus, is deactivated in the next step.
An alternative to an active set strategy may be an *inverse barrier function*

$$P(x) = f(x) + \delta \left\| \frac{1}{F_3(x)} \right\|_2^2$$

similar to that presented in [54] with a barrier parameter $\delta > 0$. It could be used for a Filter-IP-GGN method instead of the discussed Filter-AS-GGN. However, an AS method should perform better for the problems considered in this work than an IP method as we expect that constraints for nonnegativity are activated only seldomly. Therefore, the effort to use a homotopy method and to drive the homotopy parameter to zero is not justifiable.

### Feasibility restoration phase

There might be the case that a candidate for an iterate $x_k + t_k d_k$ is not acceptable via the criteria discussed before even after several reductions (in the implementation: 5) of the step length $t_{k,j} = \gamma^j$ for $j = 0, \ldots,$ e.g. with $\gamma = 0.5$. In this case, a *feasibility restoration phase* is used. The aim of a

feasibility restoration is to find a feasible point as a new iterate $x_{k+1}$ that is "near" to $x_k$ and acceptable to the updated filter. If the feasibility restoration phase fails, this indicates an error in the optimization model or a very bad scaling. The goal to find a feasible point that is "near" to $x_k$ can be written in context of GGN methods with the last accepted iterate $x = x_k$ as the following CNLLS problem

$$\min_{\bar{x}} \ \tfrac{1}{2}\|\bar{x} - x\|_2^2 \tag{7.9a}$$

subject to

$$F_2(\bar{x}) = 0 \tag{7.9b}$$
$$F_3(\bar{x}) \geqslant 0. \tag{7.9c}$$

We solve problem (7.9) iteratively with increments $\bar{d}$ computed as solution of a CLLS optimization problem

$$\min_{\bar{d}} \ \tfrac{1}{2}\|\bar{x}_k - x + \bar{d}\|_2^2$$

subject to

$$F_2(\bar{x}_k) + J_2(\bar{x}_k)\bar{d} = 0$$
$$F_3(\bar{x}_k) + J_3(\bar{x}_k)\bar{d} \geqslant 0$$

and initial value $\bar{x}^0 := x$. We define functions $\bar{F}_1 := \bar{x}^k - x + \bar{d}$, $\bar{F}_j := F_j$, $j = 2, 3$, and their Jacobian matrices $\bar{J}_1 = I$ and $\bar{J}_j = J_j$, $j = 2, 3$; the considerations presented in Sections 7.1.1 and 7.1.2 are directly applicable and matrix factorizations, e.g. of $J_2$, can be recycled.
It would be possible to use a similar restoration phase as `Ipopt` [168], where an optimization problem with a relaxed feasibility in $F_2(\bar{x}) = 0$ is solved

$$\min_{\bar{x}} \ \tfrac{1}{2}\|F_2(\bar{x})\|_2^2 + \tfrac{\bar{\delta}}{2}\|\bar{x} - x\|_2^2$$

subject to

$$F_3(\bar{x}) \geqslant 0.$$

A homotopy parameter $\bar{\delta}$ balances the desires of a feasible point and a point that is "near" to the previous iterate. This alternative restoration phase is not implemented, yet.

### Scaling and termination

It is beneficial for the numerical stability of the algorithm to scale all variables to a similar magnitude. We assume that the starting values for the optimization (the values given by the user for a first call or the values of the Euler prediction within a warm start, see Section 8.1.2) are reasonable.

An automatic scaling is implemented following the ideas of [64]. Scaling by a diagonal matrix is considered to keep computations as simple as possible

$$\tilde{x} = D^{-1}x,$$

where $x \in \mathbb{R}^n$ is the original (specific moles and temperature) vector; $\tilde{x} \in \mathbb{R}^n$ is the scaled vector. We define the diagonal matrix $D \in \mathbb{R}^{n\times n},\ D = \operatorname{diag}(d)$ with $d \in \mathbb{R}^n$ for initial values $x_i^0 \neq 0$ in the current call of the optimization algorithm as

$$d_i = 10^{\lfloor \lg(|x_i^0|)\rfloor}, \quad i = 1, \ldots, n,$$

where $\lfloor\cdot\rfloor$ is the floor function. Otherwise, $d_i = 1$ is used.
A scaling of the form $x = D\tilde{x} + c$ with $c \in \mathbb{R}^n$ where

$$\begin{aligned} d_i &= \tfrac{1}{2}(b_i - a_i), \quad i = 1, \ldots, n \\ c_i &= \tfrac{1}{2}(b_i + a_i), \quad i = 1, \ldots, n \end{aligned}$$

with upper and lower bounds $a_i \leqslant x_i \leqslant b_i$, $i = 1, \ldots, n$, is also tested. It is necessary for this scaling to provide realistic bounds for the species, which is difficult for models including multiple scales.
In our implementation, the objective function is also scaled. It is beneficial if the objective function at the solution is $\mathcal{O}(1)$. So the magnitude of the objective function in the previous solution is used as a guess for the magnitude of the objective function at the solution of the next optimization problem.
Absolute convergence tolerances $\bar{\epsilon}_i$, $i = 1, \ldots, n$, and a relative convergence tolerance $\hat{\epsilon}$ have to be specified. If the condition

$$|d_i| \leqslant \max\{\hat{\epsilon}\,|x_i|,\, \bar{\epsilon}_i\}$$

holds for all $i = 1, \ldots, n$, the algorithm terminates at the numerical solution.

**Proof of global convergence**

Wächter and Biegler show global convergence of line search filter methods in [167]. This is done for IP- and SQP-filter methods. A number of assumptions is necessary. They mainly ensure sufficient smoothness of all functions. We can interpret the GGN method as an SQP method with Gauss–Newton approximation of the Hessian of the Lagrangian. This means, the results of [167] are directly applicable here if $H_k$ in [167, p. 22] is $H_k = J_1(x_k)^{\mathrm{T}} J_1(x_k)$ in each iteration.

## 7.2 Interior point method

The main difference of interior point (IP) methods, also called barrier methods, see e.g. the review [59], in comparison to sequential quadratic programming methods [129] is the handling of the inequality constraints. Results

presented in Chapter 9 are partly computed with the optimization software package `Ipopt`. The theory of `Ipopt` is published and discussed in detail in [165, 166, 167, 168]. We have a short overview of IP methods in this section. As it is done in [168], we consider the NLP problem

$$\min_{x \in \mathbb{R}^n} \; f(x) \tag{7.12a}$$

subject to

$$F_2(x) = 0 \tag{7.12b}$$

$$x \geqslant 0 \tag{7.12c}$$

with the equality constraint function $F_2 : \mathbb{R}^n \to \mathbb{R}^{n_2}$, inequality constraints for nonnegativity, and the objective function $f : \mathbb{R}^n \to \mathbb{R}$.
Interior point methods approximate a solution of the primal dual equations, that are the KKT conditions for problem (7.12) with a relaxed complementarity

$$\begin{aligned} \nabla_x f(x) - \nabla_x F_2(x)\lambda - \mu &= 0 \\ F_2(x) &= 0 \\ \operatorname{diag}(x)\mu - \delta e &= 0 \\ x &\geqslant 0 \end{aligned} \tag{7.13}$$

with the vector $e \in \mathbb{R}^n$, $e = (1, \ldots, 1)^{\mathrm{T}}$. The relaxation parameter $\delta > 0$ is driven toward zero iteratively.
On the other hand, this method can be interpreted as a barrier method, where the optimization problem

$$\min_{x \in \mathbb{R}^n} \; f^{\delta}(x) := f(x) - \delta \sum_{i=1}^{n} \ln(x_i)$$

subject to

$$F_2(x) = 0$$

is solved.
System (7.13) is solved with Newton's method. The algorithm always decreases the homotopy parameter $\delta$ if the maximum error in the scaled equations in (7.13) is lower than a certain tolerance. An iterate is accepted as numerical solution, if the maximum error in (7.13) with $\delta = 0$ (the KKT error) is lower than a user specified tolerance.
If it is impossible to solve the linear system in a Newton iteration due to (an almost) singularity of the KKT matrix, a regularization (inertia correction) of the KKT matrix is done. On the other hand, update formula can also be used. `Ipopt` offers a limited memory Broyden–Fletcher–Goldfarb–Shanno (BFGS) update method. The usage of the Hessian of the Lagrangian function usually leads to faster convergence in our experience.

**Remark 7.2.1**
In `Ipopt`, a scaling of the gradients is used. We use the default scaling only for the objective function and for the collocation equations in the constraints in case a collocation method is employed, see Section 6.2.1. The other conservation constraints are assumed to be well scaled. This scaling is also considered in the computation of the step size in the continuation method described in the next chapter.

**Remark 7.2.2**
We use the monotonic strategy for the choice of parameter $\delta$. The value of $\delta$ is kept constant in a hot start, see Section 8.5.

## 7.3 Computation of derivatives for the optimization algorithm

As seen in previous sections, derivatives of the objective function and the constraints with respect to the optimization variables are necessary for the evaluation of the KKT conditions in order to solve the NLP problem. Besides analytic differentiation, there are two basic ways for the computation of the derivatives: finite differences and automatic differentiation.

### Finite differences

Let $f : \mathbb{R} \to \mathbb{R}$ be the function which is supposed to be differentiated. The one-sided (forward) difference quotient with step size $h$ is given as

$$\frac{f(x+h) - f(x)}{h} = \frac{\mathrm{d}}{\mathrm{d}x} f(x) + \mathcal{O}(h),$$

and the central difference quotient is

$$\frac{f(x+h) - f(x-h)}{2h} = \frac{\mathrm{d}}{\mathrm{d}x} f(x) + \mathcal{O}(h^2).$$

In both cases, a large number of valid digits are lost due to cancellation errors. This is undesirable if one deals with systems which involve many different time scales. Hence, we prefer automatic differentiation. Finite differences are only used in our implementation for a cross check of derivatives.

### Automatic differentiation

Automatic differentiation, sometimes also called *algorithmic differentiation*, is based on the differentiation of the calculation rule of a computer code itself. The chain rule is used to derive an algorithmic expression for the computation of the derivative. There are two basic modes of automatic

differentiation: forward and reverse. The forward mode is beneficial if the range space of the function to be differentiated has a higher dimension than the space in which its domain is located and vice versa. We use the code `CppAD` [17] for automatic differentiation.
The theory of automatic differentiation is not topic of this thesis and can be found e.g. in [79].

### Imaginary finite differences

It can be useful to use imaginary finite differences [153]. This is the case if only first order derivative information is necessary. It can be used in our implementation for the computation of the derivative of the objective function with respect to the optimization variables. If `Ipopt` [168] is used as optimization tool, a BFGS update formula can be applied instead of an evaluation of the Hessian matrix of the Lagrangian function. Consider the real-valued, analytical function $f : \mathbb{R} \to \mathbb{R}$. The derivative approximation is given as

$$\frac{\mathrm{d}}{\mathrm{d}x} f(x) \doteq \frac{\Im f(x + \mathrm{i}h)}{h},$$

where $\Im(y)$ is the imaginary part of $y \in \mathbb{C}$ and i is the complex unit, see [135]. In contrast to finite differences, no cancellation error is introduced with this imaginary step.

*I must continue to follow the path I take now. If I do nothing, if I study nothing, if I cease searching, then, woe is me, I am lost.*

Vincent van Gogh

# 8 Path following

The approximation of points on the SIM, that is computed as solution of optimization problem (5.1) introduced in Chapter 5, can be used e.g. in computational fluid dynamics (CFD) and other applications. In this context, a large number of approximation points of the SIM for different values of the reaction progress variables is needed. This means, problem (5.1) has to be solved repeatedly for varying values of $z_j^{t_*}$, $j \in \mathcal{I}_{\text{pv}}$.
In order to achieve this, a warm start or hot start method for initialization of the algorithm (the corrector) to solve a neighboring optimization problem can be useful to save computation time. The initialization of the corrector algorithm (with a predictor) is done by means of the computed solution of the previously solved optimization problem. Together with such a warm start method, a homotopy method with a step size control can be of benefit to save computation time as it is shown for an example in Section 9.3.2. Such *path following* or *continuation* or *homotopy methods* are considered in this chapter. The theoretical basis of continuation methods is discussed in Section 3.3 with the theory of parametric optimization problems.
The predictor corrector scheme and the computation of parameter sensitivities of NLP problems are described in the first section of this chapter. Afterward, the step size strategy is explained. If the sequential approach (see Chapter 6) is used to solve the general optimization problem (5.1) or (5.6) for SIM approximation, the computation of the tangent space of the SIM calls for more explanation, described in Section 8.3. Finally, aspects of the implementation of the homotopy method in the `C++` code developed together with this work are explained, such as the scaling of linear equation systems and problems with the warm start of interior point methods.
For the presentation in this chapter, we adapt content of [9] to our purpose.

## 8.1 Predictor corrector scheme

In the following, we consider the finite parametric optimization problem

$$\min_{x \in \mathbb{R}^n} \; f(x) \tag{8.1a}$$

subject to

$$0 = g(x) \tag{8.1b}$$

$$0 = x_{j(i)} - r^i, \quad i = 1, \ldots, n_r \tag{8.1c}$$

$$0 \leqslant x, \tag{8.1d}$$

where the functions $f : D \to \mathbb{R}$ and $g : D \to \mathbb{R}^{n_2}$ are $\mathcal{C}^2(D)$ in the open domain $D \subset \mathbb{R}^n$. The reaction progress variables in (8.1c) are denoted by the parameter vector $r \in \tilde{D} \subset \mathbb{R}^{n_r}$, $r^i = z^{t_*}_{j(i)}$, $i = 1, \ldots, n_r$, $n_r < n - n_2$ with the notation of Equation (5.6e), where $j : \{1, \ldots, n_r\} \to \mathcal{I}_{\text{pv}}$, $i \mapsto j(i)$ is a bijective map to the index set $\mathcal{I}_{\text{pv}} \subset \{1, \ldots, n\}$ of the reaction progress variables and $r^i$ is the $i$-th component of $r$.
The optimization problem (8.1) can be considered in different ways in dependence of the solution method to solve (5.6): In case a collocation method is applied to solve (5.6), $x$ corresponds to all discrete approximations of $z(t_i)$, $T(t_i)$ at the Gauss–Radau points $t_i$, see Section 6.2.1. Equality constraints other than the fixation of the reaction progress variables, e.g. from the collocation discretization of the ODE constraints in (5.6) as described in Section 6.2.1, are collected in the nonlinear function $g$. If the BDF integration method is used in a shooting approach to solve (5.6), see Section 6.3, nonnegativity is only demanded for the optimization variables $x$ that correspond to the initial values $z(t_0)$, $T(t_0)$ in (5.6). The optimization problem (8.1) can also be considered as the NLP problem (5.7) with the previously described notation for the reaction progress variables, objective function, and constraints.
In Section 3.2, the KKT conditions of the parametric optimization problem are written in short form as

$$K(x, \lambda, \mu, r) = 0 \tag{8.2}$$

with the primal variables $x$, the dual variables $\lambda$ and $\mu$, and the parameter vector $r$.

### 8.1.1 Parameter sensitivities

The derivative of a solution $(x^*, \lambda^*, \mu^*)$ of the parametric optimization problem with respect to the parameters is given via

$$\mathrm{D}_{(x,\lambda,\mu)} K(x^*, \lambda^*, \mu^*, r)\, \mathrm{D}_r(x^*, \lambda^*, \mu^*) = -\mathrm{D}_r K(x^*, \lambda^*, \mu^*, r) \tag{8.3}$$

if second order sufficient optimality conditions, LICQ, and strict complementarity are fulfilled, cf. Theorem 3.2.1 in Section 3.2. These parameter sensitivities are needed to derive the tangent space of the SIM that is considered in Section 2.3.2.
In the following subsection, the computation of the derivatives $\mathrm{D}_r(x^*, \lambda^*, \mu^*)$ is described. This depends on the collocation or shooting approach employed to solve (5.6) that leads to problem (8.1) and the solution method for (8.1). In case of an active set method for the treatment of (8.1d), see Section 7.1.3, function $K^{\mathrm{AS}}$ replacing $K$ in (8.2) which can be used in an optimization algorithm to compute a numerical solution of (8.1) can be written as

$$K^{\mathrm{AS}}(x, \lambda, \mu, r) := \begin{cases} \nabla f(x) - \nabla_x g(x)\lambda^1 - \Xi^{\mathrm{T}}\lambda^2 - \mu \\ g(x) \\ x_{j(i)} - r^i, \quad i = 1, \ldots, n_r \\ x_i, \quad i \in \mathcal{A}(x), \end{cases}$$

where only active inequality constraints are under consideration whose indices are collected in the active set $\mathcal{A}(x)$ in $x$. Matrix $\Xi := (\xi_{i,m})$ with $i = 1, \ldots, n_r$ and $m = 1, \ldots, n$ is given via

$$\xi_{i,m} := \frac{\mathrm{d}}{\mathrm{d}x_m}(x_{j(i)} - r^i)$$

which yields

$$\xi_{i,m} = \begin{cases} 1, & \text{if } m = j(i), \\ 0, & \text{else.} \end{cases}$$

The Lagrange multipliers that correspond to the equality constraints in (8.1b) are denoted $\lambda^1 \in \mathbb{R}^{n_2}$. The Lagrange multipliers corresponding to the equality constraints for the fixation of the reaction progress variables in (8.1c) are denoted $\lambda^2 \in \mathbb{R}^{n_r}$.
In the case that an interior point method is employed to compute a solution of (8.1) numerically, the inequality constraints (8.1d) are coupled to the objective function via a barrier term, see Section 7.2. Consequently and analogously to $K^{\mathrm{AS}}$, $K^{\mathrm{IP}}$ can be formulated as

$$K^{\mathrm{IP}}(x, \lambda, \mu, r) := \begin{cases} \nabla f(x) - \nabla_x g(x)\lambda^1 - \Xi^{\mathrm{T}}\lambda^2 - \mu \\ g(x) \\ x_{j(i)} - r^i, \quad i = 1, \ldots, n_r \\ \mathrm{diag}(x)\mu - \delta e \end{cases} \tag{8.4}$$

with $x, \mu > 0$, $e^{\mathrm{T}} = (1, \ldots, 1) \in \mathbb{R}^n$, and a homotopy parameter $\delta > 0$.

### Sensitivities in the GGN method

If Newton's method is used to find a solution of optimization problem (8.1) representing (5.7) with an active set strategy, i.e. to compute a root of $K^{\mathrm{AS}}$, the KKT matrix $\mathrm{D}_{(x,\lambda,\mu)}K(x_k, \lambda_k, \mu_k, r)$ has to be available in every iteration. This is different if a generalized Gauss–Newton method is employed.
We return to the notation used in Section 7.1: The objective function is written as $f(x) = \|F_1(x)\|_2^2$ with a function $F_1 : D \subset \mathbb{R}^n \to \mathbb{R}^{n_1}$, sufficiently smooth. The constraints are given by the condition $F_2(x) = 0$ with a function $F_2 : D \subset \mathbb{R}^n \to \mathbb{R}^{\bar{n}_2}$, $\bar{n}_2 = n_2 + n_r + |\mathcal{A}(x)|$ as

$$F_2(x) = \begin{cases} g(x) \\ x_{j(i)} - r^i, \quad i = 1, \ldots, n_r \\ x_i, \quad i \in \mathcal{A}(x). \end{cases}$$

The Jacobian matrices of $F_1$ and $F_2$ are denoted as $J_1$ and $J_2$, respectively. In the GGN method, one solves in every iteration the equation system

$$\begin{bmatrix} J_1^{\mathrm{T}} J_1 & J_2^{\mathrm{T}} \\ J_2 & 0 \end{bmatrix} \begin{bmatrix} d \\ -\lambda \end{bmatrix} = - \begin{bmatrix} J_1^{\mathrm{T}} F_1 \\ F_2 \end{bmatrix} \tag{8.5}$$

(where the argument $x_k$ is omitted and the symbol $\lambda$ is used for all equality and active inequality constraints); that is the KKT system of the CLLS problem (7.2), see Section 7.1. By contrast, one solves

$$\begin{bmatrix} \mathcal{L}_{xx} & -J_2^{\mathrm{T}} \\ J_2 & 0 \end{bmatrix} \begin{bmatrix} \Delta x \\ \Delta\lambda \end{bmatrix} = - \begin{bmatrix} \nabla_x \mathcal{L} \\ F_2 \end{bmatrix} \tag{8.6}$$

if Newton's method is applied to find a KKT point of the original CNLLS problem (7.1). The derivative of the Lagrangian function of the CNLLS problem is $\nabla_x \mathcal{L}^{\mathrm{T}} = F_1(x)^{\mathrm{T}} J_1(x) - \lambda^{\mathrm{T}} J_2(x)$. The difference in the KKT matrices in Equations (8.6) and (8.5) is the difference in the Hessians of the different Lagrangian functions: In the GGN method, $J_1^{\mathrm{T}} J_1$ is used; whereas Newton's method applied to find a KKT point of the original CNLLS problem (7.1) exploits

$$\begin{aligned} \mathcal{L}_{xx} &= \nabla_{xx} \tfrac{1}{2} \|F_1(x)\|_2^2 - \sum_{i=1}^{\bar{n}_2} \lambda_i \nabla_{xx} F_2^i(x) \\ &= J_1^{\mathrm{T}} J_1 + \left(\partial_x J_1^{\mathrm{T}}\right) F_1 - \sum_{i=1}^{\bar{n}_2} \lambda_i \nabla_{xx} F_2^i(x), \end{aligned} \tag{8.7}$$

where $F_2^i$ is the $i$-th component of $F_2$.
This work aims at the solution of optimization problem (8.1) for model reduction of chemical combustion models. In this case, the constraints $g$, here included in $F_2$, represent the linear elemental mass conservation as given

in Equation (4.6) and eventually a nonlinear energy balance, see (4.8) and (4.9).
So the second derivative of $F_2$ with respect to the optimization variables $x$ is zero besides the second derivatives of the functions in Equations (4.8) or (4.9). If, e.g., energy conservation

$$\tilde{g}(z,T) := \sum_{s=1}^{n_{\text{spec}}} \bar{H}_s^\circ \, z_s - RT \sum_{s=1}^{n_{\text{spec}}} z_s - \check{e} = 0 \tag{8.8}$$

is considered (for the notation see Chapter 4), the following derivatives of second order have to be computed additionally

$$\frac{\mathrm{d}^2}{\mathrm{d}z_i \mathrm{d}z_s} \tilde{g}(z,T) = 0, \quad \forall s,i = 1,\ldots,n_{\text{spec}} \tag{8.9a}$$

$$\frac{\mathrm{d}^2}{\mathrm{d}T^2} \tilde{g}(z,T) = \sum_{s=1}^{n_{\text{spec}}} z_s \frac{\mathrm{d}}{\mathrm{d}T} \bar{C}_{p,s}^\circ(T) \tag{8.9b}$$

$$\frac{\mathrm{d}^2}{\mathrm{d}T \mathrm{d}z_s} \tilde{g}(z,T) = \bar{C}_{p,s}^\circ(T) - R, \quad s = 1,\ldots,n_{\text{spec}}. \tag{8.9c}$$

If enthalpy conservation is considered, the term $-R$ (the difference of the molar heat capacity at constant pressure and the molar heat capacity at constant volume) falls away in (8.9c). In the case that $F_2$ represents the conservation laws of isothermal systems as described in Chapter 4, $\nabla_{xx} F_2^i(x) = 0$ holds for all $i = 1,\ldots,\bar{n}_2$.

**Remark 8.1.1**
The evaluation of the cubic polynomials $\frac{\mathrm{d}}{\mathrm{d}T}\bar{C}_{p,s}^\circ(T)$ for (8.9b), see also Equation (4.10), is computed fast. Typically $\frac{\mathrm{d}}{\mathrm{d}T}\bar{C}_{p,s}^\circ(T)$ is small as the heat capacity only changes slightly in dependence of the temperature. The main additional computational effort for the computation of the Hessian of the Lagrangian function (8.7) of problem (7.1) is the computation of $\left(\partial_x J_1^{\mathrm{T}}\right) F_1$. This can be evaluated using automatic differentiation as a directional derivative of $J_1$ in direction $F_1$, see Section 7.3.

The `LAPACK` [13] solver `dsysvx` is used to solve equation system (8.3) with the KKT matrix including the Hessian (8.7).

### Sensitivities in the interior point approach

If an interior point method is used to solve (8.1), the parameter sensitivity equation (8.3) of the barrier problem, i.e. (8.3) with $K = K^{\text{IP}}$ as in (8.4), can be written as

$$\begin{bmatrix} \mathcal{L}_{xx} & g_x^{\mathrm{T}} & -\Xi^{\mathrm{T}} & -I_n \\ g_x & 0 & 0 & 0 \\ \Xi & 0 & 0 & 0 \\ \mathrm{diag}(\mu) & 0 & 0 & \mathrm{diag}(x) \end{bmatrix} \begin{bmatrix} x_r \\ \lambda_r^1 \\ \lambda_r^2 \\ \mu_r \end{bmatrix} = - \begin{bmatrix} \mathcal{L}_{x,r} \\ g_r \\ -I_{n_r} \\ 0 \end{bmatrix}, \tag{8.10}$$

where $I_n$ is the unit matrix of dimension $n$.
In case of (8.1), $\mathcal{L}_{x,r} = 0$ and $g_r = 0$ hold. The KKT matrix is invertible if second order sufficient optimality conditions and LICQ are fulfilled. System (8.10) can be solved efficiently via the transformed system

$$\begin{bmatrix} \mathcal{L}_{xx} + \operatorname{diag}(x)^{-1} \operatorname{diag}(\mu) & g_x^{\mathrm{T}} & -\Xi^{\mathrm{T}} \\ g_x & 0 & 0 \\ \Xi & 0 & 0 \end{bmatrix} \begin{bmatrix} x_r \\ \lambda_r^1 \\ \lambda_r^2 \end{bmatrix} = \begin{bmatrix} 0 \\ 0 \\ I_{n_r} \end{bmatrix}, \tag{8.11}$$

see [124]. The parameter sensitivity of the multipliers of the inequality constraints is given as

$$\mathrm{D}_r \mu_i = -\frac{\mu_i}{x_i} \mathrm{D}_r x_i, \quad i = 1, \ldots, n,$$

where $x_i$, $i = 1, \ldots, n$, are in the interior of the feasible set. If nonnegativity constraints (8.1d) are not required in the model, the term $\operatorname{diag}(x)^{-1} \operatorname{diag}(\mu)$ is omitted in Equation (8.11).

**Remark 8.1.2**
There is an open source extension of `Ipopt` called `sIPOPT`. This toolbox is implemented by H. Pirnay and provides the necessary parameter sensitivities. The theory for `sIPOPT` is described in [127]. However, an early implementation used derivatives of the last pre-optimal iterate of `Ipopt` to compute the sensitivities.

**Sensitivities in the simultaneous approach** If the dynamics in the constraints (5.1b) or (5.6b) and (5.6c), respectively, are discretized with a collocation scheme, see Section 6.2.1, the KKT matrix of the resulting NLP problem (8.1) is large and sparse. Also the right hand side in (8.11) is sparse. Therefore, we use the linear solver `MUMPS` [12] to solve (8.11) as it is suited for sparse equation systems.

**Sensitivities in the sequential approach** If the BDF integrator in the sequential approach is used to solve the ODE (5.1b) or (5.6b) and (5.6c), respectively, see Section 8.3, all necessary derivatives in the KKT matrix of the resulting NLP problem (8.1) are computed via sensitivity differential equations solved in the BDF integration algorithm. The matrices in system (8.11) are dense in this case, and the `LAPACK` [13] solver `dsysvx` is used.

**Remark 8.1.3**
All linear solvers check if the KKT matrix, which has to be decomposed, has full rank, and an error is reported otherwise. If the KKT matrix does not have full rank, this indicates that the second order sufficient optimality conditions as stated in Theorem 3.1.10 are not fulfilled at the computed "solution" of (8.1), as LICQ is always fulfilled in our case, see Remark 7.1.2. If such an error is reported, there may be trouble in the problem formulation.

We use several possibilities for equilibration of the KKT matrix for the solution of the linear system (8.3) in case of a bad conditioning. This is described in Section 8.4.

### 8.1.2 Predictor with full step

We define a curve $c$ as a mapping from the parameter space to the space of the primal and dual variables of (8.1)

$$c : \tilde{D} \subset \mathbb{R}^{n_r} \to \mathbb{R}^{2n+n_2}$$
$$r \mapsto c(r) := \begin{pmatrix} x^*(r) \\ \lambda^*(r) \\ \mu^*(r) \end{pmatrix}$$

such that the notation coincides with the notation in Section 3.3. For each value of the parameter $r$, $c(r)$ is a local solution $(x^{*,\mathrm{T}}(r), \lambda^{*,\mathrm{T}}(r), \mu^{*,\mathrm{T}}(r))^{\mathrm{T}}$ of (8.1).
We assume that the vector $c^{\mathrm{T}}(r_0) = (x^{*,\mathrm{T}}(r_0), \lambda^{*,\mathrm{T}}(r_0), \mu^{*,\mathrm{T}}(r_0))$ for an initial $r_0 \in \tilde{D}$ and its derivative with respect to $r$ at $r_0$ are given. We predict a solution of (8.1) with new parameter values $r_{i+1}$ to be $c^0_{i+1}$ (where the index $i+1$ denotes the iteration index)

$$c^0_{i+1} = \mathrm{P}(r_{i+1}, c_i(r_i), h_i, \tfrac{\mathrm{d}}{\mathrm{d}r} c_i(r_i)), \quad i = 0, \dots$$

as a function of the old solution $c_i(r_i)$, its derivative with respect to the parameters $\frac{\mathrm{d}}{\mathrm{d}r} c_i(r_i)$, and a step size $h_i = 1$ in the full step method without step size control. The prediction $c^0_{i+1}$ is used as initialization of an optimization algorithm (the corrector) to compute a solution of (8.1) with parameter $r_{i+1}$. As the derivative $\frac{\mathrm{d}}{\mathrm{d}r} c_i(r_i)$ must be computed to obtain the tangent space of the SIM (see Section 2.3.2) with the numerical solution of (8.1), the Euler prediction

$$c^0_{i+1} = c_i(r_i) + h_i (r_{i+1} - r_i)^{\mathrm{T}} \tfrac{\mathrm{d}}{\mathrm{d}r} c_i(r_i), \quad i = 0, \dots \tag{8.12}$$

is calculable with the main additional computational effort of one matrix vector multiplication and used in our implementation. Predictors of higher order could be constructed based on Aitken–Neville interpolation as described in [16] or Hermite interpolation. These strategies are not used in our implementation.

**Linear step** Optimization problem (8.1) has to be solved several times for different values of the parameter $r$. Especially if the approximation of points on a SIM is needed *in situ* in a CFD simulation, it is necessary to compute the next point for SIM approximation fast.

If the values $r^{\text{new}}$ for the reaction progress variables, for which a SIM approximation is needed, are near (in the sense of the Euclidean distance) to the values $r^*$ for which the optimization problem is already solved

$$\|r^{\text{new}} - r^*\|_2 < \epsilon_{\text{tol}}, \tag{8.13}$$

it can be beneficial to save computing time and not to use the corrector algorithm but to use the Euler prediction directly. In this case, it is assumed that the SIM is only slightly curved. So there is no update for the approximation of the tangent vectors of the SIM.
This means, we use $z^{\text{lin}}$ and $T^{\text{lin}}$ as approximation of the SIM, see also Section 4.1 for the notation. These are defined as

$$\begin{aligned} z^{\text{lin}} &:= z^*(t_*) + (r^{\text{new}} - r^*)^{\mathrm{T}} \frac{\mathrm{d}z^*(t_*)}{\mathrm{d}r}(r^*) \\ T^{\text{lin}} &:= T^*(t_*) + (r^{\text{new}} - r^*)^{\mathrm{T}} \frac{\mathrm{d}T^*(t_*)}{\mathrm{d}r}(r^*), \end{aligned} \tag{8.14}$$

where the notation is in accordance with the notation in (5.6), $r^i = z^{t_*}_{j(i)}$, $i = 1, \ldots, n_r$, $n_r = |\mathcal{I}_{\text{pv}}|$, $j$ is the bijection described in Section 8.1, and $r^i$ is the $i$-th component of $r$. This linear approximation step is analogous to the prediction in (8.12).

## 8.2 Step size strategy in the predictor corrector method

A step size strategy is discussed in this section. It is used within the continuation method described in the section before to determine a step length for the prediction, see also Section 3.3. The strategy is originally published in [45] and extensively discussed and modified in [8, 9, 10]. We follow the discussion in [9].
The aim of the step size strategy of den Heijer and Rheinboldt [45] is to determine a desired number of corrector iterations which altogether form the *corrector step*. The strategy allows for the computation of a step length based on the contraction rate of the corrector iterations and an error model for the corrector such that the desired number of iterations is achieved.
We denote the Euler predictor step with

$$c^0_{i+1}(h_i) = c_i + h_i(r_{i+1} - r_i)^{\mathrm{T}} \tfrac{\mathrm{d}}{\mathrm{d}r} c_i(r_i), \quad i = 0, \ldots,$$

and the subsequent corrector iterations as

$$c^{j+1}_i(h_i) = \mathrm{C}(c^j_i(h_i)), \quad j = 0, \ldots$$

with the corrector C. It is assumed that the iterates computed in the corrector iterations converge to the solution

$$c_i^\infty(h_i) := \lim_{j\to\infty} c_i^j(h_i) \in K^{-1}(0)$$

with the function $K$ given in (8.2). Furthermore, it is assumed that the angle between the vector of the initial value in direction of the solution $c_i^\infty(h_i) - c_i^0(h_i)$ and the tangent $\frac{\mathrm{d}}{\mathrm{d}r}c_{i-1}$ is $\frac{\pi}{2} + \mathcal{O}(h_i)$.
The sophisticated aspect in the work of den Heijer and Rheinboldt [45] is the error model $\phi$. This error model estimates the error of the iterates

$$\epsilon_j(h_i) = \|c_i^\infty(h_i) - c_i^j(h_i)\|_2$$

via an expression of the form

$$\epsilon_{j+1}(h_i) \leqslant \phi(\epsilon_j(h_i)).$$

The concise form of the error model depends on the contraction rate of the corrector. In case of the quadratically convergent Newton method as corrector, den Heijer and Rheinboldt [45] suggest the two error models (see [9, p. 52])

$$\phi_1(\epsilon) = \frac{\epsilon^2}{3-2\epsilon}, \quad 0 \leqslant \epsilon \leqslant 1$$
$$\phi_2(\epsilon) = \frac{\epsilon + \sqrt{10-\epsilon^2}}{5-\epsilon^2}\epsilon^2, \quad 0 \leqslant \epsilon \leqslant 1$$

that they derive via estimates of Newton–Kantorovitch theory. For superlinear convergence (as in case of a quasi-Newton method with limited memory BFGS update as in `Ipopt` [168] as corrector), the function

$$\phi_3(\epsilon) = \epsilon^p, \quad p > 1$$

with $p = 1$ in the limit of linear convergence (e.g. in case of a GGN method as corrector, see Section 7.1) is suggested [9, p. 53].
The contraction $\omega$ of the last computed numerical solution of optimization problem (8.1) is the ratio of the length of the last corrector iteration to the length of the overall corrector step after termination with a certain error tolerance after, say, $k$ iterations, see the next section.
We define

$$\omega(h_i) := \frac{\|c_i^k(h_i) - c_i^{k-1}(h_i)\|_2}{\|c_i^k(h_i) - c_i^0(h_i)\|_2} \approx \frac{\epsilon_{k-1}(h_i)}{\epsilon_0(h_i)},$$

with $c_i^k(h_i) \approx c_i^\infty(h_i)$. This can be estimated with $\epsilon_{k-1}(h_i) \leqslant \phi^{k-1}(\epsilon_0(h_i))$ such that

$$\omega(h_i) \leqslant \frac{\phi^{k-1}(\epsilon_0(h_i))}{\epsilon_0(h_i)}.$$

The solution $\epsilon_1$ of

$$\omega(h_i) = \frac{\phi^{k-1}(\epsilon_1)}{\epsilon_1}$$

is an estimate for $\epsilon_0(h_i)$. The goal is a step length $\tilde{h}$ such that after $\tilde{k}$ iterations the stopping criterion for the corrector step is fulfilled. The error $\epsilon_{\tilde{k}}(\tilde{h}) \leqslant \phi^{\tilde{k}}(\epsilon_0(h_i))$ is estimated with the solution $\epsilon_2$ of

$$\phi^{\tilde{k}}(\epsilon_2) = \phi^k(\epsilon_1).$$

The ratio

$$f^2 = \left(\frac{h_i}{\tilde{h}}\right)^2 \approx \frac{\epsilon_1}{\epsilon_2}$$

to compute the new step size $\tilde{h}$ can be derived with a Taylor series for the distance $\|c_i^\infty(h_i) - c_i^0(h_i)\|_2$ in $h_i$.

### 8.2.1 Computation of the step size ratio

The computation of the ratio $f$ of the old step size $h_i$ to the new step size $\tilde{h}$ is done in the following way. In case of quadratic convergence of the corrector method, the contraction

$$\omega = \frac{\|c_i^k(h_i) - c_i^{k-1}(h_i)\|_2}{\|c_i^k(h_i) - c_i^0(h_i)\|_2}$$

is computed. If we use `Ipopt` [168] as the corrector method for the solution of the optimization problem (8.1), we use the scaling of the variables as `Ipopt` does, see Section 7.2. The computation of $\omega$ is done based on the scaled variables. Afterward, equation

$$\frac{\phi^{k-1}(\epsilon_1)}{\epsilon_1} = \omega \tag{8.15}$$

is solved with a Newton-bisection method as described in Section 8.2.2. The value of $\epsilon_2$ is computed via

$$\phi^{\tilde{k}}(\epsilon_2) = \phi^k(\epsilon_1) \tag{8.16}$$

with the same Newton-bisection method. The stretching ratio of the step size is

$$f = \sqrt{\frac{\epsilon_1}{\epsilon_2}}.$$

In case of superlinear convergence of the corrector method, an analytic expression for $f$ can be evaluated directly. It is [9, p. 53]

$$f = \omega^{\frac{1-p^{k-\tilde{k}}}{2(p^{k-1}-1)}}.$$

In the limit of linear convergence, i.e. $p \to 1$, l'Hôpital's rule yields [9, p. 54]

$$\lim_{p \to 1} f = \omega^{\frac{\tilde{k}-k}{2(k-1)}}.$$

### 8.2.2 Newton-bisection method

In the previous section, it is stated that the nonlinear equations (8.15) and (8.16) have to be solved. In order to find the root of a one-dimensional function $\bar{f} : \mathbb{R} \to \mathbb{R}$ which is sufficiently smooth, a mixture of Newton's method and a bisection method can be used if it is known that the solution is within a given interval, here $[0, 1]$. The combination of the two methods is used to exploit the quadratic convergence of Newton's method in its region of contraction near the solution. On the other hand, a bisection method converges if Newton's method is not contracting. The method is described in [132, p. 362ff.].
Let $y_{k+1} = y_k + \Delta y_k$, $y_k, \Delta y_k \in \mathbb{R}$, be the iteration step with the middle of the given start interval $y_0 \in \mathbb{R}$ as initial value. A Newton step is discarded if it exceeds the current bisection interval or if there is not enough contraction, i.e. if $|\bar{f}(x_k)| > \Delta x_{k-1} \bar{f}'(x_k)$. In that case, the current interval is bisected.

## 8.3 Computation of the tangent space in the sequential approach

As stated in Section 2.3.2, we are not only interested to approximate points on the SIM but also to approximate the tangent space of the SIM, which is needed e.g. in the linear approximation as defined in Equation (8.14).
Consider optimization problem (8.1) as the NLP problem that is solved in a sequential approach (see Section 6.3) for computation of a numerical solution of problem (5.6), where the ODE constraints (5.6b) and (5.6c) in problem (5.6) are solved numerically with a BDF integration method (see Section 6.2.2).
In that case, the parameter sensitivities of the primal optimization variables $x^{*,T} = (z^*(t_0)^{\mathrm{T}}, T(t_0))$ at the computed solution are (combining the notation as used in (8.1) and (5.6))

$$\frac{\mathrm{d}}{\mathrm{d}r} x^* = \frac{\mathrm{d} \begin{pmatrix} z^*(t_0) \\ T^*(t_0) \end{pmatrix}}{\mathrm{d}r},$$

where $r^i = z^{t_*}_{j(i)}$, $i = 1, \ldots, n_r$ is the vector of the reaction progress variables at $t_*$.

The matrix product

$$\frac{\mathrm{d}\begin{pmatrix} z^*(t_*) \\ T^*(t_*) \end{pmatrix}}{\mathrm{d}r} = \frac{\mathrm{d}\begin{pmatrix} z^*(t_*) \\ T^*(t_*) \end{pmatrix}}{\mathrm{d}\begin{pmatrix} z^*(t_0) \\ T^*(t_0) \end{pmatrix}} \frac{\mathrm{d}\begin{pmatrix} z^*(t_0) \\ T^*(t_0) \end{pmatrix}}{\mathrm{d}r}$$

yields the matrix of an approximation of the tangent vectors of the SIM in the computed point for approximation of the SIM.
The necessary derivatives of the solution of the ODE constraints at the point in time $t_*$ with respect to the initial values

$$\frac{\mathrm{d}\begin{pmatrix} z^*(t_*) \\ T^*(t_*) \end{pmatrix}}{\mathrm{d}\begin{pmatrix} z^*(t_0) \\ T^*(t_0) \end{pmatrix}}.$$

are computed as solutions of the sensitivity differential equations with the BDF integration method, see also [151].

## 8.4 Equilibration of the KKT matrix

The KKT matrix in the linear equation system (8.3) for computation of the parameter sensitivities can be ill-conditioned, see also the results in Section 9.3.2. An equilibration of the matrix $\mathrm{D}_{(x,\lambda,\mu)}K(x^*, \lambda^*, \mu^*, r)$ can overcome this problem.
We restrict ourselves to direct methods for the computation of a solution of the linear equation system (8.3). The description and notation in the following is taken from and similar to [116].
In general, we aim to solve a system of linear equations of the form

$$Ax = b \tag{8.17}$$

with the coefficient matrix $A \in \mathbb{R}^{\tilde{n}\times\tilde{n}}$, $A = (a_{ij})_{i,j=1}^{\tilde{n}}$, and $x, b \in \mathbb{R}^{\tilde{n}}$ the solution and right hand side, respectively.

**Definition 8.4.1** (Preconditioned system [116])
*The system*

$$\tilde{A}\tilde{x} = \tilde{b}$$

*with $\tilde{A} = P_{\mathrm{L}}AP_{\mathrm{R}}$, $\tilde{b} = P_{\mathrm{L}}b$, and $\tilde{x} = P_{\mathrm{R}}^{-1}x$, where $P_{\mathrm{L}}, P_{\mathrm{R}} \in \mathbb{R}^{\tilde{n}\times\tilde{n}}$ are regular matrices, is called* preconditioned system *to system (8.17).*

The goal of preconditioning is to find matrices $P_{\mathrm{L}}, P_{\mathrm{R}}$ such that the transformed coefficient matrix $\tilde{A}$ has a better condition number than the original $A$. First, one computes the matrix $\tilde{A} = P_{\mathrm{L}}AP_{\mathrm{R}}$ and the right hand side

$\tilde{b} = P_{\mathrm{L}} b$. Second, the preconditioned system is solved which results in the solution $\tilde{x}$. Finally, one gains the solution $x = P_{\mathrm{R}} \tilde{x}$.
We deal with the symmetric matrix $A = \mathrm{D}_{(x,\lambda,\mu)} K(x^*, \lambda^*, \mu^*, r)$. So we use $P := P_{\mathrm{L}} = P_{\mathrm{R}}^{\mathrm{T}}$ to preserve symmetry. A simple form for $P$ is a regular diagonal matrix $D = \mathrm{diag}(d)$ with a vector $d \in \mathbb{R}^{\tilde{n}}$. Such an equilibration is commonly called scaling. We define $D := P^{-1}$ to simplify notation.
The success of a certain scaling depends strongly on the underlying problem, and no clear suggestion can be made which scaling should be used for a specific problem. The following scaling is available in the implementation:

1. $d_i = 1.0, \quad i = 1, \ldots, \tilde{n}$
2. $d_i = |a_{ii}|^{\frac{1}{2}}, \quad i = 1, \ldots, \tilde{n}$
3. $d_i = a_{ii}, \quad i = 1, \ldots, \tilde{n}$
4. $d_i = \sum_{j=1}^{\tilde{n}} |a_{ij}|, \quad i = 1, \ldots, \tilde{n}$
5. $d_i = \left( \sum_{j=1}^{\tilde{n}} a_{ij}^2 \right)^{\frac{1}{2}}, \quad i = 1, \ldots, \tilde{n}$
6. $d_i = \max_{j=1,\ldots,\tilde{n}} |a_{ij}|, \quad i = 1, \ldots, \tilde{n}.$

In the cases 2. and 3., the machine precision eps is used instead of $a_{ii}$ if $|a_{ii}| < \mathrm{eps}$.

## 8.5 Warm start of interior point methods

The notions *warm start* and *hot start* are distinguished in context of interior point methods [176] as described in Section 7.2. The start of an algorithm to find a solution of a new optimization problem from a solution of a previously solved optimization problem is called hot start. The starting point may be at the boundary of the feasible set. This results in an ill-conditioned KKT matrix and a small step size [71]. The start from a point near to a solution of a previously solved optimization problem but sufficiently far from the boundary is called warm start [176].
Recently, an unblocking strategy for interior point methods is suggested in [71]. A survey at earlier proposed heuristics for a hot start is also given as well as examples for a warm start with a first correction step for unblocking and combinations of these strategies [71].
We do not expect the solutions of the optimization problems for model reduction as discussed in Chapter 5 at the boundary of the realizable composition space. So we always use the hot start technique as described in Section 8.1. Some tests for a comparison of a hot start with the final homotopy parameter $\delta$ of a previously solved optimization problem and an increased value of

$\delta$ show that convergence with $\delta$ from the old solution usually is faster in our experience than with an increased value. This is because the original value for $\delta$ fits together with the current prediction as described in Section 8.1.2. If convergence to the solution is blocked, this results in many corrector iterations such that the algorithm for the step size control (see Section 8.2) computes a reduced step size in the continuation algorithm.

*However beautiful the strategy, you should occasionally look at the results.*

Winston Churchill

# 9 Results of application

A computer code in form of a collection of `C++` classes named `MoRe` (short for model reduction) is developed with this thesis. The code solves the optimization problems (5.1), (5.6), or (5.7) for model reduction to reduce general ODE models, but it is tailored to particular needs of the reduction of chemical combustion models.
The implementation of the model reduction method is tested with a large number of examples. A selection of results of the tests is presented in this chapter. In the first section, test models with SIM that can be represented as the graphs of functions are used. In Section 9.2, more complicated models are treated. Test models based on kinetic mechanisms are considered in Section 9.3. Finally, results of the reduction of realistic models for combustion are shown in Section 9.4.

**Remark 9.0.1** (Choice of the objective function)
For the results presented in this chapter, we only use criterion

$$\Phi(z(t)) = \| J_{S^{\mathrm{m}}}(z(t))\, S^{\mathrm{m}}(z(t)) \|_2^2 \tag{9.1}$$

in the objective function (5.2) of the optimization problem (5.1) as the optimization problem (5.1) with this objective function is analyzed theoretically in [108].

**Remark 9.0.2** (Design of the figures)
In the following, all figures are designed in a similar way: All state variables (of importance) are plotted versus the reaction progress variables via a projection from the full composition space into the subspace spanned by the reaction progress variables and the state variable under consideration. The

state of equilibrium is shown as full red dot. Numerical solutions of different optimization problems for different values of the reaction progress variables are shown as blue x marks. This is the optimal value $z^*(t_*)$ and eventually $T^*(t_*)$. To distinguish test cases where the state variables are not given in terms of specific moles in $\mathrm{mol\,kg^{-1}}$, the symbol $y$ is used instead of $z$. If the optimization problem (5.6) is solved in the *reverse mode*, i.e. $t_* = t_\mathrm{f}$, the "reverse" trajectory pieces $\{(z^{*,\mathrm{T}}(t),\ T^{*,\mathrm{T}}(t))^\mathrm{T} \mid t \in [t_0, t_\mathrm{f}]\}$ are also shown. In all cases, trajectories through the solution points in forward direction ($t > t_*$) are shown. This allows for a consistency test as it is described in Definition 5.5.1.

## 9.1 Basic tests

As a first test, we aim at the computation of an approximation of SIM in case of models, where analytic expressions as descriptions of SIM are given. A qualitative and quantitative comparison between the numerical results and the analytical evaluation can be made.

### 9.1.1 Davis–Skodje model

The Davis–Skodje model is a standard test model for model reduction purposes due to an existing analytical expression for the SIM. The Davis–Skodje model is given in [43, 149] via the two-dimensional system of ODE

$$\begin{aligned} \mathrm{D}y_1 &= -y_1 \\ \mathrm{D}y_2 &= -\gamma y_2 + \frac{(\gamma-1)y_1 + \gamma y_1^2}{(1+y_1)^2}. \end{aligned} \tag{9.2}$$

The parameter $\gamma > 1$ serves as a measure for the spectral gap of the system. The model is constructed in such a way that there is an exact SIM described by the graph of the map

$$y_2 = \frac{y_1}{1+y_1}.$$

In case of the Davis–Skodje model, there is also an explicit representation for a one-dimensional ILDM, see the explanation in Section 2.4.2. It is given as the graph of the map

$$y_2 = \frac{y_1}{1+y_1} + \frac{2y_1^2}{\gamma(\gamma-1)(1+y_1)^3}.$$

Results of our model reduction method in application to the Davis–Skodje model are shown in [105, 108, 135, 161]. So we restrict ourselves to some basic examples.
In this model, $y_1$ is the slow variable. Solutions of the optimization problem (5.6) are visualized in Figures 9.1 and 9.2 for different values of the reaction

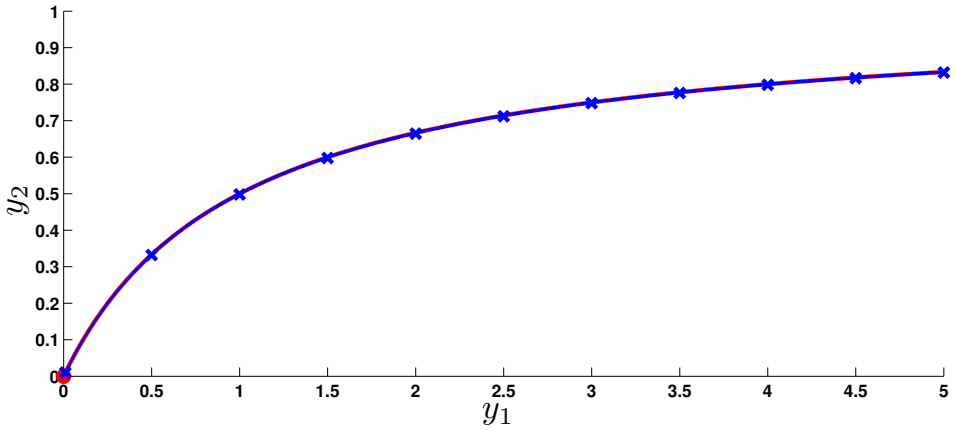


**Figure 9.1:** Visualization of numerical solutions of the semi-infinite optimization problem (5.6) in reverse mode $t_* = t_\mathrm{f}$ with $t_\mathrm{f} - t_0 = 5$ to reduce the Davis–Skodje model with a spectral gap $\gamma = 3$. The x marks are the solution points $y^*(t_*)$ for several values of the reaction progress variable $y_1$ at $t_*$, for each of which the optimization problem is solved.

progress variable $y_1$ at $t_*$. In all cases, a small value for the spectral gap $\gamma$ is chosen. The optimization problem in reverse mode formulation ($t_* = t_\mathrm{f}$) is solved for a time horizon of $t_\mathrm{f} - t_0 = 5$. The plots show the exact SIM as red curve. It can be seen that the results $y^*(t_*)$ are near this invariant one-dimensional manifold. Only for the small value $y_1^{t_*} = 0.01$ for the reaction progress variable in case of the small spectral gap $\gamma = 1.1$, the solution $y^*(t_*)$ is not close to the invariant manifold, see Figure 9.2. A better result could be achieved with a larger time horizon $t_\mathrm{f} - t_0$ as it is proven in [108]. A comparison of our results to the ILDM is shown in [105].

To obtain the results shown in Figure 9.3, the same spectral gap for the Davis–Skodje model is used as for the results visualized in Figure 9.1, but solutions of the optimization problem (5.7) are computed. The presented numerical solutions $y^*(t_*)$ are inconsistent in the sense of Definition 5.5.1; however, the computation is less time-consuming.

For the results shown in Figure 9.4, the same spectral gap for the Davis–Skodje model is used as for the results depicted in Figure 9.1, but the forward mode $t_* = t_0$ in the semi-infinite optimization problem (5.6) is used with the same time horizon. The presented numerical solutions $y^*(t_*)$ deviate stronger from the exact SIM than the results do which are shown in Figure 9.3.

We want to illustrate the linear step as defined in Equation (8.14) by means of the results shown in Figure 9.5. We choose the problem formulation as the same that we have chosen for the results shown in Figure 9.1. However, we set the linear step tolerance, see Equation (8.13), to a very large value of $\epsilon_\mathrm{tol} = 0.75$ for demonstration. In regions where the SIM has a large

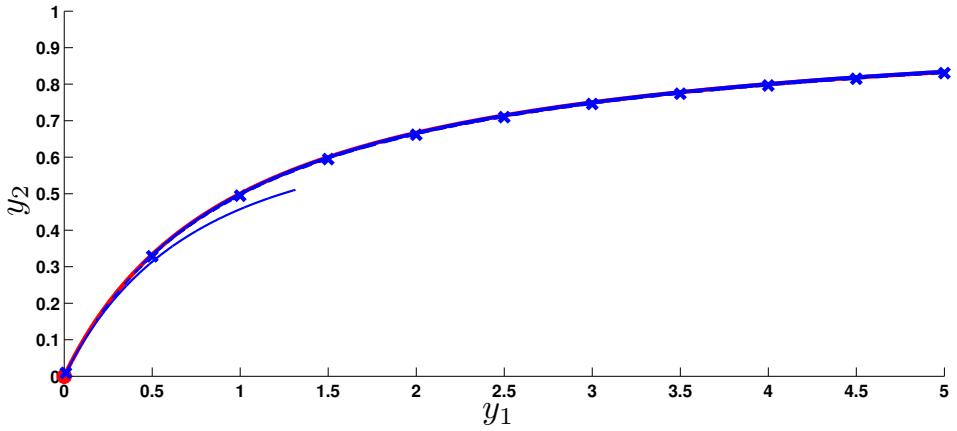


**Figure 9.2:** Illustration of numerical solutions of the optimization problem (5.6) to reduce the Davis–Skodje model with the same setting ($t_* = t_\mathrm{f}$, $t_\mathrm{f} - t_0 = 5$) as for the computation of the results shown in Figure 9.1 but with a spectral gap $\gamma = 1.1$.

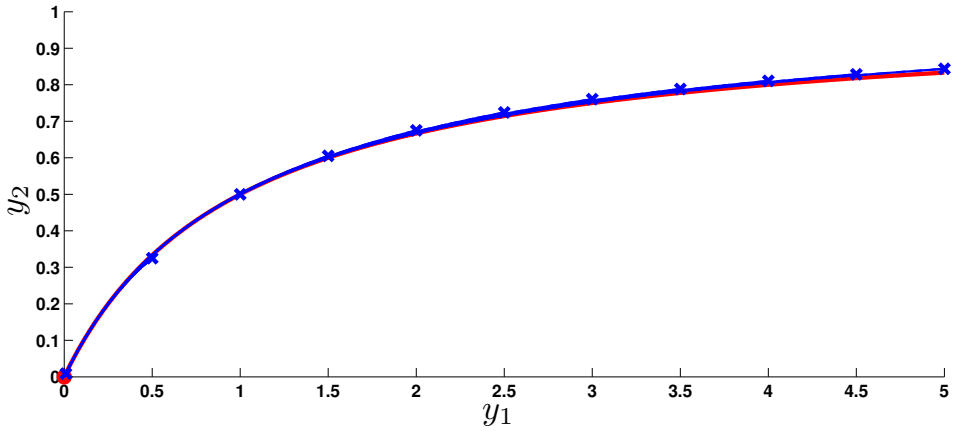


**Figure 9.3:** Visualization of numerical solutions of the local (in the point in time $t_*$) optimization problem (5.7) to reduce the Davis–Skodje model with $\gamma = 3$.

curvature, the results deviate from the invariant slow manifold.

### 9.1.2 Verhulst model

An interesting model is discussed in [164, Example 1.2]. It is given as the two-dimensional system of ODE

$$\begin{aligned} \mathrm{D}y_1 &= 1 \\ \mathrm{D}y_2 &= \frac{y_1 y_2 - y_2^2}{\varepsilon} = \frac{(y_1 - y_2) y_2}{\varepsilon} \end{aligned} \tag{9.3}$$

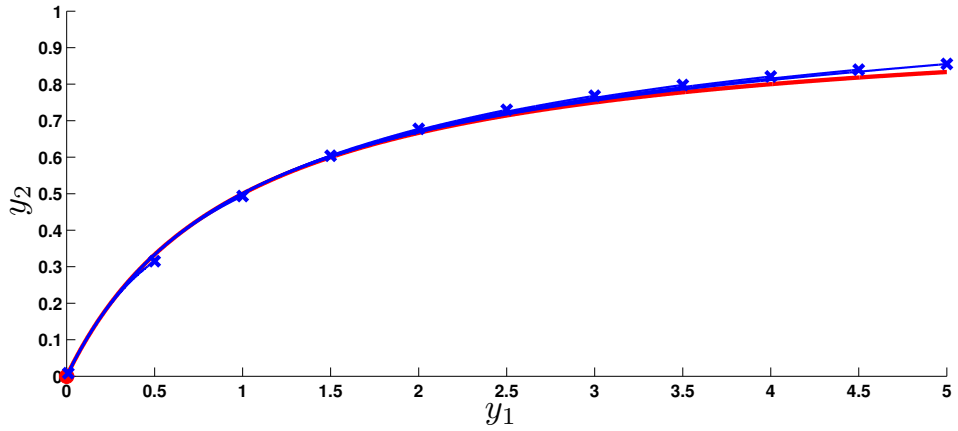


**Figure 9.4:** Visualization of numerical solutions of the optimization problem (5.6) in forward mode $t_* = t_0$ with $t_\mathrm{f} - t_0 = 5$ to reduce the Davis–Skodje model with $\gamma = 3$.

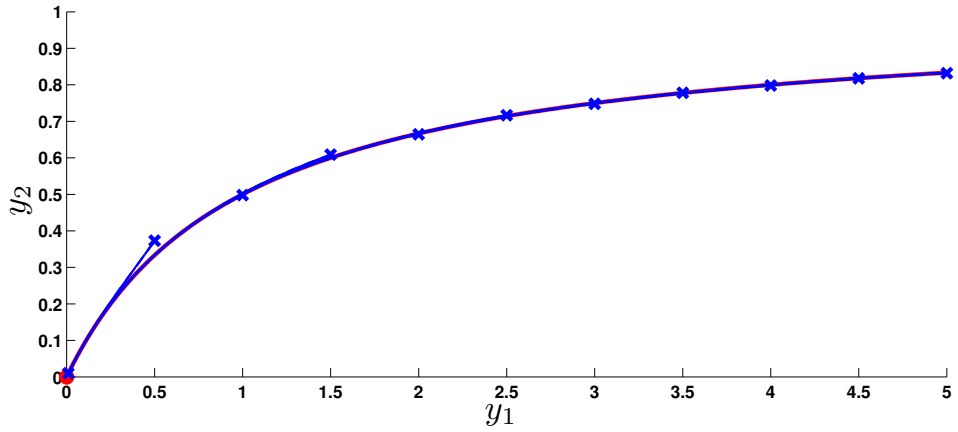


**Figure 9.5:** Illustration of numerical solutions of (5.6) in reverse mode $t_* = t_\mathrm{f}$ with $t_\mathrm{f} - t_0 = 5$ to reduce the Davis–Skodje model with $\gamma = 3$, but the linear step tolerance $\epsilon_\mathrm{tol} = 0.75$ (see Equation (8.13)) is chosen.

with the small parameter $\varepsilon > 0$. The right hand side of the fast variable $y_2$ is $\mathrm{D}y_2 = 0$ at the two critical points $y_2 = 0$ and $y_2 = y_1$. The stability of the critical points depends on the value of the slow variable $y_1$. If $y_1 < 0$, $y_2 = 0$ is stable and $y_1 = y_2$ is instable, and vice versa. This means, there are two slow manifolds: the $y_1$-axis for $y_1 < 0$ and the line of identity for $y_1 > 0$. Consider the stable SIM given as the graph of the map

$$y_2 = \begin{cases} 0, & y_1 < 0 \\ y_1, & y_1 \geqslant 0. \end{cases}$$

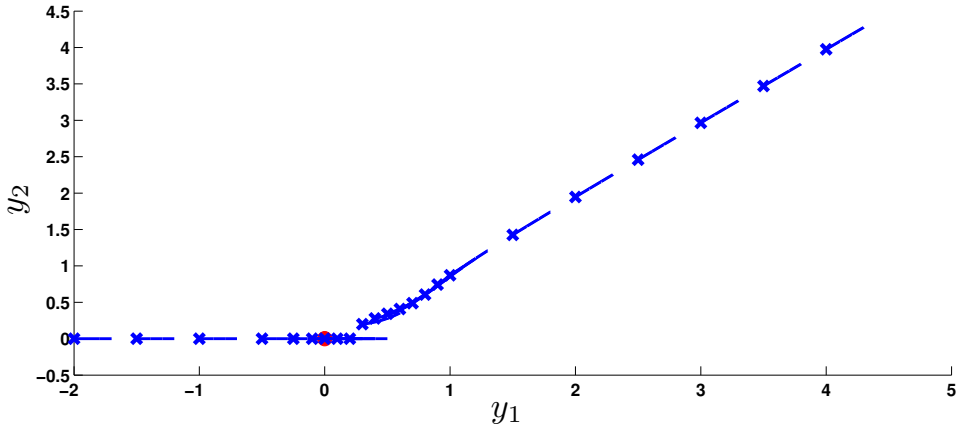


**Figure 9.6:** Visualization of numerical solutions of (5.6) in forward mode $t_* = t_0$ to reduce the Verhulst model (9.3). The time horizon is $t_\mathrm{f} - t_0 = 0.3$, and the spectral gap is $\varepsilon = 0.01$.

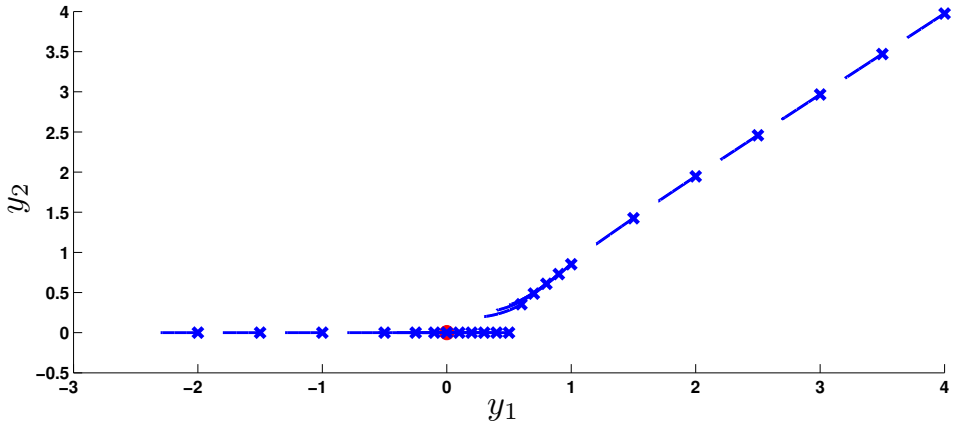


**Figure 9.7:** Visualization of numerical solutions of (5.6) in reverse mode $t_* = t_\mathrm{f}$ to reduce the Verhulst model (9.3). The time horizon is $t_\mathrm{f} - t_0 = 0.3$, and the spectral gap is $\varepsilon = 0.01$.

This function is not continuously differentiable at $y_1 = 0$ such that the region near $y_1 = y_2 = 0$ is of special interest.
The results of an application of our model reduction method are shown in Figures 9.6 and 9.7. In both cases, a collocation method is used for discretization of (5.6) as this solution method shows fast convergence in our experience in the region where the stability of the SIM changes near $y_1 = 0$. Different optimization problems are solved starting with the reaction progress variable at a value of $y_1^{t_*} = 4$. More solution points $y^*(t_*)$ of (5.6) with $t_* = t_0$ for the reduction of the Verhulst model (9.3) with different $y_1^{t_*}$ are nearer to the stable SIM than the corresponding solution points of (5.6) with the reverse mode $t_* = t_\mathrm{f}$; compare the results for $0 < y_1^{t_*} < 0.5$ in

Figures 9.6 and 9.7.

### 9.1.3 Singularly perturbed system of catalysis

As introduced in Section 2.2.2, we want to approximate a SIM in the phase space of the singularly perturbed system which arises in catalytic reactions. The approximation of zeroth order of the SIM can be computed by setting the right hand side of Equation (2.7b) to zero for $B_Z = 0$. With the value $B_A = 1.0$, this leads to the expression

$$-k_1^+ y_A y_Z + k_1^- y_{AZ} + k_2^+ y_{AZ} - k_2^- y_Z y_P = 0.$$

Hence, an approximation of the one-dimensional SIM is the graph of

$$y_Z = -\frac{k_1^- + k_2^+}{(-k_1^+ + k_2^-)y_A - k_1^- - k_2^+ - k_2^-}. \tag{9.4}$$

The test to identify candidates for reaction progress variables based on the comparison of $\hat{\sigma}_i(\bar{y})$ defined in Equation (5.11) suggests to use $y_A$. Solutions of optimization problem (5.6) with $t_* = t_f$ for the reduction of the model for catalysis with different values for $y_A^{t_*}$ are shown in Figure 9.8. The parameters of the model are given in Section 2.2.2.

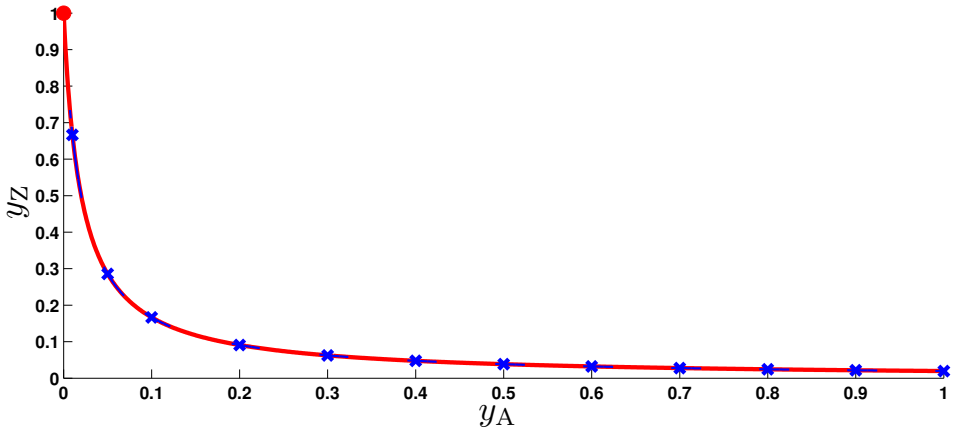


**Figure 9.8:** Illustration of numerical solutions of the optimization problem (5.6) with $t_* = t_f$ for the reduction of the singularly perturbed system for catalysis as given in Equation (2.7). The integration interval is $t_f - t_0 = 2.5$. The red curve is the SIM approximation as given via Equation (9.4).

The SIM approximation given via the graph of the map in Equation (9.4) is shown as red curve in Figure 9.8. The presented numerical solutions of the optimization problem coincide with the analytical result.

## 9.2 Advanced tests

The models in the previous section involve simple ODE and have a known SIM, that is representable as the graph of an explicit function. In this section, the examples are more complicated as they involve features of realistic models.

### 9.2.1 Simple three species model

In the original article [101] and [102, 104], the MEPT model reduction method is tested with a small three component reaction model as given in Table 9.1. The realizable composition space has an effective dimension of two due to mass conservation. This model is further discussed by Al-Khateeb et al. in [6, 7]. They compute an exact one-dimensional slow manifold for the model via heteroclinic orbits. In [105, 108], comparisons of our results with those of Al-Khateeb et al. are discussed.

**Table 9.1:** Three component test mechanism. The rate coefficients are given directly.

| Reaction | | | $k_\mathrm{f}$ | $k_\mathrm{r}$ |
|---|---|---|---|---|
| A+A | $\rightleftharpoons$ | B | 1 | $10^{-5}$ |
| B | $\rightleftharpoons$ | C | 0.01 | $10^{-5}$ |

A scaled ODE system for this model is given by the equations

$$\begin{aligned}
\mathrm{D}y_\mathrm{A} &= -k_{\mathrm{f},1}\, y_\mathrm{A}^2 + k_{\mathrm{r},1}\, y_\mathrm{B} \\
\mathrm{D}y_\mathrm{B} &= k_{\mathrm{f},1}\, y_\mathrm{A}^2 - k_{\mathrm{r},1}\, y_\mathrm{B} - k_{\mathrm{f},2}\, y_\mathrm{B} + k_{\mathrm{r},2}\, y_\mathrm{C} \\
\mathrm{D}y_\mathrm{C} &= k_{\mathrm{f},2}\, y_\mathrm{B} - k_{\mathrm{r},2}\, y_\mathrm{C},
\end{aligned}$$

and the conservation relation $y_\mathrm{A} + y_\mathrm{B} + y_\mathrm{C} = 1.0$ holds.
The authors of [6] find two finite equilibria $R_1$ and $R_2$

$$\begin{aligned}
R_1 &= (9.9945 \times 10^{-5}, 9.9890 \times 10^{-4}, 9.9890 \times 10^{-1}) \\
R_2 &= (-9.9955 \times 10^{-5}, 9.9910 \times 10^{-4}, 9.9910 \times 10^{-1}).
\end{aligned}$$

The heteroclinic orbit connecting the saddle $R_2$ with the sink $R_1$ is a one-dimensional SIM of the system.
As in [101, 105], we choose $y_\mathrm{C}$ as reaction progress variable. It is fixed at several grid point values between $9.9890 \times 10^{-1}$ and $9.9910 \times 10^{-1}$. Computed solution points $y^*(t_*)$ of the optimization problem (5.6) in reverse mode $t_* = t_\mathrm{f}$ for the different values of $y_\mathrm{C}^{t_*}$ are shown in Figure 9.9. Arbitrary trajectories shown as green dashed curves converge to the SIM. The SIM is well identified.

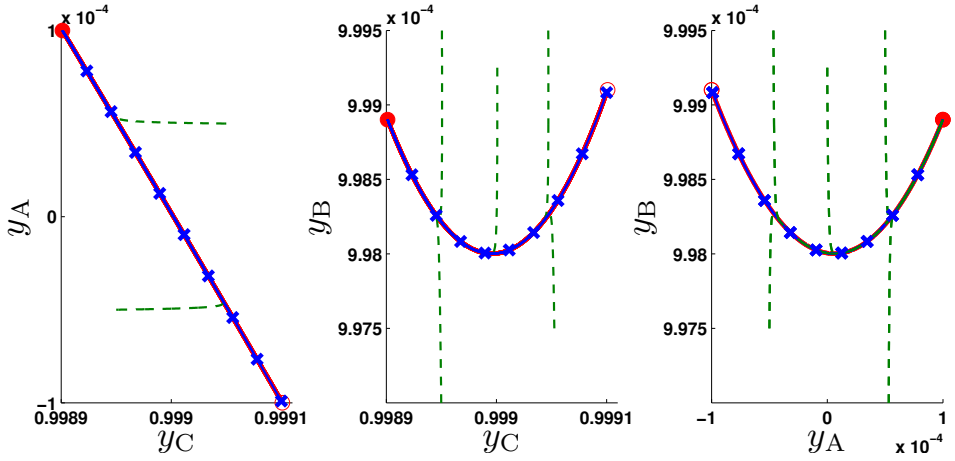


**Figure 9.9:** Visualization of numerical solutions of optimization problem (5.6) with reverse mode $t_* = t_\mathrm{f}$ for the reduction of the three species example with a time horizon $t_\mathrm{f} - t_0 = 300$. Arbitrary trajectories are plotted green, dashed. The full red dot denotes the sink $R_1$, the open red dot denotes the saddle $R_2$. An integration from a slightly disturbed value of $R_2$ leads to $R_1$. This trajectory is shown as approximation of the heteroclinic orbit depicted as red curve. Our results are shown as blue crosses.

### 9.2.2 Lindemann mechanism

The Lindemann mechanism is given in a dimensionless form via the equations

$$\begin{aligned} \mathrm{D}y_1 &= +\frac{y_2}{\varepsilon}(y_2 - y_1) - y_1 \\ \mathrm{D}y_2 &= -\frac{y_2}{\varepsilon}(y_2 - y_1) \end{aligned}$$

in [77], where $0 < \varepsilon \ll 1$ is a small parameter measuring the time gap and $y_1$ is the slow variable. Dissociation-recombination processes are modeled with this mechanism [77]. A value of $\varepsilon = 10^{-3}$ is proposed for the test problem. The special feature of this mechanism is the fact, that the SIM exits or vanishes in different areas of the two-dimensional phase space. The slow manifold can be described with the equations

$$y_1 \approx y_2 - \frac{\varepsilon}{2} + \frac{\varepsilon^2}{4y_2}, \quad (y_1, y_2) > \mathcal{O}(\varepsilon) \tag{9.5a}$$

$$\varepsilon y_1 \approx y_2^2 + \frac{y_2^3}{\varepsilon} - \frac{5y_2^5}{\varepsilon^3}, \quad (y_1, y_2) < \mathcal{O}(\varepsilon). \tag{9.5b}$$

In case of $(y_1, y_2) = \mathcal{O}(\varepsilon)$, there is no time gap. A reasonable choice for an initial value is $y_0 = (1, 4)^\mathrm{T}$. The trajectory started at this point is first attracted to the SIM described by the graph of the first equation (9.5a), near

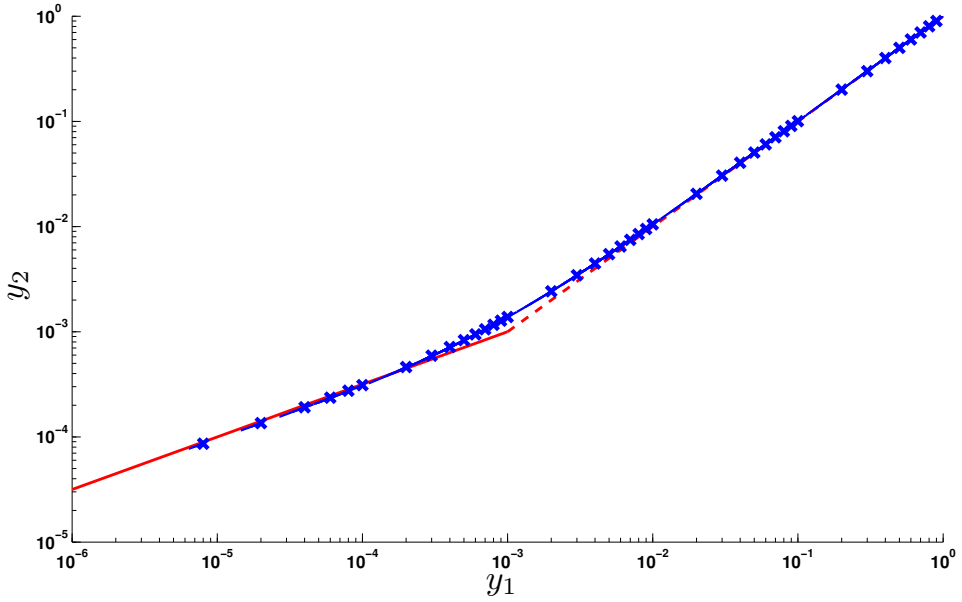


**Figure 9.10:** Visualization of numerical solutions $y^*(t_*)$ of the optimization problem (5.7) for the reduction of the Lindemann mechanism as blue x marks. The axes have logarithmic scale. The red and red dashed curves show the two different parts of the SIM. A parameter value of $\varepsilon = 10^{-3}$ is used in the computation.

which the fast time scale is exhausted. On the further way to equilibrium (the origin), this manifold degenerates and re-emerges again in form of the graph of Equation (9.5b).

Solutions of the optimization problem (5.7) for the reduction of the Lindemann model with $\varepsilon = 10^{-3}$ are shown in Figure 9.10. There is no time scale separation present if the value of the reaction progress variable is near $y_1^{t_*} \approx \varepsilon = 10^{-3}$.

The method seems to identify a transition between the two parts of the SIM in the region where $(y_1, y_2) = \mathcal{O}(\varepsilon)$. In case optimization problem (5.6) is solved for the reduction of the Lindemann mechanism (results not shown), the *middle mode* $t_* = \frac{1}{2}(t_\mathrm{f} + t_0)$ shows fast convergence and good results in our experience.

### 9.2.3 Bioreactor

An idealistic model describing the processes in a bioreactor is given and reduced in [91]. It consists of three species and the corresponding ODE

system

$$\begin{aligned}
\mathrm{D}s_\mathrm{p} &= \tilde{D}s_\mathrm{p,f} - \tilde{D}s_\mathrm{p} \\
\mathrm{D}x &= -\tilde{D}x + \frac{\mu_\mathrm{max} s x}{K_\mathrm{s} + s} \\
\mathrm{D}s &= \tilde{D}(s_\mathrm{f} - s) + cKs_\mathrm{p} - \frac{\mu_\mathrm{max} s x}{Y(K_\mathrm{s} + s)}.
\end{aligned}$$

The parameters are taken from [91]:

$$\begin{aligned}
s_\mathrm{f} &= 0 & \tilde{D} &= 0.2544\,\mathrm{d}^{-1} \\
\mu_\mathrm{max} &= 4.2\,\mathrm{d}^{-1} & K_\mathrm{s} &= 23.0\,\mathrm{mg\,l}^{-1} \\
Y &= 0.11 & s_\mathrm{p,f} &= 50\,000\,\mathrm{mg\,l}^{-1} \\
K &= 0.1\,\mathrm{d}^{-1} & c &= 1.
\end{aligned}$$

There is a two-dimensional slow manifold in the phase space of this model. The variable $s$ is considered as fast. The equilibrium is taken from [91] as

$$\begin{aligned}
s_\mathrm{p}^\mathrm{eq} &= \frac{\tilde{D}s_\mathrm{p,f}}{\tilde{D} + K} \\
x^\mathrm{eq} &= Y\left(s_\mathrm{f} + \frac{cKs_\mathrm{p,f}}{\tilde{D} + K} + \frac{\tilde{D}K_\mathrm{s}}{\mu_\mathrm{max} - \tilde{D}}\right) \\
s^\mathrm{eq} &= \frac{\tilde{D}K_\mathrm{s}}{\mu_\mathrm{max} - \tilde{D}}.
\end{aligned} \tag{9.6}$$

Solutions of optimization problem (5.6) with $t_* = t_\mathrm{f}$ are shown in Figure 9.11. A two-dimensional slow manifold is approximated, where the slow variables $x$ and $s_\mathrm{p}$ are used as reaction progress variables.

## 9.3 Models based on kinetic mechanisms

In this section, applications of the model reduction algorithm to test models which are based on kinetic mechanisms are presented. The models range from a model based on a small hypothetical test mechanism to models for realistic ozone decomposition.

### 9.3.1 Six species test mechanism

A small mechanism which is used for tests of model reduction methods is raised in [74]. It is also used for demonstrations in [38, 102, 103, 104, 105, 106, 135, 136, 161, 175]. It consists of six species involved in six (forward and reverse) elementary reactions, cf. Table 9.2.
The model is based on this mechanism. A system in an isochoric and isothermal thermodynamic environment is considered. Units are meaningless in

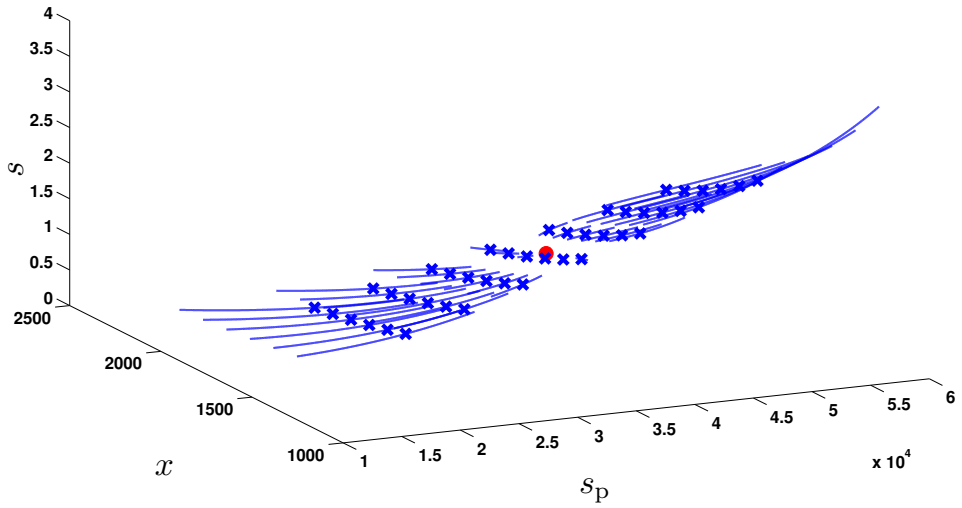


**Figure 9.11:** Visualization of numerical solutions of (5.6) in reverse mode $t_* = t_\mathrm{f}$ with time horizon $t_\mathrm{f} - t_0 = 1$ for the reduction of the bioreactor model (9.6), where $x$ and $s_\mathrm{p}$ are the reaction progress variables.

**Table 9.2:** Six species test mechanism as in [74], where the forward rate coefficients and equilibrium constants are given.

| Reaction | | | $k_\mathrm{f}$ | $k_\mathrm{r}$ |
|---|---|---|---|---|
| $H_2$ | $\rightleftharpoons$ | $2\,H$ | 2.0 | 216.0 |
| $O_2$ | $\rightleftharpoons$ | $2\,O$ | 1.0 | 337.5 |
| $H_2O$ | $\rightleftharpoons$ | $H + OH$ | 1.0 | 1400.0 |
| $H_2 + O$ | $\rightleftharpoons$ | $H + OH$ | 1000.0 | 10800.0 |
| $O_2 + H$ | $\rightleftharpoons$ | $O + OH$ | 1000.0 | 33750.0 |
| $H_2 + O$ | $\rightleftharpoons$ | $H_2O$ | 100.0 | 0.7714 |

this academic example and are skipped in the following. There are only two chemical elements – hydrogen and oxygen – involved. The corresponding mass conservation relations are chosen as in [74] in terms of concentration as

$$\begin{aligned} 2\,c_{\mathrm{H}_2} + 2\,c_{\mathrm{H}_2\mathrm{O}} + c_\mathrm{H} + c_\mathrm{OH} &= 2 \\ 2\,c_{\mathrm{O}_2} + c_{\mathrm{H}_2\mathrm{O}} + c_\mathrm{O} + c_\mathrm{OH} &= 1. \end{aligned}$$

This leads to a mass density of $\rho = 0.0180$. The values given in the figures in the following are in terms of concentration to allow for comparison to the results published in the articles cited above.
The realizable composition space of the model has an effective dimension

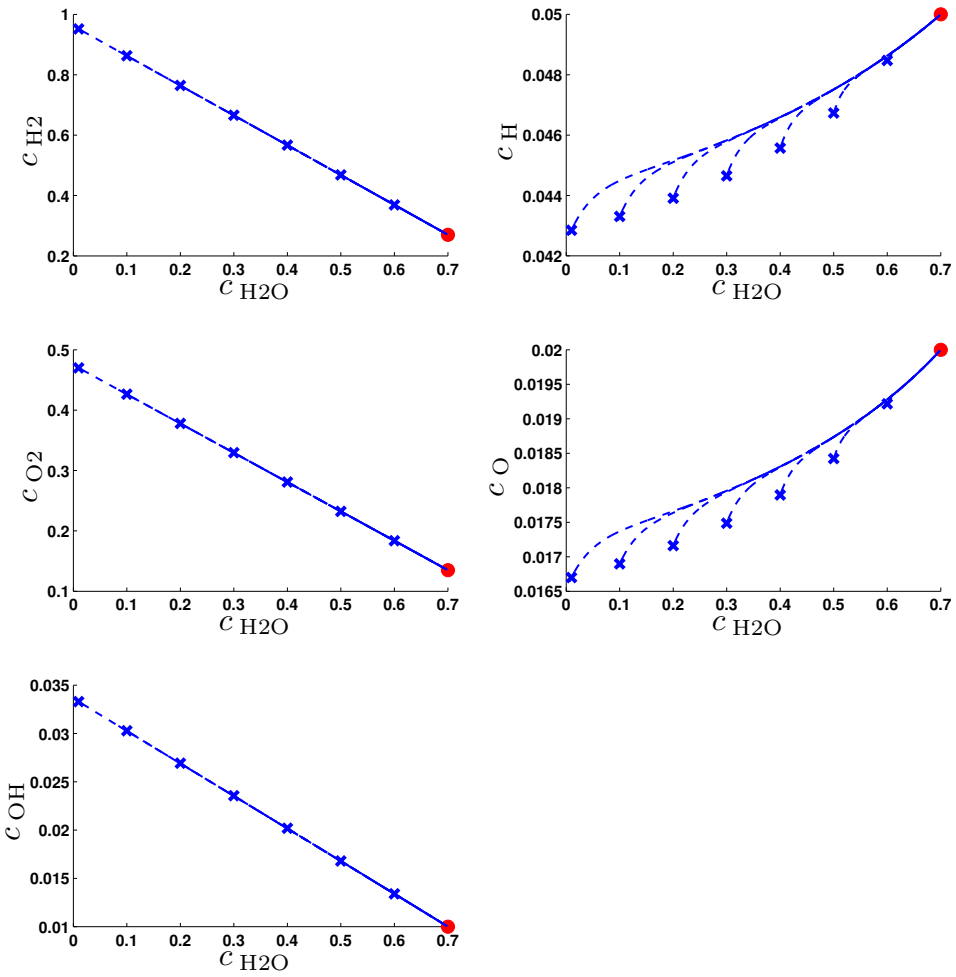


**Figure 9.12:** Illustration of numerical solutions of the optimization problem (5.6) with reverse mode $t_* = t_\mathrm{f}$ to approximate a one-dimensional manifold in the phase space of the six species test model. The time horizon $t_\mathrm{f} - t_0 = 0.001$ is chosen.

of four. We aim to approximate a one- and a two-dimensional manifold. The test to identify candidates for reaction progress variables (see Equation (5.11)) leads to the suggestion to use the specific moles of $H_2O$, $H_2$, H, O, $H_2$, and OH in descending preference.

### One-dimensional manifold

We choose $z_{H_2O}$ as reaction progress variable, where only values smaller than the equilibrium value $z^{\mathrm{eq}}_{H_2O} = 0.7$ are of interest. Solutions of (5.6) with reverse mode $t_* = t_\mathrm{f}$ for the reduction of the six species test model are shown in Figure 9.12. Solutions of the least squares optimization problem (5.7) for

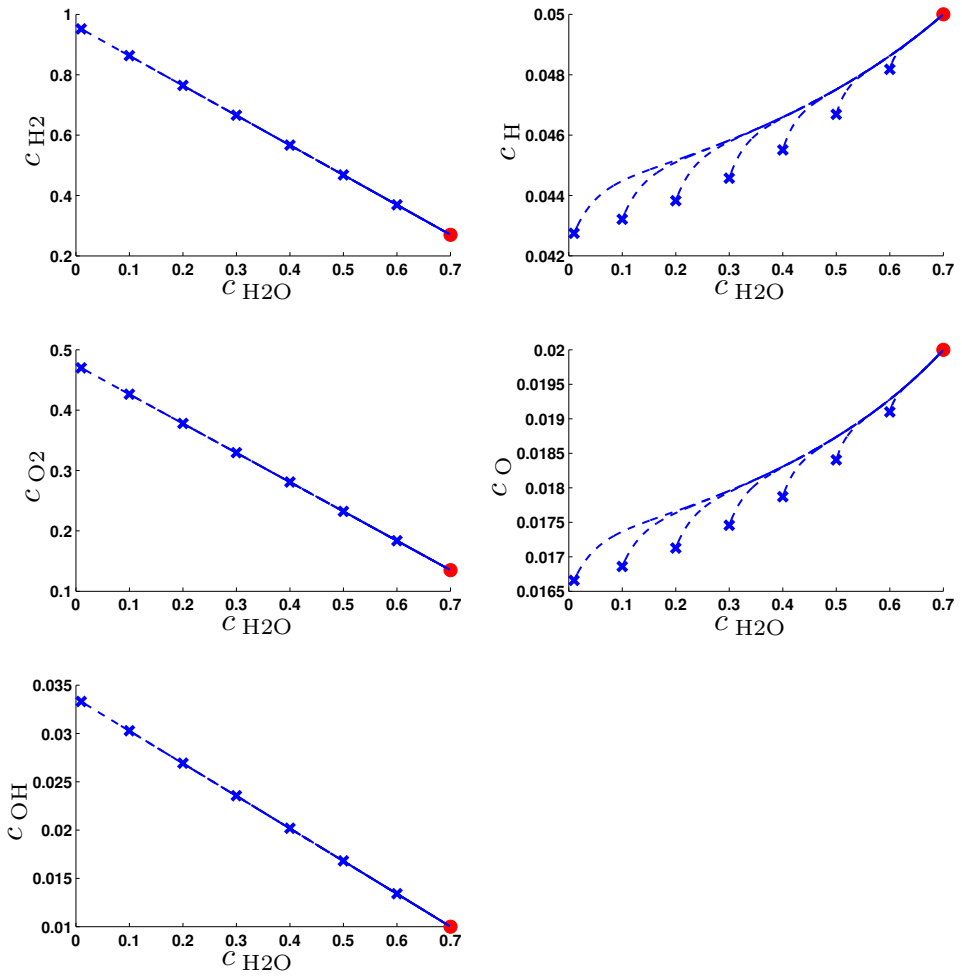


**Figure 9.13:** Visualization of numerical solutions of (5.7) to approximate a one-dimensional slow manifold in the phase space of the six species test mechanism.

the reduction of the six species test model are shown in Figure 9.13. A large inconsistency in the sense of Definition 5.5.1 can be seen in both cases. This is especially the case for the unstable "radical" species H and O that occur at small concentration.

### Two-dimensional manifold

To approximate a two-dimensional SIM, $z_{H_2}$ and $z_{H_2O}$ serve as reaction progress variables. These are fixed at different values in the region where the value of $z_{H_2}$ is higher than its equilibrium value and $z_{H_2O}$ is lower than its equilibrium value. Combinations of these values which violate mass conservation and nonnegativity are identified and sorted out automatically in

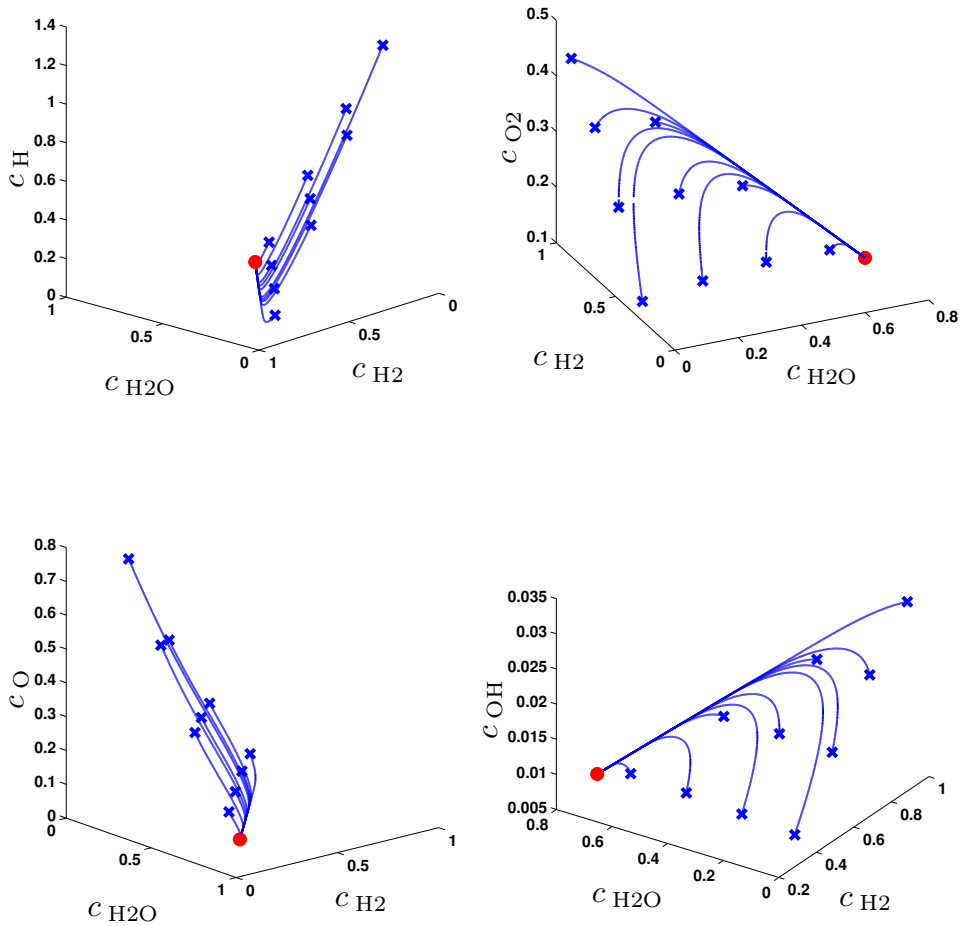


**Figure 9.14:** Visualization of numerical solutions of the optimization problem (5.6) in reverse mode ($t_* = t_\mathrm{f}$) to approximate a two-dimensional slow manifold in the phase space of the six species test mechanism. As the norm of the right hand side of the ODE model as a measure of the rate of change of the state variables is larger near the two-dimensional SIM than it is near the one-dimensional SIM, a smaller integration interval of $t_\mathrm{f} - t_0 = 10^{-5}$ is used in comparison to the time horizon used for the results shown in Figure 9.12.

the implementation. Solutions of the optimization problem (5.6) in reverse mode ($t_* = t_\mathrm{f}$) for the reduction of the six species test model are shown in Figure 9.14. An approximation of an invariant manifold can be asserted.

### 9.3.2 Simplified six species hydrogen combustion

In this section, we consider a test case that includes a simplified combustion mechanism. The presented results are partly discussed in [108, 148], where

we show a comparison of solutions of our method to the results of Al-Khateeb et al. [6, 7].
The reaction mechanism is given in Section A.1, see also [140]. It consists of five reactive species and inert nitrogen. The reaction system is considered in an isothermal and isobaric thermodynamic environment at a temperature of $T = 3000\,\mathrm{K}$ and a pressure of $p = 101\,325\,\mathrm{Pa}$.
Conservation relations for the elemental mass in this model are given in terms of amount of substance as [140]

$$\begin{aligned} n_{\mathrm{H}} + 2\,n_{\mathrm{H_2}} + n_{\mathrm{OH}} + 2\,n_{\mathrm{H_2O}} &= 1.25 \times 10^{-3}\,\mathrm{mol} \\ n_{\mathrm{OH}} + n_{\mathrm{O}} + n_{\mathrm{H_2O}} &= 4.15 \times 10^{-4}\,\mathrm{mol} \\ 2\,n_{\mathrm{N_2}} &= 6.64 \times 10^{-3}\,\mathrm{mol}. \end{aligned} \tag{9.7}$$

The total mass in the system can be computed with the values in Equation (9.7) and has a value of $m = 1.01 \times 10^{-4}\,\mathrm{kg}$.
An analysis which variables should be used as reaction progress variables is done by comparing the values $\hat{\sigma}_i(\bar{z})$, $i = 1, \ldots, n_{\mathrm{spec}}$, defined in Equation (5.11). This results in the recommendation to use the specific moles $z_i$ of the following species (where constant species are ignored) in descending preference: $H_2O$, $H_2$, H, OH, O. Another analysis based on the time scales for an appropriate dimension of a SIM to approximate, see Section 5.5.1, gives the following recommendation in descending preference: 0, 1, 3, 2. As a zero-dimensional manifold corresponds to the equilibrium state and a three-dimensional manifold to the full system, we conclude that it would be more appropriate to approximate a one-dimensional manifold than to approximate a two-dimensional one.

### One-dimensional manifold

We aim to approximate a one-dimensional SIM. Solutions of the optimization problem (5.6) with $t_* = t_{\mathrm{f}}$ and the simplified hydrogen combustion model are computed with the shooting approach and `Ipopt` [168]. The reaction progress variable $z_{\mathrm{H_2O}}$ is fixed at different values between 0.0 and 4.0. The results are shown in a three-dimensional sketch in Figure 9.15 for a comparison with the SIM of Al-Khateeb et al. [6, 7]. The authors of [6, 7] identify the heteroclinic orbits that connect two instable fixed points with the stable equilibrium. The plot is designed as Figure 9 in [6]. The numbering of the species is $z_1 = z_{\mathrm{H_2}}$, $z_2 = z_{\mathrm{O}}$, and $z_3 = z_{\mathrm{H_2O}}$. The unit $\mathrm{mol\,kg^{-1}}$ is omitted in the plots. Figure 9.15 shows a good agreement of our result with theirs.

**Initialization** Fast convergence of the algorithm to compute solutions of optimization problems (5.6) and (5.7) depends strongly on the initial value, that should be chosen near a (still unknown) solution. For a first initialization of the algorithm, we solve the ODE system (5.6b) and (5.6c) initialized

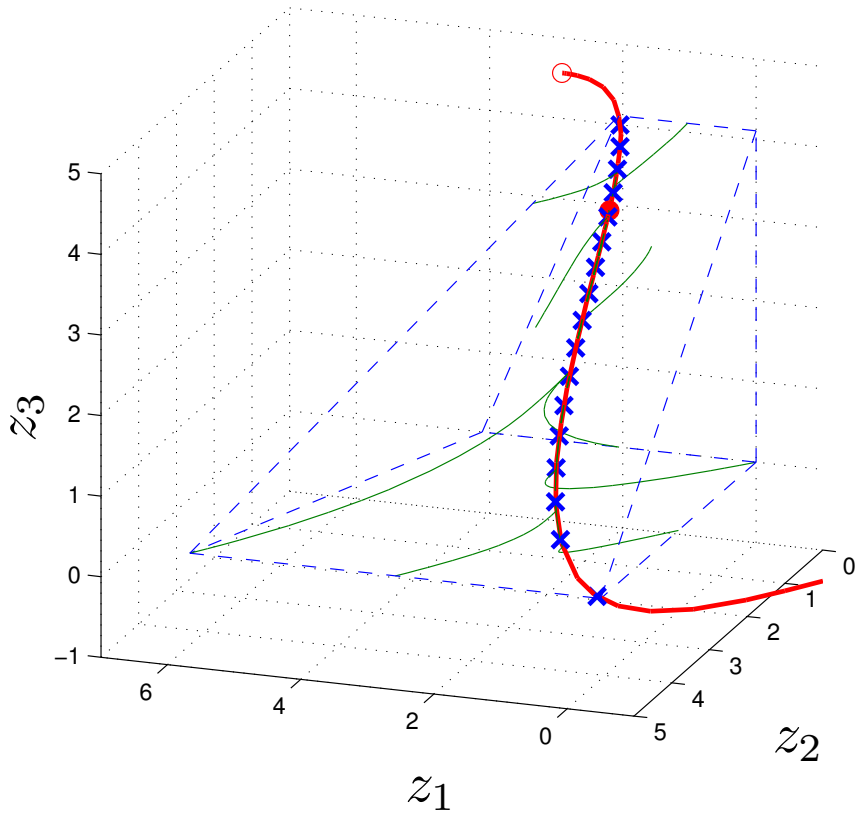


**Figure 9.15:** Three-dimensional visualization of the results illustrated as in Figure 9 in [6]. The blue bounded polytope depicts the realizable state space. Green curves correspond to some arbitrary trajectories to illustrate their bundling near the one-dimensional SIM. The red curve depicts the two branches of the SIM as derived in [6]. The open red dot represents the instable fixed point named $R_6$ in [6]; the full red dot represents the equilibrium $R_7$ [6]. Our results are included as blue x marks: numerical solutions $z^*(t_*)$ of the optimization problem (5.6) with $t_* = t_\mathrm{f}$ and a time horizon $t_\mathrm{f} - t_0 = 10^{-7}\,\mathrm{s}$ to reduce the model for hydrogen combustion. The state of the system is given as $z_1 = z_{\mathrm{H}_2}$, $z_2 = z_\mathrm{O}$, and $z_3 = z_{\mathrm{H}_2\mathrm{O}}$ in $\mathrm{mol\,kg^{-1}}$.

with the desired "unburned" mixture in the sense that $z_{\mathrm{H}_2}$ and $z_\mathrm{O}$ are at their maximum possible value restricted by the given elemental specific moles until reaching the equilibrium state, i.e. until the state variables do not change significantly.

We use a state near the equilibrium state as initial point in the optimization algorithm as we assume this point near a slow manifold. We set the values of the reaction progress variables near their values in that state; see Table 9.3 for the concrete values. This allows for a fast computation of a solution of the first optimization problem with $z^{t_*}_{\mathrm{H}_2\mathrm{O}} = 3\,\mathrm{mol\,kg^{-1}}$.

**Table 9.3:** Initial value (unscaled) for the algorithm and a solution of the optimization problem (5.6) as solved for the results depicted in Figure 9.15 to reduce the simplified hydrogen combustion model with $z^{t_*}_{\mathrm{H_2O}} = 3\,\mathrm{mol\,kg^{-1}}$.

| State | Initial value $z^0(t_0)$, $T^0(t_0)$ | Numerical solution $z^*(t_*)$, $T^*(t_*)$ |
|---|---|---|
| $z_{\mathrm{O}}$ | $0.345\,464\,41\,\mathrm{mol\,kg^{-1}}$ | $0.345\,637\,63\,\mathrm{mol\,kg^{-1}}$ |
| $z_{\mathrm{H_2}}$ | $2.027\,973\,2\,\mathrm{mol\,kg^{-1}}$ | $2.028\,161\,5\,\mathrm{mol\,kg^{-1}}$ |
| $z_{\mathrm{H}}$ | $1.519\,563\,9\,\mathrm{mol\,kg^{-1}}$ | $1.519\,360\,6\,\mathrm{mol\,kg^{-1}}$ |
| $z_{\mathrm{OH}}$ | $0.764\,549\,59\,\mathrm{mol\,kg^{-1}}$ | $0.764\,376\,37\,\mathrm{mol\,kg^{-1}}$ |
| $z_{\mathrm{H_2O}}$ | $3.000\,000\,0\,\mathrm{mol\,kg^{-1}}$ | $3.000\,000\,0\,\mathrm{mol\,kg^{-1}}$ |
| $z_{\mathrm{N_2}}$ | $32.905\,130\,\mathrm{mol\,kg^{-1}}$ | $32.905\,130\,\mathrm{mol\,kg^{-1}}$ |
| $T$ | 3000 K | 3000 K |

**Condition number** We want to show by means of this example that scaling of the KKT matrix as described in Section 8.4 can improve convergence. Therefore, we consider optimization problem (5.6) with $t_* = t_\mathrm{f}$, $t_\mathrm{f} - t_0 = 10^{-7}\,\mathrm{s}$ as it is solved to obtain the results presented in Figure 9.15. The value of the reaction progress variable is fixed to $z^{t_*}_{\mathrm{H_2O}} = 2\,\mathrm{mol\,kg^{-1}}$. The shooting approach and `Ipopt` [168] are used to solve this optimization problem. In Table 9.4, we list the condition numbers of the KKT matrix with different scaling at the solution of this optimization problem denoted as $\mathrm{D}_{(x,\lambda,\mu)}K(x^*, \lambda^*, \mu^*, r)$ in Chapter 8, where $x^* = z^*(t_0)$ are the primal variables in the current context, $\lambda^*, \mu^*$ are the dual variables at the solution, and $r = z^{t_*}_{\mathrm{H_2O}} = 2\,\mathrm{mol\,kg^{-1}}$.
We use the 2-norm condition number $\kappa$

$$\kappa = \frac{\sigma_{\max}(P\mathrm{D}_{(x,\lambda,\mu)}K(x^*, \lambda^*, \mu^*, r)P)}{\sigma_{\min}(P\mathrm{D}_{(x,\lambda,\mu)}K(x^*, \lambda^*, \mu^*, r)P)}$$

computed with `MATLAB` [113], i.e. the ratio of the largest singular value of the equilibrated matrix $P\mathrm{D}_{(x,\lambda,\mu)}K(x^*, \lambda^*, \mu^*, r)P$ to the smallest singular value of the equilibrated $P\mathrm{D}_{(x,\lambda,\mu)}K(x^*, \lambda^*, \mu^*, r)P$ with the regular matrix $P = \mathrm{diag}(d)^{-1}$ and $d \in \mathbb{R}^{n_{\mathrm{spec}}+1}$, see Section 8.4.
The scalings 4., 5., and 6. lead to an improved condition number of the (scaled) KKT matrix at the solution of the optimization problem, which is needed to compute the parameter sensitivities as described in Section 8.1.1, in the case of the presented example.

**Warm start with step size strategy** We want to demonstrate that a step size strategy for the prediction in the predictor corrector scheme of the algorithm to solve neighboring optimization problems can have a benefit. So we consider on the one hand the optimization problem (5.6) with $t_* = t_\mathrm{f}$, $t_\mathrm{f} - t_0 = 10^{-7}\,\mathrm{s}$ to be solved for $z^{t_*}_{\mathrm{H_2O}} = 3\,\mathrm{mol\,kg^{-1}}$ with the shooting approach

**Table 9.4:** Condition number $\kappa$ of the *equilibrated* KKT matrix $P\mathrm{D}_{(x,\lambda,\mu)}K(x^*,\lambda^*,\mu^*,r)P$ with the six different scalings introduced in Section 8.4.

| Scaling | $\kappa$ |
|---|---|
| 1. | $1.7730 \times 10^{13}$ |
| 2. | $1.2344 \times 10^{9}$ |
| 3. | $1.4499 \times 10^{19}$ |
| 4. | $3.0251 \times 10^{5}$ |
| 5. | $3.2546 \times 10^{5}$ |
| 6. | $3.5504 \times 10^{5}$ |

and `Ipopt` [168]. As neighboring problem we consider the same optimization problem but with the parameter value $z^{t_*}_{\mathrm{H_2O}} = 0.5\,\mathrm{mol\,kg^{-1}}$. (Such a rather large change in the parameter can occur e.g. if the presented method for model reduction is used *in situ* in a CFD simulation and grid refinements are performed in different regions of the spatial domain.)
We solve the optimization problem at hand first with $z^{t_*}_{\mathrm{H_2O}} = 3\,\mathrm{mol\,kg^{-1}}$ and second with $z^{t_*}_{\mathrm{H_2O}} = 0.5\,\mathrm{mol\,kg^{-1}}$ with a *full step method* and the Euler prediction. For the scaling of the KKT matrix to compute the parameter sensitivities, we use scaling 4. as this results in the best condition number, see Table 9.4.
The computations are done on an Intel® Core™ 2 Duo CPU E6550 with 2.33 GHz, operating system is openSUSE 11.4 (i586) including the Linux 2.6.37.6 kernel and GCC 4.5. Four iterations in `Ipopt` [168] have to be preformed to solve the first optimization problem and nine iterations to solve the second optimization problem. In sum, 13 iterations are necessary which take 3.63 s.
If we initialize the step size strategy, see Section 8.2, with initial step size $h_{\mathrm{init}} = \frac{1}{2.5}$ and the desired number of iterations $\tilde{k} = 10$, we need one intermediate step in the predictor corrector scheme described in Section 8.1.2. This intermediate step is to solve the optimization problem with the parameter $z^{t_*}_{\mathrm{H_2O}} = 2\,\mathrm{mol\,kg^{-1}}$. In this case, we need in sum $4 + 4 + 6 = 14$ iterations that only take 2.95 s.
The difference in the computation time arises as the point for initialization of the algorithm to solve the second optimization problem in the full step method is not near a solution such that the KKT matrix is badly scaled. The inertia correction in `Ipopt`, see [168], is activated, and 17 line search iterations are performed. In case of an activated step size strategy, the initial value for the algorithm to solve the optimization problem in case of a warm start is near to a solution of the optimization problem such that no inertia correction and only 14 line search iterations (one per Newton iteration) are necessary in the presented example.

### Two-dimensional manifold

We aim to approximate a two-dimensional SIM. We choose the values of $z_1$ and $z_2$ as reaction progress variables in opposition to the results of the analysis which reaction progress variables to choose stated before. Numerical results are shown in Figures 9.16 and 9.17.

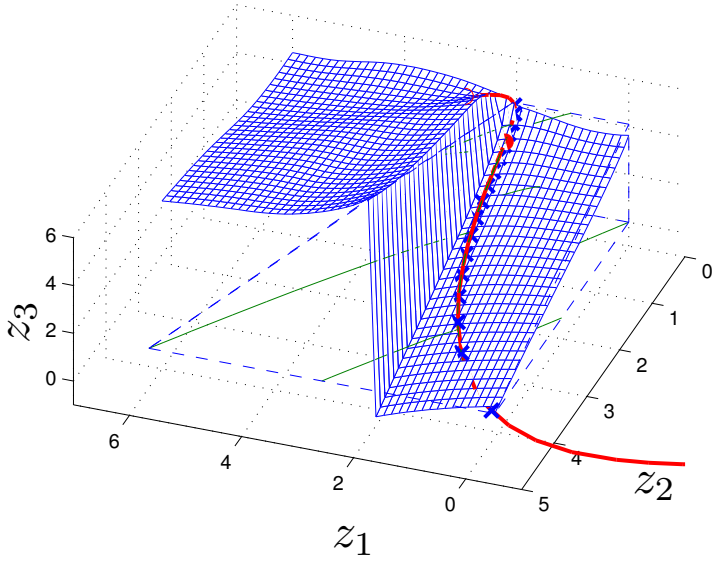


**Figure 9.16:** Visualization of numerical solutions of the optimization problem (5.6) with $t_* = t_\mathrm{f}$, $t_\mathrm{f} - t_0 = 10^{-7}\,\mathrm{s}$ to reduce the simplified hydrogen combustion model with the reaction progress variables $z_1$ and $z_2$. The solution points $z^*(t_*)$ for different values of $(z_1^{t_*}, z_2^{t_*})$ are shown as a blue mesh in addition to the results shown in Figure 9.15.

Solutions of the optimization problem (5.6) approximate different two-dimensional "SIM" for different values of the reaction progress variables. At the turning point of the heteroclinic orbit (in the top left corner of the blue-bounded polytope in Figure 9.16) the two SIM merge. Such phenomena can lead to severe numerical problems in the optimization algorithms as well as in the continuation algorithms as there are regions where the KKT matrix might be singular at least to machine precision.

### Optimization landscapes

We want to further analyze this problem via optimization landscapes, i.e. graphical representations of the objective function versus the (free) optimization variables.

**One reaction progress variable** In Figure 9.18, the value of (the objective function of the optimization problem (5.7)) $\Phi = \|J_{S^\mathrm{m}}(z)\ S^\mathrm{m}(z)\|_2^2$ is

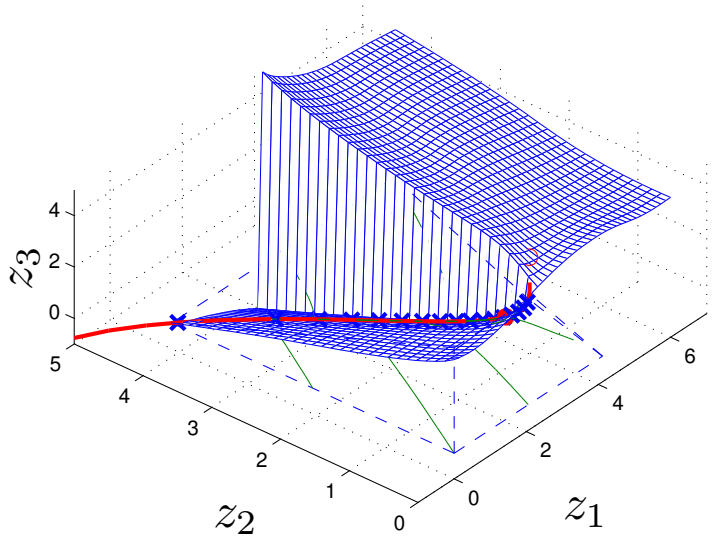


**Figure 9.17:** The same plot as shown in Figure 9.16, but shown from another angle.

plotted versus two degrees of freedom in (5.7) for one exemplary value of one reaction progress variable $z_3^{t_*} = z_{\mathrm{H_2O}}^{t_*} = 1\,\mathrm{mol\,kg^{-1}}$ for the simplified hydrogen combustion model.

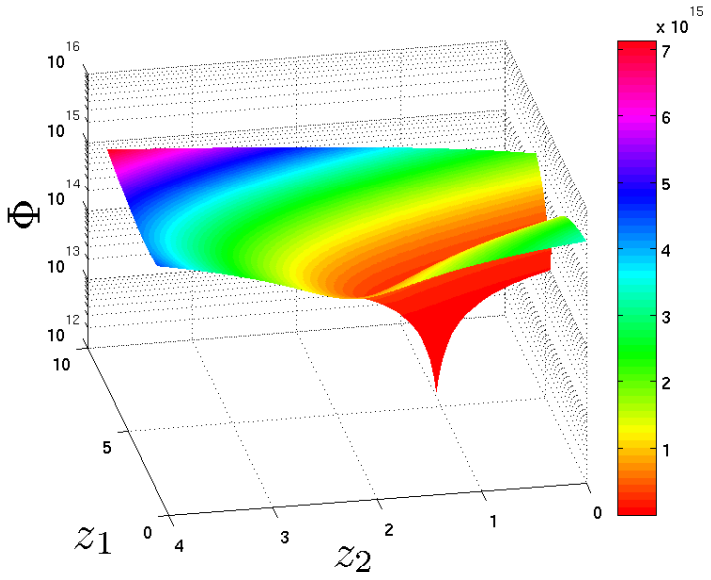


**Figure 9.18:** Visualization of $\Phi = \|J_{S^{\mathrm{m}}}(z)\ S^{\mathrm{m}}(z)\|_2^2$ in dependence of $z_1$ and $z_2$ to illustrate the location of the computed solution of the optimization problem (5.7) with $z_3^{t_*} = z_{\mathrm{H_2O}}^{t_*} = 1\,\mathrm{mol\,kg^{-1}}$ for the reduction of the simplified hydrogen combustion model.

The Φ-axis has logarithmic scale. One local solution of the optimization problem (5.7) for the reduction of the simplified hydrogen combustion model can be seen.

**Two reaction progress variables** To compute an optimization landscape in case of two reaction progress variables, we fix $z_2^{t*} = z_{\mathrm{O}}^{t*} = 0.3\,\mathrm{mol\,kg^{-1}}$. The other reaction progress variable $z_1 = z_{\mathrm{H_2}}$ varies as well as the optimization variable $z_3 = z_{\mathrm{H_2O}}$. This means, we are interested in (the objective function of the optimization problem (5.7)) $\Phi = \|J_{S^{\mathrm{m}}}(z)\, S^{\mathrm{m}}(z)\|_2^2$ in dependence of $z_3$ for fixed $z_1$.

The optimization landscape is shown in Figure 9.19. It can be seen that

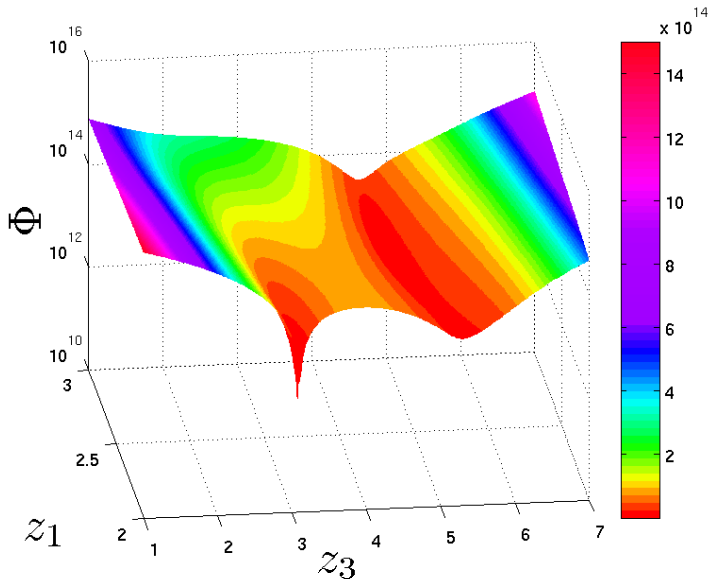


**Figure 9.19:** Visualization of $\Phi = \|J_{S^{\mathrm{m}}}(z)\, S^{\mathrm{m}}(z)\|_2^2$ for the simplified hydrogen combustion model in dependence of $z_1$ and $z_3$ for a fixed value of $z_2^{t*} = 0.3\,\mathrm{mol\,kg^{-1}}$. The scale for Φ is logarithmic. Consider the value of Φ in dependence of $z_3$ for a fixed value of $z_1$, e.g. for $z_1^{t*} = 2\,\mathrm{mol\,kg^{-1}}$.

there are two distinct local minima of $\Phi = \|J_{S^{\mathrm{m}}}(z)\, S^{\mathrm{m}}(z)\|_2^2$ for a fixed value of e.g. $z_1 = 2\,\mathrm{mol\,kg^{-1}}$: There is no unique local solution of the optimization problem (5.7) for the reduction of the simplified hydrogen combustion model with the reaction progress variables $z_2^{t*} = z_{\mathrm{O}}^{t*} = 0.3\,\mathrm{mol\,kg^{-1}}$ and $z_1^{t*} = z_{\mathrm{H_2}}^{t*} = 2\,\mathrm{mol\,kg^{-1}}$.

This is also visualized in Figure 9.20. One solution is near the value $z_3' = z_{\mathrm{H_2O}}' = 3.1020\,\mathrm{mol\,kg^{-1}}$ and the other one near $z_3'' = 5.2977\,\mathrm{mol\,kg^{-1}}$.

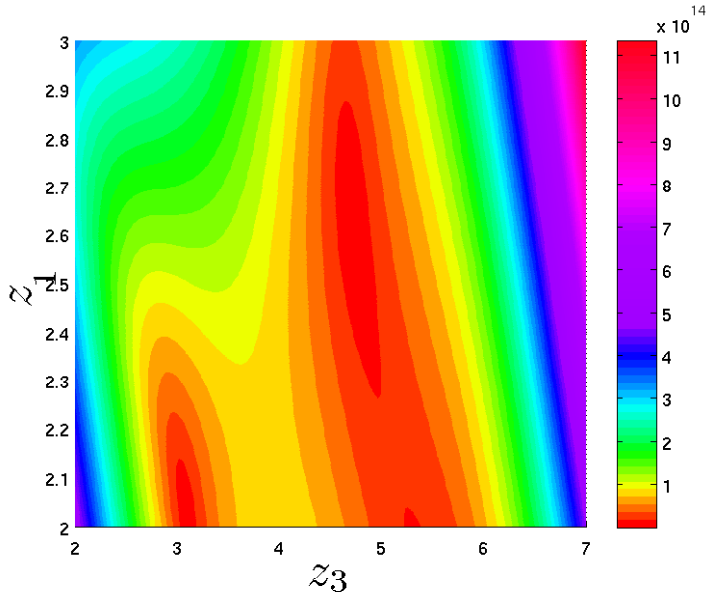


**Figure 9.20:** Same plot as in Figure 9.19 but with the value $z_3 \in [2\,\mathrm{mol\,kg^{-1}}, 7\,\mathrm{mol\,kg^{-1}}]$ and shown from a different angle (view on top).

### Performance test

We use the specific moles of $H_2O$ and $H_2$ (based on the comparison of $\hat{\sigma}_i(\bar{z})$ defined as in Equation (5.11) as stated before) for parametrization of a two-dimensional SIM approximation in a performance test.
We consider a test situation of a two-dimensional grid of 108 points defined by $(z^{t_*}_{H_2O}, z^{t_*}_{H_2}) \in [0.001, 0.5, 1, 1.5, \ldots, 5, 5.5] \times [0.001, 0.5, 1, \ldots, 3.5, 4]$, where points which violate mass conservation in combination with the non-negativity constraints are ignored such that 80 points remain. Solutions of the optimization problem (5.7) to reduce the model at hand, which are computed with the GGN method with Euler prediction for initialization of the algorithm to solve neighboring problems, are shown in Figure 9.21.
In Table 9.5, we compare the performance of our algorithm using the different implemented solution methods. We use the generalized Gauss–Newton method as described in Section 7.1 for solving (5.7). We apply a shooting approach for the semi-infinite optimization problem (5.6) with $t_* = t_f$. The NLP problem (after solving the ODE with the BDF integrator) is solved with the interior point algorithm `Ipopt` [168]. As a third alternative, we use a Gauss–Radau collocation with linear polynomials (backward Euler) for (5.6) with $t_* = t_f$. The resulting high-dimensional NLP problem is also solved with `Ipopt` [168]. For the optimization problem (5.6), an integration horizon of $t_f - t_0 = 10^{-8}\,\mathrm{s}$ is used.
An initialization of neighboring problems is done without step size control,

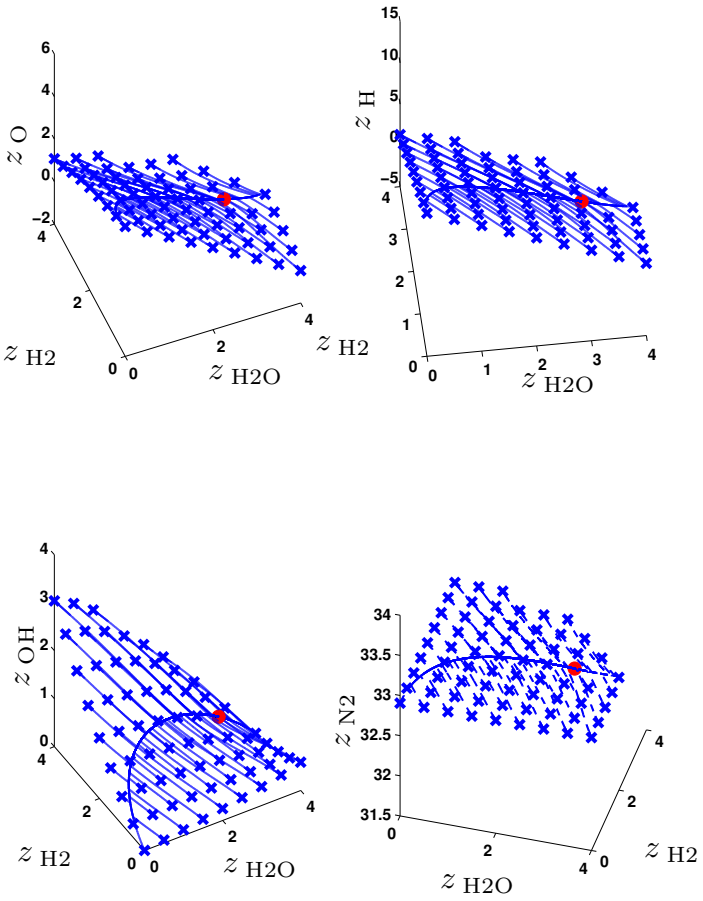


**Figure 9.21:** Illustration of an approximation of a two-dimensional SIM in the phase space of the simplified model for hydrogen combustion. The optimization problem (5.7) is solved with the GGN method. The absolute tolerance for convergence is $10^{-10}$, see Section 7.1.3. The relative tolerance is $10^{-9}$. The values of the optimization variables at the computed solution are plotted versus the given values of the reaction progress variables shown as x marks. The trajectories started with the solution $z^*(t_*)$ as initial values converge toward the equilibrium (full red dot).

as we concentrate on the benefit of the Euler prediction. The computations are done on an Intel® Core™ 2 Duo CPU E6550 with 2.33 GHz.

It can be seen that the relative gain in the computation time achieved by the Euler prediction in case of the collocation method, where we use 100 collocation points, is the largest with about 19%. This is reasonable because of the strong dependence of the collocation method on the initialization on all collocation points in the time interval $[t_0, t_f]$.

The benefit of the Euler prediction if the shooting approach is used to solve

**Table 9.5:** Comparison of the performance of the algorithm for the reduction of the simplified model for hydrogen combustion with two reaction progress variables and full step method for the initialization of neighboring problems.

| Method | Prediction | # Iter. w/o fail | Time | Fail | Time w/o fail |
|---|---|---|---|---|---|
| GGN | Constant | 804 | 0.67 s | 11 | 0.33 s |
| | Euler | 723 | 0.64 s | 11 | 0.30 s |
| Shooting | Constant | 335 | 77.39 s | 0 | 77.39 s |
| | Euler | 258 | 66.48 s | 0 | 66.48 s |
| Collocation | Constant | 315 | 119.28 s | 0 | 119.28 s |
| | Euler | 234 | 96.96 s | 0 | 96.96 s |

(5.6) is about 14%. In case of the GGN method, the benefit is only 10% if we do not regard failures. The eleven failures only occur in the region, where $z_{H_2O}^{t_*}$ is larger than the equilibrium value $z_{H_2O}^{eq}$. The numbers of iterations in Table 9.5 are given without the failures, where the code stops after the predefined maximum of 100 iterations. This drawback can not be overcome neither with the step size control for the continuation method nor with a larger tolerance for convergence in the GGN method. It can be seen that the algorithm to solve (5.7) with the GGN method is about a factor of 100 faster than the algorithm to solve (5.6). The computation of one approximation of a point on the SIM takes about $0.33\,\mathrm{s}/69 = 4.78\,\mathrm{ms}$.

### 9.3.3 Ozone decomposition

As a small realistic test problem, we consider an ozone decomposition mechanism which includes three allotropes of oxygen, namely atomic oxygen, dioxygen, and ozone. The mechanism is given in Section A.2. The following results are also discussed in [107, 148].

The elemental specific mole has to be given for mass conservation. It is always

$$\check{z}_O = \frac{1}{15.999\,\mathrm{g\,mol^{-1}}} = 62.5\,\mathrm{mol\,kg^{-1}}$$

for this composition of species. We consider a density of $\rho = 0.2\,\mathrm{kg\,m^{-3}}$ in the isochoric case and a pressure of $p = 10^5\,\mathrm{Pa}$ for isobaric conditions, respectively. In the isothermal cases, $T = 1000\,\mathrm{K}$ is chosen. The specific internal energy or enthalpy, respectively, of $\check{z}_O$ at a temperature of 1000 K is used as a fixed specific internal energy or enthalpy of adiabatic systems.

In case of the ozone mechanism as given in Table A.2, it is not necessary to demand nonnegativity of specific moles to guarantee that the right hand side of the ODE model is evaluable, because no pressure dependent reactions are

present, which could lead to undefined values in the model equations. Therefore, the model can be evaluated also in nonphysical regions. That means that negative specific moles of the species are visible in the following figures. The analysis for identification of candidates for reaction progress variables (see Equation (5.11)) yields the proposal $z_{\mathrm{O}}$, $z_{\mathrm{O}_2}$, and $z_{\mathrm{O}_3}$ in descending preference. Hence, we use $z_{\mathrm{O}}$.
Solutions of the optimization problem (5.6) for the reduction of the ozone decomposition model in case of all four different thermodynamic environments are shown in Figures 9.22, 9.23, 9.24, and 9.25.
We present the optimization problem (5.6) for the reduction of the model for adiabatic, isobaric ozone decomposition as example. We solve* with $t_* = t_{\mathrm{f}}$, $t_* = 10^{-8}$, $t_0 = 0$, $t \in [t_0, t_{\mathrm{f}}]$

$$\min_{z,T} \int_0^{10^{-8}} \| J_{S^{\mathrm{m}}}(z(t))\ S^{\mathrm{m}}(z(t)) \|_2^2 \,\mathrm{d}t \tag{9.8a}$$

subject to

$$\mathrm{D}z_s(t) = S_s^{\mathrm{m}}(z(t), T(t)) = \frac{\omega_s(t)}{\rho(t)}, \quad s = 1, \ldots, n_{\mathrm{spec}}. \tag{9.8b}$$

$$\mathrm{D}T(t) = -\frac{RT(t) \sum_{s=1}^{n_{\mathrm{spec}}} \left(\bar{H}_s^\circ(T(t))\ \omega_s(t)\right) \sum_{s=1}^{n_{\mathrm{spec}}} z_s(t)}{p\ \sum_{s=1}^{n_{\mathrm{spec}}} \left(z_s(t)\ \bar{C}_{p,s}^\circ(T(t))\right)} \tag{9.8c}$$

$$0 = \check{z}_{\mathrm{O}} - \sum_{s=1}^{n_{\mathrm{spec}}} \chi_{\mathrm{O},s}\, z_s(0) \tag{9.8d}$$

$$0 = \check{h} - \sum_{s=1}^{n_{\mathrm{spec}}} \bar{H}_s^\circ(T(0))\ z_s(0) \tag{9.8e}$$

$$0 = z_{\mathrm{O}}(10^{-8}) - z_{\mathrm{O}}^{t_*} \tag{9.8f}$$

with $\chi_{\mathrm{O},\mathrm{O}} = 1$, $\chi_{\mathrm{O},\mathrm{O}_2} = 2$, and $\chi_{\mathrm{O},\mathrm{O}_3} = 3$. The production rate $\omega_s(t)$ is

$$\omega_s = \sum_{r=1}^{n_{\mathrm{reac}}} \nu_{sr} \left( \sum_{s=1}^{n_{\mathrm{spec}}} \alpha_{sr} c_s \right) \left( k_{\mathrm{f},r} \prod_{s=1}^{n_{\mathrm{spec}}} c_s^{\nu'_{sr}} - k_{\mathrm{r},r} \prod_{s=1}^{n_{\mathrm{spec}}} c_s^{\nu''_{sr}} \right), \ s = 1, \ldots, n_{\mathrm{spec}},$$

with the concentrations

$$c_s = z_s\ \rho, \quad s = 1, \ldots, n_{\mathrm{spec}},$$

the density $\rho$ given via

$$p\bar{M} = \rho RT,$$

and the mean molar mass

$$\bar{M} = \left( \sum_{s=1}^{n_{\mathrm{spec}}} z_s \right)^{-1}.$$

*See Chapter 4 and Section B.2 for the notation.

The forward rate coefficients are computed with the parameters given in Table A.2 as

$$k_{\mathrm{f},r}(T) = A\, T^b\, \mathrm{e}^{-\frac{E_\mathrm{a}}{RT}}, \quad r = 1, \ldots, n_\mathrm{reac},$$

and the reverse rate coefficients via the equilibrium constant

$$K_{c,r} = K_{p,r} \left( \frac{p^\circ}{RT} \right)^{\nu_r}, \quad r = 1, \ldots, n_\mathrm{reac}$$

with

$$\nu_r := \sum_{s=1}^{n_\mathrm{spec}} \nu_{sr}, \quad r = 1, \ldots, n_\mathrm{reac}$$

and

$$K_{p,r} = \exp\left( \frac{\Delta S^\circ_{\mathrm{r},r}(T)}{R} - \frac{\Delta H^\circ_{\mathrm{r},r}(T)}{RT} \right), \quad r = 1, \ldots, n_\mathrm{reac}. \tag{9.9}$$

The entropy and enthalpy of the reactions, the standard molar enthalpy of the species, and the standard molar heat capacity at constant pressure of the species needed in (9.9), (9.8c), and (9.8e) are computed via the NASA polynomials as discussed in Section 4.2.3.

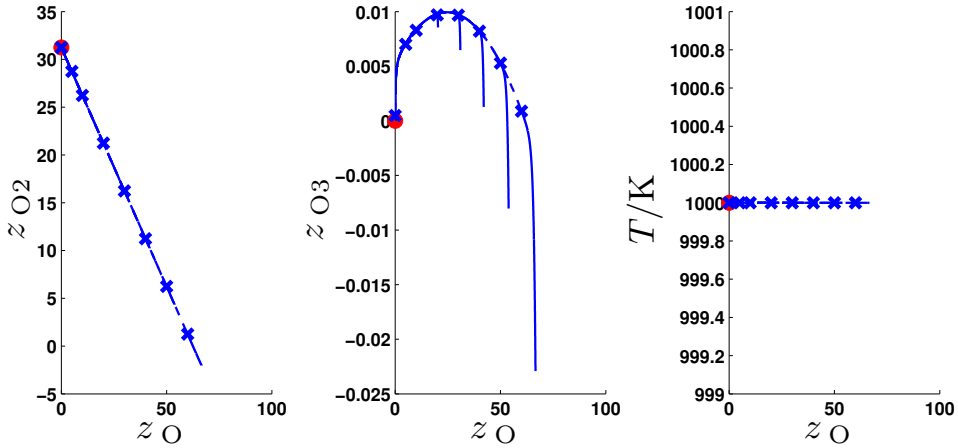


**Figure 9.22:** Illustration of numerical solutions of the optimization problem (5.6) with reverse mode ($t_* = t_\mathrm{f}$) for an approximation of a one-dimensional SIM in the phase space of the ozone decomposition model for an isothermal and isochoric thermodynamic environment. The value of $z_\mathrm{O}$ serves as reaction progress variable and is varied between zero and the largest meaningful value $\check{z}_\mathrm{O}$. We use an integration interval of $t_\mathrm{f} - t_0 = 10^{-6}\,\mathrm{s}$.

For the reduction of the models in all four traditional thermodynamic environments, good results can be achieved as the SIM approximation is nearly consistent in the sense of Definition 5.5.1. However, no consistent SIM approximation can be identified due to a lack of time scale separation in the

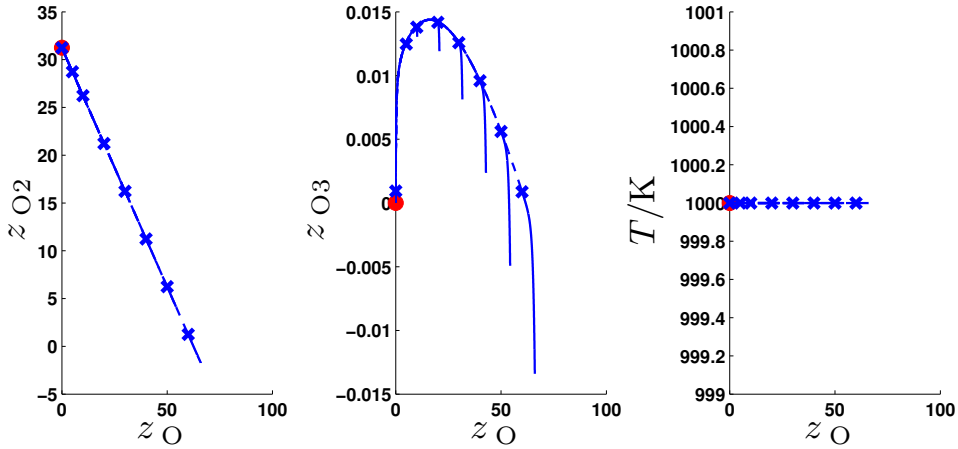


**Figure 9.23:** Visualization of numerical solutions of the same optimization problem as solved for the results shown in Figure 9.22, but the ozone decomposition is modeled in an isothermal and isobaric thermodynamic environment.

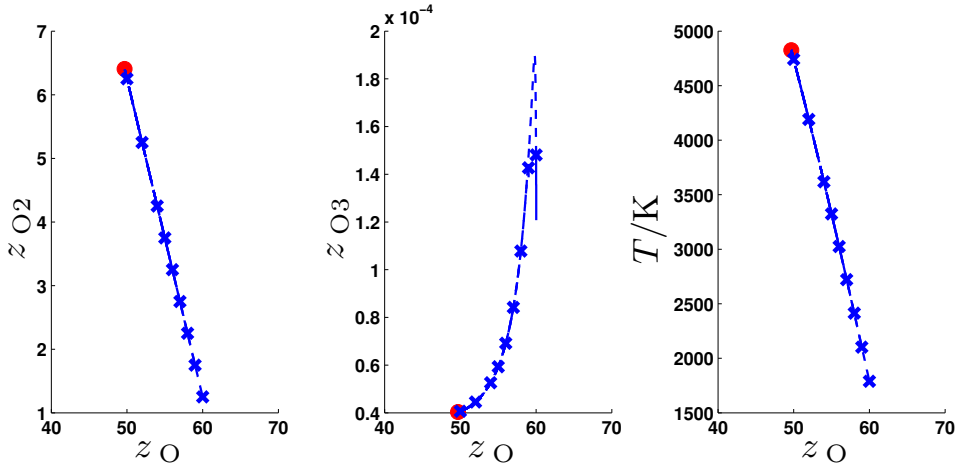


**Figure 9.24:** Visualization of numerical solutions of the same optimization problem as solved for the results shown in Figure 9.22, but the ozone decomposition is modeled in an adiabatic and isochoric thermodynamic environment, and the integration interval is reduced to $t_\mathrm{f} - t_0 = 10^{-8}\,\mathrm{s}$.

region far from equilibrium at large values of $z_\mathrm{O}$ for unstable O, but the values are in a reasonable range. In the isothermal and isobaric case, where the results are shown in Figure 9.23, $O_3$ is more stable than in the isothermal and isochoric case with the results shown in Figure 9.22. Chemical processes in the models of adiabatic systems, where the results are shown in Figures 9.24 and 9.25, are faster such that a shorter integration interval is sufficient.

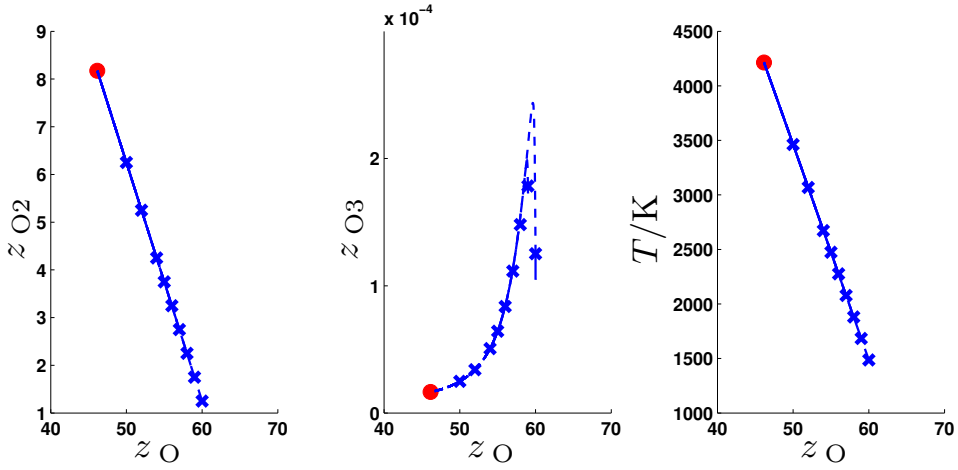


**Figure 9.25:** Visualization of numerical solutions of the same optimization problem as solved for the results shown in Figure 9.22, but the ozone decomposition is modeled in an adiabatic and and isobaric thermodynamic environment: This is optimization problem (9.8).

We want to demonstrate the importance of the inequality constraints for nonnegativity in (5.6f) and (5.7d), respectively, by means of the ozone decomposition model for a system in an isothermal, isochoric thermodynamic environment. Solutions of optimization problem (5.6) for the reduction of this model are shown in Figure 9.22.
A numerical solution of (5.6) with $t_* = t_\mathrm{f}$ and $t_\mathrm{f} - t_0 = 10^{-6}\,\mathrm{s}$ to reduce the model for isothermal, isochoric ozone decomposition with $z_\mathrm{O}^{t_*} = 62\,\mathrm{mol\,kg^{-1}}$ for the reaction progress variable is given by $z^*_{\mathrm{O}_2}(t_*) = 2.50 \times 10^{-1}\,\mathrm{mol\,kg^{-1}}$ and $z^*_{\mathrm{O}_3}(t_*) = -1.67 \times 10^{-4}\,\mathrm{mol\,kg^{-1}}$. The negative value might cause problems in the further use of the SIM approximation, e.g. in a CFD simulation.

## 9.4 Models for combustion

We aim for the reduction of realistic models for combustion in this section. The GRI-Mech 3.0 mechanism [152] serves as basis for these models in the following. We subsume all relevant reactions in Section A.3. With the thermodynamic data for the GRI-Mech 3.0 mechanism, that can be found on the internet, a confirmation of the results presented here is possible.

### 9.4.1 Hydrogen combustion

In this section, we restrict ourselves to the combustion of hydrogen without nitrogen chemistry. This means, the model is based on the reactions from the GRI-Mech 3.0 mechanism listed in Listing A.1.

We choose a temperature for the isothermal cases of $T = 1500\,\mathrm{K}$. We consider a density of $\rho = 0.3\,\mathrm{kg\,m^{-3}}$ in the isochoric cases and a pressure of $p = 10^5\,\mathrm{Pa}$ for isobaric conditions, respectively.
The overall reaction can be stated as

$$2\,H_2 + O_2 \rightarrow 2\,H_2O. \tag{9.10}$$

Nitrogen is considered as inert. We assume a homogeneous mixture at a ratio of $n_{H_2} : n_{O_2} = 2 : 1$ and a ratio of $n_{O_2} : n_{N_2} = 1 : 3.76$. This leads to an unburned mixture of oxygen $z_{O_2} = 7.070\,243\,7\,\mathrm{mol\,kg^{-1}}$, hydrogen $z_{H_2} = 14.140\,487\,\mathrm{mol\,kg^{-1}}$, and nitrogen $z_{N_2} = 26.584\,116\,\mathrm{mol\,kg^{-1}}$. The specific internal energy or enthalpy, respectively, of this mixture at a temperature of $T = 1000\,\mathrm{K}$ is used as a fixed specific internal energy or enthalpy for the models of adiabatic systems.

### One-dimensional SIM

As in case of the ozone decomposition model, we aim for the reduction of hydrogen combustion models for systems in all four standard thermodynamic environments. The results for these are shown in Figures 9.26, 9.27, 9.28, and 9.29.
We use $z_{H_2O}$ as reaction progress variables as it is the product of the overall reaction (9.10). It can be seen that over the whole range of meaningful values of $z_{H_2O}$ an approximation of a one-dimensional SIM can be computed for the models of isothermal hydrogen combustion, see Figures 9.26 and 9.27. However, this is different in the case of the adiabatic hydrogen combustion models, cf. Figures 9.28 and 9.29. Only near the equilibrium value for the reaction progress variable $z^{t_*}_{H_2O} < z^{\mathrm{eq}}_{H_2O}$, $z^{t_*}_{H_2O} \approx z^{\mathrm{eq}}_{H_2O}$, a reasonable one-dimensional SIM approximation can be identified. Results for low values of $z^{t_*}_{H_2O}$ are not satisfying and not shown.

### Two-dimensional SIM

We consider an approximation of a two-dimensional SIM for the model of adiabatic and isochoric hydrogen combustion for which an approximation of a one-dimensional SIM is shown in Figure 9.28. We choose $z_{O_2}$ as second reaction progress variable as this is the oxidizer in the overall reaction (9.10). Numerical solutions of the corresponding optimization problem (5.7) are shown in Figure 9.30.
A two-dimensional SIM approximation can be seen in the visualization. The solution is not satisfying for highly reactive species as e.g. $H_2O_2$: The results are inconsistent in the sense of Definition 5.5.1. An increase in the number of reaction progress variables can be beneficial, but consistency in the sense of Definition 5.5.1 cannot be checked for approximation of high-dimensional SIM in an easy manner.

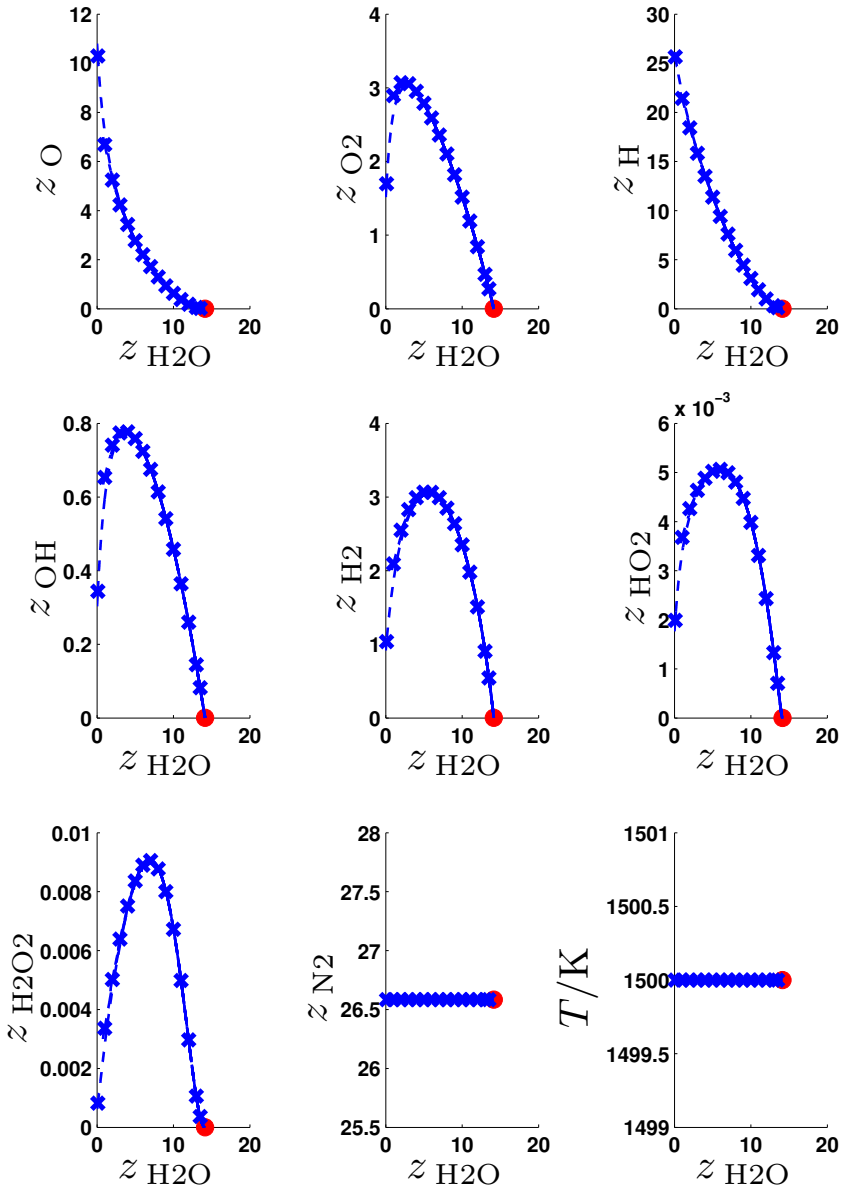


**Figure 9.26:** Visualization of numerical solutions $z^*(t_*)$ of the optimization problem (5.6) with $t_* = t_\mathrm{f}$ for an approximation of a one-dimensional SIM in the phase space of the model for hydrogen combustion. The system is modeled with all reactions given in Listing A.1 in an isothermal and isochoric thermodynamic environment. The specific mole of the product of the overall reaction $z_{\mathrm{H_2O}}$ serves as reaction progress variable and is varied between zero and the equilibrium value. We use an integration horizon of $t_\mathrm{f} - t_0 = 10^{-7}\,\mathrm{s}$.

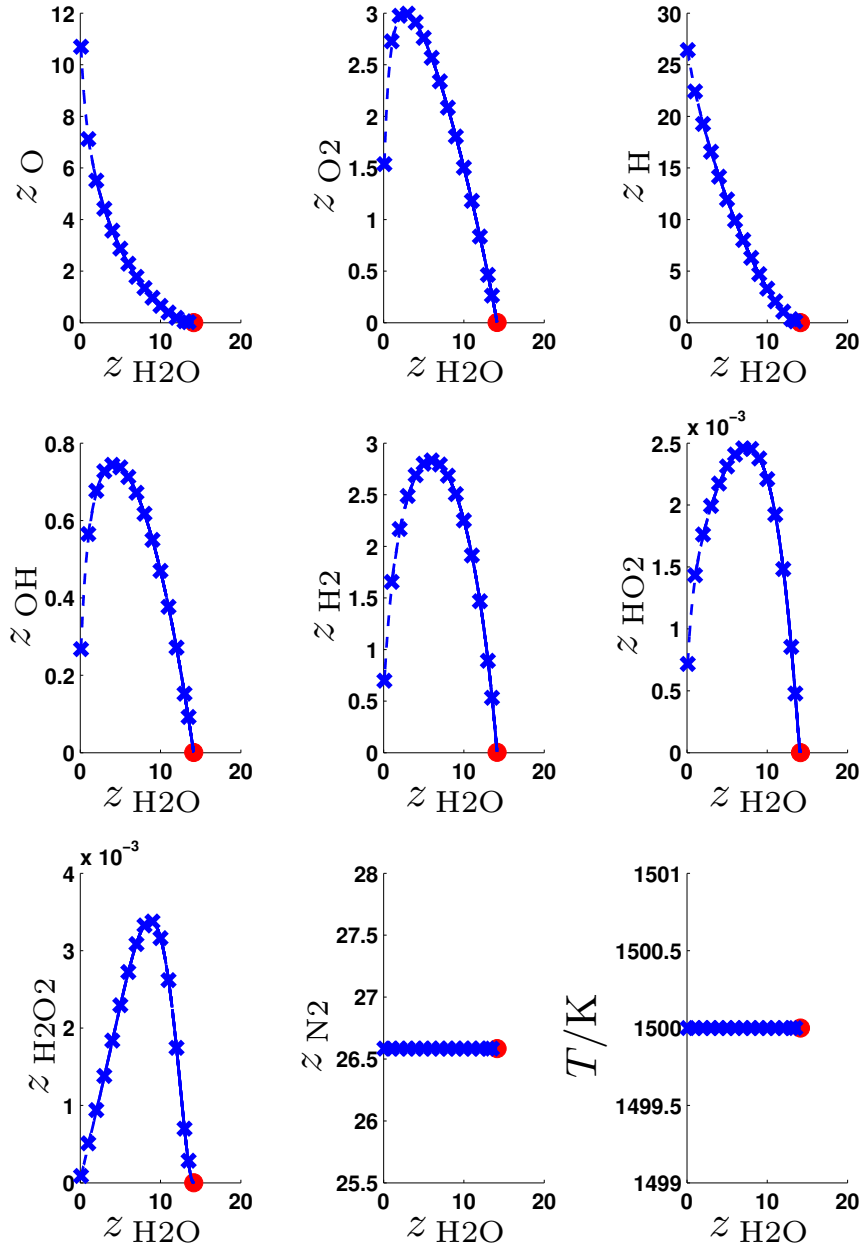


**Figure 9.27:** Visualization of numerical solutions of the same optimization problem as solved for the results shown in Figure 9.26, but the hydrogen combustion is modeled in an isothermal and isobaric thermodynamic environment.

### 9.4.2 Syngas combustion

We consider a syngas combustion model as largest combustion model in this thesis. It includes all species of the hydrogen combustion mechanism as used

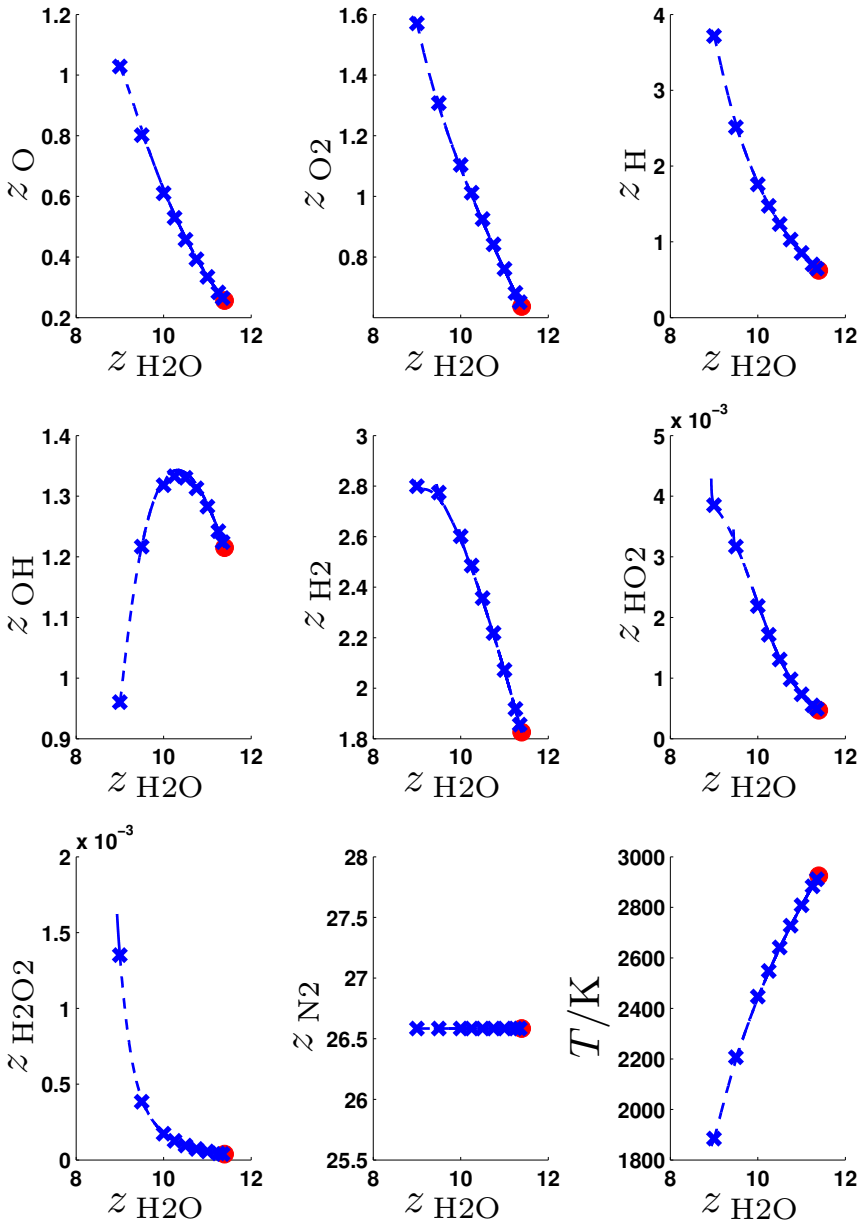


**Figure 9.28:** Visualization of numerical solutions of the same optimization problem as solved for the results shown in Figure 9.26 but with a model for hydrogen combustion in an adiabatic, isochoric thermodynamic environment.

in Section 9.4.1, additionally the two species CO, $CO_2$, and some nitrogen compounds. We consider $N_2$ as inert species in the following section. In a second step, reactive nitrogen is also considered.

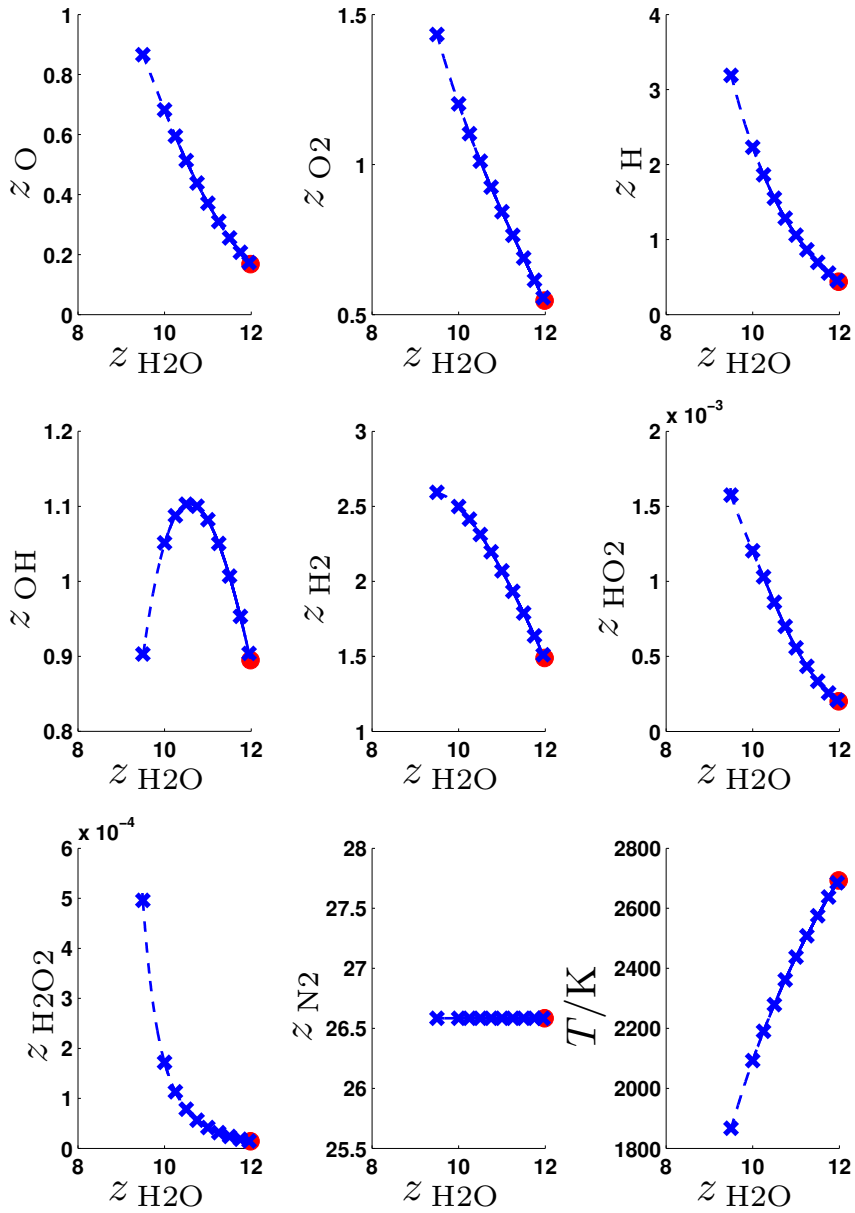


**Figure 9.29:** Visualization of numerical solutions of the same optimization problem as solved for the results depicted in Figure 9.26 but in case of a model for adiabatic and isochoric hydrogen combustion.

### Syngas combustion with inert nitrogen

We use all species and reactions listed in Listings A.1 and A.2, i.e. thirty-three reactions of the GRI-Mech 3.0 mechanism [152] which include no other species than O, $O_2$, H, OH, $H_2$, $HO_2$, $H_2O_2$, $H_2O$, $N_2$, CO, and $CO_2$. Those thirty-three reactions can be split up into thirty-one reactions of Arrhenius-

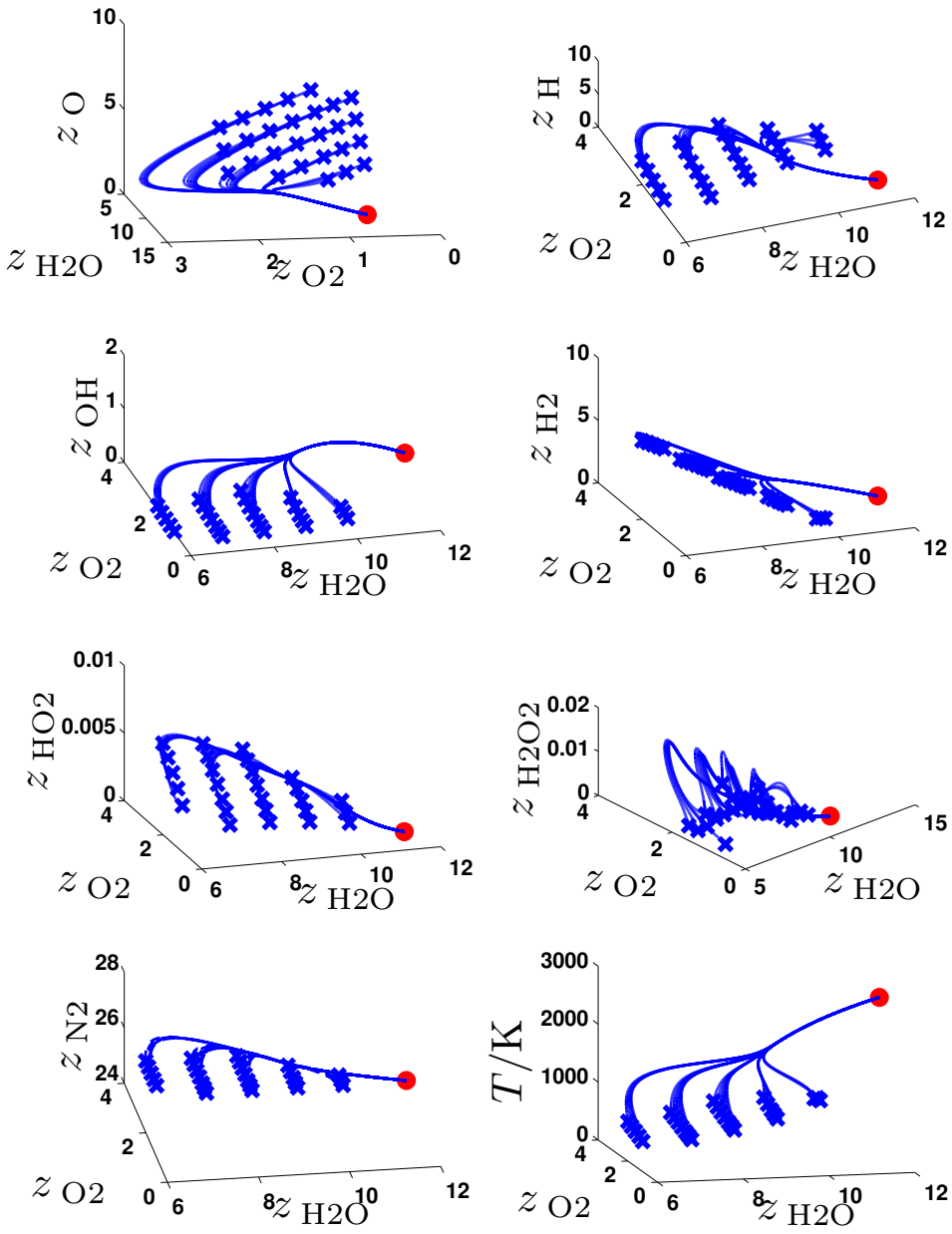


**Figure 9.30:** Visualization of numerical solutions of optimization problem (5.7) for the approximation of a two-dimensional SIM in the phase space of the model for adiabatic and isochoric hydrogen combustion. Reaction progress variables are $z_{H_2O}$ and $z_{O_2}$.

type and two pressure-dependent reactions of Troe-type.
The overall reaction can be stated as

$$H_2 + CO + O_2 \rightarrow H_2O + CO_2,$$

where $N_2$ is a collision partner. We assume a homogeneous stoichiometric mixture of syngas with air in an adiabatic and isochoric thermodynamic environment. We use $\rho = 0.3\,\mathrm{kg\,m^{-3}}$ as fixed mass density. We assume a ratio of $n_{H_2} : n_{CO} = 1 : 1$ and a ratio of $n_{O_2} : n_{N_2} = 1 : 3.76$. This leads to an unburned mixture of $z_{CO} = z_{H_2} = z_{O_2} = 5.972\,579\,6\,\mathrm{mol\,kg^{-1}}$ and $z_{N_2} = 22.456\,899\,\mathrm{mol\,kg^{-1}}$. The specific internal energy of this mixture at a temperature of $T = 1000\,\mathrm{K}$ is used as a fixed specific internal energy for the model. The specific moles of water and carbon dioxide are used as reaction progress variables as we assume the emission of these species of interest in a reactive flow simulation where the reduced model can be used.
Solutions of the optimization problem (5.6) with $t_* = t_f$ for the reduction of the syngas combustion model are shown in Figure 9.31. Only a small region near the equilibrium is considered, where the results are satisfying.

### Syngas combustion with reactive nitrogen

We additionally consider chemical reactions with reactive nitrogen in the model that is discussed in the preceding section. That means, we consider the submechanism of the GRI-Mech 3.0 mechanism [152] that includes all reactions in the Listings A.1, A.2, A.3, and A.4. Hence, the model also includes pollutants such as $NO_x$.
We use the same ratios as in the example before: A stoichiometric mixture of air and the fuel is chosen where the fuel fulfills the ratio $n_{H_2} : n_{CO} = 1 : 1$. As nitrogen takes part in the reaction, argon plays the role of the inert gas, and we further assume $n_{O_2} : n_{N_2} : n_{Ar} = 21 : 78 : 1$. Therefore, we consider an unburned mixture of $z_{H_2} = z_{O_2} = z_{CO} = 5.953\,224\,66\,\mathrm{mol\,kg^{-1}}$, $z_{N_2} = 22.112\,059\,\mathrm{mol\,kg^{-1}}$, and $z_{Ar} = 0.283\,487\,9\,\mathrm{mol\,kg^{-1}}$. We consider an adiabatic, isobaric thermodynamic environment at standard pressure $p = p^\circ$. The value for the fixed enthalpy is the enthalpy of the unburned mixture at standard state for a temperature of $T = 1000\,\mathrm{K}$ analogous to the case discussed before.
Solutions of the optimization problem (5.7) for the reduction of the model of syngas combustion with reactive nitrogen are shown in Figure 9.32. The constant value of argon is not shown. Reactions with nitrogen interaction are much slower (on a larger time scale) than reactions that involve only carbon, hydrogen, and oxygen. Therefore, $z_{N_2}$ is chosen as one reaction progress variable. The specific mole of carbon dioxide serves as second reaction progress variable.
The algorithm (with GGN method) needs a computation time of 0.73 s to solve the 9 optimization problems with different values of the reaction progress variables where the results are depicted in Figure 9.32. Always one intermediate homotopy step is done, such that a total of 17 optimization problems are solved with 62 Gauss–Newton iterations.
The values of ammonia and radicals which include nitrogen, e.g. $NH_2$, NH,

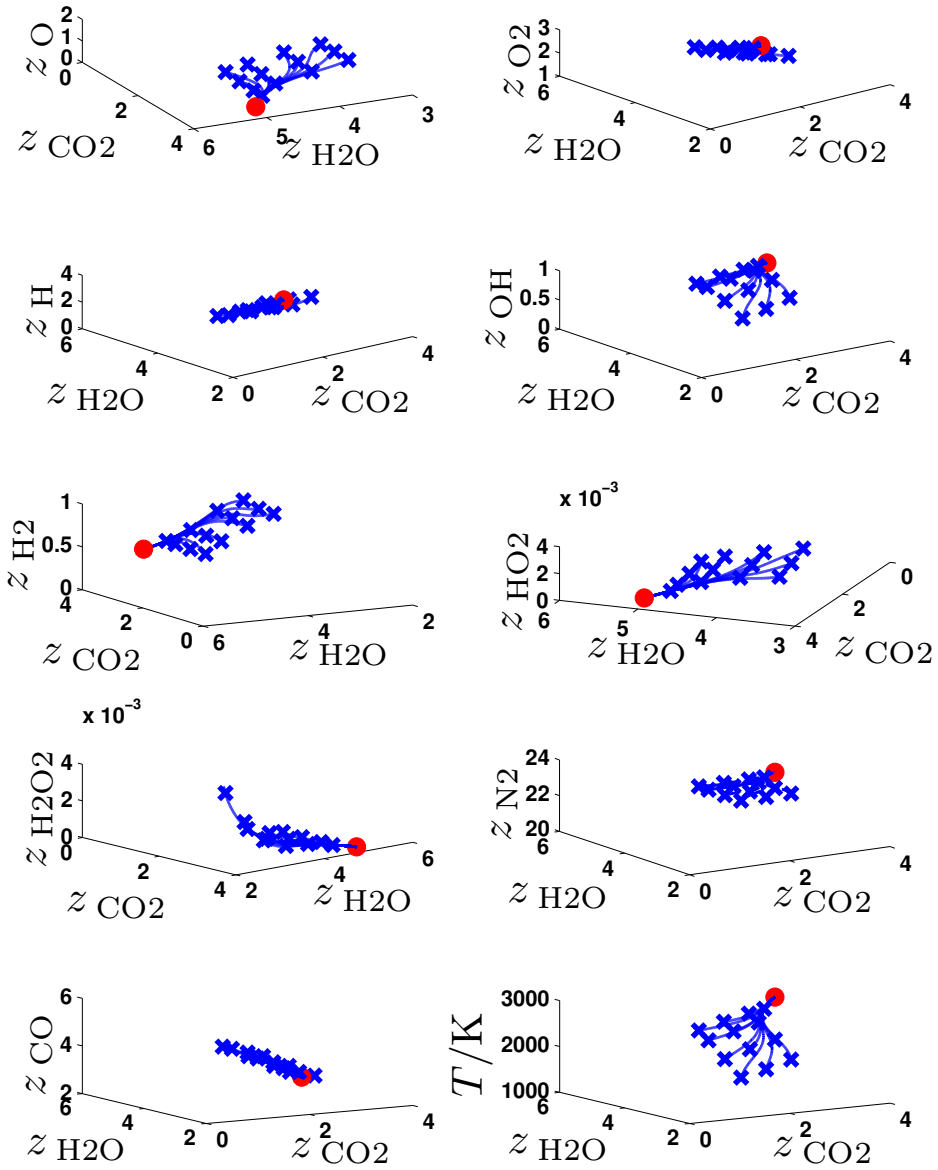


**Figure 9.31:** Visualization of numerical solutions $z^*(t_*)$ of the optimization problem (5.6) with $t_* = t_\mathrm{f}$ for the reduction of the syngas combustion model. The integration horizon $t_\mathrm{f} - t_0 = 10^{-7}\,\mathrm{s}$ is used. We aim to approximate a two-dimensional SIM. The overall products $z_{\mathrm{H_2O}}$ and $z_{\mathrm{CO_2}}$ serve as reaction progress variables.

and CN, deviate from a smooth manifold and are inconsistent in the sense of Definition 5.5.1, but they are of reasonable magnitude.

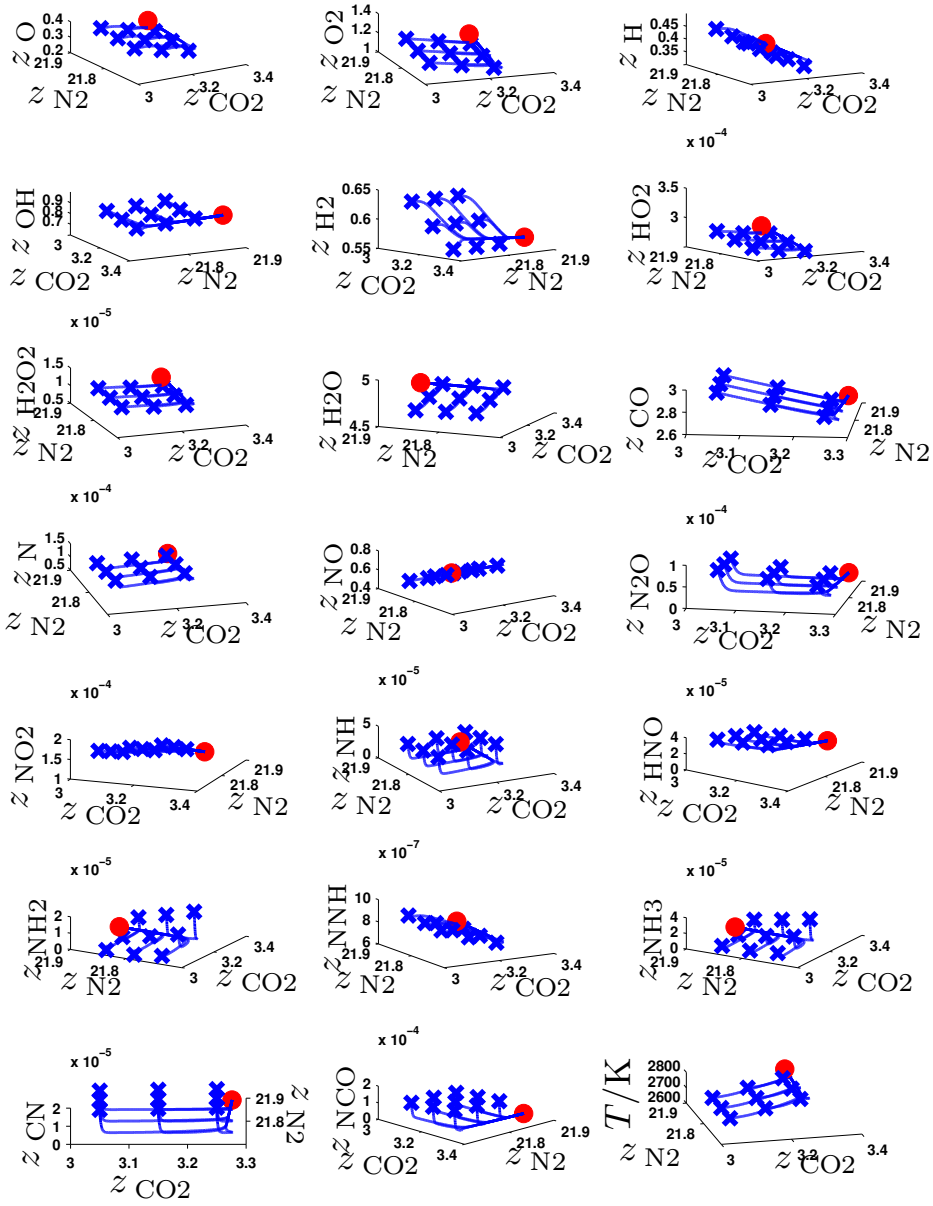


**Figure 9.32:** Visualization of solutions $z^*(t_*)$ of the optimization problem (5.7) for the reduction of the syngas combustion model including reactive nitrogen. As for the results shown in Figure 9.31, we aim to approximate a two-dimensional SIM. The variables $z_{N_2}$ and $z_{CO_2}$ serve as reaction progress variables. Constant $z_{Ar}$ is not shown.

*Systems seem, like certain worms, to be formed by a kind of generatio aequivoca – by the mere confluence of conceptions, and to gain completeness only with the progress of time.*

Immanuel Kant

# 10 Summary, conclusion, and outlook

The thesis is summarized in this chapter, and conclusions are drawn. An outlook on future work is given.

## 10.1 Summary and conclusion

This work deals with the numerical solution of optimization problems. These problems arise in an optimization based model reduction method that is raised in [101]. The method for kinetic model reduction is applied to models of chemical combustion.
The theory of kinetic model reduction methods is reviewed shortly. The aim of model reduction as discussed here is the identification of slow invariant manifolds (SIM) in the state space of the dynamical system which forms the model under consideration. Species reconstruction is an important issue for an efficient usage of a model reduction method within other applications: The values of unrepresented species are computed locally as approximation of a slow manifold in dependence of the given values of the represented species, which are also called reaction progress variables and parametrize the slow manifold. In addition to the values of the unrepresented species, the computation of the derivative of these with respect to the reaction progress variables is of great importance. In this work, the method for model reduction based on optimization of trajectories is further analyzed toward these aims.
Parametric optimization techniques are considered for the computation of the tangent space of the manifold. The tangent space of the manifold can be used together with the results of the species reconstruction in applications that make use of reduced models. Furthermore, parameter sensitivities, that

are computed for the tangent space, can serve for an Euler prediction of solutions of neighboring optimization problems.
The main focus of this work is the reduction of models that describe combustion chemistry. It is shown, that the optimization problem that is solved to approximate points on the SIM in the realizable composition space of standard models for combustion of a homogeneous mixture always has a solution if the feasible set is nonempty. A simple strategy is used for the selection of the reaction progress variables based on the Jacobian matrix of the right hand side of the ordinary differential equation (ODE) of the model.
The aim of this work is an efficient application of the model reduction method to models of combustion chemistry. Therefore, we discuss these models in detail. It becomes clear that negative values of third body concentrations in pressure dependent reactions result in undefined values of the right hand side of the ODE of the model. Such values have to be avoided in the optimization algorithm e.g. with an active set strategy or an interior point method. It turned out that discontinuities can occur at the switch temperature of the NASA polynomials for the standard molar heat capacity of the species. As we need sufficiently smooth functions for optimization, this problem is solved with a smooth transition function.
Two methods are tested to solve the semi-infinite optimization problem (5.6) for model reduction: collocation and shooting approaches. The resulting nonlinear programming problem is solved with a state-of-the-art open source interior point algorithm [168]. It turns out that all variants for solving the semi-infinite optimization problem are too slow for an *in situ* application of the model reduction method e.g. in a computational fluid dynamics simulation.
A finite optimization problem in form of a constrained nonlinear least squares problem is solved instead. This can be solved efficiently with a generalized Gauss–Newton method. A filter approach is used for globalization of convergence. Second order correction iterations prevent the Maratos effect. The problem that has to be solved in the feasibility restoration phase of the filter algorithm can also be formulated as a least squares problem such that matrix factorizations can be reused.
Parameter sensitivities of the optimization problem are used in a predictor corrector homotopy method. The reaction progress variables for parametrization of the slow manifold are considered as parameters in the optimization problem. This problem has to be solved several times for different values of the parameters. An Euler prediction based on the (computed) solution of neighboring problems is employed for initialization of the corrector algorithm. This linear prediction can be used directly within a certain tolerance as an approximation of a point on the slow manifold. It can also be used in the continuation scheme in combination with a sophisticated step size strategy. The step size is computed according to [45] in dependence of the contraction of the corrector method (i.e. the solution method for the non-

linear programming problem) and the iterations needed to solve a previous optimization problem.
Results of applications are shown. A computer code associated with this work implements the model reduction approach as presented in this thesis in `C++`. The model reduction method is applied to a large variety of test problems. They range from test problems with known slow manifolds, which can be represented as the graphs of functions, to singularly perturbed systems of ODE and models with instable manifolds in their phase space. Ozone decomposition is considered in form of a small realistic mechanism. Stoichiometric hydrogen and syngas combustion with and without reactive nitrogen are used as samples of combustion models.

It can be stated that the current implementation of the model reduction method including all features described in this thesis can efficiently solve models for chemical combustion. There is a large flexibility in the implementation, and a user has to make a lot of deliberate decisions, where the following considerations and statements can help.

1. A model has to be provided. This can be done in form of a combustion mechanism in `HOMREA` format [172] with a specification of the assumed thermodynamic environment and additional parameters. The model can also be given as the right hand side of an ODE implemented as `C++` class in an appropriate format.

2. If a model is provided that includes reactions with Troe kinetics, non-negativity of the variables should be considered in the algorithm, see Section 9.3.3. This is also the case if the application where the reduced model is supposed to be used can only deal with positive specific moles, concentrations, etc.

3. Initial values for the algorithm have to be given. These should be near to the solution as the scaling is based on the magnitude of the initial values and convergence depends strongly on a good initialization, see Section 9.3.2.

4. The reaction progress variables have to be chosen appropriately. The strategy described in Section 5.5.1 can give a hint, but also depends strongly on the initial values as a nearest feasible point to the initial values in the Euclidean distance is analyzed. In general, the application in which the reduced model is needed also poses criteria for the selection of the reaction progress variables; the product or educt of the overall reaction are often of interest. Either way, it is not guaranteed that a satisfying approximation of a point on a SIM can be computed for all values of the reaction progress variables that are given.

5. The decision has to be made which optimization problem (5.6) or (5.7) should be used to determine an approximation of a point on a SIM. In

general, (5.7) can be solved faster than (5.6) as the constraints do not include the ODE. Sometimes the algorithm fails to solve (5.7) for the given combination of reaction progress variables, see Section 9.3.2, and its solution deviates stronger from the SIM than the solution of (5.6) in some test examples.

6. If the user decides to compute a solution of (5.6) as an approximation of a point on a SIM, the solution method for (5.6) has to be specified. Usually a collocation method needs more computation time but converges more reliable in case of instable systems as e.g. in the case of the Verhulst model described in Section 9.1.2. The shooting method has an error control for the numerical solution of the ODE constraints on the other hand.

7. If the shooting approach is chosen to solve (5.6), tolerances for the BDF integrator have to be given. If on the other hand the collocation method is used, the user has to specify the number of finite elements, the order of the collocation polynomials, and the ratio of the size of the collocation intervals, see Chapter 6 and Section D.3.

8. The time horizon has to be given and the point in time $t_*$ in the interval $[t_0, t_\mathrm{f}]$ has to be specified for (5.6), too. The choice $t_* = t_\mathrm{f}$ is recommendable is case of systems that converge to a stable equilibrium whereas $t_* = t_0$ is advisable in the case of systems that diverge, see Section 9.1.2.

9. If optimization problem (5.1) is chosen to be solved for an approximation of points on the SIM, the user has also to specify, which criterion should be used in the objective function, see also Section 5.2. For the results shown in this work, we restrict ourselves to $\Phi$ as given in Equation (5.5), but currently twenty possibilities are implemented.

10. If (5.7) is chosen as optimization problem to be solved, the user has to specify, if this optimization problem should be solved with the GGN method as described in Section 7.1 or with `Ipopt` [168].

11. If an approximation of several points on the SIM is needed quickly, it can save much computation time to choose a large linear step tolerance $\epsilon_\mathrm{tol}$, see Equation (8.13). This can lead to large deviations from the SIM (see Section 9.1.1), and the approximation might not fulfill all desired conservation laws.

12. If `Ipopt` [168] is used to solve one of the discussed optimization problems for model reduction, the limited memory BFGS (l-BFGS) update for an approximation of the Hessian of the Lagrangian function can be used. In our experience, the `Ipopt` iterations are computed much

faster with l-BFGS, but more iterations are needed such that the overall computation takes longer.

13. A scaling of the KKT matrix has to be specified as described in the Sections 8.4 and 9.3.2. Is has to be tested by the user which scaling works best for the current problem. In case of an indefinite KKT matrix near the solution, only another problem formulation can produce relief.

14. The step size control in the homotopy method to solve neighboring optimization problems as discussed in Section 8.2 can shorten the computation time as shown for an example in Section 9.3.2. This is only the case if the initial step size and the desired number of corrector iterations are chosen carefully. The algorithm typically slows down if the step size strategy is activated for solving families of simple problems.

15. The *a posteriori* checks as described in Section 5.5.2 can help to identify outliers, but permanent deviation from a smooth invariant manifold can not be identified with these strategies.

It becomes clear that the model reduction tool `MoRe` is not a black box but must be used with care and experience. Knowledge of the model which is supposed to be reduced, an idea of the rough magnitude of the specific moles of the different species, and an anticipation of the time scales are inevitable. It can not be guaranteed that a solution of the optimization problem for the reduction of models of chemical combustion with a certain value for the reaction progress variables can be computed with the `MoRe` code even though we have proven a solution to exist (see Section 5.4). Many numerical strategies are presented in this work to overcome the difficulties. It still is up to the user of the model reduction code to find the best way to overcome the (numerical) difficulties that arise in each problem.

## 10.2 Outlook

A lot of open questions remain. The use of reduced models – the approximation of the slow manifold with its tangent space – for the simulation of reaction-diffusion-convection problems which include combustion kinetics is the aim of [48]. An application of reduced models in optimal control problems with ODE constraints is discussed in [134].
The homotopy method described in Chapter 8 is only implemented for variations in the reaction progress variables. An analogous implementation is possible for changes of the fixed values of elemental specific moles or the fixed specific enthalpy or internal energy, respectively.
There are also open fields in the numerical implementation of the model reduction method. The choice of the homotopy parameter for a better hot

start of the interior point algorithm is not clear; an unblocking strategy could improve computational time as it is shown in [71]. A relaxed version of the problem to find a feasible point close to the last iterate in the feasibility restoration phase could be used as in [167]. Eventually, this can be realized efficiently in the context of a generalized Gauss–Newton method.
Yet it is not clear to our knowledge how to make a good selection of the reaction progress variables. A good choice depends on the location in the phase space where the slow dynamics are approximated. It seems rather laborious to vary the reaction progress variables in a reactive flow simulation in dependence of space and time. Such an approach can only be made with a close coupling of the reduction of the chemistry model with the usage of the reduced model.
Recently, an approach for the selection of the reaction progress variables is published by V. Hiremath et al. in [83] based on a greedy algorithm. Their method is designed to find an optimal set of reaction progress variables such that a certain error is minimal.
Another open question is the existence of large residual solutions [27] of the least squares optimization problem (5.7). If such problems arose, an implementation of the restrictive monotonicity test [28] would be helpful.
Furthermore, the temperature could be implemented as a control function, thereby one could compute a control such that the approximation of the specific moles of pollutants as $NO_x$ on the slow manifold are below a desired threshold.
There are integration methods for ODE which exploit a time scale separation and are based on reduced models. The fast directions in the phase space are needed e.g. in the G-scheme [163]. These directions are not available in the optimization based model reduction method as presented here.

# A Mechanisms

Combustion mechanisms usually are given as a long-winded list of reactions and parameter values. The mechanisms for test models used in this thesis are directly given in Chapter 9. Mechanisms for realistic processes in physical chemistry as ozone decomposition and syngas combustion are collected in this section. They are noted to enable the reader to implement a code for computation and verification of the results presented in Chapter 9.

`MoRe` – the software tool developed with this thesis – has a "preprocessor" which parses the mechanism file and the thermodynamic data. The mechanism file has to be given in `HOMREA` format [172]. Molecularity of the reactions, the matrix of stoichiometry, etc. are computed. A text file is created; its content is arranged in a key word system. All numerical values are converted to SI base units. When a model based on a parsed mechanism is supposed to be reduced, `MoRe` reads the file and can evaluate the right hand side (4.19) of the model. A `C++` class is created additionally by the parser. It contains the computation of $\omega_s$ as in Equation (4.16). The same content is also written as a `MATLAB` function for eventual test computations. If a general ODE model is considered, these files have to be written manually. Values for e.g. mass, pressure, volume, and the elemental specific moles have to be given appropriately.

## A.1 Simplified six species hydrogen combustion

The reaction mechanism for a simplified six species hydrogen combustion is given in Table A.1. We use thermodynamical data in form of coefficients

**Table A.1:** Simplified six species hydrogen combustion mechanism as used in [140]. Collision efficiencies for M are: $\alpha_{\mathrm{H}} = 1.0$, $\alpha_{\mathrm{H_2}} = 2.5$, $\alpha_{\mathrm{OH}} = 1.0$, $\alpha_{\mathrm{O}} = 1.0$, $\alpha_{\mathrm{H_2O}} = 12.0$, $\alpha_{\mathrm{N_2}} = 1.0$; [140].

| Reaction | | | $A$ / (cm, mol, s) | $b$ | $E_{\mathrm{a}}$ / kJ mol$^{-1}$ |
|---|---|---|---|---|---|
| $\mathrm{O + H_2}$ | $\rightleftharpoons$ | $\mathrm{H + OH}$ | $5.08 \times 10^{04}$ | 2.7 | 26.317 |
| $\mathrm{H_2 + OH}$ | $\rightleftharpoons$ | $\mathrm{H_2O + H}$ | $2.16 \times 10^{08}$ | 1.5 | 14.351 |
| $\mathrm{O + H_2O}$ | $\rightleftharpoons$ | $\mathrm{2\,OH}$ | $2.97 \times 10^{06}$ | 2.0 | 56.066 |
| $\mathrm{H_2 + M}$ | $\rightleftharpoons$ | $\mathrm{2\,H + M}$ | $4.58 \times 10^{19}$ | −1.4 | 436.726 |
| $\mathrm{O + H + M}$ | $\rightleftharpoons$ | $\mathrm{OH + M}$ | $4.71 \times 10^{18}$ | −1.0 | 0.000 |
| $\mathrm{H + OH + M}$ | $\rightleftharpoons$ | $\mathrm{H_2O + M}$ | $3.80 \times 10^{22}$ | −2.0 | 0.000 |

of NASA polynomials that we received from J. M. Powers and A. N. Al-Khateeb. They use these coefficients for the results in [6, 7].

The mechanism is published originally in [110]. The simplified version shown in Table A.1 is used by Ren et al. in [140]. The mechanism consists of five reactive species and inert nitrogen, where in comparison to a full hydrogen combustion mechanism the species $O_2$, $HO_2$, and $H_2O_2$ are removed. The species are involved in six reactions of Arrhenius type, where three combination/decomposition reactions require a third body for an effective collision. The mechanism is used in [108, 148], too.

In prior publications, e.g. [106, 161], we use an alternative version of the mechanism, where the reverse rate coefficients are computed with fitted Arrhenius parameters for the reverse reactions.

## A.2 Ozone decomposition

An ozone decomposition mechanism is given in Table A.2. It involves three chemical species: O, $O_2$, and $O_3$.

**Table A.2:** Ozone decomposition mechanism with the forward rates as in [112]. Collision efficiencies in reactions including M: $\alpha_{\mathrm{O}} = 1.14$, $\alpha_{\mathrm{O_2}} = 0.40$, $\alpha_{\mathrm{O_3}} = 0.92$.

| Reaction | | | $A$ / (cm, mol, s) | $b$ | $E_{\mathrm{a}}$ / kJ mol$^{-1}$ |
|---|---|---|---|---|---|
| $\mathrm{O + O + M}$ | $\rightleftharpoons$ | $\mathrm{O_2 + M}$ | $2.9 \times 10^{17}$ | −1.0 | 0.0 |
| $\mathrm{O_3 + M}$ | $\rightleftharpoons$ | $\mathrm{O + O_2 + M}$ | $9.5 \times 10^{14}$ | 0.0 | 95.0 |
| $\mathrm{O + O_3}$ | $\rightleftharpoons$ | $\mathrm{O_2 + O_2}$ | $5.2 \times 10^{12}$ | 0.0 | 17.4 |

The original version with fitted reverse rate parameters as published in [112] is used for tests in [105, 135].

# A.3 GRI-Mech 3.0

We use parts of the GRI-Mech 3.0 mechanism [152]. We group the reactions in four modules: the hydrogen module in Listing A.1, the carbon monoxide module in Listing A.2, the nitrogen oxide module in Listing A.3, and the nitrogen with carbon monoxide module in Listing A.4. The third body collision efficiencies are given in Listing A.5. The listings are given in the `HOMREA` format [172] for combustion mechanisms. The activation energy is converted to SI units.
It is stated with the results in Chapter 9 which modules are used. Related thermodynamic data can be found in the original publication [152].

**Listing A.1:** Hydrogen module of the GRI-Mech 3.0 mechanism [152].

```
*******************************************************************************
**** 1. hydrogen module                                                    ****
---- Rxn                                    A         b          E_a       ----
-------- |------- |------- |------- |-------  |cm,mol,s |       |   kJ/mol   ----
-------- |------- |------- |------- |-------  |---------|------|----------------
O       +O       +M(1)    =O2      +M(1)      1.200E+17 -1.000     0.00
O       +H       +M(2)    =OH      +M(2)      5.000E+17 -1.000     0.00
O       +H2      =H       +OH                 3.870E+04  2.700   26.19184
O       +HO2     =OH      +O2                 2.000E+13   .000     0.00
O       +H2O2    =OH      +HO2                9.630E+06  2.000   16.736
H       +O2      +M(4)    =HO2     +M(4)      2.800E+18 -0.860     0.00
H       +O2      +O2      =HO2     +O2        2.080E+19 -1.240     0.00
H       +O2      +H2O     =HO2     +H2O       11.26E+18 -0.760     0.00
H       +O2      +N2      =HO2     +N2        2.600E+19 -1.240     0.00
H       +O2      +AR      =HO2     +AR        7.000E+17 -0.800     0.00
H       +O2      =O       +OH                 2.650E+16 -0.6707  71.299544
H       +H       +M(5)    =H2      +M(5)      1.000E+18 -1.000     0.00
H       +H       +H2      =H2      +H2        9.000E+16 -0.600     0.00
H       +H       +H2O     =H2      +H2O       6.000E+19 -1.250     0.00
H       +OH      +M(6)    =H2O     +M(6)      2.200E+22 -2.000     0.00
H       +HO2     =O       +H2O                3.970E+12  0.000   2.807464
H       +HO2     =O2      +H2                 4.480E+13  0.000   4.468512
H       +HO2     =OH      +OH                 0.840E+14  0.000   2.65684
H       +H2O2    =HO2     +H2                 1.210E+07  2.000   21.7568
H       +H2O2    =OH      +H2O                1.000E+13  0.000   15.0624
OH      +H2      =H       +H2O                2.160E+08  1.510   14.35112
OH      +OH      +M(2)    =H2O2    +M(2)      7.400E+13 -0.370     0.00
                                     LOW       2.300E+18 -0.900   -7.1128
                                     TROE   0.7346   94.0  1756.0  5182.0
OH      +OH      =O       +H2O                3.570E+04  2.400   -8.82824
OH      +HO2     =O2      +H2O                1.450E+13  0.000   -2.092
OH      +H2O2    =HO2     +H2O                2.000E+12  0.000   1.786568
**** BEGIN DUPLICATE REACTION
OH      +H2O2    =HO2     +H2O                1.700E+18  0.000   123.05144
**** END DUPLICATE REACTION
HO2     +HO2     =O2      +H2O2               1.300E+11  0.000   -6.81992
**** BEGIN DUPLICATE REACTION
HO2     +HO2     =O2      +H2O2               4.200E+14  0.000   50.208
**** END DUPLICATE REACTION
OH      +HO2     =O2      +H2O                0.500E+16  0.000   72.50872
*******************************************************************************
```

**Listing A.2:** Carbon monoxide module of the GRI-Mech 3.0 mechanism [152].

```
!****************************************************************************
!**** 2. carbon monoxide module                                            ****
!---- Rxn                                          A         b         E_a    ----
!-------- |------- |------- |------- |-------  |cm,mol,s |       |   kJ/mol   ----
!-------- |------- |------- |------- |-------  |---------|------|-----------------
O        +CO      +M(3)    =CO2     +M(3)       1.800E+10  0.000    9.97884
                                     LOW         6.020E+14  0.000   12.552
                                     TROE    0.0     0.0      0.0    0.0
O2       +CO      =O       +CO2                 2.500E+12  0.000  199.9952
H        +H       +CO2     =H2      +CO2        5.500E+20 -2.000    0.00
OH       +CO      =H       +CO2                 4.760E+07  1.228   0.29288
HO2      +CO      =OH      +CO2                 1.500E+14  0.000   98.7424
!****************************************************************************
```

**Listing A.3:** Nitrogen oxide module of the GRI-Mech 3.0 mechanism [152].

```
!****************************************************************************
!**** 6. nitrogen oxide module                                            ****
!---- Rxn                                          A         b         E_a    ----
!-------- |------- |------- |------- |-------  |cm,mol,s |       |   kJ/mol   ----
!-------- |------- |------- |------- |-------  |---------|------|-----------------
N        +NO      =N2      +O                   2.700E+13  0.000    1.48532
N        +O2      =NO      +O                   9.000E+09  1.000   27.196
N        +OH      =NO      +H                   3.360E+13  0.000    1.61084
N2O      +O       =N2      +O2                  1.400E+12  0.000   45.22904
N2O      +O       =NO      +NO                  2.900E+13  0.000   96.8596
N2O      +H       =N2      +OH                  3.870E+14  0.000   78.99392
N2O      +OH      =N2      +HO2                 2.000E+12  0.000   88.11504
N2O      +M(10)   =N2      +O       +M(10)      7.910E+10  0.000  234.38768
                                     LOW         6.370E+14  0.000  236.98176
                                     TROE    0.0     0.0      0.0    0.0
HO2      +NO      =NO2     +OH                  2.110E+12  0.000   -2.00832
NO       +O       +M(2)    =NO2     +M(2)       1.060E+20 -1.410    0.00
NO2      +O       =NO      +O2                  3.900E+12  0.000   -1.00416
NO2      +H       =NO      +OH                  1.320E+14  0.000    1.50624
NH       +O       =NO      +H                   4.000E+13  0.000    0.00
NH       +H       =N       +H2                  3.200E+13  0.000    1.38072
NH       +OH      =HNO     +H                   2.000E+13  0.000    0.00
NH       +OH      =N       +H2O                 2.000E+09  1.200    0.00
NH       +O2      =HNO     +O                   4.610E+05  2.000   27.196
NH       +O2      =NO      +OH                  1.280E+06  1.500    0.4184
NH       +N       =N2      +H                   1.500E+13  0.000    0.00
NH       +H2O     =HNO     +H2                  2.000E+13  0.000   57.9484
NH       +NO      =N2      +OH                  2.160E+13 -0.230    0.00
NH       +NO      =N2O     +H                   3.650E+14 -0.450    0.00
NH2      +O       =OH      +NH                  3.000E+12  0.000    0.00
NH2      +O       =H       +HNO                 3.900E+13  0.000    0.00
NH2      +H       =NH      +H2                  4.000E+13  0.000   15.2716
NH2      +OH      =NH      +H2O                 9.000E+07  1.500   -1.92464
NNH      +M(2)    =N2      +H       +M(2)       3.300E+08  0.000    0.00
NNH      +O2      =HO2     +N2                  1.300E+14 -0.110   20.83632
NNH      +O       =OH      +N2                  5.000E+12  0.000    0.00
NNH      +O       =NH      +NO                  2.500E+13  0.000    0.00
NNH      +H       =H2      +N2                  7.000E+13  0.000    0.00
NNH      +OH      =H2O     +N2                  5.000E+13  0.000    0.00
H        +NO      +M(2)    =HNO     +M(2)       2.000E+13  0.000    0.00
HNO      +O       =NO      +OH                  4.480E+19 -1.320    3.09616
HNO      +H       =H2      +NO                  2.500E+13  0.000    0.00
HNO      +OH      =NO      +H2O                 9.000E+11  0.720    2.76144
HNO      +O2      =HO2     +NO                  1.300E+07  1.900   -3.9748
NH3      +H       =NH2     +H2                  1.000E+13  0.000   54.392
NH3      +OH      =NH2     +H2O                 5.400E+05  2.400   41.48436
NH3      +O       =NH2     +OH                  5.000E+07  1.600    3.99572
!****************************************************************************
```

**Listing A.4:** Nitrogen with carbon monoxide module of the GRI-Mech 3.0 mechanism. [152].

```
!****************************************************************************
!**** 7. nitrogen - carbon monoxide module                                  ****
!---- Rxn                                          A          b          E_a      ----
!-------- |------- |------- |------- |-------  |cm,mol,s |       |   kJ/mol    ----
!-------- |------- |------- |------- |-------  |---------|------|----------------
CN       +O        =CO       +N                 7.700E+13  0.000      0.00
CN       +OH       =NCO      +H                 4.000E+13  0.000      0.00
CN       +O2       =NCO      +O                 6.140E+12  0.000     -1.84096
NCO      +O        =NO       +CO                2.350E+13  0.000      0.00
NCO      +H        =NH       +CO                5.400E+13  0.000      0.00
NCO      +OH       =NO       +H        +CO      0.250E+13  0.000      0.00
NCO      +N        =N2       +CO                2.000E+13  0.000      0.00
NCO      +O2       =NO       +CO2               2.000E+12  0.000     83.68
NCO      +M(2)     =N        +CO       +M(2)    3.100E+14  0.000    226.1452
NCO      +NO       =N2O      +CO                1.900E+17 -1.520      3.09616
NCO      +NO       =N2       +CO2               3.800E+18 -2.000      3.3472
NH       +CO2      =HNO      +CO                1.000E+13  0.000     60.0404
CN       +NO2      =NCO      +NO                6.160E+15 -0.752      1.44348
NCO      +NO2      =N2O      +CO2               3.250E+12  0.000     -2.94972
N        +CO2      =NO       +CO                3.000E+12  0.000     47.2792
!****************************************************************************
```

**Listing A.5:** Collision efficiencies (in part) of the GRI-Mech 3.0 mechanism [152].

```
!****************************************************************************
COLLISION EFFICIENCIES
!****************************************************************************
M(1)     =H2       +H2O      +CO       +CO2      +AR
          2.40      15.4      1.75      3.60      0.83
M(2)     =H2       +H2O      +CO       +CO2      +AR
          2.00      6.00      1.50      2.00      0.70
M(3)     =H2       +O2       +H2O      +CO       +CO2      +AR
          2.00      6.00      6.00      1.50      3.50      0.50
M(4)     =O2       +H2O      +CO       +CO2      +N2       +AR
          0.0       0.0       0.75      1.50      0.0       0.00
M(5)     =H2       +H2O      +CO2      +AR
          0.0       0.0       0.0       0.63
M(6)     =H2       +H2O      +AR
          0.73      3.65      0.38
M(7)     =H2       +H2O      +CO       +CO2      +AR
          2.00      6.00      1.50      2.00      0.70
M(8)     =H2       +H2O      +CO       +CO2
          2.00      6.00      1.50      2.00
M(9)     =H2       +H2O      +CO       +CO2
          2.00      0.00      1.50      2.00
M(10)    =H2       +H2O      +CO       +CO2      +AR
          2.00      6.00      1.50      2.00      0.625
M(11)    =H2       +H2O      +CO       +CO2      +AR
          2.00      6.00      1.50      2.00      1.00
!****************************************************************************
```

# B Notation

In this chapter, notations are explained, and lists of important symbols especially for combustion models are given.

## B.1 General notation

In this work, several notations for a derivative of a function are used. Consider some function $f : \mathbb{R}^n \to \mathbb{R}^m$, $n, m \in \mathbb{N}$, with argument $x \in \mathbb{R}^n$. The derivative of $f$ with respect to $x$ is written as

$$\frac{\mathrm{d}}{\mathrm{d}x} f(x) = \mathrm{d}_x f(x) = \mathrm{D} f(x),$$

where the notation $\mathrm{D}f$ usually represents the derivative of $f$ with respect to time $x = t \in \mathbb{R}$.
Consider a function $g(x, y)$ with arguments $x \in \mathbb{R}^{n_1}$ and $y \in \mathbb{R}^{n_2}$. The partial derivative of $g$ with respect to the first entry $x$ is written as

$$\frac{\partial}{\partial x} g(x, y) = \mathrm{D}_x g(x, y) = g_x(x, y) = \nabla_x g(x, y)^{\mathrm{T}}$$

and with respect to the second entry analogously.
If special interest is paid to the Jacobian matrix of a vector valued function $f$, it is written as $J_f(x)$, which can be considered as the transposed gradient

$$J_f(x) = \nabla f(x)^{\mathrm{T}}.$$

The notation d without index in application to a function is used for the total differential, e.g.

$$\mathrm{d}g = g_x \mathrm{d}x + g_y \mathrm{d}y.$$

The symbol $\|\cdot\|$ denotes any norm in $\mathbb{R}^n$. If it is necessary to specify a certain norm, $\|\cdot\|_p$ is the $p$-norm. For example, $\|\cdot\|_2$ denotes the Euclidean norm. For the corresponding scalar product $\langle\cdot,\cdot\rangle$, the same index as for the norm are used (or not, respectively).
Inequalities between vectors or matrices of the same dimension are always meant componentwise.
The term *instable* is used in the mathematical context for e.g. equilibria; the term *unstable* is used in the chemical context, e.g. for radicals.

## B.2 Symbols in combustion models

In Chapter 4 and later on, a confusing number of symbols is used for the description of combustion models. An overview of the meaning of the symbols and eventually their value and/or unit is given in the following tables. Latin symbols used in combustion models are explained in Table B.1.

**Table B.1:** List of Latin symbols used in models of combustion.

| Symbol | Description | Value or unit |
|---|---|---|
| $a$ | parameter in Troe reaction | w/o dim. |
| $A$ | pre-exponential factor in Arrhenius law | varies |
| $b$ | exponent of $T$ in Arrhenius law | |
| $c$ | concentration | $\mathrm{mol\,m^{-3}}$ |
| $c_p$ | specific heat capacity at constant pressure | $\mathrm{J\,kg^{-1}\,K^{-1}}$ |
| $C_p$ | heat capacity at constant pressure | $\mathrm{J\,K^{-1}}$ |
| $\bar{C}_p$ | molar heat capacity at constant pressure | $\mathrm{J\,mol^{-1}\,K^{-1}}$ |
| $c_{p,s}$ | specific heat capacity at constant pressure of species $s$ | $\mathrm{J\,kg^{-1}\,K^{-1}}$ |
| $\bar{C}_{p,s}$ | molar heat capacity at constant pressure of species $s$ | $\mathrm{J\,mol^{-1}\,K^{-1}}$ |
| $c_s$ | concentration of species $s$ | $\mathrm{mol\,m^{-3}}$ |
| $c_V$ | specific heat capacity at constant volume | $\mathrm{J\,kg^{-1}\,K^{-1}}$ |
| $C_V$ | heat capacity at constant volume | $\mathrm{J\,K^{-1}}$ |
| $\bar{C}_V$ | molar heat capacity at constant volume | $\mathrm{J\,mol^{-1}\,K^{-1}}$ |
| $c_{V,s}$ | specific heat capacity at constant volume of species $s$ | $\mathrm{J\,kg^{-1}\,K^{-1}}$ |
| $\bar{C}_{V,s}$ | molar heat capacity at constant volume of species $s$ | $\mathrm{J\,mol^{-1}\,K^{-1}}$ |
| $e$ | specific internal energy | $\mathrm{J\,kg^{-1}}$ |
| $E$ | internal energy | J |
| $E_\mathrm{a}$ | activation energy | $\mathrm{J\,mol^{-1}}$ |
| $e_s$ | specific partial internal energy of species $s$ | $\mathrm{J\,kg^{-1}}$ |
| $h$ | specific enthalpy | $\mathrm{J\,kg^{-1}}$ |
| $H$ | enthalpy | J |
| $h_s$ | specific partial enthalpy of species $s$ | $\mathrm{J\,kg^{-1}}$ |
| $\bar{H}_s$ | molar partial enthalpy of species $s$ | $\mathrm{J\,mol^{-1}}$ |
| $k_{\mathrm{f},r}$ | forward rate coefficient of reaction $r$ | varies |
| $k_{\mathrm{r},r}$ | reverse rate coefficient of reaction $r$ | varies |
| $K_c$ | equilibrium constant in concentration units | varies |
| $K_p$ | equilibrium constant in pressure units | w/o dim. |
| $m$ | mass | kg |

Continued on next page.

| Symbol | Description | Value or unit |
|---|---|---|
| $\bar{M}$ | mean molar mass | $\mathrm{kg\,mol^{-1}}$ |
| $m_s$ | mass of species $s$ | kg |
| $M_s$ | molar mass of species $s$ | $\mathrm{kg\,mol^{-1}}$ |
| $\bar{M}_i$ | molar mass of element $i$ | $\mathrm{kg\,mol^{-1}}$ |
| $n$ | amount of substance | mol |
| $n_{\mathrm{elem}}$ | number of elements | w/o dim. |
| $n_s$ | amount of substance of species $s$ | mol |
| $N_{\mathrm{A}}$ | Avogadro constant | $6.022 \times 10^{23}\,\mathrm{mol^{-1}}$ |
| $n_{\mathrm{reac}}$ | number of chemical reactions | w/o dim. |
| $n_{\mathrm{spec}}$ | number of chemical species | w/o dim. |
| $n_{\mathrm{tb}}$ | number of collision partners (third bodies) | w/o dim. |
| $p$ | total pressure | Pa |
| $p_s$ | partial pressure of species $s$ | Pa |
| $p_{\mathrm{r}}$ | reduced pressure | w/o dim. |
| $p^\circ$ | standard pressure | $10^5\,\mathrm{Pa}$ |
| $q_r$ | rate of progress of reaction $r$ | $\mathrm{mol\,m^{-3}\,s^{-1}}$ |
| $R$ | gas constant | $8.314\,\mathrm{J\,mol^{-1}\,K^{-1}}$ |
| $r_{\mathrm{f},r}$ | forward rate of reaction $r$ | varies |
| $r_{\mathrm{r},r}$ | reverse rate of reaction $r$ | varies |
| $s$ | specific entropy (if not a counter) | $\mathrm{J\,kg^{-1}\,K^{-1}}$ |
| $s$ | counter of species (usually as index) | w/o dim. |
| $S$ | entropy | $\mathrm{J\,K^{-1}}$ |
| $\bar{S}_s$ | molar partial entropy of species $s$ | $\mathrm{J\,K^{-1}}$ |
| $t$ | time | s |
| $T$ | temperature | K |
| $T^*$ | parameter in Troe reaction | w/o dim. |
| $T^{**}$ | parameter in Troe reaction | w/o dim. |
| $T^{***}$ | parameter in Troe reaction | w/o dim. |
| $T_{\mathrm{lb}}$ | lower bound of temperature in NASA polynomials | K |
| $T_{\mathrm{sw}}$ | switching temperature in NASA polynomials | K |
| $T_{\mathrm{ub}}$ | upper bound of temperature in NASA polynomials | K |
| $V$ | total volume | $\mathrm{m^3}$ |
| $v_s$ | specific volume of species $s$ | $\mathrm{m^3\,kg^{-1}}$ |
| $w_s$ | mass fraction of species $s$ | w/o dim. |
| $x_s$ | mole fraction of species $s$ | w/o dim. |
| $z_s$ | specific mole of species $s$ | $\mathrm{mol\,kg^{-1}}$ |
| $\check{z}_i$ | specific mole of element $i$ | $\mathrm{mol\,kg^{-1}}$ |

Greek symbols used in combustion models are listed in Table B.2.

**Table B.2:** List of Greek symbols used in models of combustion.

| Symbol | Description | Value or unit |
|---|---|---|
| $\alpha_{i,s}$ | collision efficiency of species $s$ in third body $i$ | w/o dim. |
| $\nu_r$ | sum of net stoichiometric coefficients in reaction $r$ | w/o dim. |
| $\nu_{sr}$ | net stoichiometric coefficient of species $s$ in reaction $r$ | w/o dim. |
| $\nu'_{sr}$ | stoichiom. coeff. of species $s$ in forward direction of rxn $r$ | w/o dim. |
| $\nu''_{sr}$ | stoichiom. coeff. of species $s$ in reverse direction of rxn $r$ | w/o dim. |
| $\rho_s$ | mass density of species $s$ | $\mathrm{kg\,m^{-3}}$ |

Continued on next page.

| Symbol | Description | Value or unit |
|---|---|---|
| $\rho$ | total (mass) density | $\mathrm{kg\,m^{-3}}$ |
| $\chi_{i,s}$ | atomic composition coefficient (element $i$ in species $s$) | w/o dim. |
| $\omega_s$ | molar chemical production rate of species $s$ | $\mathrm{mol\,m^{-3}\,s^{-1}}$ |
| $\omega$ | vector of $\omega_s$, $s = 1, \ldots, n_{\mathrm{spec}}$ | $\mathrm{mol\,m^{-3}\,s^{-1}}$ |

## B.3 Acronyms

A list of acronyms used in this work is given in Table B.3. We use the same acronym for an expression in singular and plural. The full expression depends on the current context.

**Table B.3:** List of acronyms.

| Acronym | Full expression |
|---|---|
| AS | active set |
| BDF | backward differentiation formula(e) |
| CFD | computational fluid dynamics |
| CLLS | constrained linearized least squares |
| CNLLS | constrained nonlinear least squares |
| CPA | close-parallel assumption |
| CSP | computational singular perturbation |
| FGM | flamelet generated manifold(s) |
| GGN | generalized Gauss–Newton |
| ICE-PIC | invariant constrained equilibrium edge preimage curve |
| ILDM | intrinsic low dimensional manifold(s) |
| IND | internal numerical differentiation |
| IVP | initial value problem(s) |
| IP | interior point |
| KKT | Karush–Kuhn–Tucker |
| LICQ | linear independence constraint qualification |
| MEPT | minimal entropy production trajectory/-ies |
| NASA | national aeronautics and space administration |
| ODE | ordinary differential equation(s) |
| PDE | partial differential equation(s) |
| PEA | partial equilibrium assumption |
| QSSA | quasi steady state assumption |
| RCCE | rate-controlled constrained equilibrium |
| SIM | slow invariant manifold(s) |
| SOC | second order correction |
| SQP | sequential quadratic programming |

# C External software and hardware

All results shown in Chapter 9 are computed on an Intel® Core™ 2 Duo CPU E6550 with 2.33 GHz. The operating system is openSUSE 11.4 (i586) including the Linux 2.6.37.6 kernel and GCC 4.5.

The following external software is used in the `MoRe` code (listed in alphabetical order).

### BDF integrator

The BDF integrator used for integration of ODE is an implementation by D. Skanda [151]. It is based on Nordsiek array interpolation. It is also possible to compute sensitivities needed in the optimization algorithm based on internal numerical differentiation [22, 23]. The detailed numerical strategy can be found in [151, Chap. 5].

### CppAD

The automatic differentiation tool `CppAD` is used for the computation of necessary derivatives. It is published by B. M. Bell with Common Public License Version 1.0 or the GNU General Public License Version 2 [17, 18]. We always use the most recent trunk version via the `svn` repository. This is currently revision 2332.

### HSL routines

We use `ma27` with the ordering routine `mc19` from the HSL routines [84] within `Ipopt`.

### Ipopt

Ipopt is a powerful optimization algorithm based on an interior point filter method. Its theory is published in [165, 166, 167, 168]. We use Ipopt 3.10 provided by A. Wächter via the svn repository. This version of Ipopt is published with the Eclipse Public License.

### LAPACK

We use LAPACK [13] as standard library for all linear algebra purposes, where MUMPS or ma27 are not used.

### MATLAB

MATLAB® R2009a [113] is used to plot the results and to compute the condition numbers that are presented in Chapter 9. The trajectory pieces shown in the figures in Chapter 9 are computed with the integrator ode15s.

### METIS

METIS is a program for graph partitioning which can be used for the computation of orderings for sparse matrices [90]. We use METIS 4.0 in combination with MUMPS.

### MUMPS

MUMPS is a multifrontal massively parallel sparse direct solver [11, 12]. In our case, it is especially useful for use in the collocation approach, where we deal with sparse systems of linear equations. The right hand side of the linear system (8.3) for the computation of the tangent space is also sparse and can be handled by MUMPS. We use MUMPS 4.9.2 which is freely available via the website http://graal.ens-lyon.fr/MUMPS/.

# D

# Work flow of the model reduction code

In this chapter, the work flow of the model reduction code `MoRe` is shown in form of flowcharts. We present the usage of our collection of `C++` headers in an overview.

## D.1 First call

After creating an instance of the `MoRe` class, a first call of the model reduction tool has to be made either with the method `first()` or with `reduction()`. In both cases the code works as depicted in Figure D.1. All input data has to be given in the form of text files. Only the names and values for the reaction progress variables can be given directly to the code for species reconstruction in an *in situ* application with the methods `first()` and `warm()`.
The path to the text files which contain the parameters can be specified in the `makefile`. The easiest way to provide the combustion model which is supposed to be reduced is to use the mechanism parser which directly converts the mechanism from `HOMREA` format [172] to the needed `C++` class and additional text files that contain the values of the kinetic parameters. All input data is analyzed for contradictions or an empty feasible set of (5.7), e.g. if the given values for the reaction progress variables violate the mass conservation if only nonnegative variables are allowed.
Subsequently, the code prepares the tapes for the automatic differentiation tool `CppAD` [17], where only these tapes are created that are needed for the NLP problem which is supposed to be solved afterward. In order to achieve this, the computation of the right hand side of the ODE system of the model is done once for the given initial values. This is depicted in Figure D.2.

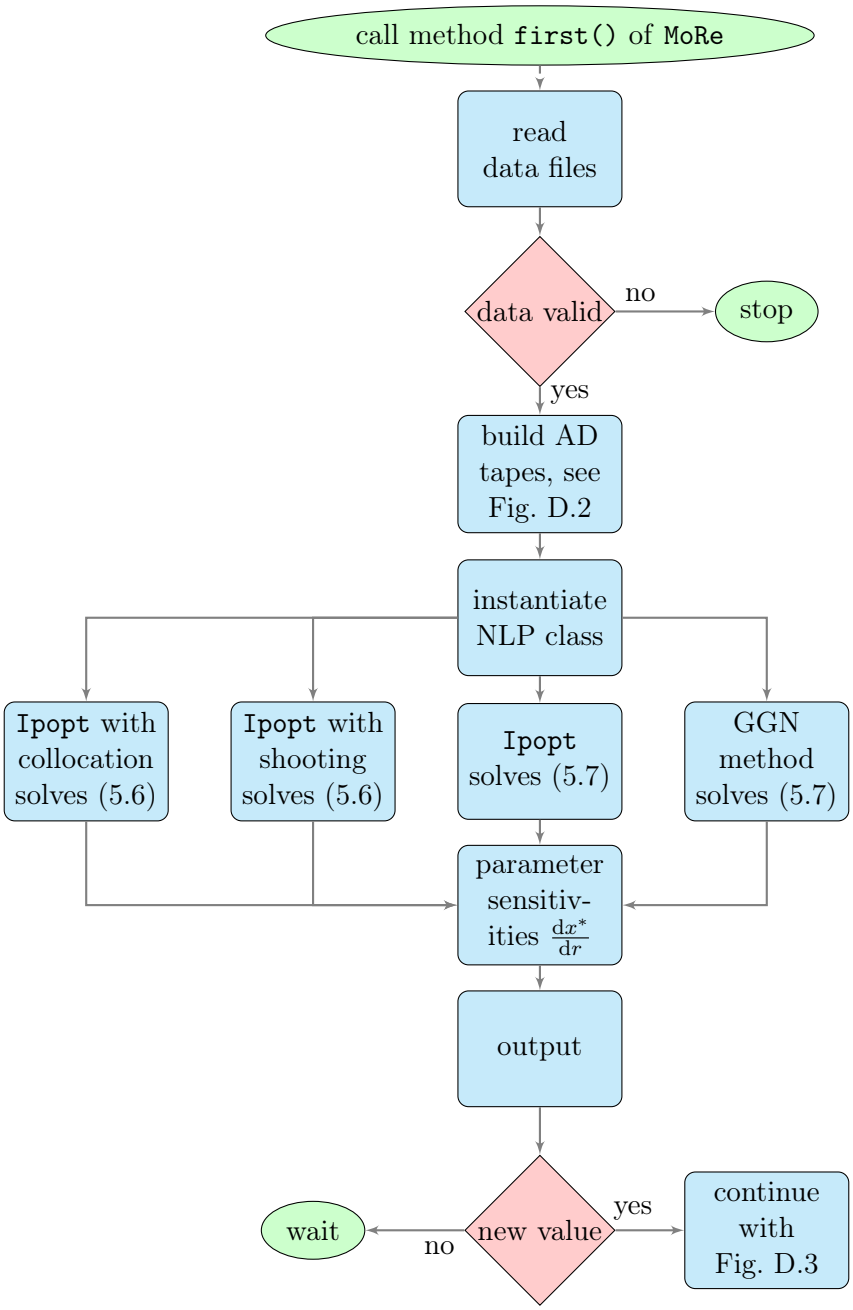


**Figure D.1:** Flowchart of a first call of the model reduction code `MoRe` with method `first()` or `reduction()`.

After the preparation of all necessary tapes, the `C++` class to solve the NLP problem is instantiated. Either `Ipopt` is called to solve the NLP problem that arises as a discretized form of (5.6) with collocation equations as constraints

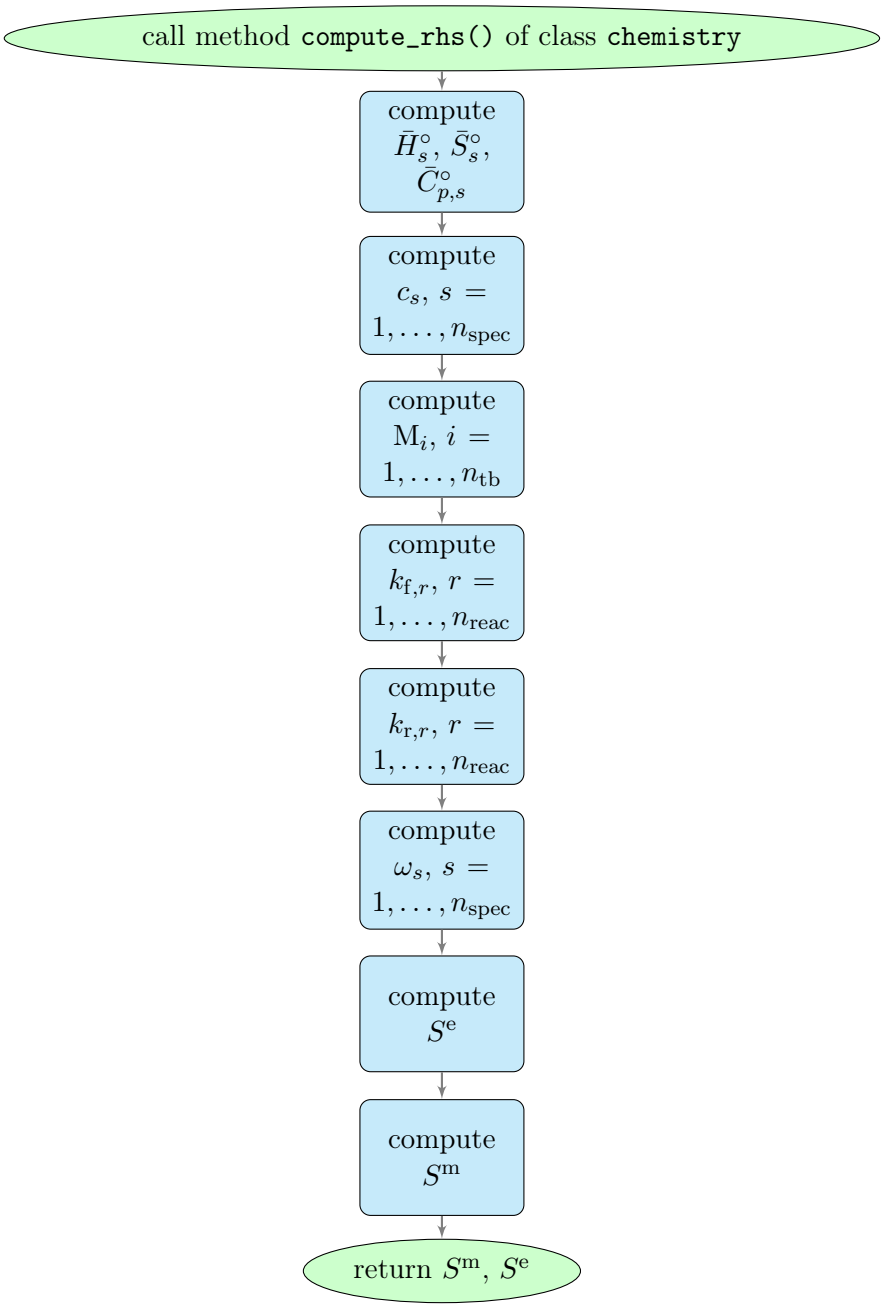


**Figure D.2:** Flowchart of the computation of the right hand side of the ODE of the combustion model in the model reduction code `MoRe`.

and a quadrature method for the evaluation of the objective function. Alternatively, `Ipopt` is used to solve the NLP problem that results within a shooting approach to solve (5.6) with the BDF integrator to solve the ODE

of the model. As a third choice, `Ipopt` can be used to solve (5.7). As a fourth possibility, this problem can also be solved with the GGN method as described in Section 7.1. The different ways to solve the different optimization problems merge with the computation of the derivatives of the solution $x^*$ with respect to the parameters $r$, i.e. to solve Equation (8.3). Here the choice of the linear solver (`MUMPS` or a `LAPACK` solver) depends on the size and sparsity of the KKT matrix and right hand side of the linear system.
*A posteriori* checks can be done. That means, the values introduced in Section 5.5.2 can be computed and saved with the regular output. Here again the BDF integrator or the Gram–Schmidt algorithm may be used as described in Section 5.5.2. The results in the sense of the approximation of a point on the SIM and of the tangent vectors of the SIM in that point are written to a file (if required) and/or returned by the method `first()`.
If the `MoRe` code is used for tabulation of the SIM approximation with a grid of values for the reaction progress variables by means of the method `reduction()`, the algorithm continues to solve the optimization problem for the next grid point according to the warm start depicted in Figure D.3. Otherwise, the instance of the `MoRe` class can be newly called with `warm()`.

## D.2 Warm start

The work flow of the model reduction code if a neighboring optimization problem has to be solved in a warm start is similar to the case of a first call, see Figure D.3, but less input data has to be provided.
After testing the input data for contradictions, it is checked if (8.13) holds. If this is the case, the values computed as a linear approximation of the SIM defined in (8.14) are returned. If (8.13) does not hold, the homotopy step size is computed. This is either a full step (if requested by the user) or the step size computed with the step size strategy presented in Section 8.2.
An NLP class is instantiated. The same choice for the corrector algorithm is made as in the preceding call with `first()`, `warm()`, or `reduction()`. After a solution of the NLP problem is computed, parameter sensitivities are computed as well. If the code fails to solve the NLP problem in a given number of iterations, the homotopy step size is reduced and another attempt to compute a solution is made until a maximum number is exceeded.
Repeatedly, a new homotopy step size is computed and the next optimization problem is solved until the desired values for the reaction progress variables are achieved (or the algorithm stops after the maximum allowed number of attempts). An *a posteriori* check of the solution is possible before the output is written to a text file and/or returned by the method `warm()`. If another requested value for the reaction progress variables is present in a call of the method `reduction()`, the algorithm continues. Otherwise a new call with the method `warm()` is awaited.

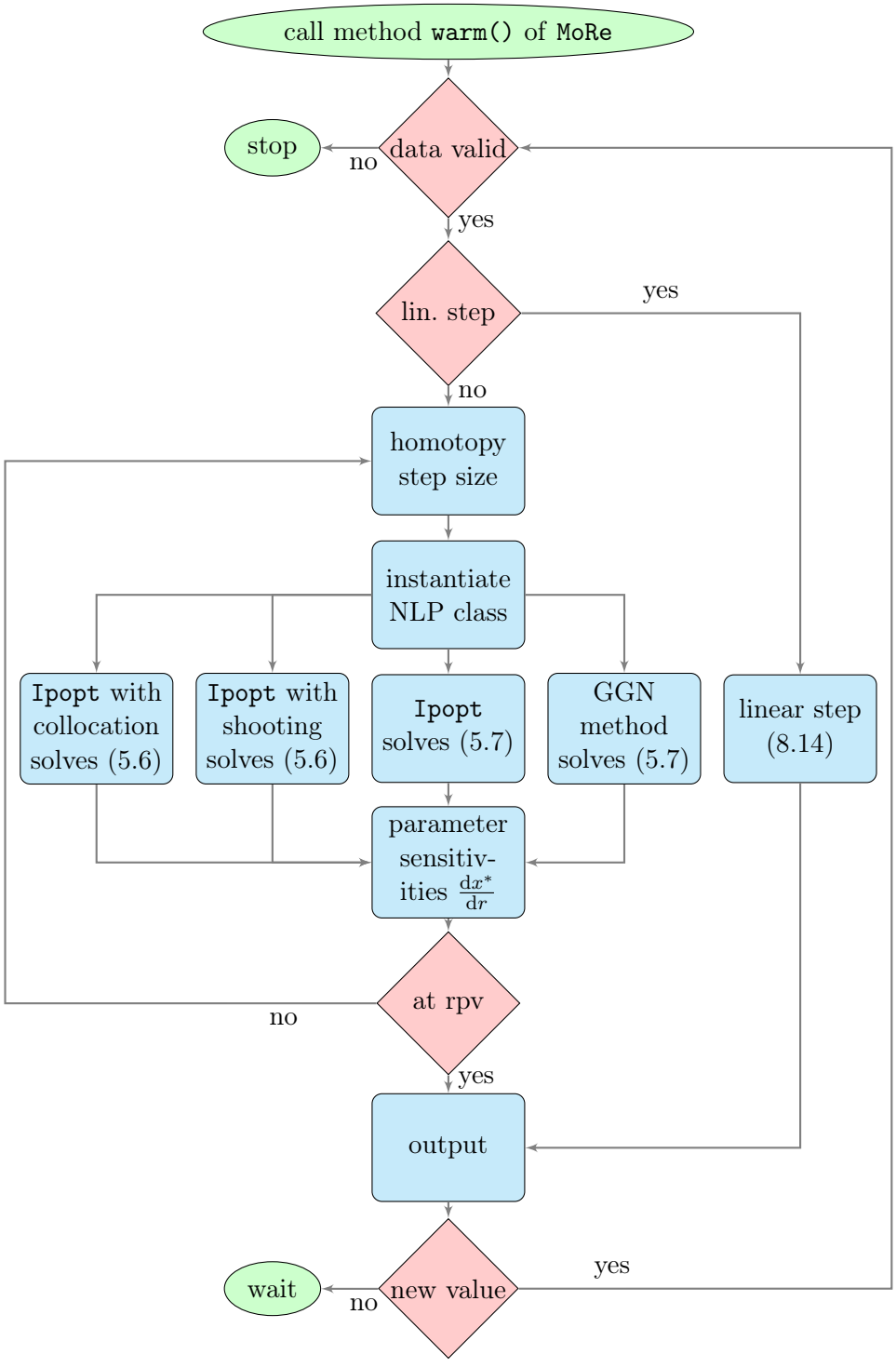


**Figure D.3:** Flowchart for a warm start in the model reduction code `MoRe` implicitly with method `reduction()` or explicitly with `warm()`.

## D.3 Input variables and options

In this section, we present input data that is needed to compute the numerical solutions of optimization problem (9.8) that are presented in Figure 9.25 in Section 9.3.3. We choose to solve optimization problem (5.6) with reverse mode $t_* = t_f$ in a collocation approach. The time horizon is chosen as $t_f - t_0 = 10^{-8}$ s. Therefore, we set the options as given in Table D.1 and use the default values for the remaining options.

**Table D.1:** General settings for the example problem (9.8) to reduce the model for ozone decomposition.

| Key word | Value |
|---|---|
| `<method>` | `c` or `collocation` |
| `<criterion>` | `12` |
| `<condition>` | `4` |
| `<tf>` | `1e-8` |
| `<t*>` | `tf` |
| `<combustion>` | `1` |
| `<positivity>` | `0` |
| `<obj_scal>` | `1e-10` |
| `<output_style>` | `js` |

The option `<criterion>` selects the objective function, where `12` is the form given via Equation 5.5. Option `<condition>` decides on the thermodynamic environment for the combustion model (if option `<combustion>` is set to `1`), where `4` represents adiabatic and isobaric. Nonnegativity of the variables is not demanded by setting `<positivity>` to `0`. The objective function is scaled with a factor of $10^{-10}$.
We specify the collocation settings by choosing the options as depicted in Table D.2, where `<ncp>` defines the degree of the collocation polynomials and `<nfe>` defines the number of collocation intervals. For the rest of the options, we choose the default values.

**Table D.2:** Collocation settings for the example problem (9.8) to reduce the model for ozone decomposition.

| Key word | Value |
|---|---|
| `<nfe>` | `150` |
| `<ncp>` | `1` |

The step size control for the homotopy steps in the predictor corrector scheme is switched off. This means, we set the option `<step_size_control>` to `0` in

the homotopy settings and do not have to specify any other options for the requested homotopy full step method.
The mechanism given in the `HOMREA` format [172] and the thermodynamic data (the coefficients of NASA polynomials) are automatically transformed by the mechanism parser. We choose the parameters of the model as given in Table D.3.

**Table D.3:** Parameters for the example problem (9.8) to reduce the model for ozone decomposition.

| Key word | Value |
|---|---|
| `p` | `100000` |
| `T` | `1000` |
| `O` | `62.5` |

This means, we assume a pressure of 1 bar and an elemental specific mole of $\check{z}_\mathrm{O} = 62.5\,\mathrm{mol\,kg^{-1}}$. The temperature is given to define the fixed specific enthalpy of the system indirectly: It is the enthalpy of the given value for $\check{z}_\mathrm{O}$ at $T = 1000\,\mathrm{K}$.
We also give initial values for the algorithm. We should specify points that we expect near the solution $z^*(t_0)$ and $z^*(t_\mathrm{f})$ of the optimization problem (9.8) for the first given value for the reaction progress variables. In the chosen collocation approach, a linear interpolation is made on the collocation points based on the given initial values. For this small example, we make a constant initialization with the initial values $z^0(t_0) = z^0(t_\mathrm{f})$ given in Table D.4.

**Table D.4:** Initial values for the example problem (9.8) to reduce the model for ozone decomposition.

| Variable | Initial value |
|---|---|
| `O` | `4.968970151960297e+01` |
| `O2` | `6.405088761730501e-00` |
| `O3` | `4.031922778342857e-05` |
| `T` | `4.825580760386146e+03` |

The grid of values for the reaction progress variable $z_\mathrm{O}$ is given as a file `grid.dat` with first line `0` and in every subsequent line one value for $z_\mathrm{O}^{t_*}$ $(50, 51, \ldots, 60)$.
One instance `More` of the `MoRe` class is created. To compute the results, the method `More.reduction()` is used. The approximation of the points on the SIM can be found in the file `sim_solution.out`, and the approximations of the manifold tangent vectors are saved in `mtv_solution.out`. The performance of the algorithm is documented in `status_solution.out`.

# Bibliography


[1] M. Abramowitz and I. A. Stegun, eds. *Handbook of mathematical functions*. Courier Dover Publications, New York, 1964.

[2] A. Adrover, F. Creta, S. Cerbelli, M. Valorani, and M. Giona. "The structure of slow invariant manifolds and their bifurcational routes in chemical kinetic models." *Computers and Chemical Engineering*, vol. 31(11), pp. 1456–1474, 2007. doi:10.1016/j.compchemeng.2006.12.008.

[3] A. Adrover, F. Creta, M. Giona, and M. Valorani. "Stretching-based diagnostics and reduction of chemical kinetic models with diffusion." *Journal of Computational Physics*, vol. 225(2), pp. 1442–1471, 2007. doi:10.1016/j.jcp.2007.01.030.

[4] A. Adrover, F. Creta, M. Giona, M. Valorani, and V. Vitacolonna. "Natural tangent dynamics with recurrent biorthonormalizations: A geometric computational approach to dynamical systems exhibiting slow manifolds and periodic/chaotic limit sets." *Physica D: Nonlinear Phenomena*, vol. 213(2), pp. 121–146, 2006. doi:10.1016/j.physd.2005.05.021.

[5] R. Aglave. "CFD Simulation of Combustion Using Automatically Reduced Reaction Mechanisms: A Case for Diesel Engine." Ph.D. thesis, University of Heidelberg, Heidelberg, Germany, 2007.

[6] A. N. Al-Khateeb, J. M. Powers, S. Paolucci, A. J. Sommese, J. A. Diller, J. D. Hauenstein, and J. D. Mengers. "One-dimensional slow invariant manifolds for spatially homogenous reactive systems." *Journal of Chemical Physics*, vol. 131(2), p. 024 118, 2009. doi:10.1063/1.3171613.

[7] A. N. S. Al-Khateeb. "Fine Scale Phenomena in Reacting Systems: Identification and Analysis for their Reduction." Ph.D. thesis, University of Notre Dame, Notre Dame, Indiana, USA, 2010.

[8] E. Allgower and K. Georg. "Simplicial and Continuation Methods for Approximating Fixed Points and Solutions to Systems of Equations." *SIAM Review*, vol. 22(1), pp. 28–85, 1980. doi:10.1137/1022003.

[9] E. L. Allgower and K. Georg. *Numerical Continuation Methods: An Introduction*. No. 13 in Series in Computational Mathematics, Springer, Berlin, 1990.

[10] E. L. Allgower and K. Georg. "Numerical path following." In P. G. Ciarlet and J. L. Lions, eds., "Techniques of Scientific Computing (Part 2)," *Handbook of Numerical Analysis*, vol. 5, pp. 3–207. Elsevier, 1997. doi: 10.1016/S1570-8659(97)80002-6.

[11] P. R. Amestoy, I. S. Duff, J. Koster, and J.-Y. L'Excellent. "A Fully Asynchronous Multifrontal Solver Using Distributed Dynamic Scheduling." *SIAM Journal on Matrix Analysis and Applications*, vol. 23(1), pp. 15–41, 2001. doi:10.1137/S0895479899358194.

[12] P. R. Amestoy, A. Guermouche, J.-Y. L'Excellent, and S. Pralet. "Hybrid scheduling for the parallel solution of linear systems." *Parallel Computing*, vol. 32(2), pp. 136–156, 2006. doi:10.1016/j.parco.2005.07.004.

[13] E. Anderson, Z. Bai, J. Dongarra, A. Greenbaum, A. McKenney, J. Du Croz, S. Hammerling, J. Demmel, C. Bischof, and D. Sorensen. "LAPACK: a portable linear algebra library for high-performance computers." In "Proceedings of the 1990 ACM/IEEE conference on Supercomputing," pp. 2–11. Supercomputing '90, IEEE Computer Society Press, Los Alamitos, CA, USA, 1990.

[14] L. Armijo. "Minimization of functions having Lipschitz continuous first partial derivatives." *Pacific Journal of Mathematics*, vol. 16, pp. 1–3, 1966.

[15] U. Ascher and L. Petzold. *Computer methods for ordinary differential equations and differential-algebraic equations*. SIAM, Philadelphia, 1998.

[16] I. Bauer. "Numerische Verfahren zur Lösung von Anfangswertaufgaben und zur Generierung von ersten und zweiten Ableitungen mit Anwendungen bei Optimierungsaufgaben in Chemie und Verfahrenstechnik." Ph.D. thesis, University of Heidelberg, Heidelberg, Germany, 1999.

[17] B. M. Bell. "Automatic differentiation software CppAD.", 2012. URL `http://www.coin-or.org/CppAD/`.

[18] B. M. Bell and J. V. Burke. "Algorithmic Differentiation of Implicit Functions and Optimal Values." In C. H. Bischof, H. M. Bücker, P. D. Hovland, U. Naumann, and J. Utke, eds., "Advances in Automatic Differentiation," pp. 67–77. Springer, Berlin, 2008.

[19] A. Ben-Israel and T. N. Greville. *Generalized Inverses: Theory and Applications*. Springer, New York, second edn., 2003.

[20] E. A. Bender. *An introduction to mathematical modeling*. Wiley, New York, 2000.

[21] L. T. Biegler. "An overview of simultaneous strategies for dynamic optimization." *Chemical Engineering and Processing: Process Intensification*, vol. 46(11), pp. 1043–1053, 2007. doi:10.1016/j.cep.2006.06.021.

[22] H. G. Bock. "Numerical treatment of inverse problems in chemical reaction kinetics." In K. H. Ebert, P. Deuflhard, and W. Jäger, eds., "Modelling of Chemical Reaction Systems," *Springer Series in Chemical Physics*, vol. 18, pp. 102–125. Springer, Heidelberg, 1981.

[23] H. G. Bock. "Recent advances in parameter identification techniques for ODE." In P. Deuflhard and E. Hairer, eds., "Numerical Treatment of Inverse Problems in Differential and Integral Equations," pp. 95–121. Birkhäuser, Boston, 1983.

[24] H. G. Bock. "Randwertproblemmethoden zur Parameteridentifizierung in Systemen nichtlinearer Differentialgleichungen." In "Bonner Mathematische Schriften," vol. 183. University of Bonn, Germany, 1987.

[25] H. G. Bock. "Numerische Mathematik 2." Lecture, Heidelberg, 2006.

[26] H. G. Bock. "Algorithmische Optimierung I." Lecture, Heidelberg, 2007.

[27] H. G. Bock. "Numerische Mathematik 3 – Ausgewählte Kapitel des Wissenschaftlichen Rechnens." Lecture, Heidelberg, 2007.

[28] H. G. Bock, E. Kostina, and J. P. Schlöder. "On the Role of Natural Level Functions to Achieve Global Convergence for Damped Newton Methods." In M. J. D. Powell and S. Scholtes, eds., "System Modelling and Optimization. Methods, Theory and Applications," Kluwer, 2000.

[29] H. G. Bock and K. J. Plitt. "A multiple shooting algorithm for direct solution of optimal control problems." In "Proceedings of the Ninth IFAC World Congress, Budapest," Pergamon, Oxford, 1984.

[30] M. Bodenstein. "Geschwindigkeit der Bildung des Bromwasserstoffs aus seinen Elementen." *Zeitschrift für Physikalische Chemie (Leipzig)*, vol. 57, pp. 168–192, 1907.

[31] M. Bodenstein. "Eine Theorie der photochemischen Reaktionsgeschwindigkeiten." *Zeitschrift für Physikalische Chemie (Leipzig)*, vol. 85, pp. 329–397, 1913.

[32] M. Braack. "An Adaptive Finite Element Method for Reactive-Flow Problems." Ph.D. thesis, University of Heidelberg, Heidelberg, Germany, 1998.

[33] C. Büskens and H. Maurer. "Sensitivity analysis and real-time optimization of parametric nonlinear programming problems." In M. Grötschel, S. O. Krumke, and J. Rambau, eds., "Online Optimization of Large Scale Systems," chap. 1, pp. 3–16. Springer, Berlin, 2001.

[34] V. Bykov and U. Maas. "Reaction-Diffusion Manifolds and Global Quasi-linearization: Two Complementary Methods for Mechanism Reduction." *The Open Thermodynamics Journal*, vol. 4, pp. 92–100, 2010. doi:10.2174/1874396X01004010092.

[35] D. L. Chapman and L. K. Underhill. "The interaction of chlorine and hydrogen. The influence of mass." *Journal of the Chemical Society, Transactions*, vol. 103, pp. 496–508, 1913. doi:10.1039/CT9130300496.

[36] E. Chiavazzo. "Invariant Manifolds and Lattice Boltzmann Method for Combustion." Ph.D. thesis, ETH Zürich, Zürich, Switzerland, 2009.

[37] E. Chiavazzo, A. N. Gorban, and I. V. Karlin. "Comparison of Invariant Manifolds for Model Reduction in Chemical Kinetics." *Communications in Computational Physics*, vol. 2(5), pp. 964–992, 2007.

[38] E. Chiavazzo and I. V. Karlin. "Quasi-equilibrium grid algorithm: Geometric construction for model reduction." *Journal of Computational Physics*, vol. 227(11), pp. 5535–5560, 2008. doi:10.1016/j.jcp.2008.02.006.

[39] E. Chiavazzo, I. V. Karlin, A. N. Gorban, and K. Boulouchos. "Combustion simulation via lattice Boltzmann and reduced chemical kinetics." *Journal of Statistical Mechanics: Theory and Experiment*, vol. 2009(6), p. P06 013, 2009. doi:10.1088/1742-5468/2009/06/P06013.

[40] F. Creta, A. Adrover, S. Cerbelli, M. Valorani, and M. Giona. "Slow Manifold Structure in Explosive Kinetics. 1. Bifurcations of Points-at-Infinity in Prototypical Models." *Journal of Physical Chemistry A*, vol. 110(50), pp. 13 447–13 462, 2006. doi:10.1021/jp0636064.

[41] C. F. Curtiss and J. O. Hirschfelder. "Integration of stiff equations." *Proceedings of the National Academy of Sciences of the United States of America*, vol. 38(3), pp. 235–243, 1952.

[42] D. Davidenko. "On a new method of numerically integrating a system of nonlinear equations." *Doklady Akademii Nauk SSSR*, vol. 88, pp. 601–604, 1953.

[43] M. J. Davis and R. T. Skodje. "Geometric investigation of low-dimensional manifolds in systems approaching equilibrium." *Journal of Chemical Physics*, vol. 111(3), pp. 859–874, 1999. doi:10.1063/1.479372.

[44] S. Delhaye, L. M. T. Somers, J. A. van Oijen, and L. P. H. de Goey. "Incorporating unsteady flow-effects in flamelet-generated manifolds." *Combustion and Flame*, vol. 155(1–2), pp. 133–144, 2008. doi:10.1016/j.combustflame.2008.03.023.

[45] C. den Heijer and W. C. Rheinboldt. "On Steplength Algorithms for a Class of Continuation Methods." *SIAM Journal on Numerical Analysis*, vol. 18(5), pp. 925–948, 1981. doi:10.1137/0718066.

[46] P. Deuflhard and F. Bornemann. *Numerische Mathematik II: Gewöhnliche Differentialgleichungen*. Walter de Gruyter, Berlin, third edn., 2008.

[47] B. A. Dubrovin, A. T. Fomenko, and S. P. Novikov. *Modern geometry – methods and applications. Part II. The geometry and topology of manifolds*. No. 104 in Graduate texts in mathematics, Springer, New York, 1985.

[48] M. Fein. Ph.D. thesis, University of Freiburg, Freiburg im Breisgau, Germany. In preparation.

[49] N. Fenichel. "Persistence and smoothness of invariant manifolds for flows." *Indiana University Mathematics Journal*, vol. 21(3), pp. 193–226, 1972. doi:10.1512/iumj.1972.21.21017.

[50] N. Fenichel. "Asymptotic Stability with Rate Conditions." *Indiana University Mathematics Journal*, vol. 23(12), pp. 1109–1137, 1974. doi:10.1512/iumj.1974.23.23090.

[51] N. Fenichel. "Asymptotic Stability with Rate Conditions II." *Indiana University Mathematics Journal*, vol. 26(1), pp. 81–93, 1977. doi:10.1512/iumj.1977.26.26006.

[52] N. Fenichel. "Geometric singular perturbation theory for ordinary differential equations." *Journal of Differential Equations*, vol. 31(1), pp. 53–98, 1979. doi:10.1016/0022-0396(79)90152-9.

[53] H. J. Ferreau, H. G. Bock, and M. Diehl. "An online active set strategy to overcome the limitations of explicit MPC." *International Journal of Robust and Nonlinear Control*, vol. 18(8), pp. 816–830, 2008. doi:10.1002/rnc.1251.

[54] A. Fiacco and G. McCormick. *Nonlinear programming: sequential unconstrained minimization techniques*. No. 4 in Classics in applied mathematics, SIAM, Philadelphia, PA, 1990.

[55] A. V. Fiacco. "Sensitivity analysis for nonlinear programming using penalty methods." *Mathematical Programming*, vol. 10(1), pp. 287–311, 1976. doi:10.1007/BF01580677.

[56] R. Fletcher. *Practical methods of optimization*, vol. 2. Wiley, Chichester, NY, 1981.

[57] R. Fletcher and S. Leyffer. "Nonlinear programming without a penalty function." *Mathematical Programming*, vol. 91(2), pp. 239–269, 2002. doi:10.1007/s101070100244.

[58] R. Fletcher, S. Leyffer, and P. L. Toint. "On the Global Convergence of a Filter–SQP Algorithm." *SIAM Journal on Optimization*, vol. 13(1), pp. 44–59, 2002. doi:10.1137/S105262340038081X.

[59] A. Forsgren, P. E. Gill, and M. H. Wright. "Interior Methods for Nonlinear Optimization." *SIAM Review*, vol. 44(4), pp. 525–597, 2002. doi:10.1137/S0036144502414942.

[60] S. J. Fraser. "The steady state and equilibrium approximations: A geometrical picture." *Journal of Chemical Physics*, vol. 88, pp. 4732–4738, 1988. doi:10.1063/1.454686.

[61] R. W. Freund and R. H. W. Hoppe. *Stoer/Bulirsch: Numerische Mathematik 1*. Springer, Berlin, tenth edn., 2007. doi:10.1007/978-3-540-45390-1.

[62] C. W. Gear, T. J. Kaper, I. G. Kevrekidis, and A. Zagaris. "Projecting to a Slow Manifold: Singularly Perturbed Systems and Legacy Codes." *SIAM Journal on Applied Dynamical Systems*, vol. 4(3), pp. 711–732, 2005. doi:10.1137/040608295.

[63] R. Gilbert, K. Luther, and J. Troe. "Theory of Thermal Unimolecular Reactions in the Fall-off Range. II. Weak Collision Rate Constants." *Berichte der Bunsen-Gesellschaft für Physikalische Chemie*, vol. 87, pp. 169–177, 1983.

[64] P. E. Gill, W. Murray, and M. H. Wright. *Practical optimization*. Academic Press, London, 1981.

[65] J.-M. Ginoux. *Differential Geometry Applied to Dynamical Systems*, *World Scientific Series on Nonlinear Science, Series A*, vol. 66. World Scientific, Singapore, 2009.

[66] J.-M. Ginoux and B. Rossetto. "Differential Geometry and Mechanics: Applications to Chaotic Dynamical Systems." *International Journal of Bifurcation and Chaos*, vol. 16(4), pp. 887–910, 2006. doi:10.1142/S0218127406015192.

[67] J.-M. Ginoux and B. Rossetto. "Slow Invariant Manifolds as Curvature of the Flow of Dynamical Systems." *International Journal of Bifurcation and Chaos*, vol. 18(11), pp. 3409–3430, 2008. doi:10.1142/S0218127408022457.

[68] M. Giona, A. Adrover, F. Creta, and M. Valorani. "Slow Manifold Structure in Explosive Kinetics. 2. Extension to Higher Dimensional Systems." *Journal of Physical Chemistry A*, vol. 110(50), pp. 13 463–13 474, 2006. doi:10.1021/jp063608o.

[69] S. S. Girimaji. "Reduction of Large Dynamical Systems by Minimization of Evolution Rate." *Physical Review Letters*, vol. 82(11), pp. 2282–2285, 1999. doi:10.1103/PhysRevLett.82.2282.

[70] G. H. Golub and C. F. V. Loan. *Matrix Computations*. Johns Hopkins University Press, Baltimore, 1996.

[71] J. Gondzio and A. Grothey. "A New Unblocking Technique to Warmstart Interior Point Methods Based on Sensitivity Analysis." *SIAM Journal on Optimization*, vol. 19(3), pp. 1184–1210, 2008. doi:10.1137/060678129.

[72] A. N. Gorban and I. V. Karlin. *Invariant Manifolds for Physical and Chemical Kinetics*. No. 660 in Lecture Notes in Physics, Springer, Berlin, 2005.

[73] A. N. Gorban, I. V. Karlin, and A. Zinovyev. "Invariant Grids: Method of Complexity Reduction in Reaction Networks." *Complexus*, vol. 2(3–4), pp. 110–127, 2005. doi:10.1159/000093684.

[74] A. N. Gorban, I. V. Karlin, and A. Y. Zinovyev. "Constructive methods of invariant manifolds for kinetic problems." *Physics Reports*, vol. 396(4–6), pp. 197–403, 2004. doi:10.1016/j.physrep.2004.03.006.

[75] A. N. Gorban, O. Radulescu, and A. Y. Zinovyev. "Asymptotology of chemical reaction networks." *Chemical Engineering Science*, vol. 65(7), pp. 2310–2324, 2010. doi:10.1016/j.ces.2009.09.005.

[76] D. A. Goussis. "On the validity and relation of the QSSA and PEA." In "13th International Conference on Numerical Combustion," Corfu, Greece, 2011.

[77] D. A. Goussis and M. Valorani. "An efficient iterative algorithm for the approximation of the fast and slow dynamics of stiff systems." *Journal of Computational Physics*, vol. 214(1), pp. 316–346, 2006. doi: 10.1016/j.jcp.2005.09.019.

[78] G. Gramelsberger. *Computerexperimente*. Science studies, Transcript-Verlag, Bielefeld, 2010.

[79] A. Griewank. *Evaluating Derivatives: Principles and Techniques of Algorithmic Differentiation*. No. 19 in Frontiers in Applied Mathematics, SIAM, Philadelphia, PA, 2000.

[80] S. Hafner, A. Rashidi, G. Baldea, and U. Riedel. "A detailed chemical kinetic model of high-temperature ethylene glycol gasification." *Combustion Theory and Modelling*, vol. 15(4), pp. 517–535, 2011. doi: 10.1080/13647830.2010.547602.

[81] E. Hairer, S. P. Nørsett, and G. Wanner. *Solving Ordinary Differential Equations I: Nonstiff Problems*. No. 8 in Springer Series in Computational Mathematics, Springer, Berlin, second edn., 2008.

[82] E. Hairer and G. Wanner. *Solving Ordinary Differential Equations II: Stiff and Differential-Algebraic Problems*. No. 14 in Springer Series in Computational Mathematics, Springer, New York, second edn., 2010.

[83] V. Hiremath, Z. Ren, and S. B. Pope. "A greedy algorithm for species selection in dimension reduction of combustion chemistry." *Combustion Theory and Modelling*, vol. 14(5), pp. 619–652, 2010. doi:10.1080/13647830.2010.499964.

[84] HSL. "A Collection of Fortran codes for large-scale scientific computation.", 2007. URL `http://www.hsl.rl.ac.uk`.

[85] P. Humphreys. *Extending Ourselves: Computational Science, Empiricism, and Scientific Method*. Oxford University Press, New York, 2004. doi:10.1093/0195158709.001.0001.

[86] C. K. R. T. Jones. "Geometric Singular Perturbation Theory." In R. Johnson, ed., "Dynamical Systems," chap. 2, pp. 44–118. No. 1609 in Lecture Notes in Mathematics, Springer, Heidelberg, 1995.

[87] S. Kameswaran and L. T. Biegler. "Convergence rates for direct transcription of optimal control problems using collocation at Radau points." *Computational Optimization and Applications*, vol. 41(1), pp. 81–126, 2008. doi:10.1007/s10589-007-9098-9.

[88] J. Kammerer. "Numerische Verfahren zur dynamischen Komplexitätsreduktion biochemischer Reaktionssysteme." Ph.D. thesis, University of Heidelberg, Heidelberg, Germany, 2007.

[89] H. G. Kaper and T. J. Kaper. "Asymptotic analysis of two reduction methods for systems of chemical reactions." *Physica D*, vol. 165(1–2), pp. 66–93, 2002. doi:10.1016/S0167-2789(02)00386-X.

[90] G. Karypis and V. Kumar. "A Fast and Highly Quality Multilevel Scheme for Partitioning Irregular Graphs." *SIAM Journal on Scientific Computing*, vol. 20(1), pp. 359–392, 1999. doi:10.1137/S1064827595287997.

[91] N. Kazantzis, C. Kravaris, and L. Syrou. "A new model reduction method for nonlinear dynamical systems." *Nonlinear Dynamics*, vol. 59(1–2), pp. 183–194, 2010. doi:10.1007/s11071-009-9531-y.

[92] J. C. Keck and D. Gillespie. "Rate-controlled partial-equilibrium method for treating reacting gas mixtures." *Combustion and Flame*, vol. 17(2), pp. 237–241, 1971. doi:10.1016/S0010-2180(71)80166-9.

[93] R. J. Kee, M. E. Coltrin, and P. Glarborg. *Chemically Reacting Flow: Theory and Practice*. Wiley-Interscience, Hoboken, NJ, 2003.

[94] H. B. Keller. *Numerical methods for two-point boundary-value problems*. Blaisdell Publishing, Boston, 1968.

[95] A. Ketelheun, C. Olbricht, F. Hahn, and J. Janicka. "NO Prediction in Turbulent Flames Using LES/FGM With Additional Transport Equations." *Proceedings of the Combustion Institute*, vol. 33(2), pp. 2975–2982, 2011. doi:10.1016/j.proci.2010.07.021.

[96] K. Kohse-Höinghaus, P. Oßwald, T. Cool, T. Kasper, N. Hansen, F. Qi, C. Westbrook, and P. Westmoreland. "Biofuel Combustion Chemistry: From Ethanol to Biodiesel." *Angewandte Chemie International Edition*, vol. 49(21), pp. 3572–3597, 2010. doi:10.1002/anie.200905335.

[97] J. Kuehne, A. Ketelheun, and J. Janicka. "Analysis of sub-grid PDF of a progress variable approach using a hybrid LES/TPDF method." *Proceedings of the Combustion Institute*, vol. 33(1), pp. 1411–1418, 2011. doi:10.1016/j.proci.2010.08.001.

[98] Y. A. Kuznetsov. *Elements of Applied Bifurcation Theory*. No. 112 in Applied Mathematical Sciences, Springer, New York, third edn., 2004.

[99] S. Lam. *Recent Advances in the Aerospace Sciences*, chap. Singular Perturbation for Stiff Equations using Numerical Methods, pp. 3–20. Plenum Press, New York and London, 1985.

[100] S. H. Lam and D. A. Goussis. "The CSP Method for Simplifying Kinetics." *International Journal of Chemical Kinetics*, vol. 26(4), pp. 461–486, 1994. doi:10.1002/kin.550260408.

[101] D. Lebiedz. "Computing minimal entropy production trajectories: An approach to model reduction in chemical kinetics." *Journal of Chemical Physics*, vol. 120(15), pp. 6890–6897, 2004. doi:10.1063/1.1652428.

[102] D. Lebiedz. "Optimal Control, Model- and Complexity-Reduction of Self-Organized Chemical and Biochemical Systems: A Scientific Computing Approach." Habilitation thesis, University of Heidelberg, Heidelberg, Germany, 2006.

[103] D. Lebiedz. "Entropy-related extremum principles for model reduction of dynamical systems." *Entropy*, vol. 12(4), pp. 706–719, 2010. doi: 10.3390/e12040706.

[104] D. Lebiedz, V. Reinhardt, and J. Kammerer. "Novel trajectory based concepts for model and complexity reduction in (bio)chemical kinetics." In A. N. Gorban, N. Kazantzis, I. G. Kevrekidis, and C. Theodoropoulos, eds., "Model reduction and coarse-graining approaches for multi-scale phenomena," pp. 343–364. Springer, Berlin, 2006. doi: 10.1007/3-540-35888-9.

[105] D. Lebiedz, V. Reinhardt, and J. Siehr. "Minimal curvature trajectories: Riemannian geometry concepts for slow manifold computation in chemical kinetics." *Journal of Computational Physics*, vol. 229(18), pp. 6512–6533, 2010. doi:10.1016/j.jcp.2010.05.008.

[106] D. Lebiedz, V. Reinhardt, J. Siehr, and J. Unger. "Geometric criteria for model reduction in chemical kinetics via optimization of trajectories." In A. N. Gorban and D. Roose, eds., "Coping with Complexity: Model Reduction and Data Analysis," pp. 241–252. No. 75 in Lecture Notes in Computational Science and Engineering, Springer, first edn., 2011. doi:10.1007/978-3-642-14941-2.

[107] D. Lebiedz and J. Siehr. "Simplified reaction models for combustion in gas turbine combustion chambers." Submitted, 2012.

[108] D. Lebiedz, J. Siehr, and J. Unger. "A variational principle for computing slow invariant manifolds in dissipative dynamical systems." *SIAM Journal on Scientific Computing*, vol. 33(2), pp. 703–720, 2011. doi: 10.1137/100790318.

[109] J. M. Lee. *Introduction to Topological Manifolds*. No. 202 in Graduate Texts in Mathematics, Springer, New York, second edn., 2011. doi: 10.1007/978-1-4419-7940-7.

[110] J. Li, Z. Zhao, A. Kazakov, and F. L. Dryer. "An updated comprehensive kinetic model of hydrogen combustion." *International Journal of Chemical Kinetics*, vol. 36(10), pp. 566–575, 2004. doi: 10.1002/kin.20026.

[111] U. Maas and S. B. Pope. "Simplifying Chemical Kinetics: Intrinsic Low-Dimensional Manifolds in Composition Space." *Combustion and Flame*, vol. 88(3–4), pp. 239–264, 1992. doi:10.1016/0010-2180(92)90034-M.

[112] U. Maas and J. Warnatz. "Simulation of Thermal Ignition Processes in Two-Dimensional Geometries." *Zeitschrift für Physikalische Chemie, Neue Folge*, vol. 161(1–2), pp. 61–81, 1989. doi:10.1524/zpch.1989.161.Part_1_2.061.

[113] MathWorks Inc. "MATLAB 7.8.0 (R2009a)." Natick, MA, USA, 2009.

[114] K. D. Mease, S. Bharadwaj, and S. Iravanchy. "Timescale Analysis for Nonlinear Dynamical Systems." *Journal of Guidance, Control, and Dynamics*, vol. 26(2), pp. 318–330, 2003.

[115] K. D. Mease, U. Topcu, and E. Aykutluğ. "Characterizing Two-Timescale Nonlinear Dynamics Using Finite-Time Lyapunov Exponents and Vectors." arXiv:0807.0239, 2008.

[116] A. Meister. *Numerik linearer Gleichungssysteme*. Vieweg+Teubner, fourth edn., 2011. doi:10.1007/978-3-8348-8100-7.

[117] L. Michaelis and M. L. Menten. "Die Kinetik der Invertinwirkung." *Biochemische Zeitschrift*, vol. 49, pp. 333–369, 1913.

[118] A. Mitsos, G. M. Oxberry, P. I. Barton, and W. H. Green. "Optimal automatic reaction and species elimination in kinetic mechanisms." *Combustion and Flame*, vol. 155(1–2), pp. 118–132, 2008. doi:10.1016/j.combustflame.2008.03.004.

[119] P. J. Mohr, B. N. Taylor, and D. B. Newell. "CODATA recommended values of the fundamental physical constants: 2006." *Reviews of Modern Physics*, vol. 80(2), pp. 633–730, 2008. doi:10.1103/RevModPhys.80.633.

[120] J. Nafe and U. Maas. "Modelling of NO-formation Based on ILDM Reduced Chemistry." *Proceedings of the Combustion Institute*, vol. 29(1), pp. 1379–1385, 2003. doi:10.1016/S1540-7489(02)80169-9.

[121] H. N. Najm, M. Valorani, D. A. Goussis, and J. Prager. "Analysis of methane-air edge flame structure." *Combustion Theory and Modelling*, vol. 14(2), pp. 257–294, 2010. doi:10.1080/13647830.2010.483021.

[122] A. H. Nguyen and S. J. Fraser. "Geometrical picture of reaction in enzyme kinetics." *Journal of Chemical Physics*, vol. 91(1), pp. 186–193, 1989. doi:10.1063/1.457504.

[123] D. Nilsson. "Automatic analysis and reduction of reaction mechanisms for complex fuel combustion." Ph.D. thesis, Lund Institute of Technology, Lund, Sweden, 2001.

[124] J. Nocedal and S. J. Wright. *Numerical Optimization*. Springer Series in Operations Research and Financial Engineering, Springer, New York, second edn., 2006.

[125] J. A. van Oijen and L. P. H. de Goey. "Modelling of Premixed Laminar Flames using Flamelet-Generated Manifolds." *Combustion Science and Technology*, vol. 161(1), pp. 113–137, 2000. doi:10.1080/00102200008935814.

[126] L. Petzold and W. Zhu. "Model Reduction for Chemical Kinetics: An Optimization Approach." *AIChE Journal*, vol. 45(4), pp. 869–886, 1999. doi:10.1002/aic.690450418.

[127] H. Pirnay, R. López-Negrete, and L. T. Biegler. "Optimal sensitivity based on IPOPT." *Mathematical Programming Computation*, pp. 1–27, submitted, 2011.

[128] K. J. Plitt. "Ein superlinear konvergentes Mehrzielverfahren zur direkten Berechnung beschränkter optimaler Steuerungen." Master's thesis, University of Bonn, Bonn, Germany, 1981.

[129] M. J. D. Powell. "A Fast Algorithm For Nonlinearly Constrained Optimization Calculations." In A. Dold and B. Eckmann, eds., "Numerical Analysis," *Lecture Notes in Mathematics*, vol. 630, pp. 144–157. Springer, Berlin, 1978.

[130] J. M. Powers and S. Paolucci. "Uniqueness of chemical equilibria in ideal mixtures of ideal gases." *American Journal of Physics*, vol. 76(9), pp. 848–855, 2008. doi:10.1119/1.2919742.

[131] J. Prager, H. N. Najm, M. Valorani, and D. A. Goussis. "Skeletal mechanism generation with CSP and validation for premixed $n$-heptane flames." *Proceedings of the Combustion Institute*, vol. 32(1), pp. 509–517, 2009. doi:10.1016/j.proci.2008.06.074.

[132] W. H. Press, S. A. Teukolsky, W. T. Vetterling, and B. P. Flannery. *Numerical Recipes in C – The Art of Scientific Computing*. Cambridge University Press, Cambridge, second edn., 1997.

[133] R. Rannacher. "Numerische Mathematik (Numerik gewöhnlicher und einfacher partieller Differentialgleichungen)." Lecture notes, University of Heidelberg, Heidelberg, Germany, 2011.

[134] M. Rehberg. Ph.D. thesis, University of Freiburg, Freiburg im Breisgau, Germany. In preparation.

[135] V. Reinhardt. "On the Application of Trajectory-based Optimization for Nonlinear Kinetic Model Reduction." Ph.D. thesis, University of Heidelberg, Heidelberg, Germany, 2008.

[136] V. Reinhardt, M. Winckler, and D. Lebiedz. "Approximation of Slow Attracting Manifolds in Chemical Kinetics by Trajectory-Based Optimization Approaches." *Journal of Physical Chemistry A*, vol. 112(8), pp. 1712–1718, 2008. doi:10.1021/jp0739925.

[137] V. Reinhardt, M. Winckler, J. Warnatz, and D. Lebiedz. "Kinetic Mechanism Reduction by Trajectory-Based Optimization Methods." In "Proceedings of the Third European Combustion Meeting," ECM, 2007.

[138] Z. Ren and S. Pope. "Species reconstruction using pre-image curves." *Proceedings of the Combustion Institute*, vol. 30(1), pp. 1293–1300, 2005. doi:10.1016/j.proci.2004.07.017.

[139] Z. Ren and S. B. Pope. "The use of slow manifolds in reactive flows." *Combustion and Flame*, vol. 147(4), pp. 243–261, 2006. doi:10.1016/j.combustflame.2006.09.002.

[140] Z. Ren, S. B. Pope, A. Vladimirsky, and J. M. Guckenheimer. "The invariant constrained equilibrium edge preimage curve method for the dimension reduction of chemical kinetics." *Journal of Chemical Physics*, vol. 124(11), p. 114 111, 2006. doi:10.1063/1.2177243.

[141] Z. Ren, S. B. Pope, A. Vladimirsky, and J. M. Guckenheimer. "Application of the ICE-PIC method for the dimension reduction of chemical kinetics coupled with transport." *Proceedings of the Combustion Institute*, vol. 31(1), pp. 473–481, 2007. doi:10.1016/j.proci.2006.07.106.

[142] C. Rhodes, M. Morari, and S. Wiggins. "Identification of low order manifolds: Validating the algorithm of Maas and Pope." *Chaos*, vol. 9(1), pp. 108–123, 1999. doi:10.1063/1.166398.

[143] L. B. Ryashko and E. E. Shnol. "On exponentially attracting invariant manifolds of ODEs." *Nonlinearity*, vol. 16(1), pp. 147–160, 2003. doi:10.1088/0951-7715/16/1/310.

[144] S. Sager. *Numerical methods for mixed–integer optimal control problems*. Der andere Verlag, Tönning, 2005.

[145] L. A. Segel and M. Slemrod. "The Quasi-Steady-State Assumption: A Case Study in Perturbation." *SIAM Review*, vol. 31(3), pp. 446–477, 1989. doi:10.1137/1031091.

[146] S. Shahshahani. "A new mathematical framework for the study of linkage and selection." *Memoirs of the American Mathematical Society*, vol. 17(211), 1979.

[147] J. Siehr and D. Lebiedz. "A continuation method for the solution of parametric optimization problems in kinetic model reduction." Tentative title, in preparation.

[148] J. Siehr and D. Lebiedz. "An optimization approach to kinetic model reduction for combustion chemistry." Submitted, 2012.

[149] S. Singh, J. M. Powers, and S. Paolucci. "On slow manifolds of chemically reactive systems." *Journal of Chemical Physics*, vol. 117(4), pp. 1482–1496, 2002. doi:10.1063/1.1485959.

[150] S. Singh, Y. Rastigejev, S. Paolucci, and J. M. Powers. "Viscous detonation in $H_2$–$O_2$–Ar using intrinsic low-dimensional manifolds and wavelet adaptive multilevel representation." *Combustion Theory and Modelling*, vol. 5(2), pp. 163–184, 2001. doi:10.1088/1364-7830/5/2/303.

[151] D. Skanda. "Robust Optimal Experimental Design for Model Discrimination of Kinetic ODE Systems." Ph.D. thesis, University of Freiburg, Freiburg im Breisgau, Germany, 2012. Submitted.

[152] G. P. Smith, D. M. Golden, M. Frenklach, N. W. Moriarty, B. Eiteneer, M. Goldenberg, C. T. Bowman, R. K. Hanson, S. Song, W. C. Gardiner Jr., V. V. Lissianski, and Z. Qin. "GRI-Mech 3.0." Published online, 1999. URL `http://www.me.berkeley.edu/gri_mech`.

[153] W. Squire and G. Trapp. "Using Complex Variables to Estimate Derivatives of Real Functions." *SIAM Review*, vol. 40(1), pp. 110–112, 1998. doi:10.1137/S003614459631241X.

[154] J. Stoer. "On the Numerical Solution of Constrained Least-Squares Problems." *SIAM Journal on Numerical Analysis*, vol. 8(2), pp. 382–411, 1971. doi:10.1137/0708038.

[155] J. Stoer and R. Bulirsch. *Introduction to Numerical Analysis*. No. 12 in Texts in Applied Mathematics, Springer, New York, third edn., 2002.

[156] P. Tannenbaum. *Excursions in modern mathematics*. Pearson Education, New York, seventh edn., 2011.

[157] A. S. Tomlin, T. Turányi, and M. J. Pilling. "Mathematical tools for the construction, investigation and reduction of combustion mechanisms." In M. Pilling and G. Hancock, eds., "Low temperature combustion and autoignition," pp. 293–437. Elsevier, Amsterdam, 1997.

[158] J. Troe. "Theory of Thermal Unimolecular Reactions in the Fall-off Range. I. Strong Collision Rate Constants." *Berichte der Bunsen-Gesellschaft für Physikalische Chemie*, vol. 87, pp. 161–169, 1983.

[159] T. Turányi, A. S. Tomlin, and M. J. Pilling. "On the error of the quasi-steady-state approximation." *Journal of Physical Chemistry*, vol. 97(1), pp. 163–172, 1993. doi:10.1021/j100103a028.

[160] M. Ulbrich, S. Ulbrich, and L. N. Vicente. "A globally convergent primal-dual interior-point filter method for nonlinear programming." *Mathematical Programming, Series A*, vol. 100(2), pp. 974–1002, 2004. doi:10.1007/s10107-003-0477-4.

[161] J. Unger. "On the Analysis of an Optimization Approach to Slow Manifold Computation in Chemical Kinetics." Diploma Thesis, University of Freiburg, Freiburg im Breisgau, Germany, 2010.

[162] M. Valorani, D. A. Goussis, F. Creta, and H. N. Najm. "Higher order corrections in the approximation of low-dimensional manifolds and the construction of simplified problems with the CSP method." *Journal of Computational Physics*, vol. 209(2), pp. 754–786, 2005. doi:10.1016/j.jcp.2005.03.033.

[163] M. Valorani and S. Paolucci. "The G-Scheme: A framework for multi-scale adaptive model reduction." *Journal of Computational Physics*, vol. 228(13), pp. 4665–4701, 2009. doi:10.1016/j.jcp.2009.03.011.

[164] F. Verhulst. "Singular perturbation methods for slow–fast dynamics." *Nonlinear Dynamics*, vol. 50(4), pp. 747–753, 2007. doi:10.1007/s11071-007-9236-z.

[165] A. Wächter. "An Interior Point Algorithm for Large-Scale Nonlinear Optimization with Applications in Process Engineering." Ph.D. thesis, Carnegie Mellon University, Pittsburgh, PA, USA, 2002.

[166] A. Wächter and L. T. Biegler. "Line Search Filter Methods for Nonlinear Programming: Local Convergence." *SIAM Journal on Optimization*, vol. 16(1), pp. 32–48, 2005. doi:10.1137/S1052623403426544.

[167] A. Wächter and L. T. Biegler. "Line Search Filter Methods for Nonlinear Programming: Motivation and Global Convergence." *SIAM Journal on Optimization*, vol. 16(1), pp. 1–31, 2005. doi:10.1137/S1052623403426556.

[168] A. Wächter and L. T. Biegler. "On the Implementation of a Primal-Dual Interior Point Filter Line Search Algorithm for Large-Scale Nonlinear Programming." *Mathematical Programming*, vol. 106(1), pp. 25–57, 2006. doi:10.1007/s10107-004-0559-y.

[169] K. Walter. "The Internal Combustion Engine at Work." In "Science and Technology Review," pp. 4–10. Lawrence Livermore National Laboratory, Livermore, CA, USA, 1999.

[170] W. Walter. *Gewöhnliche Differentialgleichungen*. Springer, Berlin, seventh edn., 2000.

[171] J. Warnatz. "Rate Coefficients in the C/H/O System." In W. C. Gardiner, ed., "Combustion chemistry," chap. 5. Springer, New York, 1984.

[172] J. Warnatz. "HOMREA User Guide." Version 2.5, 2002.

[173] J. Warnatz, U. Maas, and R. W. Dibble. *Combustion: Physical and Chemical Fundamentals, Modeling and Simulation, Experiments, Pollutant Formation*. Springer, Berlin, fourth edn., 2006.

[174] S. Wiggins. *Introduction to Applied Nonlinear Dynamical Systems and Chaos*. No. 2 in Texts in Applied Mathematics, Springer, New York, third edn., 1996.

[175] M. Winckler. "Towards optimal criteria for trajectory-based model reduction in chemical kinetics via numerical optimization." Diploma thesis, University of Heidelberg, Heidelberg, Germany, 2007.

[176] Y.-C. Wu and A. S. Debs. "Initialisation, decoupling, hot start, and warm start in direct nonlinear interior point algorithm for optimal power flows." *IEE Proceedings Generation Transmission and Distribution*, vol. 148(1), pp. 67–75, 2001. doi:10.1049/ip-gtd:20010008.

[177] A. Zagaris, C. W. Gear, T. J. Kaper, and Y. G. Kevrekidis. "Analysis of the accuracy and convergence of equation-free projection to a slow manifold." *ESAIM: Mathematical Modelling and Numerical Analysis*, vol. 43(4), pp. 757–784, 2009. doi:10.1051/m2an/2009026.

[178] A. Zagaris, H. G. Kaper, and T. J. Kaper. "Analysis of the Computational Singular Perturbation Reduction Method for Chemical Kinetics." *Journal of Nonlinear Science*, vol. 14(1), pp. 59–91, 2004. doi:10.1007/s00332-003-0582-9.

[179] A. Zagaris, H. G. Kaper, and T. J. Kaper. "Fast and Slow Dynamics for the Computational Singular Perturbation method." *Multiscale Modeling and Simulation*, vol. 2(4), pp. 613–638, 2004. doi:10.1137/040603577.

[180] V. M. Zavala and L. T. Biegler. "The advanced-step NMPC controller: Optimality, stability and robustness." *Automatica*, vol. 45(1), pp. 86–93, 2009. doi:10.1016/j.automatica.2008.06.011.

# List of Figures


2.1 Sketch of slow manifolds in phase space . . . . . 18
2.2 Sketch of species reconstruction . . . . . 19
2.3 Sketch of species reconstruction with tangent space . . . . . 20

4.1 Heat capacity $\bar{C}^{\circ}_{p,\mathrm{O}}$ versus $T$ . . . . . 42
4.2 Heat capacity with smooth transition . . . . . 43

5.1 Illustration of consistency . . . . . 66

9.1 Davis–Skodje: opt. prob. (5.6), reverse mode, $\gamma = 3$ . . . . . 109
9.2 Davis–Skodje: opt. prob. (5.6), reverse mode, $\gamma = 1.1$ . . . . . 110
9.3 Davis–Skodje: opt. prob. (5.7), $\gamma = 3$ . . . . . 110
9.4 Davis–Skodje: opt. prob. (5.6), forward mode, $\gamma = 3$ . . . . . 111
9.5 Davis–Skodje: large linear step tolerance . . . . . 111
9.6 Verhulst model: optimization problem (5.6), forward mode . . 112
9.7 Verhulst model: optimization problem (5.6), reverse mode . . 112
9.8 Catalysis: optimization problem (5.6), reverse mode . . . . . 113
9.9 Three species: optimization problem (5.6), reverse mode . . . 115
9.10 Lindemann mechanism: optimization problem (5.7) . . . . . 116
9.11 Bioreactor: optimization problem (5.6), reverse mode . . . . . 118
9.12 Six species test: opt. prob. (5.6), reverse mode, 1-dim. SIM . 119
9.13 Six species test: optimization problem (5.7), 1-dim. SIM . . . 120
9.14 Six species test: opt. prob. (5.6), reverse mode, 2-dim. SIM . 121
9.15 Six species $H_2$ comb.: reverse mode, 1-dim. SIM, comparison 123
9.16 Six species $H_2$ comb.: reverse mode, 2-dim. SIM, comparison 1 126
9.17 Six species $H_2$ comb.: reverse mode, 2-dim. SIM, comparison 2 127
9.18 Six species $H_2$ comb.: opt. landscape, 1-dim. SIM . . . . . 127
9.19 Six species $H_2$ comb.: opt. landscape, 2-dim. SIM, side view . 128
9.20 Six species $H_2$ comb.: opt. landscape, 2-dim. SIM, top view . 129
9.21 Six species $H_2$ comb.: optimization problem (5.7), 2-dim. SIM 130
9.22 $O_3$ decomp.: opt. prob. (5.6), rev. mode, isothermal, isochoric 133
9.23 $O_3$ decomp.: opt. prob. (5.6), rev. mode, isothermal, isobaric 134
9.24 $O_3$ decomp.: opt. prob. (5.6), rev. mode, adiabatic, isochoric . 134
9.25 $O_3$ decomp.: opt. prob. (5.6), rev. mode, adiabatic, isobaric . 135
9.26 $H_2$ comb.: rev. mode, 1-dim. SIM, isothermal and isochoric . 137

9.27 $H_2$ comb.: rev. mode, 1-dim. SIM, isothermal and isobaric . . 138
9.28 $H_2$ comb.: rev. mode, 1-dim. SIM, adiabatic and isochoric . . 139
9.29 $H_2$ comb.: rev. mode, 1-dim. SIM, adiabatic and isobaric . . . 140
9.30 $H_2$ comb.: rev. mode, 2-dim. SIM, adiabatic and isochoric . . 141
9.31 Syngas combustion with inert $N_2$: rev. mode, 2-dim. SIM . . 143
9.32 Syngas combustion with reactive $N_2$: (5.7), 2-dim. SIM . . . . 144

D.1 Flowchart, `MoRe` first call . . . . . 164
D.2 Flowchart, `MoRe` right hand side of ODE . . . . . 165
D.3 Flowchart, `MoRe` warm start . . . . . 167

# List of Tables


6.1 Butcher tableau, Radau collocation, order 1. . . . . 73
6.2 Butcher tableau, Radau collocation, order 3. . . . . 73
6.3 Butcher tableau, Radau collocation, order 5. . . . . 73

9.1 Three component mechanism . . . . . 114
9.2 Six species test mechanism . . . . . 118
9.3 Simplified hydrogen combustion: initial values and solution . 124
9.4 Condition number $\kappa$ . . . . . 125
9.5 Comparison of the performance of the algorithm . . . . . 131

A.1 Simplified six species hydrogen combustion . . . . . 152
A.2 Ozone decomposition mechanism . . . . . 152

B.1 Latin symbols in combustion . . . . . 158
B.2 Greek symbols in combustion . . . . . 159
B.3 Acronyms . . . . . 160

D.1 Ozone example: general settings . . . . . 168
D.2 Ozone example: collocation settings . . . . . 168
D.3 Ozone example: parameters . . . . . 169
D.4 Ozone example: initial values . . . . . 169

# List of Listings

4.1 NASA polynomial coefficients for $H_2O$. . . . . 40
4.2 NASA polynomial coefficients for O . . . . . 41
A.1 Hydrogen module of the GRI-Mech 3.0 mechanism . . . . . 153
A.2 Carbon monoxide module of the GRI-Mech 3.0 mechanism . . 154
A.3 Nitrogen oxide module of the GRI-Mech 3.0 mechanism . . . 154
A.4 Nitrogen with carbon monoxide module of GRI-Mech 3.0 . . . 155
A.5 Collision efficiencies of the GRI-Mech 3.0 mechanism . . . . . 155

# Index


**A**

active set . . . . . 27, 86, 95
amount of substance . . . . . 33
Armijo condition . . . . . 82, 85
Arrhenius kinetics . . . . . 46, 47
atomic composition coefficient . . . . 34
automatic differentiation . . . . . 90

**B**

barrier function . . . . . 89
barrier method . . . . . 88
BDF method . . . . . 74
BFGS update . . . . . 89
bioreactor . . . . . 117
Bolza term . . . . . 26
Bolzano–Weierstrass theorem . . . . . 61
Butcher tableau . . . . . 72, 73

**C**

chemical reaction
    elementary . . . . . 44, 45
    net . . . . . 44
CLLS problem . . . . . 78
close parallel assumption . . . . . 19
CNLLS problem . . . . . 78
collocation
    Gaussian . . . . . 73
    Radau . . . . . 73
complementarity . . . . . 27
    strict . . . . . 29
composition space . . . . . 17
concentration . . . . . 34
condition number . . . . . 124
consistency property . . . . . 65
CppAD . . . . . 43
critical cone . . . . . 28
CSP . . . . . 21, 22

**D**

Davidenko differential equation . . . 31
Davis–Skodje model . . . . . 108
difference quotient
    central . . . . . 90
    forward . . . . . 90
differential algebraic equation . . . . 15
divergence to infinity . . . . . 59
dynamical system . . . . . 9

**E**

enthalpy . . . . . 36
entropy . . . . . 36
entropy production . . . . . 55
equilibrium . . . . . 10, 108
equilibrium constant . . . . . 46
Euler prediction . . . . . 99
exponentially attracting manifold 13

**F**

feasibility restoration phase . . . 61, 86
feasible set . . . . . 26
Fenichel . . . . . 15
filter . . . . . 84
fixed point . . . . . 10, 108
flowcharts . . . . . 165
Fraser's algorithm . . . . . 23

**G**

gas constant . . . . . 35
Gaussian collocation . *see* collocation
Gaussian quadrature . *see* quadrature
GGN method . . . . . 77
Gibbs free energy . . . . . 37

Gram–Schmidt algorithm . . . . . 65
GRI-Mech 3.0 . . . . . 155

**H**

heat capacity . . . . . 36
Heine–Borel theorem . . . . . 60
heteroclinic orbit . . . . . 23
high performance computing . . . . . 2
HOMREA . . . . . 153
hot start . . . . . 105
hydrogen combustion . . . . . 136

**I**

ICE-PIC method . . . . . 23
ideal gas . . . . . 35
ILDM . *see* intrinsic low dimensional manifold
implicit function theorem . 15, 30, 31
inertia correction . . . . . 89
initial value problem . . . . . 10
interior point method . . . . . 88
internal energy . . . . . 35
intrinsic low dimensional manifold 21
invariant grids . . . . . 23
invariant manifold theorem . . . . . 15
invariant set . . . . . 11

**K**

Kelvin . . . . . 33
KKT conditions . . . . . 27
KKT matrix . . . . . 30
KKT point . . . . . 28

**L**

Lagrange interpolation . . . . . 70
Lagrange multiplier . . . . . 27, 82
Lagrange term . . . . . 26, 54, 74
Lagrangian function . . . . . 27, 29, 80
law of thermodynamics
    first . . . . . 35
    second . . . . . 36
    third . . . . . 36
LICQ . . . . . 27
Lindemann mechanism . . . . . 115
linear multistep method . . . . . 74
linearized feasible directions . . . . . 28
Lipschitz continuity . . . . . 11
local contraction theorem . . . . . 80
local minimizer . . . . . 26
    strict . . . . . 26
locally invariant set . . . . . 15
Lyapunov exponent . . . . . 23, 63
Lyapunov function . . . . . 48
Lyapunov stability . . . . . *see* stability

**M**

Maratos effect . . . . . 83
mass . . . . . 34
mass density . . . . . 34
mass fraction . . . . . 34
mathematical model . . . . . 1
Mayer term . . . . . 26, 75
mean molar mass . . . . . 35
merit function . . . . . 82
Michaelis–Menten kinetics . . . 20, 113
molar mass . . . . . 34
mole . . . . . 33
mole fraction . . . . . 34
multiple shooting . . . . . 75
my favorite figure . . . . . 123

**N**

NASA polynomial . . . . . 39
necessary opt. condition . . . . . 28
Newton–Cotes formulae . . . . . 69
Newton-bisection method . . . . . 103
NLP problem . . . . . 26
    parametric . . . . . 28
normal space . . . . . 12

**O**

optimization
    finite . . . . . 26
    semi-infinite . . . . . 25

optimization landscapes . . . . . 127
ordinary differential equation . . . . . 10
autonomous . . . . . 10
ozone decomposition . . . . . 131, 154

**P**

parameter sensitivity . . . . . 29
parser . . . . . 153
partial equilibrium assumption 15, 19
partial pressure . . . . . 34
PEA . . . . . *see* partial equilibrium assumption
Peano, Theorem of . . . . . 11
phase space . . . . . 10, 17
realizable . . . . . 17, 48
Picard–Lindelöf, Theorem of . . . . . 11
preconditioned system . . . . . 104
pressure . . . . . 35
primal dual equations . . . . . 89
proper map . . . . . 59

**Q**

QSSA . . . . . *see* quasi steady state assumption
quadrature
Gaussian . . . . . 70
Radau . . . . . 71
quasi steady state assumption 14, 19

**R**

Radau collocation . . . . *see* collocation
Radau quadrature . . . *see* quadrature
reaction order . . . . . 45
reaction progress variable . . 3, 18, 54, 61, 108
reactive flow . . . . . 2
represented species . . . . . *see* reaction progress variable
Runge–Kutta method . . . . . 72

**S**

scaling . . . . . 87, 105
second order correction . . . . . 83
sequential approach . . . . . 74
SIM . . . . . *see* slow invariant manifold
simultaneous approach . . . . . 74
singular values . . . . . 63
singularly perturbed system . . . . . 14
slow invariant manifold . . . . . 3, 17
smooth transition function . . . . . 41
species reconstruction . . . . . 3, 18, 54
specific mole . . . . . 34
specific volume . . . . . 34
SSC . . . . . 28
stability
asymptotic . . . . . 11
Lyapunov . . . . . 11
standard state . . . . . 37
state space . . . . . 9
stretching rate . . . . . 23, 64
syngas combustion . . . . . 140
system
closed . . . . . 35
isolated . . . . . 35
open . . . . . 35

**T**

tangent space . . . . . 12
temperature . . . . . 33
thermodynamic environment . . . . . 34
time scale . . . . . 61
time scale separation . . . . . 14, 62
trajectory . . . . . 10
Troe kinetics . . . . . 47

**U**

unrepresented species . . . *see* reaction progress variable

**V**

volume . . . . . 35

**W**

warm start . . . . . 105
Weierstrass theorem . . . . . 61